SYNERGISM OF LIPOATES AND ESTABLISHED ANTICANCER DRUGS IN CELL AND MOUSE MODELS OF COLORECTAL CANCER

Vom Fachbereich Chemie der Technischen Universität Kaiserslautern zur Verleihung des akademischen Grades „Doktor der Naturwissenschaften“ genehmigte

Dissertation

D386

vorgelegt von

Carina Neitzel

Betreuer: Prof. Dr. Jörg Fahrer

Datum der wissenschaftlichen Aussprache: 07. Januar 2021

Kaiserslautern 2020

Der experimentelle Teil dieser Arbeit wurde in der Zeit von September 2016 bis Oktober 2019 im Institut für Toxikologie der Unimedizin der Johannes-Gutenberg-Universität Mainz, im Rudolf-Buchheim-Institut für Pharmakologie der Justus-Liebig-Universität Gießen und in der Fachrichtung Lebensmittelchemie und Toxikologie am Fachbereich Chemie der Technischen Universität Kaiserslautern in der Arbeitsgruppe von Prof. Dr. Jörg Fahrer durchgeführt.

Eröffnung des Promotionsverfahrens: 15. Januar 2020
Datum der wissenschaftlichen Aussprache: 07. Januar 2021

Promotionskommission

Vorsitz: Prof. Dr. Elke Richling

1. Berichterstatter: Prof. Dr. Jörg Fahrer

2. Berichterstatter: Prof. Dr. Zuzana Storchová

ERKLÄRUNG

Hiermit erkläre ich, Carina Neitzel, die vorliegende Dissertation mit dem Titel „Synergism of Lipoates and Established Anticancer Drugs in Cell and Mouse Models of Colorectal Cancer“ selbstständig verfasst und dabei nur die in der Arbeit angegebenen Quellen und Hilfsmittel benutzt zu haben. Bestandteile dieser Arbeit wurden während der Promotion bereits vor der Erstellung dieser Dissertation auf Kongressen veröffentlicht (siehe Kongressteilnahme). Die vorliegende Dissertation habe ich weder im Ganzen noch in Teilen als Prüfungsarbeit bei einem anderen Fachbereich eingereicht und kein anderes Promotionsverfahren bei einer Hochschule beantragt oder eröffnet. Die geltende Promotionsordnung des Fachbereichs Chemie der Universität Kaiserslautern vom 07.Oktober 1999 ist mir bekannt.

Kaiserslautern, _____

Carina Neitzel

„ If a man will begin with certainties, he shall end in doubts;

but if he will be content to begin with doubts, he shall end in certainties. “

FRANCIS BACON

„ Wenn eine Idee nicht zuerst absurd erscheint, taugt sie nichts. ”

ALBERT EINSTEIN

ZUSAMMENFASSUNG

Das kolorektale Karzinom (KRK) ist eine der am häufigsten auftretenden Krebsentitäten und zeigt aktuell eine erhöhte Inzidenz und Mortalität bei Erwachsenen unter 50 Jahren in Europa und den USA auf. Zumeist im fortgeschrittenen Stadium diagnostiziert, ist die 5-Jahres-Überlebensrate des KRKs immer noch gering. Daher besteht eine Notwendigkeit neuer Therapieansätze und Angriffspunkte für Wirkstoffkandidaten, wenngleich Standardtherapien mit den Zytostatika 5-Fluorouracil (5-FU) oder Irinotecan (IT) und Biologika existieren. Einen solchen Angriffspunkt könnte der Energiemetabolismus darstellen, der für Krebszellen charakteristische Veränderungen aufweist. Das Lipoat CPI-613 ist ein Derivat der natürlich vorkommenden α-Liponsäure (LA) und gehört aufgrund seiner einzigartigen Hemmung des veränderten Energiemetabolismus in Krebszellen als Vorreiter zu einer neuen Klasse von Wirkstoffsubstanzen. CPI-613 erwies sich bereits als Inhibitor mitochondrieller Multienzymkomplexe wie der Pyruvatdehydrogenase und der α-Ketoglutaratdehydrogenase. Diese Wirkung wurde vorrangig in Krebszellen beschrieben.

Der Fokus dieser Arbeit lag zunächst auf der Untersuchung zellulärer Antworten auf die Behandlung von KRK-Zellen mit dem Lipoat CPI-613 und schlossen neben Effekten auf die mitochondrielle Integrität und Funktion der oxidativen Phosphorylierung auch die Endpunkte Zelltod, DNA-Schädigung und Autophagie ein. Hierfür wurde ein Panel an KRK-Zellen und auch nicht maligne transformierte humane Kolonepithelzellen (HCEC) untersucht. Darüber hinaus wurde in isolierten murinen Mitochondrien die Wirkungsweise von CPI-613 geprüft. Weiterhin sollte ein möglicher Synergismus durch eine Kombinationsbehandlung von Lipoaten wie CPI-613 oder dessen Muttersubstanz LA und Standardchemotherapeutika in der KRK-Behandlung wie 5-FU und IT charakterisiert werden. Nach Identifizierung der aussichtsreichsten Kombination *in vitro* folgten Studien zur Wirksamkeitssteigerung der Kombinationsbehandlung im Vergleich zur Einzelbehandlung *in vivo* sowie eine Beurteilung zu möglichen hämatotoxischen Nebeneffekten. Zu diesem Zwecke wurden sowohl das Xenograft-Modell in immundefizienten Mäusen (BALB/c nu/nu) als auch das Azoxymethan (AOM)/Dextran Natriumsulfat (DSS)-Model zur chemischen Induktion von KRK-Tumoren in C57BL/6-Mäusen genutzt.

Es konnte gezeigt werden, dass CPI-613 sowohl in isolierten Mitochondrien als auch in KRK-Zelllinien zu einer Reduktion des mitochondriellen Membranpotentials neben einer vermehrten Bildung von reaktiven Sauerstoffspezies führte. Dies ging mit einer deutlichen Verminderung der zellulären Atmung einher und äußerte sich in KRK-

Zelllinien zudem in einer Reduktion der Mitochondrien-Anzahl. Während kein Zellzyklusarrest durch die Behandlung mit CPI-613 ausgelöst wurde, konnte in einem Panel von diversen KRK-Zelllinien Zelltod nachgewiesen werden. Dies war mit gleicher Potenz in den verschiedenen Zelllinien unabhängig des p53- und MSS/MSS-Status zu beobachten. Dabei wurden verschiedene und teils redundante Zelltodmechanismen wie Apoptose, Nekroptose und Caspase-unabhängigem Zelltod nach CPI-613 Behandlung nachgewiesen. Als Folge einer Behandlung mit CPI-613 kam es des Weiteren zu einer gesteigerten Autophagie-Rate in KRK-Zellen. Analysen zum genotoxischen Potential von CPI-613 ergaben keine Hinweise auf DNA-Schädigungen. Verschiedene Kombinationen von Lipoaten und Standardchemotherapeutika wurden *in vitro* auf deren Synergismus charakterisiert. Neben einer synergistischen Wirkung von CPI-613 in Kombination mit IT in KRK-Zellkulturmodellen konnte ebenfalls ein positiver Effekt in Mausmodellen des KRKs verzeichnet werden. Während CPI-613 bereits alleine in Xenograft-Modellen zu einer Reduktion des Tumorwachstums und somit zu einer verlängerten Überlebenszeit und damit einem Therapieerfolg führte, verstärkten sich diese Effekte deutlich in der Kombinationsbehandlung mit IT. In chemisch-induzierten Tumoren hingegen zeigte vor allem IT einen therapeutischen Effekt, welcher ebenfalls in der Kombination mit CPI-613 zu verzeichnen war. Eine Monotherapie mit CPI-613 führte in diesem Modell zu keinem signifikanten Therapieerfolg. Der Synergismus *in vitro* und *in vivo* gründet vornehmlich auf einer gesteigerten Zelltodrate, der Depletion von p53 sowie einer Reduktion der Autophagierate und nicht auf einer erhöhten DNA-Schädigung. Ein hämatotoxisches Nebenwirkungsprofil von CPI-613 wurde hier im Allgemeinen nicht beobachtet.

Zusammenfassend wurde in dieser Arbeit demonstriert, dass CPI-613 im Kontext von KRK den veränderten Energiemetabolismus angreift und zum Zelltod führt. Darüber hinaus konnte eine Genotoxizität von CPI-613 ausgeschlossen werden. Eine Kombination aus CPI-613 und IT führte in Xenograft- und chemisch-induzierten KRK-Tumoren zu einer gesteigerten Wirksamkeit in Bezug auf die Hemmung des Tumorwachstums und der Überlebenszeit. Die Befunde in Zellkultur- und Maus-Modellen des KRKs identifizierten CPI-613 als vielversprechenden Therapiebaustein für die Behandlung des KRKs.

ABSTRACT

Colorectal Cancer (CRC) is one of the most commonly diagnosed cancer entities and incidences as well as mortalities are currently rising in adults younger than 50 years of age in Europe and the USA. While patients are often diagnosed at advanced stage, the 5-year-survival rate of these patients is detrimental. Therefore, novel therapeutic targets and drug candidates are urgently needed although standard chemotherapy using 5-fluorouracil (5-FU) or irinotecan (IT) next to the use of biologicals is available. The altered energy metabolism in cancer cells represents a hallmark of cancer and at the same time a potential drug target. The lipoate CPI-613 is a derivative of the naturally occurring α-lipoic acid (LA) and pioneers as a new class of agents due to its unique intervention into altered energy metabolism of cancer cells. It was shown to inhibit mitochondrial multi-enzyme complexes, such as pyruvate dehydrogenase and α-ketoglutarate dehydrogenase. This mode of action was primarily shown in cancerous cells.

The focus of this work was to investigate cellular responses upon the treatment of CRC cells with the lipoate CPI-613. Endpoints included mitochondrial integrity and function in oxidative phosphorylation next to cell death, DNA damage and autophagy. For this purpose, a panel of CRC cell lines and non-malignant transformed human colonic epithelial cells (HCEC) were used. Furthermore, the mode of action of CPI-613 in isolated murine mitochondria was assessed. Apart from that, the potential synergism of combination treatments using lipoates such as CPI-613 or its mother compound LA and standard chemotherapeutics in the treatment of CRC such as 5-FU or IT was elucidated. Upon identification of the most favourable combination *in vitro*, studies comparing the combination treatment with monotreatment using either CPI-613 or IT *in vivo* were conducted. For this purpose, xenograft models in immunodeficient mice (BALB/c nu/nu) as well as the azoxymethane (AOM)/dextran sodium sulphate (DSS)-model for the chemical induction of CRC tumours in C57BL/6 mice were used. Alongside, an assessment of possible haematotoxic side effects was performed.

At first, CPI-613 elicited a reduction in mitochondrial membrane potential as well as an increased formation of reactive oxygen species in both isolated mitochondria and CRC cell lines. These effects were accompanied by a decrease in cellular respiration and, in CRC cells, with a decline in mitochondrial number. While treatment with CPI-613 did not trigger a cell cycle arrest, cell death could be detected in a panel of CRC cell lines. This could be observed with the same potency among different cell lines independent of the p53- and MSS/MSI-status. In this context, several partially redundant types of cell death, such as apoptosis, necroptosis and caspase-independent cell death, were observed.

Furthermore, autophagy levels were increased as a consequence of treatment with CPI-613. Analysis regarding the genotoxic potential of CPI-613 did not reveal any DNA damage. Different combinations of lipoates and standard chemotherapeutics were characterised in respect of their synergism *in vitro*. Next to the synergistic action of CPI-613 in combination with IT in cell culture models of CRC, a positive effect could also be recorded in mouse models of CRC. Whereas CPI-613 alone reduced tumour growth in Cenograft models with prolonged survival and therapy benefit, this effect was enhanced in a combination regimen with IT. In chemically-induced tumours, however, IT in particular showed a therapeutic effect, which was also observed in combination with CPI-613. In this model, monotherapy with CPI-613 did not lead to a significant therapeutic success. The synergism *in vitro* and *in vivo* is mainly based on an increased cell death rate, the depletion of p53 and a reduction of the autophagy rate and not on increased DNA damage. Generally, a haematotoxic side effect profile of CPI-613 was not observed.

Concluding, this work demonstrated CPI-613 to attack altered energy metabolism in CRC and to cause cancer cell death. Importantly, a genotoxicity of CPI-613 could be excluded. A combination of CPI-613 and IT in xenograft and chemically-induced CRC tumours lead to an enhanced efficacy with respect to tumour growth reduction and overall survival. These findings in cell culture and mouse models of CRC present CPI-613 as a promising building block in CRC treatment.

TABLE OF CONTENTS

Erklärung IV

Zusammenfassung VII

Abstract IX

Table of Contents XI

List of Abbreviations XVI

List of Figures XIX

List of Tables XXI

1. Introduction 1

1.1. Colorectal Cancer 1

1.1.1 Aetiology, classification and staging of CRC 1

1.1.2 Treatment of CRC 4

1.1.2.1 Adjuvant chemotherapy 5

1.1.2.2 Common drugs in the treatment of CRC 8

1.1.2.2.1 Irinotecan 9

1.1.2.2.2 5-FU 11

1.2. Reprogrammed Energy Metabolism in Cancer 14

1.2.1. Altered energy metabolism as a hallmark of cancer 14

1.2.2. TCA cycle and its targetability in altered energy metabolism 17

1.2.2.1. Oncogene-mediated alterations of energy metabolism 20

1.2.2.2. Altered energy metabolism in CRC 22

1.2.3. PDH – composition and function 25

1.2.3.1. PDH in CRC 26

1.2.4. KGDH – composition and function 28

1.2.4.1. KGDH in CRC 29

1.3. Lipoates as Anti-Cancer Drugs 29

1.3.1. Lipoic acid 29

1.3.1.1. LA as mitochondrial mediator 30

1.3.1.2. Inherent properties and metabolism 30

1.3.1.3. Cytotoxicity of LA, cellular response and anti-tumour activity 31
1.3.2. CPI-613 33
1.3.2.1. Chemical Structure and Synthesis 33
1.3.2.2. Mode of Action 34
1.3.2.3. Cytotoxicity and Cellular Effects 36
1.3.2.4. Biotransformation and Pharmacokinetics 38
1.3.2.5. *In vivo* Studies 39
1.3.2.6. Clinical Trials 41
2. Objectives 46
3. Materials & Methods 48
3.1. Materials 48
3.1.1. Chemicals 48
3.1.2. Buffer and solutions 51
3.1.3. Kits 53
3.1.4. Consumables 53
3.1.5. Equipment 54
3.1.6. Software 55
3.2. Methods 55
3.2.1. Cell culture 55
3.2.1.1. Cell lines 56
3.2.1.2. Cultivation of cells 56
3.2.1.3. Treatment of cells 57
3.2.2. Protein isolation and analysis 57
3.2.2.1. Preparation of protein lysates using whole cell lysis 57
3.2.2.2. Protein analysis based on SDS-PAGE and Western Blotting 58
3.2.3. Cell viability assays based on cellular ATP content 59
3.2.3.1. Generation of arrested cells 60
3.2.4. Synergy assessment using CompuSyn and Combenefit 60
3.2.5. Flow-cytometric analysis 61

3.2.5.1. Flow-cytometric cell cycle distribution analysis 61
3.2.5.2. Flow-cytometric measurement of cell death using Annexin V/PI-staining 61
3.2.5.3. Flow-cytometric measurement of autophagy levels using CytoID® Green Detection Kit 62
3.2.5.4. Flow-cytometric quantification of reactive oxygen species 62
3.2.5.5. Flow-cytometric monitoring of mitochondrial membrane potential 62
3.2.6. Methods to assess DNA damage induction 63
3.2.6.1. Determination of DNA damage levels using InCellWestern assay 63
3.2.6.2. Assessment of genotoxicity via Alkaline Comet Assay 64
3.2.6.2.1. Modification using FPG 64
3.2.7. Immunofluorescence staining of intact mitochondria using MitoTracker™ Orange 64
3.2.8. Invasion and migration analysis 65
3.2.8.1. Assessment of migratory ability via wound healing assay 65
3.2.8.2. Assessment of invasive ability using CytoSelect™ Invasion Assay 65
3.2.9. Experiments using isolated mitochondria 66
3.2.9.1. Animals 66
3.2.9.2. Isolation of mitochondria 66
3.2.9.3. Generation of reactive oxygen species 66
3.2.9.4. Mitochondrial oxygen consumption 67
3.2.9.5. Mitochondrial membrane potential 67
3.2.10. Assessment of mitochondrial function using the Seahorse Cell Mito Stress Test Kit 67
3.2.11. Animal studies 67
3.2.11.1. Acute toxicity 68
3.2.11.2. Xenograft studies 68
3.2.11.2.1. Cell inoculation 68
3.2.11.2.2. Tumour volume determination 68
3.2.11.2.3. Tumour therapy and isolation 69

3.2.11.2.4. Western Blot analysis of xenograft tumours 69
3.2.11.2.5. Haematoxylin and eosin staining of cryosections 70
3.2.11.3. AOM/DSS model 70
3.2.11.3.1. Tumour induction 70
3.2.11.3.2. Colonoscopy 71
3.2.11.3.3. Tumour scoring 71
3.2.11.3.4. Tumour therapy 71
3.2.11.3.5. Tissue collection and conservation 72
3.2.11.3.6. Blood analysis 73
3.3. Statistical Analysis 73
4. Results 74
4.1. Disruption of Mitochondria and Their Function by CPI-613 74
4.1.1. Isolated mitochondria are impaired by CPI-613 74
4.1.2. Mitochondria in CRC cells lose function upon CPI-613 75
4.2. CPI-613 as a Promising Building Block in the Treatment of CRC 79
4.2.1. Cytotoxicity of CPI-613 displays uniform, dose- and time-dependent and tumour-selective character 79
4.2.2. CPI-613 induces cell death, which is not mediated by caspases 83
4.2.3. Autophagy is increased upon CPI-613 87
4.2.4. Genotoxicity testing of CPI-613 89
4.3. Synergism of Lipoates and Standard Chemotherapeutic Agents in the Treatment of CRC 92
4.3.1. Synergism modelling indicates beneficial combination effect 93
4.3.2. Cell death potentiates upon combination treatment 94
4.3.3. Beneficial combination effect is not related to DNA damage levels 96
4.3.4. Influence of autophagy levels on combination effect 99
4.4. Proof of Therapeutic Efficacy of CPI-613 in Combination Treatments *in vivo* 101
4.4.1. Xenograft mouse studies confirm synergism of CPI-613 with IT 101

4.4.2. Chemically-induced CRC can be efficiently treated with CPI-613 plus IT in mice 106

5. Discussion 112

5.1. The Mode of Action of CPI-613: Targeting Mitochondria and Disrupting Their Function in Energy Metabolism in CRC 112

5.2. CPI-613 Shows Benefits as a Potential Building Block in the Treatment of CRC 114

5.2.1. Cell death induction by CPI-613 in CRC cells 114

5.2.2. DNA damage is not induced upon CPI-613 120

5.2.3. CPI-613 treatment modulates autophagy 121

5.3. Synergism of CPI-613 With Standard Chemotherapeutics in the Treatment of CRC 123

5.3.1. Efficacy of standard chemotherapeutics is improved in combination with CPI-613 in cell culture models 124

5.3.2. Inhibition of tumour progression in murine xenograft and carcinogenesis models of CRC is pronounced in combination treatment of CPI-613 and IT 126

6. Conclusion and Perspectives 132

6.1. Conclusion 132

6.2. Perspective 134

6.2.1. Suggestion for future experiments 134

6.2.2. Preliminary Data: Effect of CPI-613 on Epithelial-To-Mesenchymal Transition 136

Acknowledgements 142

Curriculum Vitae 144

Publications 145

Conference attendances 146

References 147

ANNEX i

LIST OF ABBREVIATIONS

A

AIF	apoptosis-inducing factor
AKI	acute kidney injury
AML	acute myeloid leukaemia
AOM	azoxymethane
APC	adenomatous polyposis coli
APS	ammonium persulphate
ATP	adenosine triphosphate

B

BCKDC	branched-chain α-ketoacid dehydrogenase complex
BER	base excision repair
BRAF	*v-Raf murine sarcoma viral oncogene homolog B1*
BSA	bovine serum albumin
BW	body weight

C

Cad	Cadherin
CAF	cancer-associated fibroblasts
CAPOX	capecitabine + oxaliplatin
CCCP	carbonyl cyanide *m*-chlorophenyl hydrazone
CDT	*cytolethal distending toxin*
CES	carboxylesterase
CI	combination index
CIMP	CpC-island methylated phenotype
CIN	chromosomal instability
CRC	colorectal cancer
CSC	cancer stem cell
CTC	circulating tumour cell

D

D-2HG	D-2-hydroxyglutarate
D5W	5% dextrose in water
DCA	dichloroacetate
ddH_2O	deionised water
DDR	DNA damage response
DHFU	dihydrofluorourcail
DHLA	dihydrolipoic acid
DLD	dihydrolipoamide dehydrogenase
DLST	dihydrolipoamide S-succinyltransferase
DMSO	dimethyl sulphoxide
DNA	deoxyribonucleic acid
dNTP	deoxynucleotide
DPD	dihydropyrimidine dehydrogenase
DSS	dextran sodium sulphate
dTMP	thymidine monophosphate
DTT	dithiothreitol
dTTP	thymidine triphosphate
dUMP	deoxyuridine monophosphate
dUTP	deoxyuridine triphosphate

E

ECL	enhanced chemiluminescence
ECM	extracellular matrix
EDTA	ethylenediaminetetraacetic acid
EGFR	epidermal growth factor receptor
EGTA	ethylene glycol-bis(β-aminoethyl ether)-*N,N,N',N'*-tetra acetic acid
EMA	European Medicines Agency

EMT	epithelial-to-mesenchymal transition
EtOH	ethanol

F

FACS	fluorescence-activated cell sorting
FAP	familial adenomatous polyposis
FBS	foetal bovine serum
FCCP	carbonyl cyanide-*p*-trifluoromethoxy phenyl hydrazone
FCS	foetal calf serum
FDA	(US) Food and Drug Administration
FDG	fluorine-18 (18F) fluorodeoxyglucose
FH	fumarate hydratase
FOLFIRI	5-FU + folinic acid + IT
FOLFOX	5-FU + folinic acid + oxaliplatin
FOLFOXIRI	5-FU + folinic acid + oxaliplatin + IT
FP	fluoropyrimidine
FPG	formamidopyrimidine DNA glycosylase

G

GLS	glutaminase
GLUT	glucose transporter
GSH	glutathione

H

HSA	highest single agent
HE	haematoxylin and eosin
HEPES	4-(2-hydroxyethyl)-1-piperazineethanesulphonic acid
HIF	hypoxia-inducible factor
HK2	hexokinase 2
HRP	horseradish peroxidase

I

i.p.	intraperitoneal
IC_{50}	inhibitory concentration, 50%
ICW	InCellWestern
IDH	isocitrate dehydrogenase
IT	irinotecan

K

KGDH	α-ketoglutarate dehydrogenase complex
KRAS	*Kirsten rat sarcoma*

L

LA	α-lipoic acid
LDH	lactate dehydrogenase
LIR	LC3B interacting region

M

MCT	monocarboxylate transporter
MDS	myelodysplastic syndrome
MET	mesenchymal-to-epithelial transition
MMR	mismatch repair
MOPS	3-(*N*-morpholino)propane sulphonic acid
MSI/MSS	microsatellite instable/microsatellite stable
mtDNA	mitochondrial DNA
mt	mutant

N

NAC	*N*-acetyl cysteine
NEAA	non-essential amino acids

NER	nucleotide excision repair

O

O/N	over night
OCR	oxygen consumption rate
OGDH	αKG dehydrogenase
OXPHOS	oxidative phosphorylation

P

PARP	poly (ADP-ribose) polymerase
PBS	phosphate buffered saline
PDH	pyruvate dehydrogenase complex
PDK	pyruvate dehydrogenase kinase
PDP	pyruvate dehydrogenase phophatase
PDX	patient-derived xenograft
PEG	polyethylene glycol
Pen/Strep	Penicillin / Streptomycin
PET	positron emission tomography
PFA	paraformaldehyde
PFK1	phosphofructokinase 1
PI	propidium iodide
PKM	pyruvate kinase
PLT	platelet
PMSF	phenylmethylsulphonyl fluoride

R

RBC	red blood cell
RETIC	reticulocytes
RNA	ribonucleic acid
ROS	reactive oxygen species
Rot	Rotenone
rpm	rounds per minute
RT	room temperature

S

SCO	synthesis of cytochrome c oxidase
SDH	succinate dehydrogenase
SDS	sodium dodecyl sulphate
SDS-PAGE	sodium dodecyl sulphate polyacrylamide gel electrophoresis
SEM	standard error of the mean
SSM	subsarcolemmal mitochondria

T

tBOOH	*tert*-butyl hydroperoxide
TCA	tricarboxylic acid cycle
TEA	triethanolamine
TEMED	tetramethyl ethylenediamine
TET	ten-eleven translocation
TNM	tumour, node, metastasis
topo	topoisomerase
TP	thymidine phosphorylase
TPP	thiamine pyrophosphate
TS	thymidylate synthase

V

VEGF	vascular endothelial growth factor
VM	Valinomycin

W

WBC	white blood cell

wt	wildtype
XELOX	capecitabine + oxaliplatin
αKG	α-ketoglutarate
γH2AX	phosphorylated histone 2AX at Ser139
5-FU	5-fluorouracil

LIST OF FIGURES

Figure 1: Genetic alterations in the aetiology of CRC. 2

Figure 2: Flow chart of CRC therapy options. FP = fluoropyrimidine, Ox = Oxaliplatin, BSC = best standard of care. 6

Figure 3: Cellular uptake, metabolism and mode of action of IT. 10

Figure 4: Cellular uptake, metabolism and mode of action of 5-FU.....12

Figure 5: The hallmarks of cancer as postulated by Hannahan and Weinberg. 14

Figure 6: Altered energy metabolism in cancer cells centring the TCA cycle. 18

Figure 7: The PDH complex. 26

Figure 8: The KGDH complex. 28

Figure 9: Chemical structure of lipoic acid and dihydrolipoic acid. 30

Figure 10: Summary of physiological function and anticancer properties of LA. 32

Figure 11: Chemical structure and synthesis scheme of CPI-613.....33

Figure 12: Mitochondria-targeted mode of action of CPI-613.....35

Figure 13: (Human) Metabolism of CPI-613. 39

Figure 14: Scheme for generation of arrested cells. 60

Figure 15: General experimental set-up and injection scheme of xenograft mouse studies.....69

Figure 16: General experimental set-up and injection scheme of AOM/DSS model for chemically-induced CRC studies. 70

Figure 17: Scheme for preparation of Swiss Roll technique (A) and predefined sections (B). 72

Figure 18: CPI-613 disrupts mitochondria and their function. 75

Figure 19: CPI-613 causes ROS formation and loss of membrane potential in CRC cells. 76

Figure 20: Mitochondrial number decreases upon CPI-613. 77

Figure 21: CPI-613 impairs oxygen consumption rate (OCR) of CRC cells..... 78

Figure 22: p53- and proliferation-independent as well as tumour-selective cytotoxicity of CPI-613. 82

Figure 23: Induction of cell death and influence of CPI-613 on cell cycle distribution.. 84

Figure 24: CPI-613 induces various types of cell death. 85

Figure 25: CPI-613-triggered cell death is independent of caspase activity. 87

Figure 26: CPI-613 induces autophagy in CRC cells. 88

Figure 27: CPI-613 lacks genotoxicity. 90

Figure 28: CPI-613 does not induce DNA strand breaks. 91

Figure 29: CPI-613 induces insignificant ROS-damage. 92

Figure 30: CPI-613 synergises with standard chemotherapeutics. 94

Figure 31: Cell death is potentiated upon combination of lipoates and chemotherapeutics. 95

Figure 32: Influence of lipoates on genotoxicity of standard chemotherapeutics..... 98

Figure 33: Effect on cytostatic-triggered autophagy in combination regimen. 100

Figure 34: Antitumour activity of CPI-613 in comparison to IT in HCT116 xenograft model. 102

Figure 35: Antitumour activity of CPI-613 in comparison to IT in HT29 xenograft model. 104

Figure 36: Histological overview staining of xenograft tumours..... 105

Figure 37: Effects on p53, γH2AX and LC3B protein levels in tumour tissue obtained from xenograft studies. 106

Figure 38: Chemically-induced CRC in mice. 107

Figure 39: Therapeutic efficacy of CPI-613, IT and their combination in AOM/DSS-induced colorectal tumours. 109

Figure 40: Differential blood analysis of animals undergoing AOM/DSS model coupled with therapy. 110

Figure 41: Synergism model of CPI-613 in combination with standard chemotherapeutics in the treatment of CRC. 133

Figure 42: CPI-613 impairs migration and invasion of CRC cells. 138

Figure 43: CPI-613 leads to depletion of migration-regulating N-Cadherin. 140

Figure Annex- 1: Gating strategy of flow cytometry methods. ii

LIST OF TABLES

Table 1: Molecular classification of CRC. 3

Table 2: TNM staging system of CRC. 3

Table 3: Overview of authorised drugs used in CRC therapy (in Germany). 8

Table 4: Overview of anti-cancer drugs targeting altered energy metabolism in the TCA cycle. 19

Table 5: Overview of PDK isoforms and their function in CRC and its tumourigenesis. 27

Table 6: Overview of KGDH and its function in CRC and its tumourigenesis. 29

Table 7: Overview of clinical trials related to CPI-613. 42

Table 8: List of chemicals used. 48

Table 9: List of buffers and solutions and their composition. 51

Table 10: List of kits used. 53

Table 11: List of consumables used. 53

Table 12: List of equipment used. 54

Table 13: List of software used. 55

Table 14: Panel of screened cell lines including source, culturing conditions and genetic features. 56

Table 15: Composition of SDS-PAGE-gels. 58

Table 16: Primary antibodies used including their incubation conditions. 59

Table 17: Dehydration sequence for tissue. 72

Table 18: Cytotoxicity screening in a panel of colon (cancer) cell lines based on IC_{50} values. 81

Table 19: Summary of findings with respect to cell death induction upon CPI-613 in CRC cells. 119

Table Annex- 1: Overview of seeded cell densities for the different cell culture experiments. i

1. INTRODUCTION

1.1. Colorectal Cancer

Nowadays, colorectal cancer (CRC) displays a major burden for health care systems. Ranking 3rd in men and 2nd in women, CRC incidence has a rising trend globally with over 1.8 million newly diagnosed patients in 2018 with an alarming increased incidence in young adults over the last decades (Favoriti et al., 2016; Bray et al., 2018; Keum and Giovannucci, 2019; Vuik et al., 2019). With a mortality of more than 860,000 patients, CRC is the second most common cancer-related cause of death (Murphy et al., 2019). Next to genetic predisposition as in the Lynch or FAP (familial adenomatous polyposis) syndrome, people with CRC history in a first-degree relative or suffering from inflammatory bowel disease, e.g. Crohn's disease or ulcerative colitis, are at higher risk for developing CRC (Johnson et al., 2013). Environmental or life-style risk factors include obesity, physical inactivity, cigarette smoking, alcohol consumption, and Westernised diet characterised by high calory, fat-rich, fibre-deficient diet with low fruit and vegetable consumption but high intake of red and processed meat (Johnson et al., 2013; Marley and Nan, 2016; Murphy et al., 2019; Seiwert et al., 2020). Characteristically, CRC is a disease of the elderly with advanced age being one of the risk factors to develop CRC. More than 50% of patients are older than 70 years, while less than 10% of patients are younger than 55 years (Robert Koch-Institut, 2015).

1.1.1 Aetiology, classification and staging of CRC

In 1988, Bert Vogelstein described the multistep process of the adenoma-carcinoma-sequence for CRC tumourigenesis (Vogelstein et al., 1988). Due to mutations, dysplastic cells in the form of aberrant crypt foci arise from colonic epithelial cells, which upon accumulation form a benign adenomatous polyp. Malign carcinoma can arise from this point via further mutations in oncogenes or tumour suppressor genes. Next to the description by Vogelstein, the serrated pathway and the inflammatory pathway further depict the heterogenous aetiology of CRC (Keum and Giovannucci, 2019).

Generally, tumourigenesis is subdivided into initiation (spontaneous mutations or mutations upon exposure to carcinogens), promotion (clonal expansion of initiated cells due to increased cell proliferation and suppressed cell death) and progression (development of the preneoplastic lesions to an invasive cancer). Initiating events in CRC include loss-of-function mutations in tumour suppressor genes or gain-of-function mutations in oncogenes. In CRC, the most critical mutation in early development of

sporadic and FAP-associated CRC is the inactivation of *APC* (adenomatous polyposis coli), which results in accumulation of β-catenin and a dysregulation of the Wnt signalling (Markowitz and Bertagnolli, 2009). Additionally, defects of the DNA mismatch repair pathway and associated proteins (*MLH1*, *MSH2*, *MSH6*, *PMS2*) display a major factor for the development of hereditary and sporadic CRC, respectively (Gupta et al., 2018). Oncogenic mutations in the *RAS* gene (30% of CRC), predominantly in *KRAS* (85% of *RAS* mutations) expressed as *KRAS*-G12D and *KRAS*-G13D, lead to the enhanced promotion of CRC. Mutually exclusive, oncogenic mutation in the *RAF* gene (10% of CRC), predominantly in *BRAF* expressed as *BRAF*-V600E, is another CRC promotion factor (Vogelstein et al., 1988; Tran et al., 2011). In up to 75% of CRC, the tumour suppressor p53 is mutated at chromosome 17p with subsequent loss of this chromosome (Vogelstein et al., 1988; Nguyen and Duong, 2018). Apart from genetic mutations, epigenetic alterations play a role in the development and progression of CRC, e.g. the hypermethylation of CpG islands, which is referred to as the CIMP (CpG-island methylator phenotype) phenotype (Markowitz and Bertagnolli, 2009; Bogaert and Prenen, 2014). Figure 1 illustrates the genes and growth factors crucial for the tumourigenesis of CRC as summarised by Markowitz and Bertagnolli (2009).

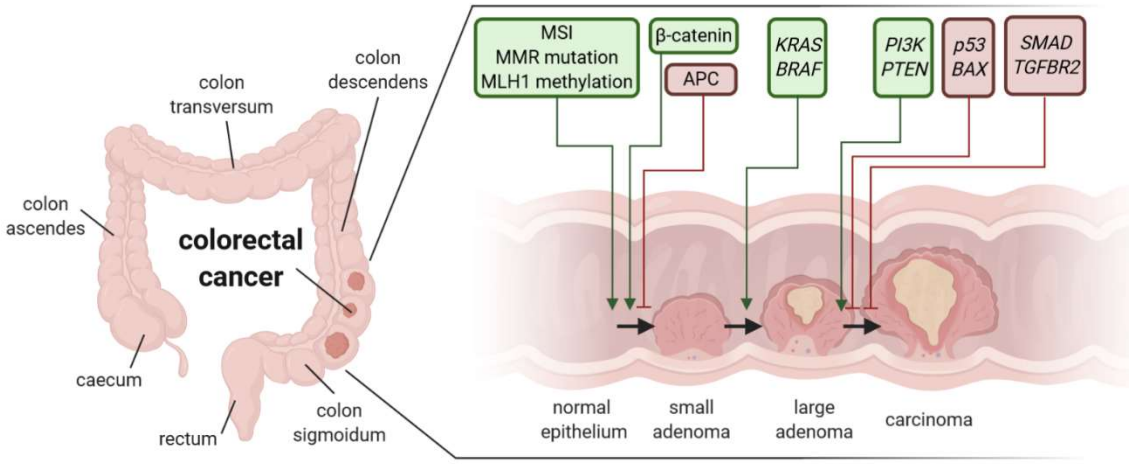

Figure 1: Genetic alterations in the aetiology of CRC.
Green colour indicates activation of oncogenic events while red colour describes inactivation of tumour suppressors. (according to Markowitz and Bertagnolli (2009), created with BioRender)

With respect to the molecular classification of CRC three pathways play a central role: the chromosomal instability (CIN) pathway, the mismatch repair (MMR) pathway and the serrated pathway (summarised in Table 1) (Jass, 2007; Cunningham et al., 2010; Armaghany et al., 2012; Müller et al., 2016). While 15% of sporadic tumours show a microsatellite instability (MSI) status associated with mutations in the MMR pathway (*MSH2*, *MLH1*, *MSH6*, *PSM2*), 85% of sporadic tumours show a CIN phenotype which is often linked to *p53* mutation (Cunningham et al., 2010; Müller et al., 2016; Gupta et

al., 2018). In approximately 5% of cases, CRC is hereditary, which is e.g. linked to the MMR deficiency-associated Lynch syndrome (Jasperson et al., 2010).

Table 1: Molecular classification of CRC.
Legend: + = present, - = absent, +/- = inconclusive, CIN = chromosomal instability, MMR = mismatch repair, MSS = microsatellite stability, MSI-H = high microsatellite instability, MSI-L = low microsatellite instability, CIMP = CpC-island methylated phenotype, *KRAS* = *Kirsten rat sarcoma*, *BRAF* = *v-Raf murine sarcoma viral oncogene homolog B1*, *MLH1* = *MutL homolog 1*. (adopted from Cunningham et al. (2010))

Pathway	***CIN***	***MMR***	***Serrated pathway***	
	hereditary / sporadic	hereditary	hereditary	sporadic
CIMP status	negative	negative	high	
MSI status	MSS	MSI-H	MSI-H	MSI-L
CIN	+	-	-	-
***KRAS* mutation**	+	+/-	-	-
***BRAF* mutation**	-	-	+	+
***MLH1* status**	normal	mutation	methylated	partial methylation

The standard for CRC staging is the tumour, node, metastasis (TNM) staging established by the International Union Against Cancer, which is summarised in Table 2. Since stage is the strongest predictor for survival and crucial for tailoring chemotherapy, an internationally recognised and accepted system is in place.

Table 2: TNM staging system of CRC.
(according to Sobin and Fleming (1997) and Compton and Greene (2004))

Stage	***Primary tumour (T)***	***Regional lymph nodes (N)***	***Distant metastasis (M)***
I	T1 or T2	N0	M0
IIA	T3	N0	M0
IIB	T4	N0	M0
IIIA	T1, T2	N1	M0
IIIB	T3, T4	N1	M0
IIIC	any	N2	M0
IV	any T	any N	M1
Legend	T1 = tumour invades the submucosa T2 = tumour invades the muscularis propria T3 = tumour invades through the muscularis propria into the subserosa or into the non-peritonealised pericolic or perirectal tissues T4 = tumour directly invades other organs or structures or perforates the visceral peritoneum	N0 = no regional lymph nodes metastasis N1 = metastasis in one to three lymph nodes N2 = metastasis in four or more lymph nodes	M0 = no distant metastasis M1 = distant metastasis

At the time of diagnosis, approximately 40% of patients developed early stage cancer (stage I and II), but about 20% of patients already have metastases at the time of diagnosis (van der Geest et al., 2015; Riihimäki et al., 2016). The most common site of metastasis are the liver (70%), the lung (32%) and the peritoneum (21%) for colon cancer (Riihimäki et al., 2016). In rectal cancer, bone metastases are found in 8% of patients (Riihimäki et al., 2016). In general, liver metastases are solitary in 48% of cases and linked to left-sided CRC, yet brain metastasis rarely occur alone and are most often found in sigmoidal and rectal CRC (Hammoud et al., 1996; Riihimäki et al., 2016; Engstrand et

al., 2018). In multi-metastases situations, liver metastases most frequently are accompanied by lung metastases followed by brain metastases, and these lung metastases in turn are accompanied by brain and bone metastases (Ko et al., 1999; Qiu et al., 2015; Riihimäki et al., 2016). Mean survival times are prognosed to be between 5.5 months (brain), 9 months (liver) and 10-11 months (lung, bone and multiple sites) in the context of metastatic spread of the primary tumour (Patanaphan and Salazar, 1993).

The overall 5-year-survival rate for CRC is approximately 62-63% among all CRC stages (Zacharakis et al., 2010; Joachim et al., 2019). However, in patients with stage III locally advanced CRC and stage IV metastatic CRC, the 5-year-survival rate is 71% and less than 10-14%, respectively (Zacharakis et al., 2010; Joachim et al., 2019). Markedly, the 5-year-survival rate for patients with unresectable metastasis drops below 5%. Median survival of stage IV CRC patients not receiving chemotherapy is as short as 5 months.

1.1.2 Treatment of CRC

Generally, standard protocols for the treatment of CRC as well as a golden standard are available. Hereafter, the treatment of patients according to German standards based on the S3 guideline is described (Leitlinienprogramm Onkologie, 2019).

For patients with CRC stage I, II and III, therapeutic intervention is regarded as curative. Furthermore, treatment of patients with CRC stage IV is not exclusively regarded as palliative, mostly depending on the intensity of metastasis spreading and resectability of metastases.

In cases of CRC stage I to III, therapy comprises of the complete surgical resection of the tumour, called hemicolectomy, including complete mesocolic excision or total mesorectal excision with at least 12 lymph nodes. Regarding patients with CRC stage II and III, surgery is followed by adjuvant chemotherapy tailored to CRC stage, age, comorbidities, risk factors and genetics. Most often, prerequisite for an adjuvant therapy is the resection of the primary tumour. In order to perform adjuvant therapy, patients must be motivated and in good general health condition. Contra-indications include bad general health condition, uncontrolled infection, liver cirrhosis, coronary heart disease, kidney insufficiency, impaired bone marrow function and other comorbidities. Moreover, age is not an exclusion criterion, while patients > 75 of age do not evidently have an advantage of receiving adjuvant chemotherapy.

1.1.2.1 Adjuvant chemotherapy

The following outlined therapy approaches are summarised as a flow chart in Figure 2 and routinely applied drugs with market authorisation in Table 3.

In patients with CRC stage I, any adjuvant chemotherapy is considered as of no additional value. With respect to patients with CRC stage II, adjuvant therapy can be performed and the decision is based on the MSS/MSI status of the tumour of whether or not adjuvant therapy is reasonable. As has been proven for microsatellite instability (MSI-H), response rates are significantly reduced in those patients and chemotherapy might be omitted due to this condition as a decision criterion. In about 20% of CRC stage II patients, however, MSI-H is genetically diagnosed. For MSS-tumour patients, a monotherapy with a fluoropyrimidine (FP; e.g. 5-fluorouracil (5-FU) or its prodrug capecitabine) is the first-choice drug. As general principle, FPs are supplemented with folinic acid in order to enhance therapy outcome. Basically, 5-FU and capecitabine are regarded as equally effective (Schmoll et al., 2018). 5-year-survival rates can be improved by 3-5% by application of a FP-based drug treatment as single agent. If this therapy approach fails, therapy approaches of stage III cancer patients apply.

Other than in stage II cancer patients, in stage III cancer patients, no biomarker is necessary in order to plead for adjuvant chemotherapy. Guiding factor for the first line therapy in these patients is primarily their age. While patients > 70 years and patients with poor general health condition do not receive oxaliplatin as an additional drug to FPs due to reduced tolerability, patients < 70 years shall receive combination regimen such as CAPOX/XELOX (capecitabine + oxaliplatin) or FOLFOX (5-FU + folinic acid + oxaliplatin). Duration of chemotherapy can be shortened from usually 6 to 3 months in patients with low risk of recurrence with the benefit of minimizing side effects and neurotoxicity. FP-based combination regimen are the golden standard in first line therapy (infusional FOLFIRI (5-FU + folinic acid + irinotecan (IT)), FOLFOX (5-FU + folinic acid + oxaliplatin), FOLFOXIRI (5-FU + folinic acid + oxaliplatin + IT) or oral CAPOX). In this context, FOLFOXIRI is the most effective therapy regimen (Souglakos et al., 2006; Falcone et al., 2007; Montagnani et al., 2011; Loupakis et al., 2014a; Cremolini et al., 2015b; Gruenberger et al., 2015).

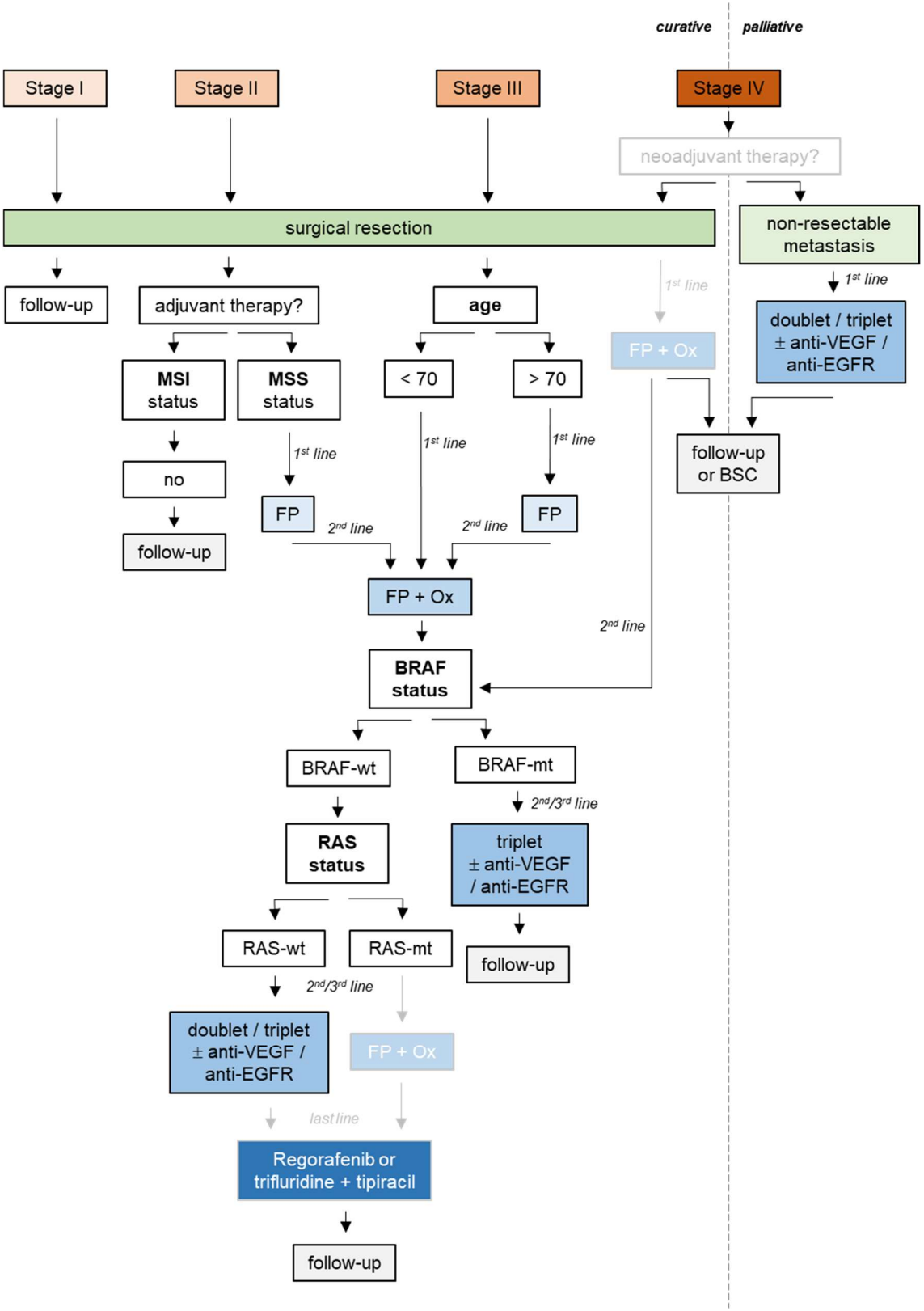

Figure 2: Flow chart of CRC therapy options.
FP = fluoropyrimidine, Ox = Oxaliplatin, BSC = best standard of care.

In cases when first line therapy failed, second and third line therapies are consulted for effectiveness. Approaches include the exchange of oxaliplatin with irinotecan (IT) and the inclusion of monoclonal antibodies against EGFR (epidermal growth factor receptor)

or a VEGF (vascular endothelial growth factor)-inhibitor (Cunningham et al., 1998; Rougier et al., 1998; Rothenberg et al., 2003). However, monoclonal antibodies or IT shall not be used as monotherapy in the treatment of CRC. If the first line of therapy shows no response, tumour genetics will guide the second line therapy. The RAS as well as the BRAF mutation status must then be determined prior to the start of the therapy. While BRAF-mt (mutant) tumours (present in 10 %) need to be treated with the most intense CRC therapy protocol currently available comprising of a triplet (i.e. FOLFIRINOX) plus either an anti-EGFR antibody or an anti-VEGF inhibitor (Tran et al., 2011; Tveit et al., 2012; Loupakis et al., 2014b; Cremolini et al., 2015a; Kopetz et al., 2015; Pietrantonio et al., 2015; Rowland et al., 2015), the genetic RAS status triggers different adjuvant therapy regimen. In all-RAS-wt (wild-type) tumour patients, patients with high risk of recurrence or patients with tumour localisation to the left hemicolon, either a doublet (e.g. FOLFOX, FOLFIRI) or a triplet cytostatic regimen either with or without an anti-EGFR antibody or an anti-VEGF inhibitor is applied (Tveit et al., 2012; Heinemann et al., 2014; Bokemeyer et al., 2015; van Cutsem et al., 2015). With respect to anti-VEGF inhibitors, Bevacizumab or Ramucirumab and Aflibercept are applicable (van Cutsem et al., 2012; Tabernero et al., 2015). As anti-EGFR antibodies, Cetuximab and Panitumumab are authorised (Sobrero et al., 2008; Peeters et al., 2010). Contrary, anti-EGFR and anti-VEGF drugs shall not be combined (Hecht et al., 2009; Tol et al., 2009; Saltz et al., 2012). It needs to be kept in mind, that an anti-EGFR therapy is less effective in cases where an anti-VEGF therapy has already been performed (Derangère et al., 2016). For RAS-mt tumours, therapy with an anti-EGFR antibody is proven to be ineffective (Peeters et al., 2010; Bokemeyer et al., 2015; van Cutsem et al., 2015) and a doublet or triplet therapy shall be applied (Saltz et al., 2012; Kubicka et al., 2013; Cremolini et al., 2015b).

As last line therapy, the multikinase inhibitor Regorafenib or the combination preparation of trifluridine + tipiracil (TAS102), acting synergistically as thymidine analogue and thymidine phosphorylase inhibitor, are nowadays in practice (Yoshino et al., 2012; Grothey et al., 2013; Li et al., 2015a; Mayer et al., 2015). Experimental medication embraces the addition of Vemurafenib in patients with BRAF mutation, the usage of Pembrolizumab or Nivolumab with or without Ipilimumab in patients with MSI or either Trastuzumab or Lapatinib in HER2-positivity as last resource (Sartore-Bianchi et al., 2016). Nivolumab and Pembrolizumab are both approved by the US-American Food and Drug Administration for the treatment of MSI-H/MMR-deficient CRC and represent immune checkpoint inhibitors that bind to the PD (programmed cell death protein)-1 receptor on T cells of the immune system (Almquist et al., 2020; Golshani and Zhang,

2020). Upon blocking the receptor, the immune system is stimulated because the interaction with the PD-1-ligand is halted. This is followed by an indirect antitumoural activity.

The most challenging therapy decision is required for patients with CRC stage IV, naturally bearing one or several metastasis sites. The strategy for patients bearing CRC stage IV depends on the resectability of the primary tumour and the extend and degree of metastasis spread and location. In some patients with direct resectability, down-sizing prior to surgery is nonetheless recommended, which normally is achieved using neoadjuvant therapy via FP and oxaliplatin (FOLFOX for 3 months). Once/if surgical resection of metastases and primary tumour are feasible, more intense regimen (doublet/triplet ± anti-EGFR/anti-VEGF) can be performed. However, for non-resectable metastases, the first line therapy comprises of doublet/triplet ± anti-EGFR/anti-VEGF for patients in good general health condition, but in palliative situations the application of the best standard of care is recommended.

1.1.2.2 Common drugs in the treatment of CRC

As outlines beforehand, a variety of drugs are authorised in the treatment of CRC in Germany. In total and as summarised in Table 3, four classes of agents can be applied: cytostatics, anti-EGFR antibodies, anti-VEGF inhibitors and multikinase inhibitors.

Next to the anti-EGFR antibodies Cetuximab and Panitumumab, the VEGF inhibitors Bevacizumab, Ramucirumab and Aflibercept and the multikinase inhibitor Regorafenib are regarded as targeted therapy components. These agents are commonly added to doublet or triplet combination regimen of cytostatics, such as 5-FU/capecitabine, IT or oxaliplatin. Of which 5-FU as FP, as first-choice drug, and IT, as key drug in advanced and metastatic CRC, are detailed in the sections to follow.

Table 3: Overview of authorised drugs used in CRC therapy (in Germany).

Class	*Name*	*Mode of Action*	*Recommendation*	*Single Agent*	*Possible Combination Regimen*
Cytostatic	5-fluorouracil	anti-metabolite (pyrimidine), thymidylate synthase inhibition	1st line therapy (first choice)	yes	FOLFOX, FOLFIRI FOLFIRINOX, ± anti-EGFR/VEGF
	Capecitabine	(oral) prodrug of 5-flurouracil	1st line therapy	yes	CAPOX / XELOX
	Trifluridine + Tipiracil	thymidine analogue / thymidine phosphorylase inhibitor	last line therapy	yes	-
	Irinotecan	topoisomerase I inhibitor	2nd line therapy (only in combination)	no	FOLFIRI, FOLFIRINOX ± anti-EGFR/VEGF
	Oxaliplatin	DNA cross-linker	1st line therapy (only in combination)	no	CAPOX / XELOX;

Class	*Name*	*Mode of Action*	*Recommendation*	*Single Agent*	*Possible Combination Regimen*
					FOLFOX, FOLFIRINOX ± anti-EGFR/VEGF
	Folinic acid	thymidylate synthase inhibition	acts in synergism with fluoropyrimidines	no	in combination with fluoropyrimidines
Anti-EGFR antibody	Cetuximab Panitumumab	monoclonal antibody against EGFR	metastatic CRC 2nd line therapy only in all-RAS-wt left-sided tumours	no	FOLFOX, FOLFIRI, FOLFIRINOX
Anti-VEGF antibody/ inhibitor	Bevacizumab Ramucirumab Aflibercept	anti-VEGF antibody/inhibitor of circulating VEGF	metastatic CRC 2nd line therapy	no	FOLFOX, FOLFIRI, FOLFIRINOX
Multikinase inhibitor	Regorafenib	inhibition of VEGFR, TIE2, KIT, RET, RAF-1, BRAF, BRAF-V600E, PDGFR, FGFR	last line therapy	yes	-

1.1.2.2.1 Irinotecan

Derived from the alkaloid camptothecin, irinotecan (7-ethyl-10-[4-(1-piperidino)-1-piperidino]carbonyloxy-camptothecin/CPT-11; IT) belongs to the class of topoisomerase I inhibitors. Camptothecin, originally isolated from the Chinese tree *Camptotheca acuminata*, exclusively targets topoisomerase I (topo I) and binds, and thus blocks, the covalent DNA and topo I complex via reversible hydrogen networks of the lactone moiety of the E-ring with Asp533 and Arg364 (Staker et al., 2002). Furthermore, the lactam moiety of the D-ring interacts with the N3 position of a cytosine base at the +1 position on the DNA strand (Staker et al., 2002). As a result, DNA breaks are preferentially formed at guanine +1 sites on the scissile strand (Staker et al., 2002). The stabilization of the DNA-topo I-complex abrogates the re-ligation of the DNA upon its unwinding, resulting in an accumulation of the cleavable complex and in both single as well as double strand breaks (Liu et al., 2000). Requiring proliferation and more particularly S-phase progression to exhibit its toxicity, not only DNA strand breaks but also replication stress due to stalked replication forks at sites of the DNA-topo I-complex are detrimental cellular effects. These effects possibly culminate in the activation of the DNA damage response (DDR), and cell cycle arrest as well as (programmed) cell death, e.g. the intrinsic apoptotic pathway, and also interfere with the RNA synthesis at transcription elongation causing premature termination (Bendixen et al., 1990; Ohdo et al., 1997; Haug et al., 2008; Kaku et al., 2015).

Since the late 1990s, IT, which consists of a pentacyclic ring structure containing a pyrrole quinolone moiety, is used in the treatment of solid tumours, e.g. colorectal, pancreatic and lung cancer. IT is used as a second line therapy in advanced/metastatic CRC (stage IV) after failure of first line chemotherapy with 5-FU and oxaliplatin and in the first line therapy for metastatic CRC. Its inclusion in therapy regimen prolongs the 1-

year, progression- and pain-free as well as overall survival and improves quality of life based on several phase II and III clinical trial (Fujita et al., 2015). Regimen used always include a doublet or triplet treatment with FPs with optional oxaliplatin combination and either anti-EGFR antibody or Bevacizumab. While IT is standardly given as an i.v. infusion in the clinic, oral and liposomal formulations are also available. In order to enhance local exposure in the situation of liver metastases, IT drug-eluting beads (DEBIRI) have been developed (Iyer and Ratain, 1998), which are administered into the hepatic artery. Most common and dose-limiting toxicities include early- and late-onset of diarrhoea (16-31%) and neutropenia (Man et al., 2018).

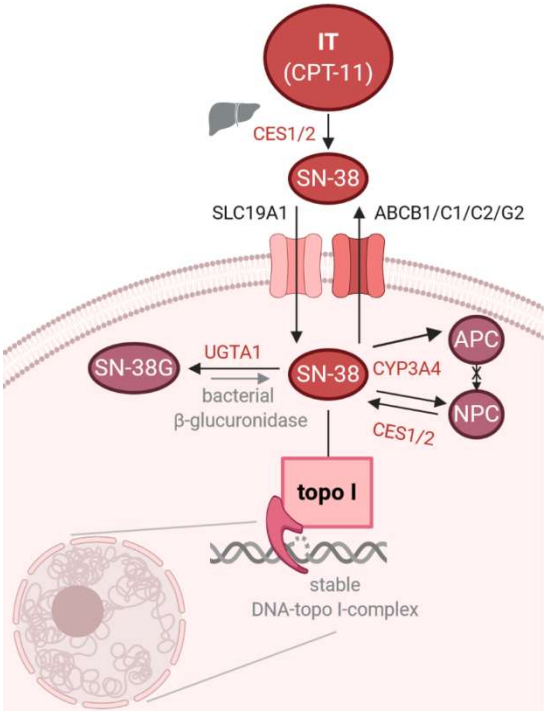

Figure 3: Cellular uptake, metabolism and mode of action of IT.
(created with BioRender)

Given as a prodrug, IT is hydrolysed by carboxylesterases (CES), especially CES2 followed by CES1, but also by butyrylcholinesterase in the liver and plasma to SN-38, its active metabolite as visualised in Figure 3 (Mathijssen et al., 2001). While only 2-3% are converted, SN-38 displays a 100- to 1000-fold higher activity (Mathijssen et al., 2001). SN-38 is inactivated by a variety of phase I and II enzymes, most importantly by oxidation via CYP3A4 to NPC and CYP3A5 to APC and glucuronidation via UGT1A1 to SN-38G (Mathijssen et al., 2001). SN-38G is subject to enterohepatic circulation upon intestinal deglucuronidation by bacterial β-glucuronidases (Iyer and Ratain, 1998). Late-onset diarrhoea as a side effect of IT is explained by the bacterial β-glucuronidase enzymatic regeneration of the active SN-38 metabolite from biliary excreted SN-38G (Collins and

Patterson, 2020). It was shown that inhibition of bacterial β-glucuronidase reduces the incidence of drug-related late diarrhoea (Wallace et al., 2010).

The involvement of these enzymes leads to susceptibility to genetic as well as environmental influences that mediate efficacy and toxicity (Iyer et al., 1998). The large interindividual pharmacokinetic variability primarily relies on the occurrence of the UGT1A1*28 polymorphism, which is found in 26-39% of the Caucasian population and is characterised by a 70% reduction of enzyme activity (Beutler et al., 1998; Hall et al., 1999). Homozygous patients exhibit higher systemic exposure of IT and SN-38 and higher rates of neutropenia irrespective of IT doses and increased risk for diarrhoea at doses above 125 mg/m², while response rates are unaffected (Hoskins et al., 2007). Based on this pharmacogenetics, genotype-adjusted dosing would be reasonable. Determination of UGT1A1 is not mandatory yet recommended prior to chemotherapy regimen including IT, but has been implemented in the guideline in particular for patients with known polymorphisms such as Gilbert's syndrome (Liu et al., 2014). As an example, the European Medicines Agency (EMA) recommends the reduction of liposomal IT from 80 to 60 mg/m² as starting dose (Man et al., 2018). Peak plasma concentrations range between 1 to 10 mg/L following an i.v. injection of 100-350 mg/m² which represents typical clinical doses (Chabot, 1997).

1.1.2.2.2 5-FU

Invented in the 1950s, FPs are widely used in the treatment of cancer taking advantage of the high demand on uracil in tumour cells. The most famous and efficient representatives of FPs are 5-FU, given infusionally, and its prodrug capecitabine, given orally. Whilst being the first-choice drug, 5-FU is given either as a monotherapy in early stage CRC or in combination with other cytostatics and in some cases together with anti-EGFR antibodies or anti-VEGF inhibitors in advanced or metastatic CRC as described in detail in section 1.1.2.1. Furthermore, 5-FU is a building block of many therapy regimen for other solid tumours, e.g. pancreatic, breast, stomach, cervical or oesophageal cancer.

The mode of action and cytotoxicity of 5-FU comprises of two mayor pathways: first, the inhibition of the thymidylate synthase (TS) and second, its pyrimidine analogy in order to act as an antimetabolite as depicted in Figure 4 (Longley et al., 2003).

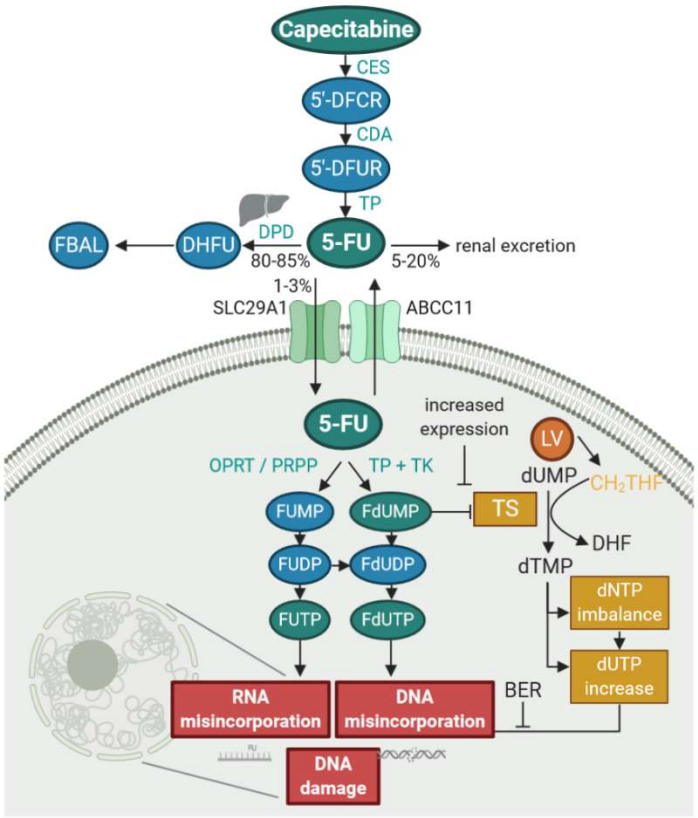

Figure 4: Cellular uptake, metabolism and mode of action of 5-FU.
(created with BioRender)

By inhibition of the TS, the pyrimidine nucleoside thymidine, required for DNA replication and repair, is no longer synthesised. Under normal conditions, deoxyuridine monophosphate (dUMP) is methylated by the catalytic activity of TS to yield thymidine monophosphate (dTMP). As a methyl-donor, 5,10-methylenetetrahydrofolat (CH_2THF) is used. CH_2THF and FdUMP bind to the nucleotide binding position of TS and competitively inhibit the binding of dUMP by forming a stable ternary complex. Consequently, 5-FU treatment leads to a depletion of the intracellular dTMP pool, followed by death due to thymine starvation in fast proliferating cells. In here, the imbalance of the deoxynucleotide (dNTP) pool in favour of the deoxyuridine triphosphate (dUTP) based on the starvation for thymidine triphosphate (dTTP) results in disrupted DNA synthesis and repair as well as severe DNA damage. In order to enhance the effect of 5-FU, adjuvant folinic acid (calcium folinate/leucovorin (LV)/5′-formyltetrahydrofolate) is given simultaneously, mimicking endogenous CH_2THF. Folinic acid stabilises the TS-5-FU-complex and thus enhances its cytotoxic effect (Danenberg et al., 2016).

Being a derivative of uracil, the tautomeric structure of 5-FU includes a Fluor atom at position C5. Acting as a pyrimidine antimetabolite and targeting enhanced DNA and RNA synthesis in cancer cells, 5-FU, in its metabolic and genotoxic form FUTP or FdUTP, is misincorporated as either thymidine (and cytosine) into the DNA or uracil (and cytosine)

into RNA. Once incorporated into DNA, miscoding RNA is transcribed, and essential protein biosynthesis blocked or DNA damage is introduced. To counteract the induced DNA damage, base excision repair involving uracil-DNA-glycosylases (UDG) named UNG2, SMUG1, TDG and MBD4 are activated (Kunz et al., 2009; Pettersen et al., 2011). However, in the presence of high (F)dUTP and dTTP, additional false nucleotides are incorporated due to concomitant inhibition of TS and futile cycling by BER, culminating in mismatches and DNA strand breaks and finally cell death (Wyatt and Wilson, 2009). Hence next to BER, also the mismatch repair pathway is induced upon 5-FU treatment (Fischer et al., 2007). Due to its mode of action, the cytotoxicity of 5-FU is cell cycle dependent and mostly limited to the interphase. With respect to RNA misincorporation, 5-FU is able to inhibit rRNA processing, post-transcriptional modification of tRNA, splicing and polyadenylation of mRNA as well as assembly of snRNA with proteins (Santi et al., 1974; Randerath et al., 1983; Kanamaru et al., 1986; Doong and Dolnick, 1988; Patton, 1993; Ghoshal and Jacob, 1994). Thus, 5-FU interferes with RNA at several levels resulting in an imbalance of cellular activities, which is regarded to be to most crucial mode of action (Pettersen et al., 2011).

Upon cellular uptake via the uracil transporter, 5-FU is deaminated (Wohlhueter et al., 1980). Approximately 80% of FPs, such as 5-FU, are metabolised and detoxified via dihydropyrimidine dehydrogenase (DPD) to dihydrofluorourcail (DHFU) in the liver (Diasio and Harris, 1989). Patients carrying a DPYD*2A variation heterozygously as well as homozygously are at risk of severe and fatal drug toxicities once treated with FPs (e.g. neurotoxicity and myelosuppression). An estimated 0.2% of the population have complete DPD deficiency (Deenen et al., 2016). However, the S3 guideline does not state DPD determination as mandatory prior to FP-based therapy treatment (Meulendijks et al., 2015). Circumventing DPD-related inactivation of 5-FU, capecitabine as its orally available prodrug undergoes metabolic change upon uptake to 5'DFUR by sequential carboxylesterase and cytidine deaminase and conversion to 5-FU by thymidine phosphorylase (TP). Advantageously, it was proven that TP is more active in cancer cells, displaying a tumour-selective cytotoxicity of capecitabine. Capecitabine, nevertheless, was shown to be as effective as 5-FU but inherits a more favourable side effect profile and a good oral bioavailability. Common side effects of 5-FU include diarrhoea, mucositis, and myelosuppression in the form of neutropenia and thrombocytopenia. A major concern represents 5-FU-induced mucositis of the entire gastrointestinal tract. In this context, the gut microbiota may play a crucial role (Gori et al., 2019). An imbalanced microbiome following 5-FU treatment is assumed to result in intestinal mucositis, bacteraemia and sepsis (Hamouda et al., 2017). While antibiotics

diminish the antitumour efficacy of 5-FU in mice, probiotics did have no effect on 5-FU efficacy (Yuan et al., 2018).

1.2. Reprogrammed Energy Metabolism in Cancer

Two decades ago, Hanahan and Weinberg (2000) postulated the six hallmarks of cancer (Figure 5). As acquired capabilities, self-sufficiency in cell growth next to insensitivity to antigrowth signals, evading apoptosis, limitless replicative potential, sustained angiogenesis as well as tissue invasion and metastasis were named. A decade later, they updated the postulated hallmarks in order to include four novel features (Hanahan and Weinberg, 2011).

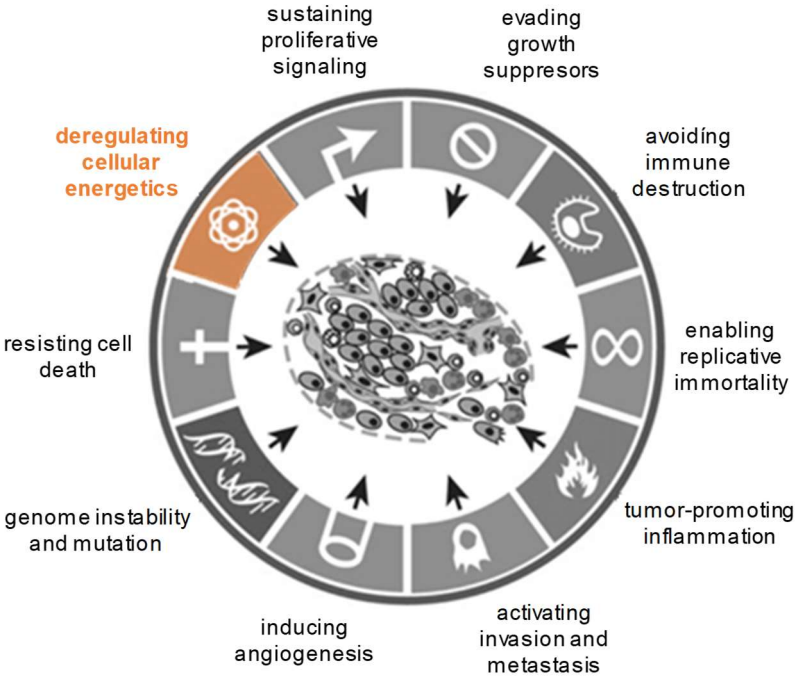

Figure 5: The hallmarks of cancer as postulated by Hannahan and Weinberg.
(modified to Hanahan and Weinberg (2000) and Hanahan and Weinberg (2011))

As next-generation hallmarks, reprogramming energy metabolism and avoiding immune destruction were added, whereas enabling characteristics included genome instability and mutation alongside tumour-promoting inflammation. Furthermore, the tumour microenvironment and its relevance for tumourigenesis were pronounced.

1.2.1. Altered energy metabolism as a hallmark of cancer

Focussing on the reprogrammed energy metabolism as a hallmark of cancer, the alteration of energy metabolism is required in order to fuel enhanced cell growth and division inherent in tumour cells, also associated with an increased need for energy

production and biosynthetic macromolecule synthesis. Going more into detail, six sub-hallmarks can be identified: I) dysregulation of glucose and amino acid (i.e. glutamine) uptake, II) usage of inconvenient sources of energy, III) need for intermediates provided by glycolysis or the TCA cycle to feed biosynthetic pathways, IV) increased demand of nitrogen, V) oncogene- and tumour suppressor-mediated alterations of the metabolic program and VI) metabolic interaction with the tumour microenvironment (Pavlova and Thompson, 2016). These changes in energy metabolism are, most importantly, of reversible nature and adjust during progression showing stage-specific metabolic traits (Valcarcel-Jimenez et al., 2017).

I) Dysregulation of Glucose and Amino Acid Uptake: under aerobic conditions, glucose is processed in the cytoplasm to pyruvate using glycolysis and is then introduced into the mitochondrial TCA cycle under oxygen-consuming conditions. However, in anaerobic conditions present primarily in cancerous cells, a shift favouring glycolysis is notable and little pyruvate is directed to oxygen-consuming mitochondria. This effect was also observed in oxygen-rich or normoxic cancerous cells and is termed “aerobic glycolysis/Warburg effect”, which was first described by Otto Warburg in the 1920s (Warburg et al., 1927). Though, the 18-times reduced efficiency of glycolysis to produce ATP in comparison to oxidative phosphorylation (OXPHOS) appears to be inefficient for cancer cells. A switch to glycolysis yet provides plenty of glycolytic intermediates required for diverse biosynthesis pathways, e.g. amino acids, fatty acids and nucleosides, and a timely supply of these intermediates (DeBerardinis et al., 2008; Reid, 2020). Counteracting the inefficiency, cancer cells upregulate glucose uptake by expression of transporters, e.g. GLUT1 (DeBerardinis et al., 2008; Hsu and Sabatini, 2008; Jones and Thompson, 2009). Prognostic positron emission tomography (PET) of the tracer fluorine-18 (^{18}F) fluorodeoxyglucose (FDG) is used in oncology to visualise tumourous sites and exploits the increase in glucose uptake. Next to enhanced glycolysis, tumours specifically rely on glutaminolysis as well in order to fuel the TCA cycle. Details are described in section 1.2.2.

II) Usage of Inconvenient Sources of Energy: Other adaptions to the altered need of energy and biosynthetic building blocks include alternative sources such as lactate, acetate, ketone bodies, fatty acids, ammonia and exogenous proteins (Sun et al., 2018).

III) Need for Intermediates Provided by Glycolysis or the TCA Cycle to Feed Biosynthetic Pathways: Cancer cells show an increase in lipid metabolism, fatty acid synthesis, amino acid synthesis and nucleotide synthesis (Pavlova and Thompson,

2016). To fuel these catabolic processes, a variety of intermediates are diverted from glycolysis and the TCA cycle. Details are described in section 1.2.2 and Figure 6.

IV) Increased Demand of Nitrogen: Although glucose is the primary source for energy production, glutamine follows second in the hierarchy (Vazquez et al., 2016). Glutamine does not only provide a source of carbon but also for nitrogen, which is readily used for amino acid and nucleotide synthesis (Romero-Garcia et al., 2011; Vazquez et al., 2016). Furthermore, ammonia and exogenous proteins containing nitrogen and recycling of these during autophagy is observed in cancer cells.

V) Oncogene- and Tumour Suppressor-Mediated Alterations of the Metabolic Program: The altered energy metabolism of tumours is not simply a passively acquired survival benefit, but the result of a plethora of alterations mediated by tumour suppressors and oncogenes. Details are described in section 1.2.2.1.

VI) Metabolic Interaction with the Tumour Microenvironment: A key observation is the formation of two distinct but symbiotic subpopulations (Semenza, 2008; Feron, 2009; Kennedy and Dewhirst, 2010). One of which is hypoxic, hence glucose-dependent and secreting lactate as waste via monocarboxylate transporters (MCTs) (Vazquez et al., 2016). Whereas the other subpopulation is highly dependent on lactate as fuel for their enhanced reliance on the TCA cycle. Cancer-associated fibroblasts (CAFs) form the tumour environment by the secretion of growth factors, cytokines and paracrine interactions (Avagliano et al., 2018). They acquire a catabolic phenotype and their activation helps cancer growth, progression, metastasis and evasion from therapy (Avagliano et al., 2018). While tumour cells rely on glycolysis, their surrounding environment compensates the requirement of crucial intermediates for bioenergetic synthesis pathways. Therefore, CAFs are more of a glycolytic phenotype and prone to a glycolytic switch, while the core of cancer cells depends on OXPHOS (Avagliano et al., 2018). Solid tumours are, therefore, metabolically heterogenous, partly based on their oxygenation status (Martinez-Outschoorn et al., 2014). This phenomenon, termed “reverse Warburg effect” describes the coupling of anabolic cancer cells with catabolic CAFs as a metabolic network (Avagliano et al., 2018). In this reciprocal interaction, energy and biomass are transferred from catabolic CAFs to anabolic cancer cells in order to fuel their growth. This compartmentalisation and heterogenicity is found in a variety of tumours, including CRC (Martinez-Outschoorn et al., 2014). Furthermore, a metabolic network is formed with surrounding immune cells, which among others uses metabolites as signalling molecules (Neitzel et al., 2020).

Mitochondria have a plethora of crucial roles within the cellular organisation: energy production, regulation of programmed apoptotic cell death, regulation of signal transduction pathways through ROS production, modulation of cytosolic calcium levels and trafficking of small metabolites and providing of intermediates for biosynthetic pathways. For a long time, mitochondria have been overlooked regarding their role in tumourigenesis and tumour progression (Anderson et al., 2018c; Dong and Neuzil, 2019). The assumption that mitochondrial dysfunction is a fundamental characteristic of tumourigenesis has largely been proven erroneous, with little exemptions. While mitochondria mediate ROS signalling via H_2O_2 and are able to regulate and induce the intrinsic apoptotic pathway via the release of cytochrome c as initiating event, mitochondrial well-functioning is central to many types of tumours.

Mitochondrial impairment resulting in a reduction of biogenesis greatly suppresses tumour formation, progression and metastasis. Thus, for cancers, enhancement of mitochondrial biogenesis is advantageous and essential (Tarrado-Castellarnau et al., 2016). A repression of mitochondrial metabolism enzymes, such as isocitrate dehydrogenase 1/2 (IDH), fumarate hydratase (FH), and succinate dehydrogenase (SDH), and genes as well as mitochondrial antioxidant pathways is associated with poor clinical outcome and linked to epithelial-to-mesenchymal transition (EMT), dissemination and metastasis as well as poor clinical outcome (Valcarcel-Jimenez et al., 2017). Contrary, increased OXPHOS is inherent in circulating tumour cells (CTCs) (Valcarcel-Jimenez et al., 2017). Autophagy as a fundamental catabolic process in tumour transformation is regarded supplementary to altered energy metabolism (Martinez-Outschoorn et al., 2014). In parallel and in interconnected pathways, autophagy and altered energy metabolism tackle oxygen and nutrient deprivation, oxidative stress, fast growth and cell death suppression (Lozy and Karantza, 2012). The role of autophagy in cancer, nevertheless, is context-dependent. To acquire therapy resistance, activated mitochondrial function and an increase in antioxidant molecules are necessary (Valcarcel-Jimenez et al., 2017). Thus, drug-resistant cancer cells are characterised by increased mitochondrial mass together with OXPHOS activity and antioxidant capacity next to autophagy (Avagliano et al., 2018).

1.2.2. TCA cycle and its targetability in altered energy metabolism

Most substantially, altered energy metabolism goes way beyond the Warburg effect. Contrary to Warburg's hypothesis, OXPHOS remains functional in most cancer cells (Avagliano et al., 2018). While the TCA cycle is mostly known for its sourcing of energy,

it also supplies biosynthetic and redox balance needs via its sequence of biochemical reactions located in the mitochondrial matrix (Anderson et al., 2018b).

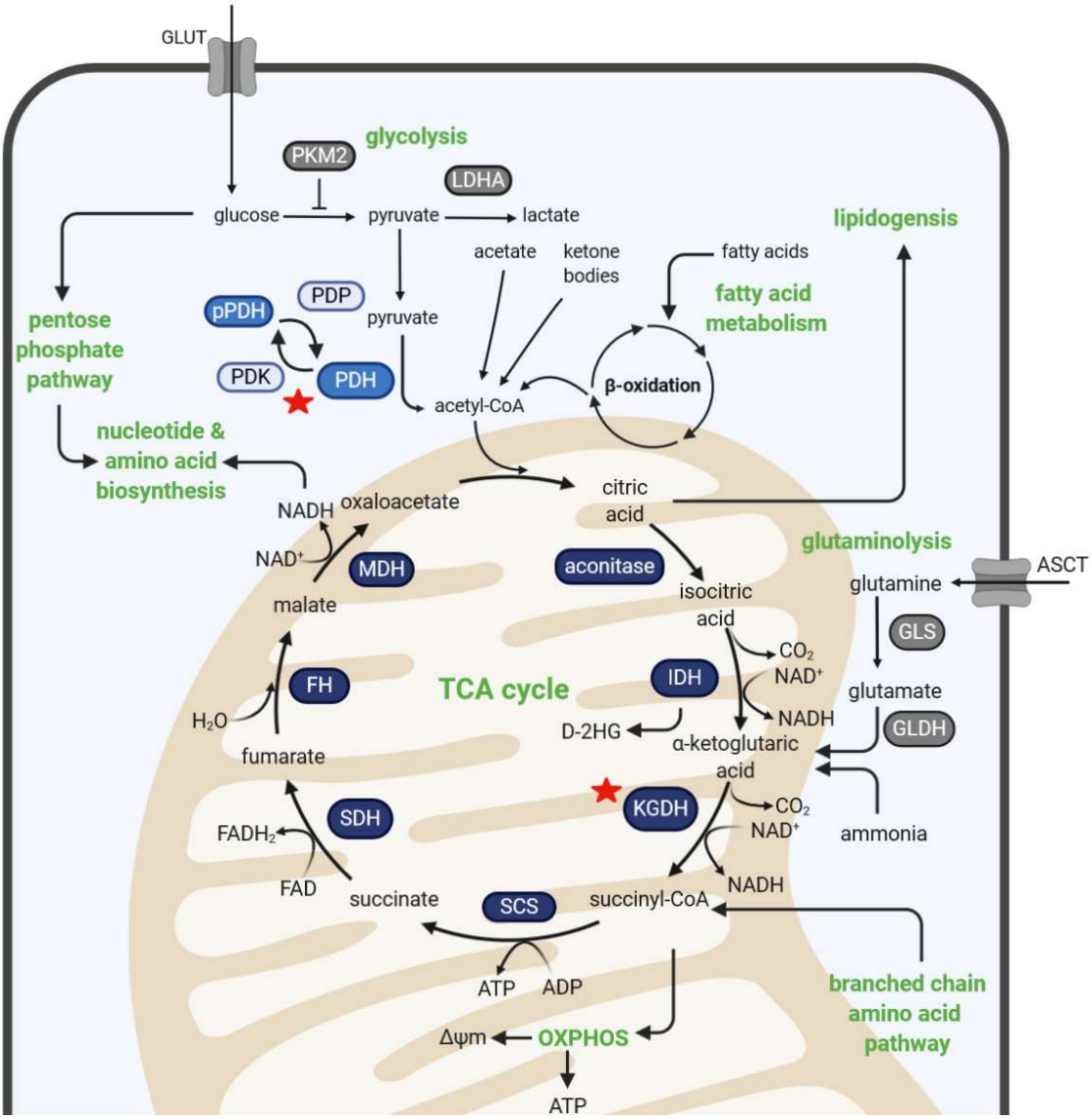

Figure 6: Altered energy metabolism in cancer cells centring the TCA cycle.
Focussing on the TCA cycle, its central role and diverse interaction with anaplerotic pathways is visualised. Crucial enzymes for this thesis are marked with a red star. (modified to Neitzel et al. (2020), created using BioRender)

The TCA cycles merges several metabolic pathways within the cellular respiration powered by three central fuels, namely glucose, glutamine and fatty acids. Not only is energy produced, but a variety of intermediates for macromolecule synthesis are generated. Regarding glucose in glycolysis, glucose yields pyruvate molecules, which upon oxidative decarboxylation are feed into the TCA cycle as acetyl-CoA. Although the Warburg effect postulates cancer cells to shunt pyruvate derived from glucose away from the TCA cycle, cancer cells nevertheless rely on the TCA cycle introducing anaplerotic carbons mainly via amino acids such as glutamine and fatty acids in order to cope with an enhanced energetic need (Pavlova and Thompson, 2016). Acetyl-CoA can not only

be generated from glucose but also from fatty acids via β-oxidation and is not only used to replenish the TCA cycle but also as starting point for lipogenesis. In the case of glutamine, this amino acid is converted to α-ketoglutarate (αKG) via glutaminolysis and thereafter introduced into the TCA cycle (Reitzer et al., 1979; Brosnan, 2003).

Driving metabolic reprogramming and reliance on the TCA cycle have been shown to be dependent on several genetic alterations of onco- or tumour suppressor genes, such as *p53*, *RAS*/*BRAF*, *MYC* and *HIF* as outlined in section 1.2.2.1. Furthermore, cells with deregulated oncogene and tumour suppressor expression have been shown to rely on the TCA cycle or to regulate uptake as well as breakdown of fuel sources via modulation of expression or activity of enzymes within the TCA cycle (Chen and Russo, 2012). Among the TCA cycle enzymes deregulated in cancer are aconitase, isocitrate dehydrogenase (IDH), fumarate hydratase (FH), succinate dehydrogenase (SDH), citrate synthase, pyruvate dehydrogenase (PDH) and α-ketoglutarate dehydrogenase (KGDH). FH, SDH and in particular mutant IDH1/2 are regarded as oncogenic enzymes, while their substrates fumarate and succinate as well as the product D-2-hydroxyglutarate (D-2HG) are declared as oncometabolites within the TCA cycle and are shown to drive tumourigenesis and tumour aggressiveness by affecting metabolic pathways (Eng et al., 2003; Juang, 2004; Yan et al., 2009; Sciacovelli and Frezza, 2016) (see section 1.2.3 and 1.2.4).

Targeting some of these aforementioned characteristics of altered energy metabolism within the TCA cycle and mutated enzymes gained attention over the past decade and a variety of small molecular inhibitors have been developed and tested, as outlined in Table 4 (Zhang and Yang, 2013; Luengo et al., 2017; Anderson et al., 2018b; Shahruzaman et al., 2018; Neitzel et al., 2020).

Table 4: Overview of anti-cancer drugs targeting altered energy metabolism in the TCA cycle.

Compound	*Target*	*Status*	*Tested in CRC*	*Reference*
3-bromo-pyruvate	broad-spectrum inhibitor of metabolic enzymes (e.g. HK2, LDH, PDH, SDH, KGDH, IDH)	mouse models	yes	Ganapathy-Kanniappan et al. (2010) Cardaci et al. (2012) Sun et al. (2015) Chong et al. (2017)
AG-120 (Ivosidenib) **IDH305** **BAY1436032** **AG-221 (Enasidenib)** **AG-881 (Vorasidenib)**	mutant IDH1 inhibitor mutant IDH2 inhibitor mutant IDH1/2 inhibitor	clinical trials	yes (e.g. AG-221)	Dang et al. (2016) Waitkus et al. (2018) Golub et al. (2019)
CB-839	glutaminase (GLS) inhibitor	clinical trials	yes	Song et al. (2018) Reckzeh et al. (2019)
Metformin	OXPHOS (complex I) inhibitor	clinical trials	yes	Kamarudin et al. (2019)
AZD7545	PDK2 inhibitor	mouse models	no	Morrell et al. (2003)

Compound	*Target*	*Status*	*Tested in CRC*	*Reference*
				Mayers et al. (2003)
VER-246608	pan-PDK inhibitor	cell culture	no	Moore et al. (2014)
Dichloroacetate (DCA)	PDK1 inhibitor	clinical trials	yes	Kankotia and Stacpoole (2014) Khan et al. (2016) Tataranni and Piccoli (2019) Liang et al. (2020)
CPI-613	PDK and KGDH inhibitor	clinical trials	yes	Stuart et al. (2014) Zachar et al. (2011)
(S)-2-[(2,6-dichlorobenzoyl) amino] succinic acid (AA6)	KGDH inhibitor	mouse model	no	Atlante et al. (2018) Spallotta et al. (2018)

Thus, the targetability of the TCA cycle in cancer cells with small molecule inhibitors is an emerging topic. Attacking these enzymes has been shown clinically to be a promising pharmacological target. In this context, the enzymes PDH and KGDH have recently gained attention, which will be detailed in sections 1.2.3 and 1.2.4.

1.2.2.1. Oncogene-mediated alterations of energy metabolism

The early belief that the metabolic signature of cancers is a passive response to damaged and unfunctional mitochondria has soon been superseded by the discovery that it is, in fact, the complex result of oncogene-directed metabolic reprogramming in order to support anabolic growth (Ward and Thompson, 2012; Hagland et al., 2013; Pavlova and Thompson, 2016). Indeed, the reprogramming of cellular energy metabolism is tightly linked to proliferation-inducing oncogenes. The most critical oncogenes as well as tumour suppressors for this metabolic reprogramming are *c-MYC*/*HIF-1/2α*, *PI3K*/*AKT*/*mTOR*, *KRAS*/*BRAF* and *p53*.

Oncogenes c-MYC and HIFs: MYC is a critical regulator of cell proliferation but also for tumourigenesis and altered energy metabolism (Tarrado-Castellarnau et al., 2016). Activated *MYC* collaborates with *HIF* (hypoxia-inducible factor) and fosters the glycolytic phenotype by upregulation of glucose transporters (GLUT1/2/4), glycolytic enzymes (hexokinase 2 (HK2), phosphofructokinase 1 (PFK1)), lactate production via LDH-A as well as lactate export via MCT1 and the inhibition of pyruvate-entry into the TCA cycle via PDK1 (Cairns et al., 2011; Cantor and Sabatini, 2012; Soga, 2013; Tarrado-Castellarnau et al., 2016). Furthermore, *MYC* targets the activation of increased mitochondrial biogenesis and glutaminolysis as well as glutamine dependency (Cairns et al., 2011; Cantor and Sabatini, 2012; Tarrado-Castellarnau et al., 2016). *MYC* has been proven to be the master mediator of glutaminolysis and glutamine addiction in cancer cells and helps to replenish the TCA cycle with anaplerotic glutamine via GLS1

and increased import via SLC1A5/SLC7A5 (Daye and Wellen, 2012; Tarrado-Castellarnau et al., 2016). Moreover, *MYC* stimulates the fatty acid, nucleotide, proline and serine synthesis next to folate and polyamine metabolism. HIFs are the major transcription factors in adaption to low oxygen conditions and downstream targets of c-MYC. Upon activation, HIF-1α increases glycolytic capacity by induction of glucose transporters (GLUT1/2/3) and glycolytic enzymes (HK2, PFK1, pyruvate kinase M2) (Cairns et al., 2011; Soga, 2013). In cancer, HIF-1/2 are oxygen-independently able to increase glucose consumption by redirecting pyruvate to lactate via lactate dehydrogenase A (LDH-A) and pyruvate kinase 2 (PDK2) (Cantor and Sabatini, 2012; Soga, 2013). Under these normoxic conditions, HIF-1α is likewise activated by PI3K, SDH and FH (Cairns et al., 2011). Furthermore, HIF-1α activates PDKs (i.e. PDK1) which in turn inhibit PDH, leading to a switch of carbon flow away from the mitochondrial TCA cycle (Cairns et al., 2011; Cantor and Sabatini, 2012; Soga, 2013). Subsidiary but not alternatively, other studies linked HIFs to increased glutaminolysis (Kroemer and Pouyssegur, 2008; Semenza, 2010a; Semenza, 2010b).

Oncogenic signalling pathway PI3K/AKT/mTOR: Key function of the PI3K/AKT/mTOR signalling pathway is cell growth, proliferation and cellular survival. The isoform AKT1 stimulates glycolysis via the expression and translocation of glucose transporters and by phosphorylating key glycolytic enzymes (HK2, PFK1) (Cairns et al., 2011; Cantor and Sabatini, 2012). However, PI3K/AKT also enhances oxidative metabolism, mitochondrial biogenesis and function (Tarrado-Castellarnau et al., 2016). Additionally, PI3K/AKT stimulates fatty acid synthesis (Cantor and Sabatini, 2012; Tarrado-Castellarnau et al., 2016). Linked to mTORC1, this signalling pathway functions as a key metabolic integration point and couples growth signals to nutrient availability next to autophagy (Cantor and Sabatini, 2012). mTORC, in this context, enhances both glycolysis and glutaminolysis (Tarrado-Castellarnau et al., 2016). In addition, protein synthesis is stimulated via mTORC1 (Cantor and Sabatini, 2012). Downstream, PI3K/AKT/mTOR regulates MYC and HIF - even under normoxic conditions (Cairns et al., 2011). Regulating cellular energy homeostasis, AMPK counteracts PI3K/AKT/mTOR under physiological conditions (Cairns et al., 2011). As a metabolic checkpoint, AMPK primarily shifts cells to an oxidative metabolic phenotype based on ATP/AMP-levels ratio and inhibits cell proliferation (Cairns et al., 2011; Cantor and Sabatini, 2012).

Oncogenes KRAS/BRAF: Both mutant *KRAS* and *BRAF* stimulates glucose metabolism via upregulation of GLUT1 conferring sensitivity to glycolytic inhibition and enhances glutaminolysis in cancer cells (Daye and Wellen, 2012; Ward and Thompson, 2012). Mutated *KRAS* is able to scavenge extracellular glutamine and promotes, thereby,

glucose anaplerosis. Also, *KRAS* activation leads to an upregulation of basal autophagy which renders cells insensitive to glucose limitation (Lozy and Karantza, 2012).

Tumoursuppressor p53: Most known for its role in cell cycle regulation and DNA damage response, p53 also controls metabolism by orchestrating two central carbon flows. Wildtype *p53* represses glycolysis by direct binding of glycolytic proteins (HK2, phosphoglycerate mutase 1) and by decreasing the expression of glucose transporters (GLUT1/3/4) (Cairns et al., 2011; Cantor and Sabatini, 2012; Soga, 2013). Moreover, p53 promotes OXPHOS by inactivating PDK2 and the expression of SCO2 (synthesis of cytochrome c oxidase 2) for the electron transport chain (Cairns et al., 2011; Cantor and Sabatini, 2012). Additionally, p53 helps redirecting glutamine to the TCA cycle via GLS2 (Daye and Wellen, 2012). A loss of p53, thus, directs/shifts cells into a glycolytic phenotype (Cairns et al., 2011). Together with OCT1 (octamer transcription factor 1), loss of p53 leads to an increase of glucose metabolism and reduction in mitochondrial respiration via PDK2 (Cairns et al., 2011).

Recent evidences show that also so-called oncometabolites are able to reprogram metabolism. The term oncometabolite refers to accumulated mitochondrial metabolites acting as oncogenic signalling molecules (Sciacovelli and Frezza, 2016). The most notable metabolite is D-2HG, which is itself able to render metabolism, cell signalling and cell differentiation. Wildtype IDH1/2 catalyses the oxidative decarboxylation of isocitrate to αKG and CO_2. A gain of function mutation of IDH1/2 is a common trait among tumours, particularly glioblastomas and acute myeloid leukaemia (AML) (Ward and Thompson, 2012; Mullen et al., 2014; DeBerardinis and Chandel, 2016). The mutation of IDH1/2 leads to conversion of αKG to D-2HG in great excess, which is a competitive inhibitor of the ten eleven translocation (TET) family orchestrating the demethylation of cytosine-rich DNA sequences. Leading to DNA and histone hypermethylation, tumourigenesis is promoted (Sciacovelli and Frezza, 2016). Both also other metabolites of the TCA cycle, such as αKG, succinate and fumarate can perform oncogenic signalling (Martínez-Reyes and Chandel, 2020).

1.2.2.2. Altered energy metabolism in CRC

In the context of CRC, altered energy metabolism could not only be found in tumour tissue but also in premalignant colorectal mucosa and benign tumours in both humans and rodents as shown using APC^{min} models/mice and models of chemically-induced CRC using azoxymethane (AOM) (Manna et al., 2014; Cruz et al., 2017; Satoh et al., 2017). This observation of altered energy metabolism in early tumourigenesis was

pronounced primarily by a Warburg effect, which was reflected by a significant increase in GLUT1, PKM2 and LDH-A (Cruz et al., 2017). Datta et al. (2017) even postulated that the Warburg effect is one of the critical initiating factors for CRC formation, which is subject for discussion. Nevertheless, a comparison of normal and CRC tissue revealed more than 120 metabolic genes to be altered indicating a more diverse picture (Satoh et al., 2008). Overall, 15 significantly altered metabolites were furthermore found and allow for prediction of recurrence and survival in CRC patients (Qiu et al., 2014). Next to anaerobic glycolysis, a deregulation of amino acid polyamine and nucleic acid metabolism were recorded (Manna et al., 2014). These alterations were primarily mediated by *c-MYC*, but also by *p53*, *KRAS*/*BRAF*, *HIF* and *PI3K/AKT*, and knockdown was demonstrated to reset the altered energy metabolism (Brown et al., 2018; Neitzel et al., 2020).

CRC cells show anaerobic metabolism mediated by HIF-1α with high glucose uptake via GLUT1 and lactate release by MCT1 (Koukourakis et al., 2006). Cancer-associated fibroblasts (CAFs) in CRC, however, are characterised by increased lactate uptake via MCT2 and lactate oxidation via LDH-5, but reduced glucose uptake. Furthermore, CAFs show reduced PDK1 activity due to increased PDH, which indicates a reliability on the TCA cycle and aerobic metabolism (Koukourakis et al., 2006). The tumour-associated epithelium, on the other hand, peaks in aerobic metabolism, high glucose absorption and a resistance to lactate uptake. This network depicts the complementary metabolic pathways in the tumour microenvironment in CRC, which comprises of a large recycling system and shows harmonised regional collaboration (Koukourakis et al., 2006). Additionally, an increase in mitochondrial gene expression (DRP1 for fission, OPA1 for fusion, PGC1a for biogenesis, UCP2 for uncoupling and mtND1 for copy number) was also noted in CRC, indicating that functionality and number of mitochondria play a crucial role (Cruz et al., 2017).

The reprogramming of energy metabolism is not only a result of oncogenic mutations but a prerequisite for (CRC) tumour formation. For instance, *MYC* enhances glycolysis but also glutamine-dependency of the TCA cycle, leading nonetheless to TCA cycle integrity and mitochondrial biogenesis promotion (Tarrado-Castellarnau et al., 2016). In this setting, *MYC* can stimulate the TCA cycle to use both glucose and glutamine and is furthermore responsible for increasing nucleotide synthesis and lipogenesis in CRC. Others, however, found MYC to negatively regulate mitochondrial biogenesis (Satoh et al., 2017). *KRAS* orchestrates multiple metabolic changes. As stated earlier, therapeutic intervention for *KRAS*-mt CRC tumours is especially difficult and *KRAS*-mt tumours are linked to poor prognosis. This goes hand in hand with the observation that *KRAS* is

responsible for altered energy metabolism and increased basal autophagy (Kawada et al., 2017). But both *KRAS*-G13D and *BRAF*-V600E mutations drive metabolic reprogramming in CRC (Hutton et al., 2016). Both mutations are characterised by enhanced glucose uptake via GLUT1 and lactate production as shown using isogenic RKO and DLD-1 cell lines as well as human biopsies (Kawada et al., 2017). This is also mirrored in increased glycolysis, nonoxidative pentose phosphate pathway, glutamine metabolism and phosphoserine biosynthetic pathway, which represent a great survival advantage. The enhanced nutrient uptake, glycolysis as well as glutaminolysis, next to elevated synthesis of fatty acids and nucleotides renders these tumours to be significantly less vulnerable to external nutritional stress (Kawada et al., 2017). However, in particular *KRAS*-mt tumour also showed an increase in numerous TCA enzymes, while mitochondrial function as well as OXPHOS were unaffected (Kawada et al., 2017). *BRAF*-V600E mutation induces a switch orchestrated by PGC1α. Yet, depletion of mitochondrial DNA can inhibit mutant *KRAS*-driven tumourigenesis in mice (Valcarcel-Jimenez et al., 2017). Suppression of glycolytic flux and increase of OXPHOS are two of several functions of p53. Consequently, mutation of p53 activates glucose transporters, glycolysis and, thus, inhibits OXPHOS also in CRC. In CRC, mutated PI3K, particularly PIK3CA, upregulates GPT2 (glutamate pyruvate transaminase 2), which renders the metabolism to be glutamine-dependent and replenishes the TCA cycle with glutamine (Hao et al., 2016). Conversely, an impaired TCA cycle with concomitantly enhanced glycolysis next to decreased gluconeogenesis and a suppressed glucuronic pathway were recorded in CRC by other research groups (reviewed in Brown et al. (2018) and Neitzel et al. (2020)).

Next to oncogenic regulation, chronic inflammation of the colon contributes to altered energy metabolism and reprogramming (Qu et al., 2017). As revealed in dextran sodium sulphate (DSS)-treated mice, chronic inflammation lead to an upregulation of key glycolytic enzymes such as PKM2, LDH-A, HK2 and PFK, which is mediated by IL-6 and STAT3/c-MYC subsequently. These changes can trigger the Warburg effect. Moreover, the Warburg effect is found to be linked to the microbiome and fostered by a concomitant dysbiosis. For instance, a dysbiosis, which preferentially no longer produce the short chain fatty acid butyrate, affects the energy metabolism in CRC (Datta et al., 2017; Brown et al., 2018). The majority of butyrate is produced by the intestinal microbiota (i.e. predominantly by *Firmicutes*) via fermentation. Butyrate is essential for the colon homeostasis and energy source for normal colonic cells, which introduce it to the TCA cycle and divert pyruvate and glutamine to other pathways. In CRC patients, the butyrate-producing species are markedly less abundant (Brown et al., 2018). In CRC

cells, the reduced amount of butyrate leads to a Warburg effect and the remaining butyrate accumulates intracellularly and ultimately leads to apoptosis (Sun et al., 2015). An alteration in the microbiome especially observed in the young due to dietary factors with a strong relationship to obesity and diabetes, connect the microbiome to altered energy metabolism and the increase of CRC incidence in the young (Datta et al., 2017).

1.2.3. PDH – composition and function

The central multi-enzyme complex linking glycolysis and the TCA cycle is the pyruvate dehydrogenase complex (PDH), which is found in aerobic eukaryotes, prokaryotes and some plants and is localised in the mitochondrial matrix (Patel and Korotchkina, 2003). It inherits a key role in regulating metabolic flux by introducing pyruvate-derived carbon into the TCA cycle (Patel and Korotchkina, 2003). Three enzymatic subunits form the PDH complex: pyruvate dehydrogenase called E1 using thiamine pyrophosphate (TPP) as co-factor, dihydrolipoyl transacetylase called E2 using lipoic acid (LA) and CoA as co-factor and dihydrolipoyl dehydrogenase termed E3 using FAD and NAD^+ as co-factors (Wieland, 1983).

PDH catalyses the irreversible oxidative decarboxylation of pyruvate to form acetyl-CoA in a three-step-reaction, which is depicted in the scheme in Figure 7A (Patel et al., 2014). PDH, more specifically its E2 subunit, uses lipoate as covalently joined catalytic co-factor. Lipoate, in the form of lipoamide/lipoic acid (LA), cycles through acylation to acetyl-LA and reduction to dihydrolipoic acid (DHLA) (also see section 1.3.1.1). Under the release of CO_2, LA is acetylated and can bind CoA via its sulphur atoms. Via the reduction to DHLA, acetyl-CoA can be formed. Acetyl-CoA is then further processed with oxal acetat to generate citrate during the TCA cycle, while $NADH/H^+$ is reoxidised within the electron transport chain.

In general, the PDH complex is regulated post-transcriptionally via phosphorylation by its associated pyruvate dehydrogenase kinases (PDKs) and phosphopyruvate dehydrogenase phosphatases (PDPs) (Korotchkina and Patel, 2001). In humans, four PDK isoenzymes bound to the lipoyl domain of E2 are known (PDK1, PDK2, PDK3, PDK4) with tissue-specific abundancy and regulatory characteristics (Korotchkina and Patel, 2001). While PDK1 and PDK3 are associated with hypoxia(/HIF-1α)-induced metabolic switch and cell survival, PDK2 and PDK4 play a role in starvation and diabetes (Korotchkina and Patel, 2001). Target of regulatory phosphorylation by PDKs are three conserved Serine residues of the E1α subunit (site 1, Ser-293; site 2, Ser-300; site 3, Ser-232), of which any type of phosphorylation leads to an inactivation of the PDH

complex, however, with a preference of site 1 and PDK1 (Korotchkina and Patel, 2001). An inhibition causes the metabolic switch from mitochondrial respiration to cytoplasmic glycolysis. PDKs are activated upon sufficient levels of acetyl-CoA, ATP and NADH (Wieland, 1983; Bunik, 2003). As a counterplayer, PDPs reverse the regulatory post-transcriptional phospho-modification in the presence of low levels of acetyl-CoA and high levels of pyruvate (Wieland, 1983). Furthermore, acetylated LA activates PDKs, which inhibit PDH via the E1α subunit (Wieland, 1983; Roche et al., 2003). The lipoate-sensitivity of PDH can be exploited to target this enzyme complex in cancer and its role in tumourigenic metabolic rewiring (Roche et al., 2001; Zachar et al., 2011; Park et al., 2018).

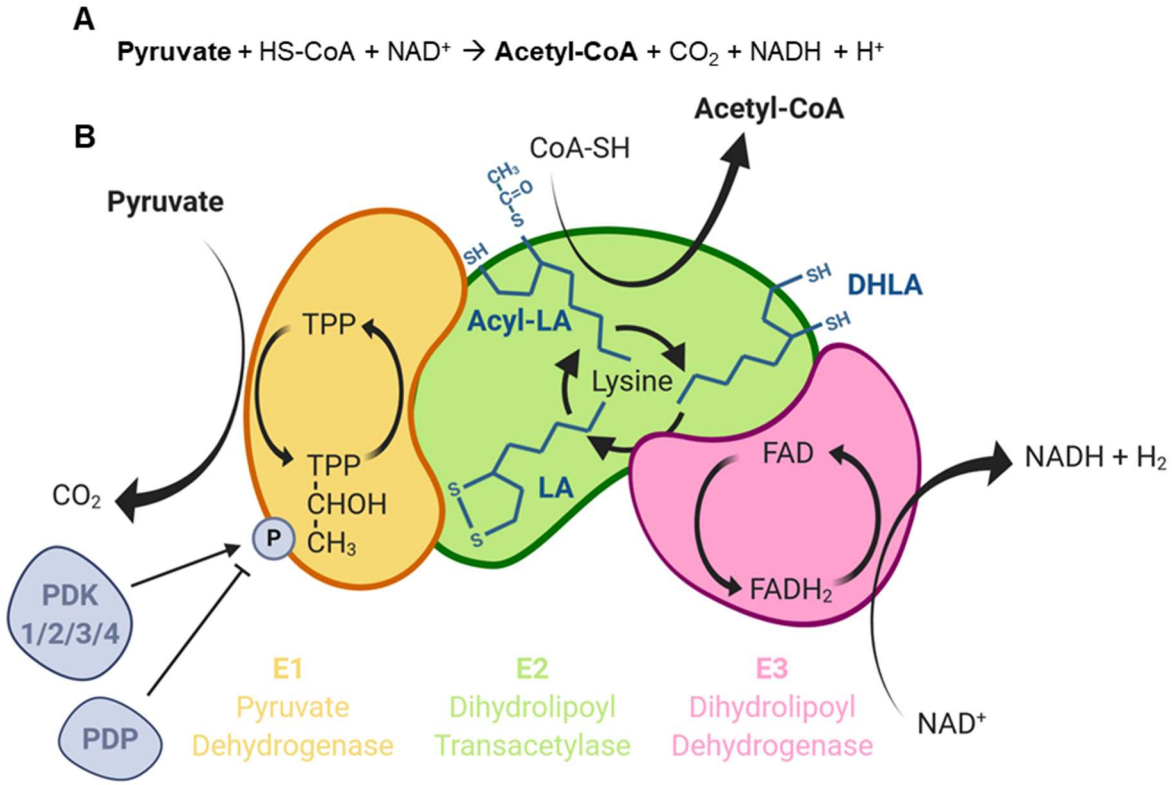

Figure 7: The PDH complex.
(A) Overall reaction scheme of the PDH complex, (B) Graphical illustration of the composition of the PDH complex and the regulating function of PDKs and PDPs. (created with BioRender)

1.2.3.1. PDH in CRC

A handful of studies assessed the condition of PDH and its regulation and activity in CRC. Suppression of PDH expression was found in 60% of colorectal adenocarcinoma tissue samples (n=70), with concomitant strong cytoplasmic PDK1 activity (Koukourakis et al., 2006). Decreased PDH activity was more frequently observed in right-sided than in left-sided CRC and correlated (together with high HK2 expression) with invasiveness and aggressiveness of tumours, resulting in a decreased recurrence-free survival of CRC patients (Hamabe et al., 2014). However, since PDH activity is determined by PDK

expression, further studies focused rather on PDK activity as a regulator of PDH than on PDH itself.

Given that PDK1 and PDK3 are regulators of metabolic switch, Lu et al. (2011) examined expression levels of these PDKs in CRC biopsies. While they observed a significant overexpression of PDK3 levels controlled by HIF-1α in all CRC cancer stages, PDK1 levels were markedly decreased in CRC tumour samples of CRC stage II to IV as compared to adjacent normal tissue. Additionally, the elevated PDK3 levels were linked to tumour aggressiveness, drug resistance and, thus, reduced survival of patients. Further investigating CRC tissue samples in comparison with adjacent normal tissue, PDK3 was found to be upregulated next to other glycolysis-regulating enzymes, indicating an impairment of the TCA cycle (Bi et al., 2006). Established CRC cell lines, i.e. LS174T and SW480, differentially express the four PDK isoforms (Ho and Coomber, 2015). While PDK1 and PDK3 are expressed sufficiently, PDK2 and PDK4 are hardly detectable. Using HCT116 isogenic cells lines, wildtype p53 was shown to decrease levels of PDK2, which in turn leads to an increase in PDH activity and results in a prevention of the Warburg effect (Contractor and Harris, 2012).

Table 5: Overview of PDK isoforms and their function in CRC and its tumourigenesis.

Isoform	*Status / Function / Effect*	*Reference*
PDK1	expression ↓	Lu et al. (2011)
	expressed in CRC cell lines	Ho and Coomber (2015)
PDK2	not found in CRC cell lines	Ho and Coomber (2015)
	expression ↓ by wildtype p53 PDH activity ↑ and subsequently Warburg effect ↓	Contractor and Harris (2012)
PDK3	expression ↑ via HIF-1α PDH activity ↓ tumour hostility and drug resistance ↑	Lu et al. (2011)
	expression ↓ PDH and TCA cycle activity ↓	Bi et al. (2006)
	expressed in CRC cell lines	Ho and Coomber (2015)
PDK4	not found in CRC cell lines	Ho and Coomber (2015)
	loss leads to growth inhibition in KRAS-mt tumours	Trinidad et al. (2017)
	oncogenic role for tumourigenesis, if expression ↑ metastatic potential ↑ apoptosis ↓	Leclerc et al. (2017)

Moreover, Leclerc et al. (2017) postulated an oncogenic role of PDK4 for CRC transformation since decreased methylation and an increased expression of the PDK4 gene was found to correlate with increased cancer cell migration and invasion and decreased apoptosis. Conversely, a loss of PDK4 was associated with strong growth inhibition of *KRAS*-mt cancer cells, which was not found in *KRAS*-wildtype cells using isogenic HCT116 cell lines (Trinidad et al., 2017).

Both resveratrol and butyrate were found to target the PDH complex in CRC. Whereas butyrate produced by a favourable colonic microbiota elicits a metabolic switch in CRC

cells to the Warburg effect by inhibiting PDH, resveratrol can reverse this effect by enhanced PDH activity *in vitro* by calcium chelation and subsequent blockage of the mitochondrial calcium uniport (Blouin et al., 2011; Saunier et al., 2017; Liu et al., 2018).

1.2.4. KGDH – composition and function

Localised in the mitochondrial matrix of eukaryotes and some bacteria and being a rate limiting enzyme in the TCA cycle, the α-ketoglutarate (also called oxoglutarate) dehydrogenase complex (KGDH) catalyses the irreversible oxidative decarboxylation of α-ketoglutarate (αKG), followed by the reaction with Coenzyme A to form succinyl-CoA in a three-step-reaction (Figure 8A) (Gibson et al., 2005). Being a member of the family of α-ketoacid dehydrogenases, KGDH consists of three components: αKG dehydrogenase (OGDH; E1), dihydrolipoyl S-succinyltransferase (DLST; E2), and dihydrolipoyl dehydrogenase (DLD; E3) (Koike and Koike, 1976). The KGDH shares many features with the PDH: the E3 subunit, the same co-factors including LA and the catalysis of a similar reaction (see section 1.2.3). In an oxidative manner, αKG is decarboxylated to succinyl-CoA and gives rise to NADH, which is fed into the respiratory chain to further generate energy (Koike and Koike, 1976; Gibson et al., 2005).

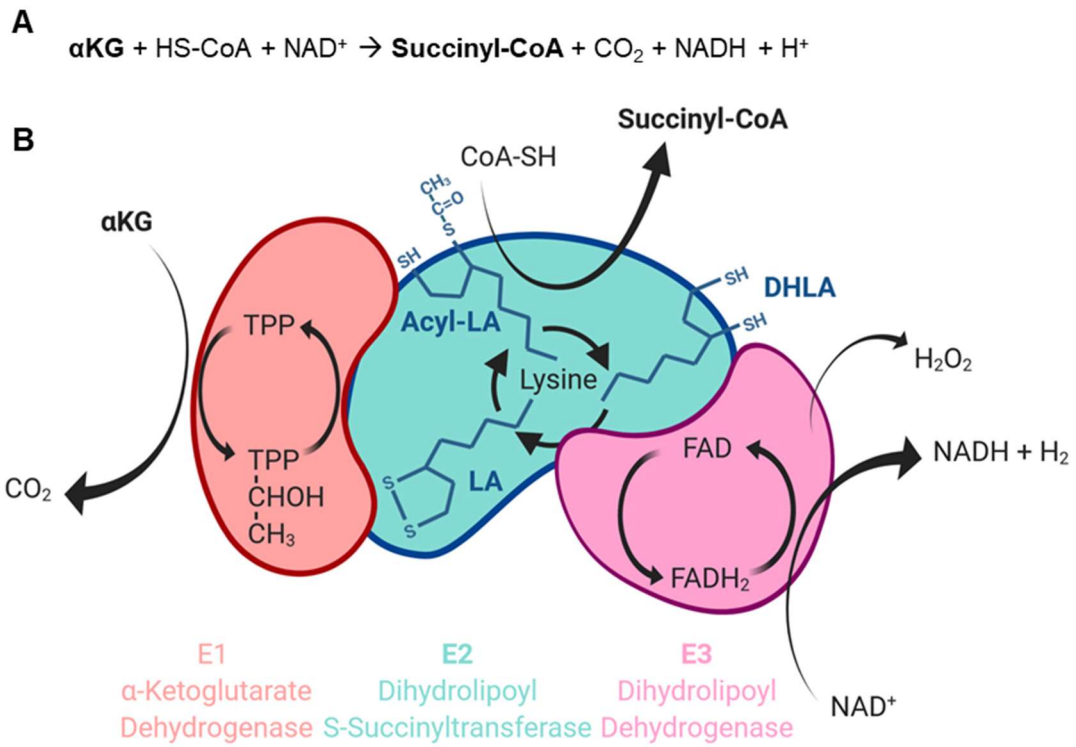

Figure 8: The KGDH complex.
(A) Overall reaction scheme of the KGDH complex, (B) Graphical illustration of the composition of the KGDH complex. (created with BioRender)

Therefore, succinyl-CoA and NADH as products are inhibitory, while ADP and Ca^{2+} are allosteric activators of the E1 component (Koike and Koike, 1976). Upon KGDH activity, oxidative stress is caused by the release of ROS as a by-product of NADH and ATP generation (Starkov et al., 2004). Upon sensing ROS, free radicals or redox imbalance, auto-regulation via the E2 subunit and its glutathionylation at the sulphhydryl of the LA-domain as posttranscriptional modification can occur and can further be reversed by glutaredoxin (Tretter and Adam-Vizi, 2005; Applegate et al., 2008; McLain et al., 2011).

1.2.4.1. KGDH in CRC

In CRC, wildtype OGDH is shown to be 8-fold downregulated via promoter hypermethylation in 50% of CRCs with CpG island methylator phenotype, but also in other types of solid tumours (Hoque et al., 2008; Ostrow et al., 2009; Fedorova et al., 2015). Aberrant hypermethylation of the OGDH gene promoter was also identified in sporadic colorectal cancer (Khalaj-Kondori et al., 2020). Overall, 19 out of 176 genes associated with metabolism including OGDH are downregulated, which was further correlating with increasing tumour size and invasiveness (Fedorova et al., 2015). A somatic frameshift mutation of the OGDH gene in exon 3 of MSI-H CRC samples was found, which is tightly linked to a loss-of-function (Jo et al., 2016). Conversely, OGDH was shown to be 4-fold upregulated in early metastatic CRC tumours (Duke's C) (Bigagli et al., 2016). Although often implied to be inactive in cancer, a distinct splice variant of OGDH is proven to be tumour-specifically overexpressed in CRC (Bunik et al., 2016). The differentially expressed transcript of OGDH (isoform uc011kby) displays a 6-fold decrease in regulatory Ca^{2+}-sensitivity upon lacking three exons (Snezhkina et al., 2016; Anderson et al., 2018b).

Table 6: Overview of KGDH and its function in CRC and its tumourigenesis.

Subunit	*Status / Function / Effect*	*Reference*
OGDH	expression ↓ via promoter hypermethylation in CIMP in sporadic CRC	Fedorova et al. (2015) Khalaj-Kondori et al. (2020)
	expression ↓ tumour growth and invasiveness ↑	Fedorova et al. (2015)
	loss of function due to frameshift in exon 3	Jo et al. (2016)
	expression ↑ due to Ca^{2+} insensitivity	Snezhkina et al. (2016)
	expression ↑ in metastatic CRC	Bigagli et al. (2016)

1.3. Lipoates as Anti-Cancer Drugs

1.3.1. Lipoic acid

Lipoates, originating from octanoic acid, are organosulphur compounds that under physiological conditions are primarily bound in multi-enzyme complexes and crucial for

aerobic metabolism. The most relevant representative of lipoates is α-lipoic acid (LA), which occurs in eukaryotes as well as prokaryotes.

1.3.1.1. LA as mitochondrial mediator

LA (1,2-dithiolane-3-pentanoic acid), an endogenously occurring chiral disulphide fatty acid (Figure 9), is a mitochondrial mediator of carbon flow due to its pivotal role in two multi-enzyme complexes. Pairing with its reduced form dihydrolipoic acid (DHLA), LA acts as co-factor in enzyme complexes performing oxidative decarboxylation of α-keto acids: the pyruvate dehydrogenase (PDH) and the α-ketoglutarate dehydrogenase (KGDH) complex.

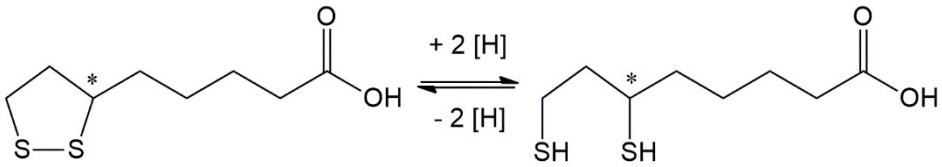

Figure 9: Chemical structure of lipoic acid and dihydrolipoic acid.
The chiral and endogenously occurring organosulphur compound LA harbours a disulphide bond, which expresses its utility as co-factor together with its reduced form DHLA in mitochondrial multi-enzyme complexes due to its high redox potential. The asterisk indicates its chiral centre. (created with ChemDraw).

As an essential co-factor, the biologically active *(R)*-enantiomer is *de novo* synthesised by the lipoyl synthase in mitochondria and covalently bound to conserved lysine residues in mitochondrial enzymes, such as the E2 dihydrolipoyl transacetylase and dihydrolipoyl S-succinyltransferase subunit of PDH and KGDH, respectively (Jordan and Cronan, (1997); Dörsam and Fahrer, 2016). In addition, at least 3 other multi-enzyme complexes are known to utilise LA (glycine cleavage complex, branched-chain oxoacid dehydrogenase complex and acetoin dehydrogenase complex, BCKDC) (Cronan et al., 2005).

1.3.1.2. Inherent properties and metabolism

A potent redox couple with anti-oxidative properties is formed with the reduced form DHLA (Dörsam and Fahrer, 2016) (Figure 10). Mechanisms include direct scavenging of reactive oxygen species (ROS) the chelation of transition metal ions (Mn^{2+}, Cu^{2+}, Mg^{2+}) and ferric iron (Fe^{3+}) (Sigel et al., 1978; Bonomi and Pagani, 1986; Haenen and Bast, 1991; Suzuki et al., 1991; Ou et al., 1995; Rochette et al., 2013). Cellular anti-oxidants such as ascorbic acid, tocopherol and glutathione are regenerated (Kagan et al., 1992; Han et al., 1997; Suh et al., 2004). LA triggers nuclear accumulation of the redox-sensitive transcription factor Nrf2 (mainly by *de novo* protein synthesis) (Shay et al., 2012). The enhanced activity of Nrf2 is responsible for cytoprotective proteins such as the phase II enzyme families GST and UGT. Apart from that, LA acts anti-inflammatory by blocking the NFκB pathway (Shay et al., 2009). Therefore, LA is accepted as dietary

supplement and granted market authorisation for the treatment of chronic diseases associated with high levels of oxidative stress, such as Alzheimer's or diabetes mellitus and associated polyneuropathy (Reljanovic et al., 1999; Smith et al., 2004).

The maximum tolerable dose in clinical trials was 1200 mg/day intravenously and 2400 mg/day orally, respectively (Yadav et al., 2005). While absorption happens rapidly with an oral bioavailability of 30% and a theoretical plasma concentration of up to 400 µM, LA has a plasma half-life of 0.5 h and is readily excreted via the urine (Teichert et al., 1998; Dörsam and Fahrer, 2016). Upon cellular uptake via either the monocarboxylate transporter or the Na^+-dependent multivitamin transporter, LA is converted to DHLA and undergoes extensive biotransformation via mitochondrial ß-oxidation and S-methylation, resulting in a spectrum of more than 10 metabolites (Handelman et al., 1994; Schupke et al., 2001; Jones et al., 2002; Teichert et al., 2003; Takaishi et al., 2007; Zehnpfennig et al., 2015). Dietary uptake of LA from animal giblets and vegetables is regarded as negligible (Packer et al., 2001; Satoh et al., 2008; Shay et al., 2009).

1.3.1.3. Cytotoxicity of LA, cellular response and anti-tumour activity

Numerous studies in cell culture models provided evidence for the cytotoxicity of LA, which itself is non-genotoxic and solely interferes with mitochondrial functionality (Dörsam et al., 2015; Dörsam and Fahrer, 2016). Vulnerable cell lines included a variety of CRC cells (HT29, HCT116, RKO, SW48, CaCo-2), hepatoma cells (HepG2, FaO, SMMC-7721), lung cancer cells (H460, A549), ovarian cancer cells (IGROC1), leukaemia cells (Jurkat), squamous carcinoma cells (FaDu) and breast cancer cells (MCF-7) of human origin as well as murine transformed fibroblasts (BALB/c-3T3). LA treatment lead to the generation of ROS (superoxide anion $\cdot O_2^-$), followed by down-regulation of the anti-apoptotic Bcl-2, Bcl-X_L and Mcl-1 protein and up-regulation of the pro-apoptotic proteins Bim and Bax. This culminated in the initiation of the mitochondrial mediated intrinsic apoptosis pathway due to the loss of mitochondrial membrane potential. The activation of the initiator Caspase-9 followed by Caspase-3/7 next to cytochrome c release, PARP-1 cleavage and DNA fragmentation were reported in this context (Wenzel et al., 2005; Simbula et al., 2007; Shi et al., 2008; Dörsam et al., 2015; Kafara et al., 2015) (Figure 10). Other pathways involved are necrosis and the apoptosis-inducing factor (AIF) as caspase-independent cell deaths (Choi et al., 2009). Generally, it was shown that both the extrinsic FasL/FasR- as well as the p53-mediated apoptotic pathways are dispensable (van de Mark et al., 2003; Dörsam et al., 2015). Recent studies by Neitzel et al. (2019) further detailed that the p53 protein is, in fact, depleted upon LA treatment in CRC cells. Some studies investigated the synergism of LA with

various anticancer drugs in combination treatment, such as 5-FU, doxorubicin, etoposide and temozolomide as well as gefitinib and γ-irradiation (Yoo et al., 2013; Dörsam et al., 2015; Göder et al., 2015; Dörsam and Fahrer, 2016; Neitzel et al., 2019).

Other cellular responses upon LA included the depletion of the direct DNA damage reversal protein O^6-methylguanine DNA-methyltransferase (MGMT) and autophagy induction (Göder et al., 2015). Regarding the PI3K-AKT-mTOR axis, LA reduced AKT phosphorylation and in turn enhanced AMPK phosphorylation as a negative regulator of mTOR (Simbula et al., 2007; Shi et al., 2008; Li et al., 2015b). Moreover, LA interferes with the EGFR/met and TGFß signalling (Michikoshi et al., 2013; Jeon et al., 2016). In addition, LA was shown to block epithelial-to-mesenchymal transition (EMT), in particular invasion, migration and motility of breast, bladder and thyroid cancer cells (Lee et al., 2010; Yamasaki et al., 2014; Jeon et al., 2016). Altogether, these cellular responses might contribute to its anti-tumour and -dissemination activity. *In vivo*, LA strongly delayed tumour growth and prolonged survival in syngenic mouse models using solid tumour cells, e.g. CRC cancer, lung cancer, breast cancer, bladder cancer and melanoma cells (Abolhassani et al., 2012; Feuerecker et al., 2012; Göder et al., 2015).

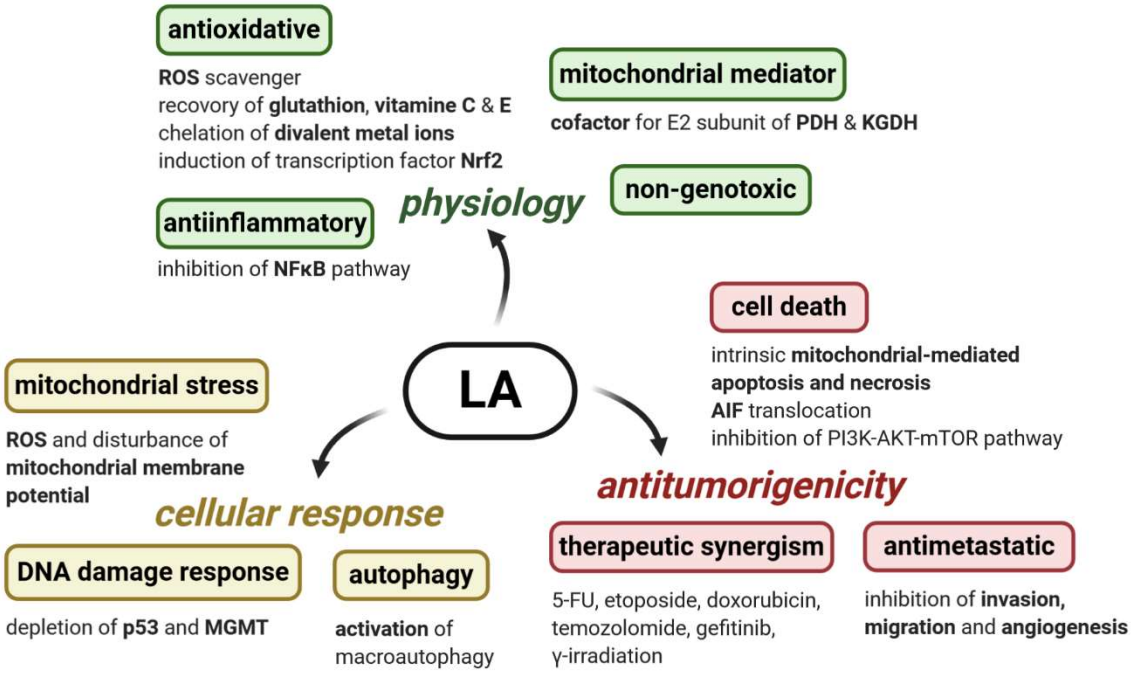

Figure 10: Summary of physiological function and anticancer properties of LA.
The physiology of LA is displayed by its mitochondrial mediating function and its pivotal role in orchestrating carbon flux through the mitochondria. LA acts anti-inflammatory and scavenges a plethora of ROS. The diverse anticancer properties of LA include the inhibition of tumour growth via the induction of ROS, cell death and displays anti-metastatic features. Additionally, LA was shown to induce autophagy and to deplete a central DNA damage reversal protein, although LA is not genotoxic itself (created with BioRender).

Due to encouraging data generated with LA, DHLA as well as a limited number of derivates (such as 17m and DHL-TauZnNa) were developed and gained attention in anti-

cancer research (Zhang et al., 2010; Hiratsuka et al., 2013). Of these, the by far most promising derivate turned out to be CPI-613 (Zachar et al., 2011; Stuart et al., 2014).

1.3.2. CPI-613

As a candidate of a set of lipoate analogues, 6,8-bis(benzylsulphanyl)octanoic acid, also called CPI-613, has been developed as a tumour-targeted antimitochondrial agent with a broad spectrum efficacy. Its mode of action is described to be distinct from any existing pharmacological class of anticancer agents used in the clinic thus far (Zachar et al., 2011; Stuart et al., 2014).

1.3.2.1. Chemical Structure and Synthesis

Belonging to the class of lipoates, CPI-613 has been derived from LA. In contrast to its parent compound, the sulphur atoms of CPI-613 are covalently linked to benzyl groups (Figure 11). This structural alteration leads to an abrogation of its potential to perform redox reactions.

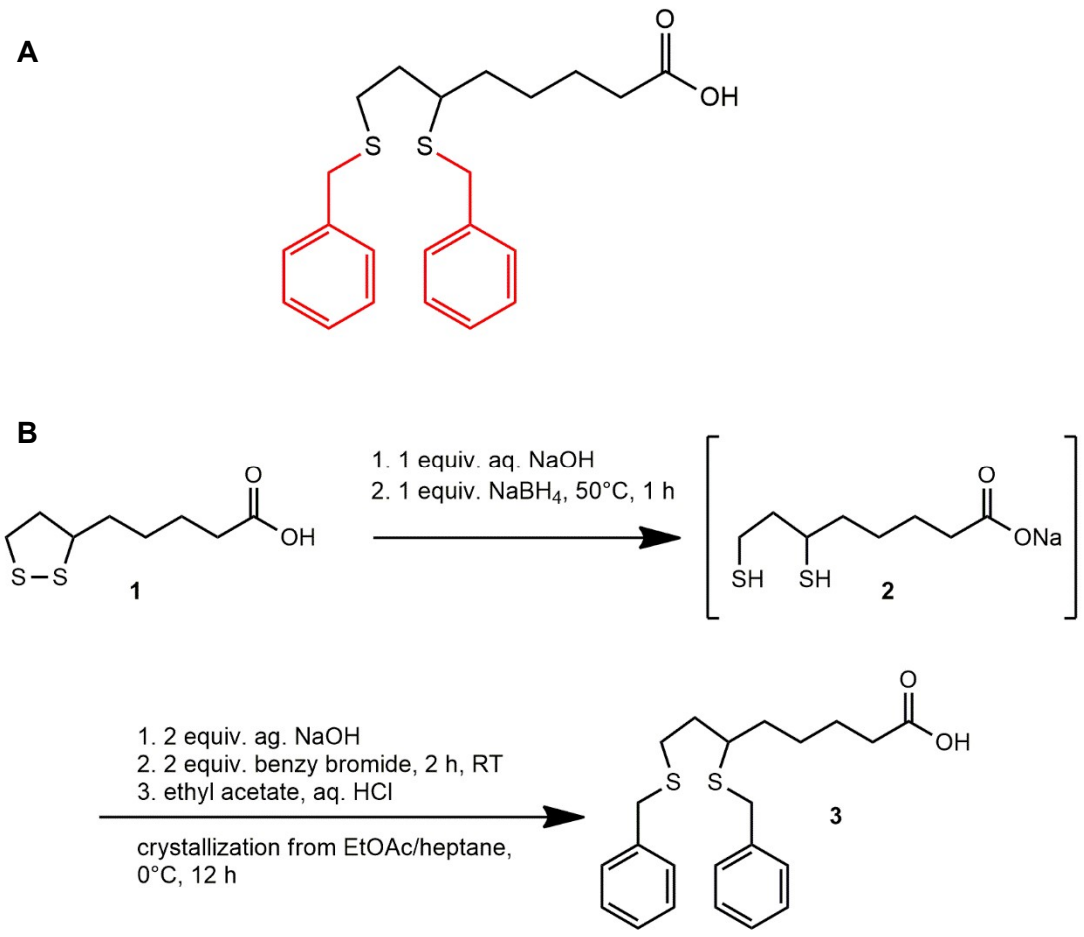

Figure 11: Chemical structure and synthesis scheme of CPI-613.
(A) Chemical structure of CPI-613 shows the covalently bound benzyl groups to the sulphur atoms (marked in red). (B) The two-step chemical synthesis pathway described by Gibson et al. (2011) allows large scale synthesis. (created with ChemDraw)

Originally designed by Rafael Pharmaceuticals Inc. (founded as Cornerstone Pharmaceuticals Inc.), CPI-613 is obtained via a two-step synthesis from its parent compound LA (Figure 11) as described by Gibson et al. (2011). First, LA is dissolved in one equivalent of aqueous sodium hydroxide (NaOH). The disulphide linkage is completely reduced within 1 h at 50°C using one equivalent of sodium borohydride ($NaBH_4$). Next, bisthiobenzylation is achieved by the addition of two equivalents of NaOH and benzyl bromide (BnBr) at ambient temperature and the reaction is completed within 2 h. At last, the reaction mixture is diluted in ethyl acetate and acidified using hydrogen chloride (HCl). The product is finally obtained as a pure single-crystal polymorph upon drying, concentration via distillation and crystallization at 0°C taking 12 h using heptane. The safe and economical one-pot synthesis in multikilogram scale yields 90% CPI-613 with a purity of 99.8% with no more than 0.16% of any single impurity, including a genotoxic sulphoxide by-product.

1.3.2.2. Mode of Action

As shown in two mechanistic landmark studies, CPI-613 targets two mitochondrial multi-enzyme complexes, which use LA as co-factor under physiological conditions (Zachar et al., 2011; Stuart et al., 2014). By mimicking lipoate catalytic intermediates, CPI-613 inhibits these enzyme complexes due to its catalytical inertness based on its inability to form a redox couple (Figure 12).

First, CPI-613 inactivates the KGDH complex in a ROS-dependent manner (Stuart et al., 2014). CPI-613 treatment leads a ROS burst, originating from the dihydrolipoyl dehydrogenase (E3) subunit of the KGDH complex in both established cell culture and purified enzyme assays. The generated ROS functions as signalling molecule and in turn disorders tumour-specific KGDH complex redox-autoregulation. CPI-613-derived ROS-modification of KGDH implies enzyme glutationylation at the lipoate residues and redox blockage of the dihydrolipoyl S-succinyltransferase (E2) subunit. Supplementation with *N*-acetyl cysteine (NAC) abrogates the formation of ROS. As a result, carbon flux is destroyed and the TCA cycle as well as OXPHOS are inhibited. Regarding respiration in terms of maximal respiration capacity measured by oxygen consumption rate, leukaemia cells (K562 and OCI-AML3) were impaired at concentrations of 5-50 µM CPI-613 (Pardee et al., 2014). Regarding OXPHOS in glioblastoma cells, however, up to 50 µM CPI-613 had no effect (Oppermann et al., 2016). Moreover, Oppermann et al. (2016) found carnosine, a glycolytic ATP production inhibitor, and CPI-613 to act synergistic by depriving all carbon sources, i.e. glucose and pyruvate, needed for energy production. Upon CPI-613, the energy-sensing AMPK pathway is activated (Pardee et al., 2019; Gao

et al., 2020). This activation represents a protection mechanism against CPI-613-induced metabolic stress, since AMPK functions as a resistance factor against TCA cycle inhibition. Consequently, metabolites down-stream of KGDH, such as succinate, fumarate and malate, are deprived (Stuart et al., 2014). Mordhorst et al. (2019) described a decrease in the cellular glycine concentration, which might be linked to an increased synthesis of glutathione (GSH) in order to cope with the increased ROS formation.

Second, the lipoate derivate CPI-613 interferes with the PDH and its tight regulation (Zachar et al., 2011). Located in the mitochondrial matrix, the PDH is regulated by lipoate-responsive phosphorylation via PDKs. CPI-613 treatment leads to an activation of pyruvate dehydrogenase kinases (PDKs) resulting in a hyperphosphorylation of the E1α subunit of PDH and, thus, its inactivation (Zachar et al., 2011). This post-translational modification has been demonstrated using Western Blot analysis of PDH-pSer360, -pSer293 and -pSer232, which all represent the major phospho-epitopes selectively altered in tumour cells. A knockdown of all PDK isoforms lead to CPI-613 resistance. In malignant transformation and ultimately in cancer cells, PDK1 and PDK3 are upregulated via HIF and their substantially elevated levels represent a suitable target for cancer therapy (see section 1.2.3). Upon PDH inhibition, glycolysis-derived mitochondrial carbon flow is truncated and energy production in the TCA cycle as well as lipid biosynthesis are impaired. The disruption of cancer cell metabolism is thought to culminate in cell death. The crucial role and mediating cytotoxicity of PDH inhibition has been proven by Pardee et al. (2018) with a rescue that is only performed using acetate as a replacement for acetyl-CoA, but was not achieved when using methyl-succinate replacing succinyl-CoA.

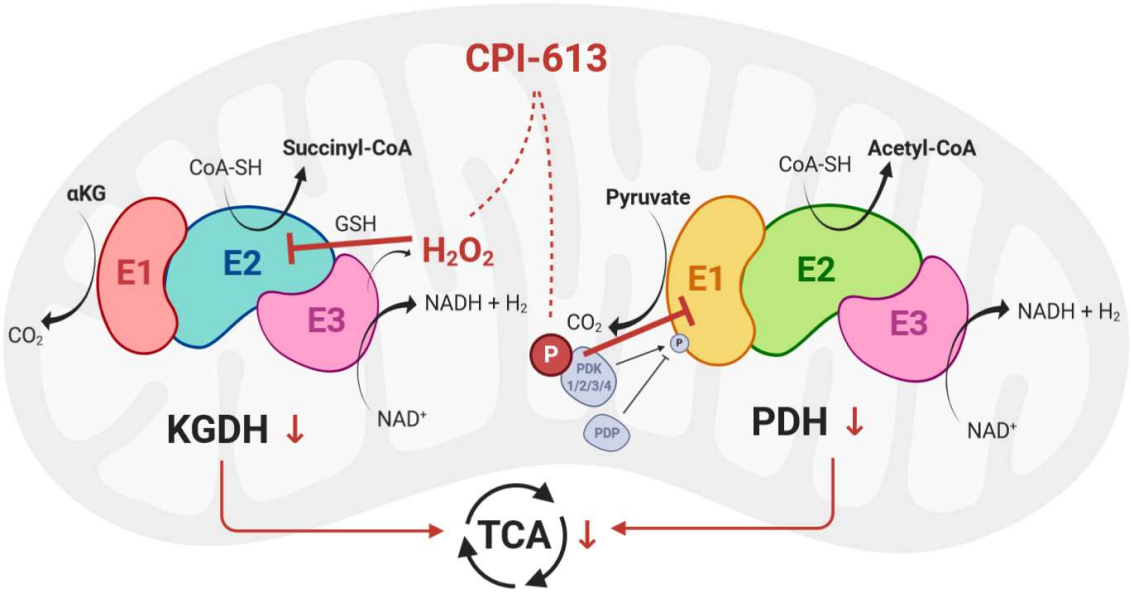

Figure 12: Mitochondria-targeted mode of action of CPI-613.
(created with BioRender, according to Zachar et al. (2011) and Stuart et al. (2014))

Work by Dahan (2014) provided evidence that CPI-613 furthermore interacts with the branched-chain α-ketoacid dehydrogenase complex (BCKDC), which catabolises leucine, isoleucine, and valine. Upon CPI-613 treatment, phosphorylation of the E1α subunit was detected in H460, BxPC3, A549 and U-87 cells. The BCKDC is, thus, the third lipoamide-regulated enzyme complex inhibited by CPI-613.

Stuart et al. (2014) have demonstrated the E3 subunit of the KGDH complex to be an important source of ROS, especially in the context of CPI-613. Contrary, CPI-613 acts as a ROS minimizing agent and pan-inhibitor for $O2^{\cdot -}$ and H_2O_2 production in isolated murine liver mitochondria in concentrations between 5 and 150 µM by inhibiting KGDH representing a high capacity site for ROS production (O'Brien et al., 2017; Slade et al., 2017). In a more mechanistic study, CPI-613 was used as a PDH inhibitor (PDHi) in order to demonstrate that lactate is indeed used as a bioenergetic fuel for mitochondrial metabolism and as affective as pyruvate in isolated murine heart, liver and muscle mitochondria (Young et al., 2020). Application of CPI-613 as a PDHi abolished mitochondrial respiration concomitant to lactate-associated ROS production. Furthermore, CPI-613 is now commonly used as KGDH inhibitor (KGDHi) in mice and yeast (Arai et al., 2020; Dogar et al., 2020).

Additionally, Gao et al. (2020) provide evidence that CPI-613 rewires lipid metabolism in pancreatic cancer cells. Suppression of lipid metabolism was proven in PANC-1 and AsPC-1 cells with concomitant AMPK-dependent ACC inhibition.

Summing up, CPI-613 targets altered energy metabolism in cancer cells by inhibiting two central enzymes orchestrating carbon flux and energy production in the mitochondria. Effectively, energy supply as well as biosynthetic intermediates are disrupted leading to cytotoxicity.

1.3.2.3. Cytotoxicity and Cellular Effects

Based on its mode of action, CPI-613 is hypothesised to be a promising candidate as anticancer therapeutic. Therefore, cytotoxicity of CPI-613 has been tested in a variety of cancer cell lines *in vitro*, including cell lines bearing a variety of different oncogenic mutations or alterations in the cell death machinery. Among these, bone marrow, breast, colorectal, kidney, lung, muscle, ovarian, pancreatic, prostate and uterine cancer cells were tested and found to be vulnerable for CPI-613-induced reduction of cell viability with inhibitory concentration 50% (IC_{50}) values ranging from 100 to 280 µM (Zachar et al., 2011; Gao et al., 2020). In comparison to non-cancerous cell lines, tumour cell lines showed a higher sensitivity to CPI-613 treatment represented by lower IC_{50} values and indicating tumour-specificity. Besides its ubiquitous efficacy against diverse cancer

types, CPI-613 was shown further to be active independent of the cell cycle phase. Furthermore, CPI-613 exhibited cytotoxicity independent of prevailing signal transduction pathways, tumour suppressor or oncogene mutations, i.e. p53-deficiency in AML or *KRAS* mutations in lung carcinoma cells (Zachar et al., 2011; Pardee et al., 2018). Additionally, CPI-613 was equally effective in cytostatic-resistant cell lines, i.e. Doxorubicin-resistant ovarian cancer cells (Lee et al., 2011). Stuart et al. 2016 pointed out that metabolite and carbon source availability is mediating the cytotoxicity of CPI-613. While cells having any glucose but pyruvate available will undergo cell death rapidly, cells having glucose present will shift their energy production away from OXPHOS. Under starving conditions with either low serum or low glucose, cytotoxicity of CPI-613 is amplified since net energy production exclusively relied on the TCA cycle/OXPHOS as shown in H460 lung cancer cells (Zachar et al., 2011).

In BxPC3 pancreatic tumour cells, but not in non-transformed NIH-3T3, CPI-613 caused a down-regulation of *cyclin D3*, *E1*, *E2*, *F*, *A2*, *B1* as analysed using a gene microarray (Lee et al., 2014). Multiple cyclins, p27, p19, and CDK2 were downregulated on RNA level in pancreatic, lung and gliosarcoma cancer cells treated with CPI-613 and hence potentially halting the cell cycle at diverse check points according to Perera et al. (2012). This halt in proliferation possibly leads to cell death as observed in a variety of cancer entities. Apoptotic as well as necrotic cell death appeared in H460 cells as early as 2 h post treatment with 240 µM CPI-613 as assessed using Annexin V/PI staining (Zachar et al., 2011). Using 160 µM CPI-613 for 24 h, both PARP as well as Caspase-3 cleavage were measured with concomitant apoptosis-associated morphological changes, e.g. membrane blebbing und nuclear subinclusions (Zachar et al., 2011). Since the pan-caspase inhibitor zVAD did not rescue cells from undergoing apoptosis, several redundant cell death pathways might be activated upon CPI-613 treatment (Zachar et al., 2011). In the prostate adenocarcinoma cell line LNCaP, CPI-613 (200 µM, 5 h) induced cell death as shown via the upregulation of NOXA (Arai et al., 2020). Apoptosis induction upon CPI-613 in pancreatic cancer cells was shown to be ROS- and AMPK-ACC-dependent and reversible by the addition of NAC as antioxidant (Gao et al., 2020). Extensive studies to detect apoptosis in the clear cell sarcoma cell line HS-MM, e.g. DNA fragmentation, by Egawa et al. (2018) failed, but necrosis in combination with chloroquine could be shown.

With respect to mitochondrial integrity, irreversible dissipation of mitochondrial membrane potential was shown in different cancer cell lines while mitochondria number and size were unchanged upon CPI-613 (Zachar et al., 2011; Mordhorst et al., 2019; Gao et al., 2020). Dramatically reduced mitochondrial cristae and overall altered

mitochondria morphology was recorded using transmission electron microscopy in pancreatic cancer cells (Gao et al., 2020).

In clear cell sarcoma cells, an induction of autophagosome formation followed by lysosome-fusion was found and an increase in autolysosome formation was observed after co-treatment with PS48, an activator of PDK1, in porcine foetal fibroblasts (Egawa et al., 2018; Mordhorst et al., 2019). In line with these observations, Gao et al. (2020) presented strong evidence of autophagy induction in pancreatic cancer cells *in vitro*, which is dispensable for the induction of apoptosis but mediated by the AMPK-ULK1-axis. Analysing lung cancer cells (H460) with induced stem cell-like properties and an EMT phenotype upon subchronic CPI-613 treatment, Perera et al. (2015) described the ability of CPI-613 to eliminate both parent and resistant cells depending solely on the duration of treatment.

In the context of AML, CPI-613 sensitised OCI-AML3 and MLF2 cells to chemotherapy, both indicating mitochondrial metabolism as a source of resistance and pointing towards a beneficial combination effect with the topoisomerase II inhibitor doxorubicin and antimetabolite cytarabine (Pardee et al., 2012). Another synergism was revealed in combination with the topoisomerase I inhibitor topotecan in lung cancer cell lines, namely DMS-114 and NCI-H69 (combination index (CI) = 0.87 and 0.51, respectively) (Lycan et al., 2016). Other studies showed CPI-613 to act synergistic with nilotinib (CI = 0.057-0.061) and with sorafenib (CI = 0.529-0.633) (Pardee et al., 2012). In these studies, knockdown of mutant p53 rendered cells more vulnerable to CPI-613.

CPI-613 has been used to induce a “reverse Warburg effect” in cells surrounding cancer, e.g. CAFs, detected by increased pyruvate and glutamine concentrations without affecting cellular proliferation or cell viability (Mordhorst et al., 2019). Overall, 27 genes and 21 metabolites switched to a “reverse Warburg effect”-like metabolism with an emphasis on lipid synthesis. The observed “reverse Warburg effect” was postulated as a driver for tumour growth and metastasis by supply of pyruvate to fuel gluconeogenesis and amino acid as well as fatty acid synthesis.

1.3.2.4. Biotransformation and Pharmacokinetics

CPI-613 was found to undergo oxidation in phase I metabolism with and without coupled *O*-glucuronidation at the terminal carboxyl moiety in phase II using human as well as animal liver S9 mixes *in vitro* (Lee et al., 2011). Only one distinct oxidation-metabolite of the parent compound is primarily formed by CYP2C8 and CYP3A4/5, although several potential reactive moieties are available. Furthermore, an uncommon sulphoxide metabolite of the CPI-613 glucuronide-metabolite is exclusively generated by human

species. In comparison to its metabolites, the parent compound is the most cytotoxic as assessed in CellTiter Blue Assays using lung and ovarian cancer cells (CPI-613 > CPI-613-O-Gluc > CPI-613-O-Gluc-SO_3 > CPI-613-OH) (Lee et al., 2011) (Figure 13).

Figure 13: (Human) Metabolism of CPI-613.
In humans, CPI-613 undergoes phase I metabolism (oxidation). Subsequently, the hydroxylated form of CPI-613 can undergo glucuronidation in phase II, which can further be transformed to an uncommon sulphoxide metabolite. The exact molecular structures are unknown. (created with PowerPoint, according to Lee et al. (2011))

In animals, metabolic half-life ranged between 8 to 47 min in minipigs and mice, respectively (Lee et al., 2011). In humans, Pardee et al. (2014) report a triphasic elimination with a first half-life of 1.34 h. In accordance, the half-life of the parent compound was calculated to be 2 h in humans compared to the major and active metabolite CPI-2850 (4,6-bis-benzylsulphanyloctanoic acid) with a half-life of 54 h, indicating enterohepatic circulation, in another study (Alistar et al., 2017). When the maximal daily dose of 2940 mg/m² CPI-613 was administered intravenously, plasma concentrations reached approx. 40 µM (Pardee et al., 2014).

Experiments revealed no sex difference in toxicokinetics, clinical and histopathological parameters as assessed in male and female rats and minipigs (Lee et al., 2011). In rats, a two-compartment toxicokinetic model with biphasic appearance, characterised by an initial distribution phase followed by a terminal elimination phase with a terminal half-life of approximately 2-5 hours could be determined. The toxicological profile of CPI-613, primarily, included inflammation in rats and minipigs. Furthermore, a rise in reticulocytes (due to haematopoietic cell proliferation of the spleen and sternal bone marrow hyperplasia) and γ-Glutamyl Transferase (due to histopathologically unconfirmed kidney or liver function) were found, but might be a secondary effect to the observed inflammation.

1.3.2.5. *In vivo* Studies

Preclinical evaluation of CPI-613 as an anticancer therapeutic agent have thus far been performed primarily on the basis of xenograft mouse models. Among these, focus has been set on lung and pancreatic cancer. In general, the maximum tolerated dose of CPI-613 was reported to be 100 mg/kg BW thrice per week in CD1-Nu/Nu female mice (Zachar et al., 2011).

Monitoring tumour growth of non-small lung cancer xenograft tumours of H460 cells in immunodeficient mice, 10 mg/kg BW CPI-613 administered once, thrice or five times per week significantly suppressed tumour growth regardless of the injection frequency (Zachar et al., 2011). Furthermore, pancreatic cancer BxPC3 tumours showed reduced growth by a factor of two and a 4-fold increased survival, when 25 mg/kg BW CPI-613 were injected once per week for four consecutive weeks (Zachar et al., 2011; Lee et al., 2014). CPI-613 performed superior to the first line therapeutic gemcitabine and post-treatment suppression was enhanced. In addition to primary tumour growth inhibition, CPI-613 (25 mg/kg BW) only in combination with chloroquine (50 mg/kg BW) using two injections per week for two weeks abolished mesenteric metastases formation in a metastasis model of clear cell sarcoma in SCID-mice with HS-MM cells (Egawa et al., 2018).

While no adverse side effects were recorded in mouse studies, neither haematologic alterations were found in minipigs in a differential blood analysis upon administration of 46 mg/kg BW CPI-613 twice per week for 21 days (Zachar et al., 2011). Maturo (2010) described the only and crucial side effect to be inflammation for high doses of CPI-613 in rats (35 mg/kg) and minipigs (55 mg/kg).

In the context of ovarian cancer, CPI-613 treatment decreased cancer stem cell frequency, represented by reduced expression of CD133 and CD117 as markers for stem-like features (Bellio et al., 2019). Consequently, ovarian cancer cells used in xenograft experiments displayed a diminished tumourigenicity upon CPI-613 treatment *in vivo*, as described by Bellio et al. (2019). Normally, olaparib, a PARP inhibitor, induces an increase in cancer stem cell frequency in ovarian cancer, which, however, can be negated using a pre-treatment with CPI-613. The sequential strategy, therefore, is of upmost importance and can delay cancer recurrence in the context of ovarian cancer. Although CPI-613 alone was able to reduce tumour growth in xenograft experiments, the combination with carboplatin/paclitaxel treatment further evidences tumour inhibiting potential *in vivo*. The combination was prior shown to negatively impact the enrichment of chemoresistant cells *in vitro* by the same research group (Bellio et al., 2019).

As a second generation of drug galenics and delivery, Li et al. (2019) invented a novel biodegradable copolymer of lysine- and PEG-based monomers in order to simultaneously co-deliver CPI-613, as apoptosis-inducing agent, and LY2109761, a TGF-β receptor I/II inhibitor, to pancreatic cancer cells in cell culture and mouse models. With a drug load of 15.13% CPI-613, CPI-613 as a hydrophobic drug is linked to the copolymer via an MMP-2-responsive moiety, whereas LY2109761 is encapsulated into

the core of the nanopolyplex. Directed to act within the tumour microenvironment, the nanopolyplex is modified to carry a plectin-1-targeting peptide next to the MMP-2-responsive element, which leads to increased accumulation within pancreatic cancer cells as confirmed using a murine biodistribution study. Beneficially, tumour growth was markedly inhibited in an orthotopic pancreatic cancer mouse model as compared to control animals and increased as compared to free drug delivery (Li et al., 2019).

Due to CPI-613 treatment and subsequent mitochondrial inhibition, glucose uptake is upregulated as cellular homeostasis response. Thus, PET scanning is not feasible in cancer patients receiving CPI-613 to monitor tumour size. However, ^{18}F-Fludeoxyglucose-PET/CT was used by Sai and colleagues to prove delivery of CPI-613 using BxPC3 pancreatic cancer cells (Sai et al., 2017). *In vivo* and *in vitro*, approx. 75% increase in ^{18}F-FDG shortly after treatment was measured. Later time points showed a decrease in glucose uptake indicating the initiation of cell killing.

The sum of the findings in *in vivo* studies demonstrate the antitumour activity of CPI-613 in a variety of cancer entities in mice next to its ability to prolong survival and to reduce the formation of cancer stem cells. These studies have proven its efficacy and mode of action and have set the basis for clinical studies in clinical cancer patients.

1.3.2.6. Clinical Trials

To date, approximately 20 clinical trials evaluated CPI-613 as monotherapy or building block in the therapy of a variety of cancers in the USA. Among these, multiple phase I, I/II, II and III studies assessed CPI-613 as single agent as well as in combination with standard drugs in patients with solid tumours and haematologic malignancies (Pardee et al., 2014). Conditions include relapsed or refractory small cell lung cancer, metastatic pancreatic cancer, metastatic bile duct cancer, metastatic colorectal cancer, Hodgkin-lymphoma or relapsed or refractory T-cell non-Hodgkin-lymphoma, previously treated myelodysplastic syndromes (MSD) and relapsed or refractory acute myeloid leukaemia (AML) or granulocytic sarcoma. In these studies, the safety, tolerability, and efficacy of CPI-613 have been evaluated. Fortunately, relatively few adverse events or toxic side effects were recorded. The most common side effects included vomiting, nausea and fatigue, headache, lymphopenia/neutropenia, diarrhoea and thus electrolyte imbalance, which is in accordance with animal studies (Maturo, 2010).

Pardee et al. (2014) reported CPI-613 in a first-in-man and phase I study in patients with advanced haematologic malignancies, including relapsed normal karyotype AML, refractory AML, Burkitt's lymphoma, and cutaneous T-cell lymphoma, to have a clinical

benefit rate of 29%. Although the toxicity profile was low with vomiting as the main side effect, acute renal failure was the main reversible complication when CPI-613 was administered twice a week for three consecutive weeks every 28 days. For patients with T-cell lymphoma, the overall response rate was 80% in combination with bendamustine and median time to response was 1.8 months (Lamar et al., 2016). In here, major side effects included lymphopenia and neutropenia. Generally, the maximum tolerable dose was 2940 mg/m² (infusion time of 2 h). Since inflammation occurred when CPI-613 was administered in the peripheral vein, infusion was given in the central vein. Responders were found to have upregulated T-cell activation, leukocyte activation and regulation of cytokine production in peripheral blood mononuclear cells, as proven with gene expression of *IFNG*, *CCL5*, *CRCR3*, *CD8A*, *CD3E* and *CD3D* (Pardee et al., 2014). Nonetheless, cytopenia improved on CPI-613 in several patients who did not meet criteria for a response.

Lee et al. (2014) demonstrated in a small phase I study that CPI-613 alone or in combination with gemcitabine improves the overall survival of stage IV pancreatic cancer patients in comparison to combinations of either abraxane and gemcitabine or FOLFIRINOX. Patients received 420-1300 mg/m² CPI-613 twice per week in a 3-week-on-1-week-off scheme.

Table 7: Overview of clinical trials related to CPI-613.
Information was retrieved from the webpage www.clinicaltrials.gov. Legend: active = active with/without recruiting, terminated = study stopped early with/without renewal, completed = ended normally. Effective date: September 2020.

Cancer Entity	*Drug(s)*	*Phase*	*Status*	*Related Publication*
		Solid Tumours		
Cancer (solid, advanced/ metastatic)	CPI-613	I (2008-2016)	Completed	Lee et al. (2014)
Small Cell Lung Cancer	CPI-613	I (2013-2015)	Completed	Lycan et al. (2016)
(Metastatic) Pancreatic Cancer	CPI-613	I (2013-2015)	Active	Anderson et al. (2018a)
(Metastatic) Pancreatic Cancer	CPI-613 + mFOLFIRINOX	I (2013-2020)	Active	Alistar et al. (2017)
Colorectal Cancer	**CPI-613 + 5-FU**	**I (2015-2022)**	**Active**	**Rocha Lima et al. (2019)**
Pancreatic Cancer	CPI-613 + Gemcitabine	I/II (2009-2017)	Terminated	Retter et al. (2010) Retter (2012) Lee et al. (2014)
Liver Cancer Bile Duct Cancer Gallbladder Cancer	CPI-613	I/II (2013-2018)	Active	Anderson et al. (2018a) further results available but not published
Biliary Tract Cancer	CPI-613 + Gemcitabine + Cisplatin	I/II (2020-2025)	Active	

Cancer Entity	*Drug(s)*	*Phase*	*Status*	*Related Publication*
Cancer (solid, advanced/ metastatic)	CPI-613	II (2013-2016)	Terminated	
(Metastatic) Pancreatic Cancer	CPI-613 + Gemcitabine + Nab-paclitaxel	II (2017-2019)	Active	Alistar et al. (2016)
Pancreatic Cancer	CPI-613 + mFOLFIRINOX	II (2018-2021)	Active	
Metastatic Pancreatic Cancer	CPI 613 + (m)FOLFIRINOX	III (2018-2022)	Active	AVENGER500 study Philip et al. (2019)
		Haematological Malignancies		
Advanced Haematologic Malignancies	CPI-613	I (2010-2014)	Completed	Pardee et al. (2014)
Acute Myeloid Leukaemia	CPI-613 + Cytarabine + Mitoxantrone	I (2013-2016)	Completed	Pardee et al. (2018) Pardee et al. (2019)
Lymphoma (B-cell / Non-Hodgkin)	CPI-613 + Bendamustine + Rituximab	I (2014-2015)	Terminated	
Lymphoma (T-Cell / Hodgkin / Non-Hodgkin)	CPI-613 + Bendamustine	I (2014-2022)	Active	Lamar et al. (2016)
Myelodysplastic Syndrome Progressive Disease	CPI-613 + Hydoxychloroquine	I/II (2020-2026)	Active	
Myelodysplastic Syndrome	CPI-613	II (2013-2020)	Terminated	Anderson et al. (2018a)
Granulocytic Sarcoma Acute Myeloid Leukaemia	CPI-613 + Cytarabine + Mitoxantrone	II (2015-2022)	Active	
Leukaemia Lymphoma (B-Cell / Burkitt)	CPI-613	II (2018-2021)	Active	
Lymphoma (T-Cell / Non Hodgkin)	CPI-613 + Bendamustine	II (2020-2025)	Active	
Acute Myeloid Leukaemia	CPI-613 + Cytarabine + Mitoxantrone	III (2018-2023)	Active	ARMADA2000 study Pardee et al. (2019)

A phase II clinical trial with CPI-613 monotreatment of patients with relapsed or refractory small cell lung carcinoma was closed early due to lack of efficacy (Lycan et al., 2016). A dose of 3000 mg/m² CPI-613 was administered to patients twice weekly for 3 weeks followed by 7 days of rest. Toxicities included nausea, vomiting and headache. However, patients receiving CPI-613 were found to be sensitised to topotecan treatment because their response rate was elevated. These results were reproducible *in vitro* (see section 1.3.2.3).

With regard to CPI-613 in the treatment of metastatic pancreatic cancer, a phase I study was conducted in combination with the modified first line therapy regimen FOLFIRINOX (Alistar et al., 2016; Alistar et al., 2017; Alistar et al., 2019). Pancreatic cancer patients received 500 mg/m² CPI-613 two days in a row at the beginning of each mFOLFIRINOX cycle, that was repeated 11 times on average. In general, the combination was feasible and tolerable and the sum of partial and complete response rate was 61% (11 out of 18 patients), which was about twice as high as in the mFOLFIRINOX control group. Moreover, CPI-613 did not add toxicity to the therapy regimen in terms of adverse side effects. Regarding these patients, *KRAS* as well as *TP53* mutations were common. Most frequent haematological toxicities were anaemia, thrombocytopenia as well as lymphopenia, although they were comparable to the control group. Other toxicities included diarrhoea, fatigue, electrolyte imbalance and sensorial neuropathy. This study encourages for the possible synergy with standard care chemotherapy without additional toxicity. Based on this phase I study, an open-label phase III trial evaluating the safety and efficacy of CPI-613 plus modified FOLFIRINOX versus FOLFIRINOX in patients with metastatic adenocarcinoma of the pancreas in the AVENGER500 study was initiated (Philip et al., 2019).

In combination with high-dose cytarabine and mitoxantrone, a phase I study for relapsed or refractory AML evaluated CPI-613 (2500 mg/m²) not to increase the 30- or 60-day mortality compared to historic data and the response rate to be 48 % (Pardee et al., 2015; Pardee et al., 2019). However, an increased response rate was detected, especially in patients of advanced age and poor performance. Pardee et al. (2018) postulated that the reason is the low spare respiratory capacity of decreased mitochondria quality associated with age, which would be the presentation of aging-derived vulnerability of cancer for the first time. Non-responders, respectively younger patients, showed a significantly increased level of superoxide dismutase 2, while responders showed an overexpression in immune system and B-cell activation (*CD79A*, *MS4A1*, *FCRL2*, *TCL1A*, *BANK1*+, *CD19*+). Side effects included nausea and diarrhoea. In the combined phase I/II study, older patients with relapsed/refractory AML treated with 2000 mg/m^2 of CPI-613 had a 52% complete remission/partial remission with incomplete hematologic recovery rate and a median survival of 12.4 months. In this study, AML cell were postulated to upregulate the TCA cycle in response to DNA damaging agents and treatment with CPI-613 increased their sensitivity. Upon successful completion of phase I/II, CPI-613 was combined with high dose cytarabine and mitoxantrone or with high dose cytarabine and mitoxantrone in older patients with relapsed/refractory AML in the ARMADA2000 phase III study (Pardee et al., 2019).

A retrospective study from three previous phase II open-label studies analysed the incidence and severity of acute kidney injury (AKI) associated with CPI-613 (Anderson et al., 2018a). Overall, 5 out of 33 patients developed a reversible AKI with moderate severity. With a median latent time of 51 days, especially older patients possessed an increased risk. Although no causality could be identified, Anderson et al. (2018a) hypothesised that ROS and increased ammoniagenesis upon truncated glutamine flux in combination with the highly metabolically active renal epithelia in the need for large amounts of ATP easily lead to AKI.

Since December 2018, CPI-613, which is now traded with its brand name Devimistat®, has been granted orphan drug status by the European Medicines Agency (EMA) for the treatment of AML and pancreatic cancer. Starting in 2006 throughout 2018, the US-American Food and Drug Agency (FDA) records list CPI-613 with orphan drug status additionally for myelodysplastic syndrome (MDS), peripheral T-cell lymphoma and Burkitt's lymphoma.

2. OBJECTIVES

The aim of this work is to assess the potential synergistic effect by implementing lipoates, e.g. LA and its derivative CPI-613, in the treatment regimen in the therapy of CRC with standard chemotherapeutics, e.g. 5-FU and IT, in cell culture and mouse models. In the scope of this assessment, a four-step-approach shall be applied as follows. The subsequent questions and principles shall be addressed and employed. Since a robust set of data on LA is available in previously performed work and the literature (see section 1.3.1), the beginning of this work shall focus on the recently developed derivative CPI-613.

1. First, the proposed **mode of action**, i.e. the disruption of mitochondrial integrity and function, shall be verified in the context of CRC. To this end, isolated mitochondria and CRC cell lines shall be treated with **CPI-613**.

- Can the proposed mode of action of CPI-613 be confirmed in isolated mitochondria and CRC cell lines?
- What are the observation and changes in terms of mitochondrial integrity and function in CRC cells?
- To which extent is the cellular energy metabolism dramatically affected upon CPI-613?

2. Second, the **cellular response to CPI-613** treatment as single agent shall be examined. In the course of this work, a panel of CRC cell lines shall be screened. Focus shall later be set to two representative cell lines, which will be used to evaluate particular endpoints in detail and the potential of lipoates in combination with standard chemotherapeutics later on.

- Are cellular responses to the treatment with CPI-613 in CRC cell lines similar to observations in other cancer entities?
- What characterises the cellular response in terms of cytotoxicity, cell death induction and autophagy?
- Does CPI-613 exclusively target the mitochondria and their function? Does CPI-613 show genotoxic traits by damaging DNA?

3. Third, lipoates (LA, CPI-613) in **combination** with standard chemotherapeutics (5-FU, IT) shall be assessed for their synergistic potential ***in vitro***. This shall provide a basis of information and selection criteria for animal experiments.

- Which lipoate is more suitable as building block in the treatment of CRC? With which standard chemotherapeutic does this lipoate show the greatest potential for synergism? This lipoate shall be used in

combination with the selected standard chemotherapeutic in the treatment regimen for murine therapy efficacy trials.

- At which dose levels does the synergism occur most prominently?
- Upon selection of dose levels, what characterises the synergism? Which endpoints in terms of cell death induction, DNA damage levels and autophagy are particularly improved?

4. Fourth, *in vitro* findings shall be **transferred to animal experiments**. Mouse models expressing CRC shall be used to assess **therapeutic efficacy** and benefits of combination treatment in comparison to monotreatment and standard chemotherapeutics ***in vivo***. The applicability of a combination of lipoates with standard chemotherapeutic agents shall be evaluated.

- Does the selected lipoate show anticancer activity as single agent in the treatment of CRC in mouse models in comparison to a standard chemotherapeutic agent?
- To which extent and with what kind of limitations does this lipoate show synergism in terms of tumour growth inhibition, survival of animals and occurrence of side effects in murine models of CRC?

3. MATERIALS & METHODS

3.1. Materials

3.1.1. Chemicals

Table 8: List of chemicals used.

Name	*Concentration*	*Manufacturer*
0.9% NaCl for injection		Braun, Kronberg, Germany
5-fluorourcail (5-FU)	50 mg/ml = 384 mM	Pharmacy of the University Medical Centre Mainz (original source: medac, Wedel, Germany)
α-lipoic acid (LA)	200 mM in EtOH (p.a.)	Merck, Darmstadt, Germany
β-mercapto-ethanol		Carl Roth GmbH & Co. KG, Karlsruhe, Germany
Acetic acid		Carl Roth GmbH & Co. KG, Karlsruhe, Germany
Agarose		Carl Roth GmbH & Co. KG, Karlsruhe, Germany
Ammonium persulphate (APS)	100 mg/ml in ddH_20	Carl Roth GmbH & Co. KG, Karlsruhe, Germany
AnnexinV-FITC		Miltenyi, Bergisch Gladbach, Germany
Azoxymethane (AOM)	stock: 10 mg/ml in H_2O working solution: 1 mg/ml in PBS	Merck, Darmstadt, Germany
Bovine serum albumin (BSA)		Carl Roth GmbH & Co. KG, Karlsruhe, Germany
Bromophenol blue		Merck, Darmstadt, Germany
Calcium chloride ($CaCl_2$)		Merck, Darmstadt, Germany
Citric acid		Carl Roth GmbH & Co. KG, Karlsruhe, Germany
CM-H_2DCFDA	50 mg/ml in DMSO	Invitrogen, Darmstadt, Germany
cOmplete protease inhibitor		Roche Diagnostics GmbH, Mannheim, Germany
Coomassie Brilliant Blue G250		Merck, Darmstadt, Germany
Corneregel®		Bausch+Lomb, Berlin, Germany
Coumaric acid	90 mM	Merck, Darmstadt, Germany
CPI-613 (for *in vitro* studies)	50 mg/ml in DMSO	Cayman / Biomol, Hamburg, Germany
CPI-613 (for *in vivo* studies)	50 mg/ml in 1 M TEA	Hölzel diagnostika, Köln, Germany (original source: ChemMedExpress, Nonmouth Junction, USA)
CPI-613 (for *in vitro* and *in vivo* studies)	see above	Hycultec GmbH, Beutelsbach, Germany (original source: ChemMedExpress, Nonmouth Junction, USA)

Name	*Concentration*	*Manufacturer*
D5W (dextrose 5% in water) for injection		Braun, Kronberg, Germany
Dextran sulphate sodium salt, colitis grade (DSS)	1% in drinking water	MP Biomedicals, Illkirch, France
Dimethylformamide		Carl Roth GmbH & Co. KG, Karlsruhe, Germany
Dimethyl sulphoxide (DMSO)		Carl Roth GmbH & Co. KG, Karlsruhe, Germany
Disodium phosphate (Na_2HPO_4)		Carl Roth GmbH & Co. KG, Karlsruhe, Germany
Dithiothreitol (DTT)	1 M	Merck, Darmstadt, Germany
DMEM/Häm F12 1:1		Gibco Life Technologies, Darmstadt, Germany
DMEM (high glucose)		Gibco Life Technologies, Darmstadt, Germany
DMEM (high glucose), phenolred-free		Gibco Life Technologies, Darmstadt, Germany
Entellan®		VWR, Darmstadt, Germany
Ethanol (EtOH)		Merck, Darmstadt, Germany
Ethylenediaminetetraacetic acid (EDTA)	100 mM	Carl Roth GmbH & Co. KG, Karlsruhe, Germany
Foetal calf serum (FCS) / foetal bovine serum (FBS)		Gibco Life Technologies, Darmstadt, Germany; PAN-Biotech GmbH, Aidenbach, Germany
Formamidopyrimidine DNA glycosylase (FPG)	13 mg/l	[redacted]
Glycerol		Carl Roth GmbH & Co. KG, Karlsruhe, Germany
Glycine		Carl Roth GmbH & Co. KG, Karlsruhe, Germany
H_2O for injection (Aqua®)		Braun, Kronberg, Germany
HEPES		Carl Roth GmbH & Co. KG, Karlsruhe, Germany
Histofix® 4%		Carl Roth GmbH & Co. KG, Karlsruhe, Germany
Hydrogen chloride (HCl)		Carl Roth GmbH & Co. KG, Karlsruhe, Germany
Hydrogen peroxide (H_2O_2; 30%)		Carl Roth GmbH & Co. KG, Karlsruhe, Germany
IMDM		Gibco Life Technologies, Darmstadt, Germany
Irinotecan (IT)	20 mg/ml = 34 mM	Pharmacy of the University Medical Centre Mainz (original source: Fresenius Kabi, Bad Homburg, Germany)
Isopropanol		Carl Roth GmbH & Co. KG, Karlsruhe, Germany
Ketamine	10%	Medistar Arzneimittelvertrieb GmbH, Ascheberg, Germany
Low melting point agarose		Carl Roth GmbH & Co. KG, Karlsruhe, Germany
Luminol	250 mM	Merck, Darmstadt, Germany

Name	*Concentration*	*Manufacturer*
Magnesium chloride ($MgCl_2$)		Carl Roth GmbH & Co. KG, Karlsruhe, Germany
MAXblock™ blocking medium		Active Motif, La Hulpe, Belgium
MEM		PAN-Biotech GmbH, Aidenbach, Germany
Methanol		Merck, Darmstadt, Germany
Milk powder (blotting grade, low fat)	5% in TBS-T	Carl Roth GmbH & Co. KG, Karlsruhe, Germany
MitoTracker™ Orange		ThermoFisher Scientific, Darmstadt, Germany
Necrostatin-1	77 mM in DMSO	SelleckChem, Houston, USA
Non-essential amino acids (NEAA)		Gibco Life Technologies, Darmstadt, Germany
NP-40		Merck, Darmstadt, Germany
Paraffin (Paraplast PLUS®)		Carl Roth GmbH & Co. KG, Karlsruhe, Germany
Paraformaldehyde (PFA)		Carl Roth GmbH & Co. KG, Karlsruhe, Germany
Penicillin/Streptomycin (Pen/Strep)	10,000 U/ml	Merck, Darmstadt, Germany
Phenyl methane sulphonyl fluoride (PMSF)	100 mM	Merck, Darmstadt, Germany
Phosphoric acid (H_3PO_4; 85%)		Carl Roth GmbH & Co. KG, Karlsruhe, Germany
Phosphate-buffered saline (PBS)		Gibco Life Technologies, Darmstadt, Germany
Polyethylene glycol (PEG) 300		Carl Roth GmbH & Co. KG, Karlsruhe, Germany
Ponceau-S		Carl Roth GmbH & Co. KG, Karlsruhe, Germany
Propidium iodide (PI)		Merck, Darmstadt, Germany
RNase A	10 mg/ml	Merck, Darmstadt, Germany
Rotenone	50 mg/ml in DMSO	Merck, Darmstadt, Germany
Rotiphorese® Gel 40 (37.5:1) Acrylamide		Carl Roth GmbH & Co. KG, Karlsruhe, Germany
RPMI 1640		Gibco Life Technologies, Darmstadt, Germany
Sodium chloride (NaCl)		Merck, Darmstadt, Germany
Sodium deoxycholate		VWR, Darmstadt, Germany
Sodium dodecyl sulphate (SDS)		Carl Roth GmbH & Co. KG, Karlsruhe, Germany
Sodium fluoride (NaF)	1 M	Merck, Darmstadt, Germany
Sodium hydroxide (NaOH)		Carl Roth GmbH & Co. KG, Karlsruhe, Germany
Sodium lauroyl sarcosinate		Carl Roth GmbH & Co. KG, Karlsruhe, Germany
Sodium orthovanadate (Na_3VO_4)	200 mM	Merck, Darmstadt, Germany

Name	*Concentration*	*Manufacturer*
TEMED (N,N,N',N'-Tetramethyl ethylenediamine)		Carl Roth GmbH & Co. KG, Karlsruhe, Germany
***tert*-Butyl hydroperoxide (tBOOH)**	10 mM in ddH_20	Merck, Darmstadt, Germany
Tissue Freezing Medium Jung		ThermoFisher Scientific, Darmstadt, Germany
TO-PRO3	1:100 in PBS	Thermo Fisher Scientific, Darmstadt, Germany
Triethanolamine (TEA)	1 M to solve CPI-613	Merck, Darmstadt, Germany
Tris		Carl Roth GmbH & Co. KG, Karlsruhe, Germany
Triton X-100		Merck, Darmstadt, Germany
Trypsin/EDTA		Merck, Darmstadt, Germany
Tween 20		Carl Roth GmbH & Co. KG, Karlsruhe, Germany
VectaShield® Mounting Medium		Vecta Laboratories, Burlingame, USA
Western Lightning Plus-ECL, Enhanced Chemiluminescence Substrate		Perkin Elmer, Waltham, USA
Xylazine	2%	Ceva Tiergesundheit GmbH, Düsseldorf, Germany
Xylol		Carl Roth GmbH & Co. KG, Karlsruhe, Germany
zVAD-FMK	20 mM in DMSO	SelleckChem, Houston, USA

3.1.2. Buffer and solutions

Table 9: List of buffers and solutions and their composition.

SDS-PAGE and Western Blotting	
Whole cell extract lysis buffer	25 mM Tris-HCl pH 8.0 500 mM NaCl 5 mM EDTA 1 mM PMSF 2 mM DTT 1 mM Na_3VO_4 2 mM NaF 0.5 % NP-40 1x cOmplete protease inhibitor
RIPA buffer for xenograft tumours	25 mM Tris-HCl (pH 7.4) 150 mM NaCl 0.1% SDS 1% sodium deoxycholate 1% NP-40 50 mM NaF 0.2 mM Na_3VO_4 2 mM EDTA 1 mM PMSF 1x cOmplete protease inhibitor
TBS-T	150 mM NaCl 10 mM Tris 0.05% Tween 20
10 x SDS-PAGE running buffer	66 g Tris

	288 g Glycine ad 2 l H_2O Diluted to 1x using H_2O and 0.1% SDS added
10 x Western Blot transfer buffer	66 g Tris 288 g Glycine ad 2 l H_2O Diluted to 1x using H_2O and 20% methanol added
5 x Lämmli buffer	312.5 mM Tris-HCl pH 6.8 10% (w/v) SDS 25% (v/v) Glycerol 0.015% (w/v) bromophenol blue 3.75% (v/v) β-mercapto-ethanol Diluted to 1x using H_2O
Bradford reagent	10 mg Coomassie Brilliant Blue G250 solved in 5 ml ethanol 10 ml H_3PO_4 (85%) added ad 100 ml H_2O
Ponceau-S staining solution	0.2% Ponceau-S 5% acetic acid
Enhanced Chemiluminescence (ECL) solutions	Solution A: 500 µl 1 M Tris-HCl pH 9 50 µl 250 mM luminol 22 µl 90 mM coumaric acid ad 5 ml H_2O Solution B: 500 µl 1 M Tris-HCl pH 9 50 µl 30% H_2O_2 ad 5 ml H_2O mixed 1:1
InCellWestern	
4 % paraformaldehyde	4 g PFA in 10 ml PBS + 50 ml ddH_2O dissolved with NaOH pH 7.4 adjusted with HCl ad 100 ml ddH_2O
Neutralisation solution	50 mM NH_4Cl in PBS
Saturation solution	1% RNase A 10% cOmplete protease inhibitor in MAXBlock solution
PST	2% FCS 0.2% Triton X-100 in PBS
Annexin V / PI staining	
Annexin binding buffer	10 mM HEPES 140 mM NaCl 2.5 mM $CaCl_2$ 0.1 % BSA pH 7.4
Propidium iodide (PI)	50 µg/ml working solution prepared from 1 mg/ml stock solution in H_2O Stored at 4°C in the dark
Alkaline Comet assay with/without FPG	
Lysis buffer	2.5 M NaCl 100 mM EDTA 10 mM Tris pH 10 directly before use: addition of 1% sodium lauroyl sarcosinate and cooling for 1 h at 4°C
Electrophoresis Buffer	30 ml NaOH

	5 ml EDTA pH 13
Neutralization Buffer	0.4 M Tris pH 7.5
Buffer F	40 mM HEPES 0.1 M HEPES 0.5 mM EDTA 0.2 mg/ml BSA pH 8.0
Anaesthesia	
Anaesthesia solution for i.p. injection	4 ml 0.9% NaCl + 400 µl Xylazine + 600 µl Ketamine

3.1.3. Kits

Table 10: List of kits used.

Name	*Manufacturer*
CellTiter-Glo® Luminescent Cell Viability Assay	Promega, Madison (WI), USA
CytoID® Green Autophagy Detection Kit	Enzo Life Sciences, Lörrach, Germany
CytoSelect™ Invasion Assay	Cell Biolabs, San Diego (CA), USA
HE Quick Staining Kit	Carl Roth GmbH & Co. KG, Karlsruhe, Germany
Mitochondria Staining Kit	Merck, Darmstadt Germany (Sigma Aldrich)
Venor® GeM Mycoplasma Detection Kit	Minerva Biolabs, Berlin, Germany
Western Lightning Plus-ECL	PerkinElmer, Waltham (MA), USA

3.1.4. Consumables

Table 11: List of consumables used.

Name	*Manufacturer*
6-well-plate	Greiner Bio-One, Frickenhausen, Germany
black 96-well-plate, clear bottom	Greiner Bio-One, Frickenhausen, Germany
cell culture dish (10 cm, 6 cm, 3.5 cm)	Greiner Bio-One, Frickenhausen, Germany
cover slips	Diagonal, Münster, Germany
cryovial	Greiner Bio-One, Frickenhausen, Germany
Eppendorf reagent tube (1.5 ml)	Eppendorf AG, Hamburg, Germany
FACS tubes	SARSTEDT AG & Co. KG, Nümbrecht, Germany
falcon (15 ml, 50 ml)	Greiner Bio-One, Frickenhausen, Germany
Injekt®-F (1 ml) syringe	Braun, Kronberg, Germany
Micro-fine+ insulin syringe 0.3 ml U100	BD Biosciences, Heidelberg, Germany
Microvette® 200 K3E	SARSTEDT AG & Co. KG, Nümbrecht, Germany
object slides	Diagonal, Münster, Germany
Omnican® lance	Braun, Kronberg, Germany
PageRuler™ Plus Prestained Protein Ladder	ThermoFisher Scientific, Darmstadt, Germany
pipette tips	Greiner Bio-One, Frickenhausen, Germany Star Lab, Hamburg, Germany

Name	*Manufacturer*
plastic pipettes (5, 10, 25, 50 ml)	Greiner Bio-One, Frickenhausen, Germany
Protran® nitrocellulose membrane (0.2 µm)	PerkinElmer, Waltham (MA), USA GE Healthcare, Chicago (IL), USA
Rotilabo® blotting paper (1mm)	Carl Roth GmbH & Co. KG, Karlsruhe, Germany
Rotilabo® embedding cassettes	Carl Roth GmbH & Co. KG, Karlsruhe, Germany
Sterican® canula (G20 and G26)	Braun, Kronberg, Germany
SuperFrost Plus™ Object Slides	ThermoFisher Scientific, Darmstadt, Germany
white 96-well-plate, half area	Greiner Bio-One, Frickenhausen, Germany

3.1.5. Equipment

Table 12: List of equipment used.

Name	*Manufacturer*
Azure c300 Chemiluminescence Imager	azure biosystems, Dublin (CA), USA
B15 Incubator	Heraeus, Hanau, Germany
Biofuge™ centrifuge	Heraeus, Hanau, Germany
Centrifuge 5424R	Eppendorf, Hamburg, Germany
Centrifuge 5804	Eppendorf, Hamburg, Germany
ChemiDoc™ Gel Imaging System	BioRad, München, Germany
Digital Caliper Digi Plus 20-2002	Vogel GmbH, Kevelaer, Germany
Endoscope Image 1 S plus H3-Z LINK and FI	Karl Storz, Tuttlingen, Germany
FACS Canto II	BD Biosciences, Heidelberg, Germany
Fluoroskan Ascent FL 2.6 Luminometer	ThermoFisher Scientific, Darmstadt, Germany
Fridge-Freezer Combination	Liebherr, Biberach an der Riß, Germany
Heracell 240i incubator	Heraeus, Hanau, Germany
Infrared imaging system Odyssey 9120	LI-COR, Bad Homburg, Germany
Leica ASP 300 S automated dehydrator	Leica Microsystems, Wetzlar, Germany
Leica CM3050 S Cyrostat	Leica Microsystems, Wetzlar, Germany
Leica DM 6000 B fluorescence microscope	Leica Microsystems, Wetzlar, Germany
Leica DMi1 Light Microscope + Leica MC170 HD camera	Leica Microsystems, Wetzlar, Germany
Leica EG1140 H embedding station	Leica Microsystems, Wetzlar, Germany
Luminometer Tristar² Multimode reader LB942	Berthold Technologies GmbH &Co KG, Bad Wildbach, Germany
Micro Scale Quintix	Sartorius, Göttingen, Germany
Mini-PROTECAN Tetra Cell System	BioRad, München, Germany
Mini-Trans Blot® Module	BioRad, München, Germany
Mr. Frosty™ Freezing Container	ThermoFisher Scientific, Darmstadt, Germany
MSC-Advantage™ Laminar Flow Cabinet	ThermoFisher Scientific, Darmstadt, Germany
Neubauer chamber	Marienfeld, Lauda-Königshofen, Germany
Pipetboy acu 2	Integra, Biebertal, Germany
Power-Pac™ Basic Power Supply	BioRad, München, Germany
Precision Balance PCB 200-2	Kern & Sohn, Balingen, Germany
ProCyte Dx	IDEXX Laboratories, Westbrook (ME), USA
Research Plus pipettes	Eppendorf, Hamburg, Germany
Rocking shaker 35 EZ	Faust, Klettgau, Germany
Rotina 35 centrifuge	Andreas Hettich GmbH & Co.KG

Name	*Manufacturer*
Sprout Minicentrifuge	Biozym, Hessisch Oldendorf, Germany
Sub Aqua Pro water bath	Grant Instruments, Cambridge, United Kingdom
Sub-Cell® Model 96 Cell	BioRad, München, Germany
ThermoMixer® C	Eppendorf, Hamburg, Germany
Thermoschüttler pro	CellMedia GmbH & Co. KG, Elsteraue, Germany
Transferpette S-8 multi-channel-pipette	Brand, Großolbersdorf, Germany
TSX Ultra Low Freezer	ThermoFisher Scientific, Darmstadt, Germany
Unimax 2010 rotating platform	Heidolph Instruments GmbH & Co. KG, Schwabach, Germany
VACUSAFE suction pump	Integra, Biebertal, Germany
Vortex-Genie 2	Scientific Industries Inc., Boehmie (NY), USA
Water Bath JB Nova	Grant, Shepreth, UK
Zeiss LSM 880	Zeiss, Oberkochen, Germany

3.1.6. Software

Table 13: List of software used.

Name	*Manufacturer*
BD FACS Diva, version 6	BD Biosciences, Heidelberg, Germany
Citavi, version 5.2	Swiss Academic Software GmbH, Wädenswill, Switzerland
Combenefit	Cancer Research UK Cambridge Institute, Cambridge, UK
Comet Assay IV	Instem Genetic Toxicology Solutiions, Bury St Edmunds, UK
CompuSyn	ComboSyn, Inc., Paramus (NJ), USA
GraphPad Prism, version 8.0	GraphPad Software, La Jolla (CA), USA
Image J	U.S. National Institutes of Health, Bethesda (MD), USA
Image Lab Software, version 6.0.1	Bio-Rad Laboratories, Hercules (CA), USA
Image Studio Light, version 5.2	LI-COR, Lincoln (NE), USA
LAS EZ, version 3.4	Leica Microsystems, Wetzlar, Germany
LAS X	Leica Microsystems, Wetzlar, Germany
Microsoft Office 365	Microsoft Cooperation, Redmond (WA), USA
Odyssey, version 3.0	LI-COR, Lincoln (NE), USA
ProCyte Dx software	IDEXX Laboratories, Westbrook (ME), USA
VLC player	VideoLAN, Châtenay-Malabry, France
ZEN blue lite, version 3	Zeiss, Oberkochen, Germany

3.2. Methods

3.2.1. Cell culture

Cell culture experiments were performed under sterile conditions and under a laminar flow cabinet. Reagents and consumables were either purchased sterile, sterile-filtered or sterilised using 70% ethanol before use. Cultivation of cell lines was performed in

incubators under standardised conditions at 37°C, 5% CO_2 and humidified atmosphere. Regarding HCEC cells, atmosphere was additionally complemented with N_2 in order to reduce the O_2 content in air to 7%.

3.2.1.1. Cell lines

In Table 14, all cell lines used in this work are listed with their corresponding culture medium and supplements as well as their genetic features (Roig et al., 2010; Ahmed et al., 2013; Maletzki et al., 2015).

Table 14: Panel of screened cell lines including source, culturing conditions and genetic features.

Name	*Medium & Supplements*	*Source*	*p53*	*MSI*	*KRAS*	*BRAF*
		Established				
		human				
HCT116	DMEM		wt	MSI	G13D	wt
HCT116-p53$^{-/-}$	DMEM		knock out	MSI	G13D	wt
LS-174T	IMDM		wt	MSI	G12D	wt
RKO	DMEM		wt	MSI	wt	V600E
SW48	RPMI		wt	MSI	wt	wt
DLD-1	DMEM		S241F	MSI	G13D	wt
HT29	RPMI		R273H	MSS	wt	V600E
CaCo-2	MEM + 1x NEAA		E204X/-	MSS	wt	wt
SW480	RPMI		R273H, P309S	MSS	G12V	wt
		Patient-derived				
HROC60	DMEM/ Häm F-12		R273H	MSS	wt	unkown
HROC278	DMEM/ Häm F-12		wt	MSI-L	unkown	unkown
		Non-transformed				
HCEC	Basal HCEC medium		wt	MSS	wt	unkown

Cell lines were routinely tested for mycoplasma contamination using the PCR-based kit Venor®GeM Mycoplasma Detection Kit (Minerva Biolabs). Morphology and morphological changes of cells were documented using Leica DMi1 Light Microscope and Leica MC170 HD camera (Leica Microsystems).

3.2.1.2. Cultivation of cells

Routinely, cell lines were passaged for a maximum of 25 passages by removal of the medium, washing with PBS, detachment with Trypsin/EDTA and resuspension in fresh medium. In order to guarantee exponential growth, cells were passaged prior to reaching confluent monolayers. All cell lines used were grown in medium supplemented with 10%

FCS and 1% Pen/Strep. Alternatively to direct passaging, cells were counted using a Neubauer counting chamber and seeding as described for each individual method.

Stocks of cell lines were prepared by freezing approximately 5 x 10^6 cells per cryotube in medium supplemented with 10% FCS and 10% DMSO at a freezing rate of 1°C/min. Long-term storage was carried out in liquid nitrogen tanks. Thawing of cells comprised of heating the cryotube to 37°C and dilution of the content with excess of warm medium. Upon mild centrifugation, cells were seeded in freshly prepared medium and passaged for one to two weeks before utilization for experiments.

3.2.1.3. Treatment of cells

Unless otherwise stated, adherent cell lines were seeded the day before treatment to allow for attachment and cell densities were chosen to guarantee exponential growth. An overview of seeded cell densities can be found in the Annex.

For cell culture experiments, LA was prepared in a 200 mM stock solution in EtOH (p.a.), stored at 4°C and protected from light for a maximum of 5 days. CPI-613 purchased from Hölzel diagnostika (Köln, Germany) or Hycultec (Beutelsbach, Germany) was dissolved in DMSO to yield a 50 mg/ml (125 mM) solution and stored at -20°C. 5-FU (50 mg/ml in 0.9% NaCl) and IT (20 mg/ml in 0.9% NaCl) were obtained from the pharmacy of the University Medical Centre Mainz and originally purchased from Fresenius Kabi (Bad Homburg, Germany) and medac (Wedel, Germany), respectively.

Treatment was performed upon change of growth medium. In combination treatments, cells were pre-treated with LA or CPI-613 for 1.5 to 2 h prior to treatment with cytostatics without an additional change of growth medium. Respective solvent controls were carried along in each experiment.

If the apoptosis inhibitor zVAD-FMK (zVAD; dissolved in DMSO; stock: 20 mM; SelleckChem; Houston, USA) was used, its supplementation was performed 8 and 24 h after drug treatment using a final concentration of 20 µM. With respect to Necrostatin-1 (Nec-1; dissolved in DMSO; stock: 77 mM; SelleckChem; Houston, USA), its treatment scheme was identical to zVAD and was used in a final concentration of 10 µM.

3.2.2. Protein isolation and analysis

3.2.2.1. Preparation of protein lysates using whole cell lysis

For protein lysate preparation, attached and detached cells were collected together using Trypsin/EDTA. Upon washing with PBS, pelleted cells were resuspended in 120 µl buffer containing 25 mM Tris-HCl pH 8, 5 mM EDTA, 0.5% NP-40, 0.5 M NaCl and the following proteases inhibitors: 1 mM PMSF, 2 mM DTT, 1 mM Na_3VO_4, 2 mM NaF and

1x cOmplete Protease Inhibitor (Roche). The cell suspension was incubated for 15 min at 4°C under constant rotation. After centrifugation for 10 min at 4°C with 10,000 rpm, the supernatant was kept as debris-free lysate and protein content was determined using the Bradford assay. Protein content was measured using dilutions of 1:25 of each sample. A standard curve was obtained by measuring BSA standards (0-200 µg/ml). Protein amounts were adjusted using miliQ H_2O and adequate volumes of 5x Lämmli buffer were added, followed by denaturation for 5 min at 95°C.

If protein lysis was not necessary, adherent cells were harvested by direct resuspension in 1x Lämmli buffer. To this end, cell culture medium was removed and dishes were washed with PBS. Afterwards, approximately 100 µl of 95°C hot 1x Lämmli buffer was added to each dish (3.5 cm, non-confluent layer of cells) and cells were detached by scratching with a pipette tip. Upon transfer into Eppendorf tubes, collected samples were denatured for 5 min at 95°C.

3.2.2.2. Protein analysis based on SDS-PAGE and Western Blotting

Proteins were separated by molecular weight using a sodium dodecyl sulphate polyacrylamide gel electrophoresis (SDS-PAGE). By uniform negative charging using SDS, proteins can be separated by size.

At first, gels were prepared by casting the stacking gel onto a separation gel using a casting stand (Mini-Protecan® Tetra Cell, Biorad) (Table 15). After complete polymerization, gels were inserted in a Mini-Protecan® Tetra Cell (Biorad) and denatured samples (5 min, 95°C) were loaded into the wells. Samples were prepared as described in 3.2.2.1. PageRuler™ Plus Prestained Protein Ladder (5 µl, ThermoFisher Scientific) was used additionally in one well. Electrophoresis was performed in 1x SDS-PAGE running buffer. During electrophoresis in the stacking gel, running conditions were set to constant voltage at 50 V. Once samples reached the separation gel, running conditions were changed to constant voltage at 100 V.

Table 15: Composition of SDS-PAGE-gels.

Components	***Separation gel***			***Stacking gel***
	10 %	12.5 %	15 %	5%
Acrylamide / Bisacrylamide (40 %)	4.5 ml	5.63 ml	6.75 ml	0.75 ml
Tris (0.625 M, pH 6.8)	-	-	-	1.2 ml
Tris (1.5 M, pH 8.8)		4.5 ml		-
ddH_2O	8.64 ml	7.52 ml	6.36 ml	3.81 ml
SDS (10 %)		180 µl		120 µl
APS (100 mg/ml)		90 µl		60 µl
TEMED		9 µl		6 µl

Secondly, proteins separated by SDS-PAGE were transferred onto a nitrocellulose membrane (Perkin Elmer, GE Healthcare) using the Mini-Trans Blot module (Biorad) in a wet blot chamber. Therefore, the SDS-PAGE-gel was lifted from the glass plates and

placed onto the nitrocellulose membrane. Flanked with blotting paper and blotting sponges, it was inserted into the Mini-Trans Blot module (Biorad) and transfer was performed in 1x blotting buffer for 2.5 h at constant 400 mA on ice. Using Ponceau-S staining for 1 min at RT, the successful transfer was confirmed. Subsequently, excess dye was removed by shaking in deionised H_2O.

In order to occupy reactive protein domains, membranes were blocked using 5% milk powder in TBS-T for 60 min at RT. After blocking, membranes were shortly washed in TBS-T and incubated with the specific primary antibody according to Table 16. Following the incubation with primary antibody, membranes were washed 3 x 5 min with TBS-T and further incubated with the corresponding secondary antibody for at least 60 min at RT or at 4°C over night (O/N). Excess of secondary antibody was washed off (3 x 5 min) in TBS-T.

Table 16: Primary antibodies used including their incubation conditions.

Antibody	*Dilution*	*Incubation*	*Origin*	*Distributor, catalogue number*
		Primary		
anti-Hsp90(α/β)	1:1000 in TBS-T	1 h, RT	mouse	Santa Cruz, sc-13119
anti-γH2AX	1:1000 in TBS-T	1 h, RT	rabbit	abcam, #81299
anti-p53 (DO-I)	1:1000 in TBS-T	1 h, RT	mouse	Santa Cruz, sc-126
anti-LC3B	1:1000 in 5% BSA/TBS-T	O/N, 4°C	rabbit	Cell Signaling, cs3868
anti-p62/SQSTM1	1:500 in 5% milk/TBS-T	O/N, 4°C	mouse	Santa Cruz, sc-28359
anti-PARP-1 (CII10)	1:1000 in TBS-T	O/N, 4°C	mouse	Prof Dr Alexander Bürkle, University of Konstanz
anti-cleaved Caspase-3	1:1000 in 5% BSA/TBS-T	O/N, 4°C	rabbit	Cell Signaling, cs9661
anti-E-Cadherin	1:1000 in TBS-T	O/N, 4°C	mouse	Santa Cruz, sc-8426
anti-N-Cadherin	1:1000 in TBS-T	O/N, 4°C	mouse	Santa Cruz, sc-59987
		Secondary		
anti-rabbit-IgG-HRP	1:2000 in 5% milk/TBS-T	1 h, RT	goat	Cell Signaling, cs7074S
anti-mouse-IgG κ BP-HRP	1:2000 in 5% milk/TBS-T	1 h, RT	-	Santa Cruz, sc-516102

Since horseradish peroxidase (HRP)-coupled secondary antibodies were used, detection of proteins was performed using enhanced chemiluminescence (ECL). Either self-made ECL reagent (composition see Table 9) or commercially available ECL reagent (Western Lightning Plus-ECL, Perkin Elmer) was applied and incubated 1-3 min prior to subjecting to the ChemiDoc (BioRad) or Azure C300 (azure biosystems) imager. Images were analysed using Image Lab software (BioRad) or ImageJ and its quantification tools.

3.2.3. Cell viability assays based on cellular ATP content

In order to measure cell viability, cells were seeded in a density of 2.5-4 x 10^3 in white 96-half-well-plates. After 72 h of incubation, cell viability was determined using the

CellTiter-Glo® Luminescent Cell Viability Assay Kit (Promega) according to the manufacturer's instructions. To this end, medium was removed completely and a 1:1-mixture of the CellTiter-Glo® reagent and fresh medium in a total volume of 30 µl was added. Excluded from light, plates were shaken for 2 min at moderate speed. Upon further incubation of 10 min, luminescence was recorded at a TriStar^2 (Berthold) or Fluoroskan (Ascent) luminometer. Cell viability was calculated as percent of the mean of control samples. Inhibitory concentrations (IC_{50}) were further calculated using GraphPad Prism by non-linear fit regressions.

3.2.3.1. Generation of arrested cells

For ATP assays with non-proliferating respectively arrested HCT116 cells (HCT116-a), cells were generated by chronic treatment with either 5 µM IT or 5 µM 5-FU for 7 days as depicted in Figure 14. Therefore, cells were seeded in 10 cm dishes (5 x 10^5 cells/dish) and treated every 48 h including change of media. Once cells were ready to be seeded for ATP assays (1 x 10^4 cells/well), cells were collected for cell cycle distribution analysis as described in 3.2.5.1. Further cells were seeded to perform a cell cycle distribution analysis at the end of the ATP assay in 6 cm dishes at a density of 5 x 10^5 cells/dish. At all times, proliferating HCT116 (HCT116-p) cells were carried along as control.

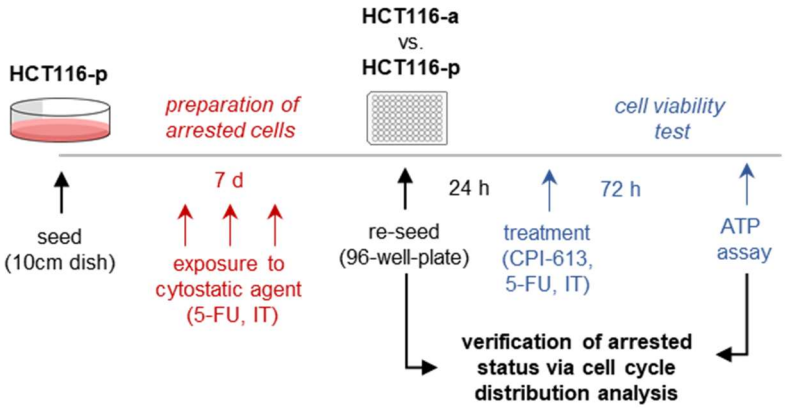

Figure 14: Scheme for generation of arrested cells.

3.2.4. Synergy assessment using CompuSyn and Combenefit

Making use of cell viability assays as described in 3.2.3, putative synergistic combination effects of LA/CPI-613 and 5-FU/IT were evaluated using two approaches. First, based on the Chou-Talalay-method, combination indexes (CI) were calculated. Therefore, inhibitory concentrations (IC_{50}) of individual drugs were determined. Next, five combination regimens were applied using doses as an x-fold of the prior determined IC_{50} values in constant ratios (0,25x, 0,5x, 1x, 2x, 4x). As recommended in Chou (2006), obtained curves were used as an input for CompuSyn software. Data input was

performed with default settings into provided template masks within the software. Output values as CI were ranked according to Chou (2010). Briefly, CI values equalling 1 represent simple additivity, CI values < 1 represent synergism and CI values > 1 indicate antagonism.

Second, based on computational-assisted Combenefit analysis and utilizing the same concentration ranges as in the Chou-Talalay-method, a total of 36 combination regimens were prepared and subjected to Combenefit analysis (Di Veroli et al., 2016). Choosing Highest Single Agent (HSA) as modelling algorithm and using the predefined Excel templates as input interface, 3D-surface-diagrams were obtained as output reflecting the synergism potential of each individual combination regimen.

3.2.5. Flow-cytometric analysis

3.2.5.1. Flow-cytometric cell cycle distribution analysis

For flow-cytometric analysis of the cell cycle distribution, HCT116 or HT29 cells were seeded in 6 cm-dishes at a density of 5, 2.5 or 1.25 x 10^5 cells for 24, 48 or 72 h, respectively. After incubation with CPI-613, detached and attached cells were harvested using Trypsin/EDTA. Prior to resuspension in ice-cold 1 ml 80% EtOH, cells were washed using PBS. EtOH-dissolved cells were frozen at -20°C for 1 to 7 days. After precipitation at -20°C, cells were centrifuged at 800 g for 8 min. EtOH was removed and cells were retrieved in 333 µl PBS and 1 µl RNase A (10 mg/ml, Merck) was added. RNA-digestion was performed at RT for 60 min. Next, 167 µl propidium iodide (PI, 50 µg/ml, Merck) was added and samples were measured using a BD Canto II (BD Biosciences). The gating strategy is described in the Annex.

3.2.5.2. Flow-cytometric measurement of cell death using Annexin V/PI-staining

Measurement of cell death rates were performed using staining with Annexin V-FITC and PI as described in Mimmler et al. (2016). To this end, cells were seeded at a density of 1 x 10^5 cells per 3.5 cm-dish and treatment lasted for 48 h. Both attached and detached cells were collected using Trypsin/EDTA. Following centrifugation (4 min, 1,000 rpm), cells were washed with PBS and stained with 0.05% Annexin V-FITC in binding buffer (2.5 µl dye plus 50 µl buffer) containing 10 mM HEPES pH 7.4, 140 mM NaCl, 2.5 mM $CaCl_2$ and 0.1% BSA for 15 min at 4°C under repeated gentle mixing. Prior to measurement at a BD Canto II flow-cytometer (FL-2-A vs. FL-3-A), samples were supplemented with 0.5 µg PI (10 µl working solution) and filled up with 430 µl binding buffer. Viable cells were defined to be double-negative labelled, (early) apoptotic cells were gated as Annexin V-positive cells and late apoptotic/necrotic cells were gates as PI- and Annexin V-positive cells using square gating. The gating

procedure is described in more detail in the Annex. Values were expressed as percentage of total population.

3.2.5.3. Flow-cytometric measurement of autophagy levels using CytoID® Green Detection Kit

Autophagy induction analysis using CytoID® Green Detection Kit (Enzo Life Sciences) were performed after 48 h of incubation and according to the manufacturer's protocol. The seeding density was 1 x 10^5 cells per 3.5 cm-dish.

Attached and detached cells were harvested using Trypsin/EDTA, centrifuged for 4 min at 1,000 rpm and washed with PBS and pelleted. Each sample was split up in two parts in each experiment. While one part was stained using 0.05% CytoID® Green reagent in phenol red-free medium (0.25 µl dye ad 500 µl medium) with thorough resuspension, the other part was resuspended in phenol red-free medium without dye (500 µl). Generally, phenol red-free medium was supplemented with 5% FCS. Cells were incubated for 30 min at 37°C in the dark prior to centrifugation (4 min, 1,000 rpm) and washed with PBS afterwards. Upon uptake in 500 µl PBS, samples were measured using a BD Canto II flow-cytometer (FL-3-A). Mean FITC intensity of the stained solvent control was set to a predefined value and subtracted with the background value assessed by the corresponding unstained sample. Illustration of the gating strategy can be found in the Annex. Values were calculated as x-fold of the solvent control.

3.2.5.4. Flow-cytometric quantification of reactive oxygen species

In order to allow the quantification of reactive oxygen species (ROS), the probe CM-H_2DCFDA (Invitrogen) was used. CM-H_2DCFDA allows for general oxidative stress detection and was prepared as a 1.25 mM solution in DMSO. Seeded in 3.5 cm-dishes at a density of 4 x 10^5 cells per dish, cells were stained after washing twice with warm PBS in phenol red-free medium plus 1.25 µl dye. For each sample, an unstained control was carried along in every experimental run. As a positive control, cells were incubated for 20 min with 200 µM tBOOH in PBS. Staining was performed at 37°C for 30 min. Upon washing with PBS, cells were harvested using Trypsin/EDTA, centrifuged (1,100 rpm, 4 min), resuspended in PBS and analysed by flow cytometry using a BD Canto II (BD Biosciences; FL-3-A). The gating procedure is described in more detail in the Annex.

3.2.5.5. Flow-cytometric monitoring of mitochondrial membrane potential

Mitochondrial membrane potential was monitored by flow cytometry using the Mitochondria Staining Kit (Sigma Aldrich) containing JC-1 dye, which allows for discrimination between polarised and depolarised mitochondria. While in polarised mitochondria JC-1 accumulates in mitochondrial matrix and forms aggregates of red

fluorescence, JC-1 is abundant in monomers of green fluorescence in cells with depolarised mitochondria.

Cells were plated in 3.5 cm-dishes at a density of 4 x 10^5 cells per dish. Upon incubation, cells were harvested including detached cells and the PBS-washing fraction using Trypsin/EDTA. Pelleted cells, which were centrifuged at 1,100 rpm for 4 min, were resuspended in 1 ml fresh medium and 1 ml staining solution (1x staining buffer supplemented with 5 µl JC-1 stain) was added. Cell suspensions were loaded for 20 min in the incubator. As positive control, cells were stained and additionally treated with the antibiotic Valinomycin (1:5000 dilution). Cells treated with Rotenone received treatment using 1 µM Rotenone for 24 h. Next, cells were centrifuged (1,100 rpm, 4 min), placed on ice and resuspended in 1 ml ice-cold 1x buffer. Upon further centrifugation, cells were picked up in 500 µl 1x buffer and subjected to FACS analysis using a BD Canto II (BD Biosciences; FL-2-A vs. FL-3-A). Figure Annex- 1 illustrates the gating strategy for the JC-1 staining in more detail.

3.2.6. Methods to assess DNA damage induction

3.2.6.1. Determination of DNA damage levels using InCellWestern assay

For InCellWestern (ICW) analysis of ɣH2AX, cells were seeded at a density of 2 x 10^4 cells per well of a black 96-well-plate with transparent bottom. After the desired time point (24 h), medium was aspirated carefully, wells were washed with PBS and subsequently cells were fixed with 100 µl 4% paraformaldehyde (PFA) in PBS for 10 min without shaking. Upon washing with PBS, cells were permeabilised with 75 µl 0.2% Triton X-100 in PBS for 5 min and later neutralised using 50 mM NH_4Cl in PBS (100 µl) for 2 min. After washing with PBS, 75 µl saturation solution composed of MAXBlock Blocking Medium with 1% RNase A and 10% cOmplete protease inhibitor was applied for 1 h at RT under continuous shaking. The plate was washed using 0.2% Triton X-100/2% FCS/PBS (PST). Incubation with the primary ɣH2AX-antibody (abcam, ab81299, rabbit; 1:200 in PST; 35 µl per well) for 90 min at RT on a rotating platform followed. After washing 3 x 5 min with PST, incubation with the secondary antibody IgG anti-rabbit-IRDye800 (Li-COR Biosciences, donkey; 1:1000 in PST), an infrared fluorescent dye-conjugated antibody, plus the nuclear staining dye TO-PRO3 (1:250 in PST; 50 µl per well) was performed for 1 h at RT on a rotating platform under the exclusion of light. Plates were scanned using an Odyssey Infrared Imaging Scanner (Li-Cor Biosciences) after 5 min washing with PBS and drying. Nuclear and *γ*H2AX staining were simultaneously visualised. Statistical analysis in the Image Studio Light (Li-Cor Biosciences) was performed to determine the *x*-fold increase in *γ*H2AX signal normalised to the DNA content per well in relation to the control.

3.2.6.2. Assessment of genotoxicity via Alkaline Comet Assay

In preparation for the alkaline Comet Assay, object slides were washed with methanol, flamed, and coated with 1.2% agarose (Carl Roth). Cells were treated for 24 h in 3.5 cm-dishes at a density of 2 x 10^5. Attached cells were harvested using Trypsin/EDTA and centrifuged. Pelleted cells were resuspended in PBS, counted and adjusted to 2 x 10^5 cells/ml. 100 µl cell suspension were supplemented with 100 µl low melting agarose (LMP, 1%, 40°C, Carl Roth). After mixing, 120 µl were given onto the agarose-coated object slide, mounted with a cover slip and placed on ice for at least 5 min. Cover slips were removed and object slides vertically placed into lysis buffer (listed in 3.1.1) and incubated at 4°C for 60 min. After lysis, object slides were placed into the electrophoresis chamber (Sub-Cell® Model 96 Cell, BioRad) containing electrophoresis buffer (see 3.1.2) and incubated for further 20 min. Electrophoresis was performed at 25 V/300 mA for exactly 15 min. Subsequently, object slides were placed in neutralization buffer (see 3.1.2) twice for 2 min, afterwards fixed in methanol at 4°C for 10 min and air-dried. When acquiring images, 45 µl PI (50 µg/ml, Merck) was added directly before measurement. Pictures were taken at a Leica DM 6000 B fluorescence microscope using Leica Application Suite X (Leica Microsystems). At least 50 cells per object slide were recorded. Evaluation was performed using ImageJ and the OpenComet plug-in or Comet Assay IV software (Instem Genetic Toxicology Solutions, Bury St Edmunds, UK).

3.2.6.2.1. Modification using FPG

In order to specifically detect oxidative DNA damage, a digestion with formamidopyrimidine DNA glycosylase (FPG, provided by [redacted]) was included. For alkaline Comet Assays with FPG, object slides were covered with 50 µl of 1 µg/ml FPG in Buffer F (40 mM HEPES, 0.1 M HEPES, 0.5 mM EDTA, 0.2 mg/ml BSA; pH 8.0) and incubated at 37°C (B15 incubator) for 38 min prior to electrophoresis. During this time, the FPG enzyme excises oxidised purines, such as 8-hydroxyguanine, and additionally introduces a DNA single strand break due to its lyase activity. The alkaline Comet Assay detects these introduced DNA single strand breaks, whose amount is directly proportional to oxidative damage.

3.2.7. Immunofluorescence staining of intact mitochondria using MitoTracker™ Orange

For immunofluorescence staining of intact mitochondria, HCT116 cells were seeded on cover slips at a density of 2 x 10^5 cells/3.5 cm dish. Cells were treated as described earlier. As positive control, 5 µM Rotenone for 24 h were used. Fresh medium with 250 nM MitoTracker™ Orange (Thermo Fisher Scientific, Darmstadt, Germany) was

added to the cells and incubated for 15 min at 37°C under the exclusion of light. Medium was removed, cells carefully washed with warm PBS (2x) and fixed using 4% PFA for 15 min at RT. Upon thorough washing (3x), cover slips were transferred into a wet chamber and permeabilised as well as blocked using 5% BSA in PBS/0.3% Triton X-100 for 30 min at RT (100 µl/cover slip). Blocking solution was discarded and nuclei stained using TO-PRO3 (1:100 in PBS, 150 µl/cover slip; Thermo Fisher Scientific) for 15 min at RT. TO-PRO3 was cleared off the cover slip and cover slips were mounted upside down on an object slide using VectaShield® Mounting Medium with DAPI (Vecta Laboratories, Burlingame, USA) and sealed using nail polish. Samples underwent confocal microscopy using a laser scanning microscope LSM 880 (Zeiss, Oberkochen, Germany) and analysis was conducted using ZEN blue lite software (Zeiss, Oberkochen, Germany).

3.2.8. Invasion and migration analysis

3.2.8.1. Assessment of migratory ability via wound healing assay

For wound healing assays, cells were seeded to reach a confluent monolayer overnight (2 x 10^6 cells/well) in 6-well-plates. Once a monolayer had formed, two scratches using a 10 µl-pipette tip were applied per well. Medium was removed, cells washed twice with warm PBS and fresh medium containing only 1% FCS was used for treatment of the cells. At defined positions, the initially generated scratches were recorded via microscopic photography (Leica Light Microscope DMi1, Leica MC170 HD camera and LAS EZ; t = 0 h). At time points 8 and 24 h, recordings were repeated. Photographs were analysed using ImageJ in order to calculate scratch area per scratch and converted into percentage of gap closure.

3.2.8.2. Assessment of invasive ability using CytoSelect™ Invasion Assay

In order to assess invasiveness of CRC cells, the Boyden chamber-based assay CytoSelect™ Invasion Assay (Cell Biolabs) was utilised according to the manufacturer's instructions. To this end, 5 x 10^5/ml cells were seeded into the insert of the plate in 300 µl serum-free medium upon activation of the membrane. The plate was filled with 500 µl FCS-supplemented medium and inserts were mounted. After 48 h of incubation, inserts were transferred to an empty well, supernatant was removed and cells from the upper part of the membrane were scrapped off with a moist cotton swab. Cells on the lower part of the membrane were stained for 10 min at RT in 400 µl staining solution and excess of dye was washed off using deionised water. Subsequently, inserts were allowed to air-dry. Under the microscope, five individual sections of view per insert were counted to quantify invaded/stained cells.

3.2.9. Experiments using isolated mitochondria

Isolation of mitochondria as well as subsequent experiments were kindly performed and analysed by the working group of [redacted]

3.2.9.1. Animals

Male C57/BL6/J mice (Janvier, Le Genest- Saint-Isle, France) were used. Mice were housed in a specific pathogen-free facility at 20-25°C and received regular laboratory animal diet *ad libitum*. Experiments were approved by the animal welfare office of the Justus-Liebig-University, [redacted].

3.2.9.2. Isolation of mitochondria

Subsarcolemmal mitochondria (SSM) were isolated as previously described in Boengler et al. (2017). Mice were sacrificed, hearts were removed and the atria were cut off. Ventricular tissue was washed in buffer A (100 mM KCl, 50 mM 3-[*N*-Morpholino]-propane sulphonic acid (MOPS), 5 mM $MgSO_4$, 1 mM ATP, 1 mM EGTA, pH 7.4) and was then minced in buffer B (buffer A + 0.04 % BSA) with scissors and further disrupted using a Potter-Elvejhem tissue homogenizer (Thomas Scientific; Svedesboro, USA). The homogenate was centrifuged for 10 min at 800 g. The supernatant containing the SSM was centrifuged for 10 min at 8,000 g. The sedimented mitochondria were washed by centrifugation in buffer A and were resuspended in a small volume of buffer A without ATP. All steps were performed at 4°C. The protein concentration of the isolated mitochondria was determined using the Lowry assay with BSA as external standard.

3.2.9.3. Generation of reactive oxygen species

Freshly isolated mitochondria (25 µg) were transferred to incubation buffer (125 mM KCl, 10 mM MOPS, 1.2 mM $MgCl_2$, 1.2 mM KH_2PO_4, 1.2 mM $MgCl_2$, 20 µM EGTA, 5 mM glutamate, 2.5 mM malate, pH 7.4) supplemented with 50 µM Amplex UltraRed (Invitrogen, A36006), 0.1 U/ml HRP and increasing doses of CPI-613 or DMSO as solvent control. H_2O_2 production was measured continuously for 4 min with a Cary Eclipse spectrophotometer (Agilent, Mulgrave, Australia) at the excitation/emission wavelengths of 565/581 nm, respectively. As positive control served SSM in the presence of 1% DMSO supplemented with 2 µM of the complex I inhibitor Rotenone. Background fluorescence of the buffer without mitochondria was subtracted and the slope of the fluorescence units over time was calculated. Measurements were performed at RT.

3.2.9.4. Mitochondrial oxygen consumption

Mitochondrial respiration of 100 µg/0.5 ml mitochondria was measured with a Clark-type oxygen electrode (Oxygen meter 782; Strathkelvin, Glasgow, UK) at 25 °C in incubation buffer. State IV respiration was recorded for 4 min, then either CPI-613 or solvent control was added and the oxygen consumption was measured for further 4 min. Oxygen consumption was analysed in nmol O_2 x min^{-1} x mg $protein^{-1}$.

3.2.9.5. Mitochondrial membrane potential

The membrane potential of 0.4 mg/ml mitochondrial proteins was measured at 25 °C with 250 nM of the potentiometric dye rhodamine 123 (Sigma, Missouri, US) in a Cary Eclipse spectrophotometer (excitation: 503 nm; emission: 535 nm; Agilent, Mulgrave, Australia). CPI-613 or DMSO was added every fifth minute to reach final concentrations of 0.1-100 µM, respectively. 1.5 µM FCCP (carbonyl cyanide-4-(trifluoromethoxy)phenylhydrazone) was used to dissipate the mitochondrial membrane potential. The effect of CPI-613 on the mitochondrial membrane potential was calculated as the difference between the fluorescence (mean value of the rhodamine 123 fluorescence for 1 min) before and after the addition of CPI-613 or DMSO, respectively.

3.2.10. Assessment of mitochondrial function using the Seahorse Cell Mito Stress Test Kit

Mitochondrial dysfunction of HCT116 and HT29 was assessed. This set of experiment was performed by [redacted] Generally, 8 x 10^5 cells per well were seeded into Seahorse XF96 Cell Culture Microplates (Agilent, Santa Clara, USA) and were treated with DMSO or CPI-613 for 24 h in their corresponding media. On the day of assay, culturing media was replaced with Seahorse assay media (glucose-free DMEM supplemented with 2 mM L-glutamine, 1 mM pyruvate and 25 mM glucose). The oxygen consumption rate (OCR) was measured with a Seahorse XF396 Analyzer (Agilent, Santa Clara, USA). Mitochondrial ATP production was defined as the difference between basal OCR reading and the OCR following the injection of 2 µM oligomycin. Maximal respiration was defined as the difference in OCR after injection of 1 µM CCCP, uncoupling the electron transport and OCR after injection of 2.5 µM Rotenone/antimycin A, inhibition of complex I and III.

3.2.11. Animal studies

All animal experiments were approved by the government of Rhineland-Palatinate or Hessia and the Animal Care and Use Committee of the University Medical Centre Mainz, the Justus-Liebig-University Gießen or the Technical University of Kaiserslautern

(approval numbers: G17-1-009 in Mainz/Kaiserslautern, G78/2017 in Gießen), and performed according to German federal law and the guidelines for the protection of animals (GV-SOLAS). After delivery, acclimatization for at least one week was allowed. Food and drinking water were supplied *ad libitum* and a maximum of 5 animals were kept per cage. Husbandry included a 12 h day-night-cycles.

3.2.11.1. Acute toxicity

Prior to pivotal mouse experiments, tolerability respectively acute toxicity of CPI-613 in desired dosages had to be excluded. Therefore, mice underwent two intraperitoneal (i.p.) injections of 50 mg/kg BW CPI-613 (dissolved in DMSO and diluted in PEG300) or vehicle control per week for 4 consecutive weeks. As primary endpoint, body weight gain was documented next to behaviour. For these experiments, male BALB/cAnNRj-FOXn1$^{nu/nu}$ nude mice (Janvier Labs, Le Genest-Saint-Isle, France) at an age of 7 weeks were used and housed in a heating cabinet at 26°C and enhanced humidified atmosphere.

3.2.11.2. Xenograft studies

Male 7- to 9-week-old BALB/cAnNRj-FOXn1$^{nu/nu}$ mice (Janvier Labs, Le Genest-Saint-Isle, France) were used for xenograft mouse studies. Nude mice housing was either performed in a heating cabinet or heated room at 26°C and humidified atmosphere.

3.2.11.2.1. Cell inoculation

HCT116 or HT29 cells were thawed and used at passage 5 to 8. Cells were expanded in 10 cm-dishes and harvested using Trypsin/EDTA. In preparation for the inoculation, cells were resuspended in medium without supplements to yield injections of 5 x 10^6 (HCT116) or 2 x 10^6 (HT29) cells / 200 µl per flank. Cell suspension was injected subcutaneously using a Sterican® cannula (G 26) to both the right and the left dorsal flank at day 0 of the experiment. Upon inoculation, mice were continuously monitored by, first, measuring body weight (BW) gain and, second, tumour size every second day (Monday, Wednesday, Friday).

3.2.11.2.2. Tumour volume determination

As mentioned above, tumour volume was determined three times per week. In order to measure tumour size, width and length were determined using a sliding calliper (Vogel GmbH, Kevelaer, Germany). Tumour volume was determined using the following equation:

$$\mathrm{V}\,[\mathrm{mm}^3] = \frac{(\mathrm{width}\,[\mathrm{mm}])^2 \times \mathrm{length}\,[\mathrm{mm}])}{2}$$

Termination criterions included a tumour volume > 1500 mm³, body weight loss > 20% and ulceration or bleeding of the tumour.

3.2.11.2.3. Tumour therapy and isolation

Once tumour volumes reached 100 mm³ (generally at day 7), mice were randomly grouped with equal mean tumour volume per group and therapy started. Groups received a) solvent controls, b) 25 mg/kg BW CPI-613, c) 40 mg/kg BW irinotecan (IT) or d) 25 mg/kg BW CPI-613 plus 40 mg/kg BW IT. Therapy included a 4-week-cycle of either two i.p. injections of CPI-613 (every Monday and Friday) or one i.p. injection of IT (every Wednesday) or the combination of both or solvent controls (Figure 15). Injection solutions of CPI-613 (dissolved in 1 M TEA) were prepared in D5W (5% Glucose in water, Braun), while injection solutions of IT (dissolved in 0.9% NaCl) were prepared in saline solution (0.9% NaCl, Braun). All injections were performed using BD Micro-Fine+ U-100 insulin syringes (BD BioSciences). Photographs of the animals back were taken at regular intervals. At the end of the experiment at day 36, tumours were photographed, isolated and snap frozen in liquid nitrogen. Next to tumour volume and body weight gain, survival based on termination criterion was noted.

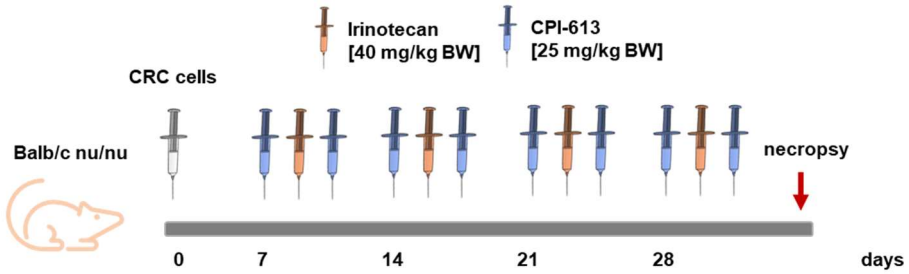

Figure 15: General experimental set-up and injection scheme of xenograft mouse studies.

3.2.11.2.4. Western Blot analysis of xenograft tumours

Protein lysates of snap frozen isolated tumours were generated and analysed by SDS-PAGE and Western Blot detection as outlined in 3.2.2.2. In order to create protein lysates, around 50 mg of snap frozen tumour were cropped at -20°C and homogenised in RIPA buffer containing 25 mM Tris-HCl (pH 7.4), 150 mM NaCl, 0.1% SDS, 1% sodium deoxycholate and 1% NP-40 as well as 0.2 mM Na_3VO_4, 50 mM NaF, 2 mM EDTA, 1 mM PMSF and 1x cOmplete Protease Inhibitor using a metal pestle on ice. After sonication for 10 sec, lysates were centrifuged for 10 min at 15,000 g at 4°C and supernatant was quantified in terms of protein concentration by the Bradford assay and subjected to analysis.

3.2.11.2.5. Haematoxylin and eosin staining of cryosections

As histopathological overview staining, haematoxylin and eosin staining (HE) was performed. Prior to HE staining, cryosections of the isolated tumours as described in 3.2.11.2.3 were prepared. Therefore, tumours were cut in half in order to yield sections of maximum diameter. Cryosections of 10 µm thickness were cut using a Leica CM3050 S cryostat and tissue freezing medium (Jung) at an ambient as well as an object temperature of -20°C. Sections were raised onto Superfrost® Plus object slides (Thermo Fisher) and stored at -80°C until use. Once slides were subjected to HE staining, the HE Quick Staining Kit by Carl Roth (Darmstadt, Germany) was utilised. Herein, slides were stained for 6 min using haematoxylin, followed by 10 sec of rinsing with tap water and 10 sec of differentiation using 0.1% hydrochloric acid. Further differentiation was achieved by running tap water for 6 min. Next, sections were counterstained for 30 seconds in eosin, followed by washing with tap water for 30 sec. Sections were mounted using Entellan® (VWR, Darmstadt, Germany) and photographed afterwards.

3.2.11.3. AOM/DSS model

In a chemically-induced model of CRC, male 7- to 9-week-old C57/BL6OlaHsd mice (Envigo, Horst, Netherlands) received a sequence of tumour initiating and tumour promoting chemicals in order to induce tumours, which were used in order to evaluate therapy success. The tumour induction was followed by a 28-days-therapy and accompanied by colonoscopy and blood sampling. Figure 16 depicts the scheme of the experimental set-up.

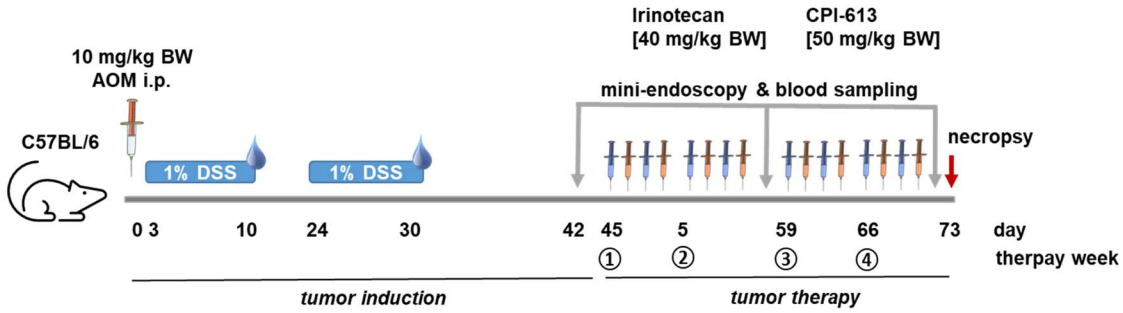

Figure 16: General experimental set-up and injection scheme of AOM/DSS model for chemically-induced CRC studies.

3.2.11.3.1. Tumour induction

While the *N*-nitroso compound azoxymethane (AOM) is used as tumour initiator by damaging DNA via DNA alkylation, dextran sodium sulphate (DSS) induces colitis and acts as a tumour promoter. In combination, the aberrant crypt foci adenoma-carcinoma-sequence is elicited (Robertis et al., 2011; Parang et al., 2016).

In detail, one i.p. injection of 10 mg/kg BW AOM (Sigma Aldrich) was given at day 0 of the experiment. For this purpose, stock solutions of 10 mg/ml AOM were thawed on ice

and diluted using 10x PBS and H_2O to yield a concentration of 1 mg/ml. Injections of 400 µl total volume were composed of diluted AOM and PBS according to the up-to-the-minute body weight. Due to its instability, a maximum of 10 injections were prepared and administered at a time using Sterican® cannulas (G 20; Braun) under sterile conditions. AOM injection was followed by a supplementation of 1% DSS (MP Biomedicals) in drinking water (Aqua, Braun) in two cycles during days 3 to 9 and 24 to 30. DSS-supplemented drinking water was renewed every two to three days and volume per cage was calculated using the formula:

$$V\ [ml] = 10 + 6\ x\ animal\ number\ x\ days$$

3.2.11.3.2. Colonoscopy

In repeating intervals, mice underwent mini-endoscopy from the rectum up to the first bend of the distal part of the colon in order to determine tumour number and tumour score. Mice were anaesthetised using 7 µl/g BW ketamine plus xylazine (i.p. injection; see Table 9). Consciousness of the mice was checked before the start of the colonoscopy. Afterwards, eye ointment (Corneregel®; Bausch+Lomb) was applied. Prior to performing the colonoscopy, the endoscope (Karl Storz, Tuttlingen, Germany) was cleaned using 70% isopropanol, the air flow was adjusted and colon lavage was performed using PBS. Videos of the colonoscopy were recorded using the integrated software and processed using the VLC player. Tumour scoring via mini-endoscopy was performed at day 42, day 56 and day 73 which represent time points before, in the middle and after tumour therapy.

3.2.11.3.3. Tumour scoring

Tumour number and tumour score were determined according to Becker et al. (2006) in order to monitor colorectal carcinogenesis. The amount of tumour per animal was noted as tumour number. For every tumour, tumour size was set into relation to the colon diameter and thereby scored. The sum of all scores per animal was recorded as tumour score.

3.2.11.3.4. Tumour therapy

After colonoscopy and tumour scoring at day 42, mice were randomly assorted to groups with equal mean tumour score per group and therapy initiated at day 45. Groups included a) solvent control, b) 50 mg/kg BW CPI-613, c) 40 mg/kg BW IT or d) 50 mg/kg BW CPI-613 plus 40 mg/kg BW IT. Therapy lasted 4 weeks with weekly two i.p. injections of CPI-613 (every Monday and Wednesday) or IT (every Tuesday and Thursday) or the combination of both or the solvent control per week. Details on injection preparation are given in 3.2.11.2.3.

3.2.11.3.5. Tissue collection and conservation

At day 73 after the last colonoscopy, mice were sacrificed by cervical dislocation. Mice were laid facing-up on tinfoil-coated polystyrene plates and fixed with needles at their legs. The abdominal cavity was opened and rinsed with ice-cold PBS. The colon was removed and flushed with ice-cold PBS until remaining stool was completely removed. Either the complete colon separated into distal and proximal part was prepared as a so-called Swiss Roll (Moolenbeek and Ruitenberg, 1981) or predefined sections were individually isolated. For generating Swiss Rolls, the colon was laid down flatly and divided into distal and proximal halves. Colon sections were then cut open longitudinally and wrapped around a toothpick with the lumen facing outwards and with the distal part inlying (see Figure 17). In order to isolate predefined sections, the colon was cut as depicted in Figure 17. Section C_A and C_B were directed for fixation and sections C_1, C_2, C_3 and C_4 were snap frozen in liquid nitrogen and stored at -80°C.

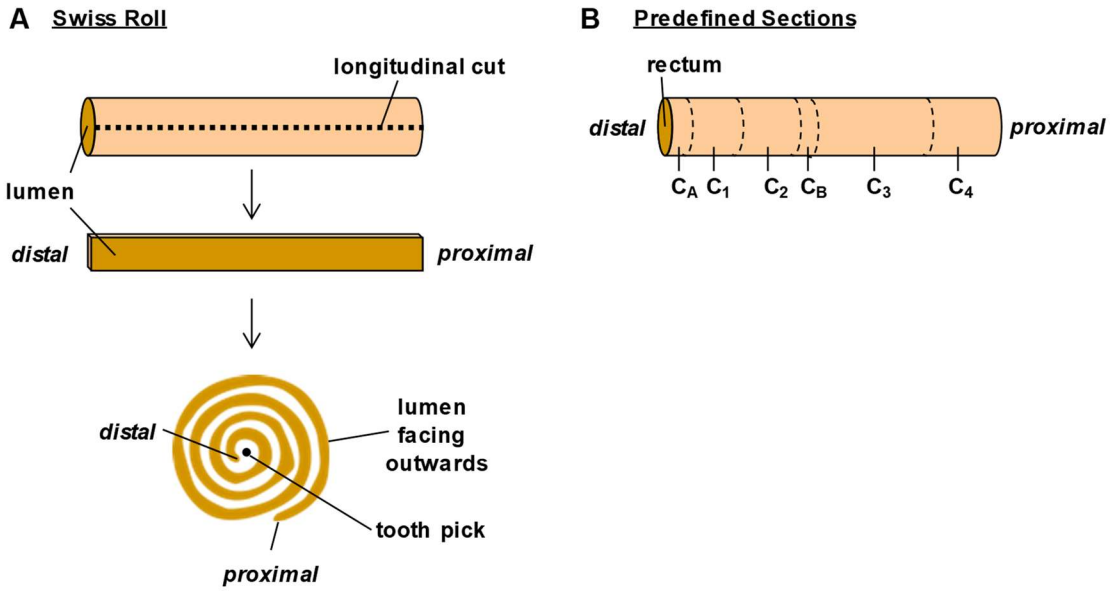

Figure 17: Scheme for preparation of Swiss Roll technique (A) and predefined sections (B).

Tissue sections and Swiss Rolls were fixed for 6 h in Histofix® (Carl Roth) at RT. Afterwards, samples were transferred into embedding cassettes (Carl Roth) and automated tissue processing with Leica ASP 300 S (Leica Microsystems) was performed using the following sequence (Table 17). At last, dehydrated samples were embedded in paraffin (Paraplast PLUS®, Carl Roth) using Leica ASP 300 S automated dehydrator (Leica Microsystems) and archived.

Table 17: Dehydration sequence for tissue.

Reagent	*Time [h]*	*Temperature [°C]*
Ethanol 70%	1	55
Ethanol 70%	1	55
Ethanol 70%	1.5	55
Ethanol 96%	1	35

Reagent	*Time [h]*	*Temperature [°C]*
Ethanol 99%	1	35
Ethanol 99%	1	35
Isopropanol 100%	1.5	35
Isopropanol 100%	1.5	35
Xylol	1	35
Xylol	1.5	35
Paraffin	1	60
Paraffin	1.5	60
Paraffin	1.5	60

3.2.11.3.6. Blood analysis

Differential blood analysis was performed with approximately 30 µl of capillary blood collected from the *vena fasciales* of anaesthetised mice at day 42, day 56 and day 73 next to colonoscopy. Blood was collected in an EDTA-coated microvette (Microvette® 200 K3E, Sarstedt AG & Co. KG). Using the veterinary haematology analyser ProCyte Dx (IDEXX), which was kindly provided by the Department of Veterinary Clinical Sciences at Justus-Liebig-University Giessen, blood samples were measured. Obtained blood parameters were set into context using reference values (Mazzaccara et al., 2008) to assess toxicity.

3.3. Statistical Analysis

All experiments were performed independently in at least three individual experiments; however, number of replicates is stated within each experiment. Results from representative experiments are shown. Values are displayed as mean + standard error of the mean (SEM) using GraphPad Prism 8.0 Software (GraphPad Software Inc., San Diego, CA, USA). For each data set, an outlier test according to Grubb was conducted. Statistical tests performed are stated within each set of experiment and significances are explained therein. Statistical analysis was performed in relation to untreated control samples or solvent control samples, respectively, as stated within each experiment.

4. RESULTS

4.1. Disruption of Mitochondria and Their Function by CPI-613

Until now, no chemotherapeutic drug candidate targeted altered energy metabolism of the mitochondria. Zachar et al. (2011) and Stuart et al. (2014), however, postulated a mitochondrial disrupting mode of action of CPI-613. The underlying mechanism includes the inhibition of mitochondrial respiration by blocking of KGDH and PDH, the release of ROS and the loss of membrane potential. In a two-step approach, the mode of action of CPI-613 should be elucidated in more detail in the context of CRC.

4.1.1. Isolated mitochondria are impaired by CPI-613

In a first step, the effects of CPI-613 on isolated mitochondria were to be assessed using bioassays directed towards ROS release, mitochondrial membrane potential integrity and flow of state IV respiration.

Effects of CPI-613 in terms of changes in mitochondrial membrane potential coupled with ROS formation and state IV respiration were to be analysed in murine mitochondria isolated from heart tissue. This set of experiment was kindly conducted and basic data analysis was performed by the working group of [redacted] Therefore, mitochondrial membrane potential was assessed using the rhodamine 123 fluorescence assay in isolated mitochondria as described in 3.2.9.5. Perpetuation of membrane potential started at 10 µM CPI-613, but strong and irreversible dissipation of membrane potential was observed at concentrations ≥ 25 µM CPI-613, while the solvent control DMSO did not affect membrane potential of isolated mitochondria at all (Figure 18A+B). Next, ROS formation in the form of H_2O_2 in isolated mitochondria was quantified employing the Amplex UltraRed assay as outlined in 3.2.9.3. While the addition of Rotenone as complex I inhibitor resulted in an increase in ROS formation, doses between 0.1 to 50 µM CPI-613 caused a substantial decline in ROS formation over increasing doses (Figure 18C). Upon 100 to 500 µM, CPI-613 ROS levels, on the other hand, increased again, reaching more than a 2.5-fold increase in the highest concentration used. Last of all, the mitochondrial respiration state IV represented by the consumption of O_2 per minute was examined (Figure 18D; 3.2.9.4). Generally, a dose of 25 µM CPI-613 or more drastically inhibited oxygen consumption by ~ 40% from 11 to 7 nmol O_2 x min^{-1} x mg^{-1} mitochondria.

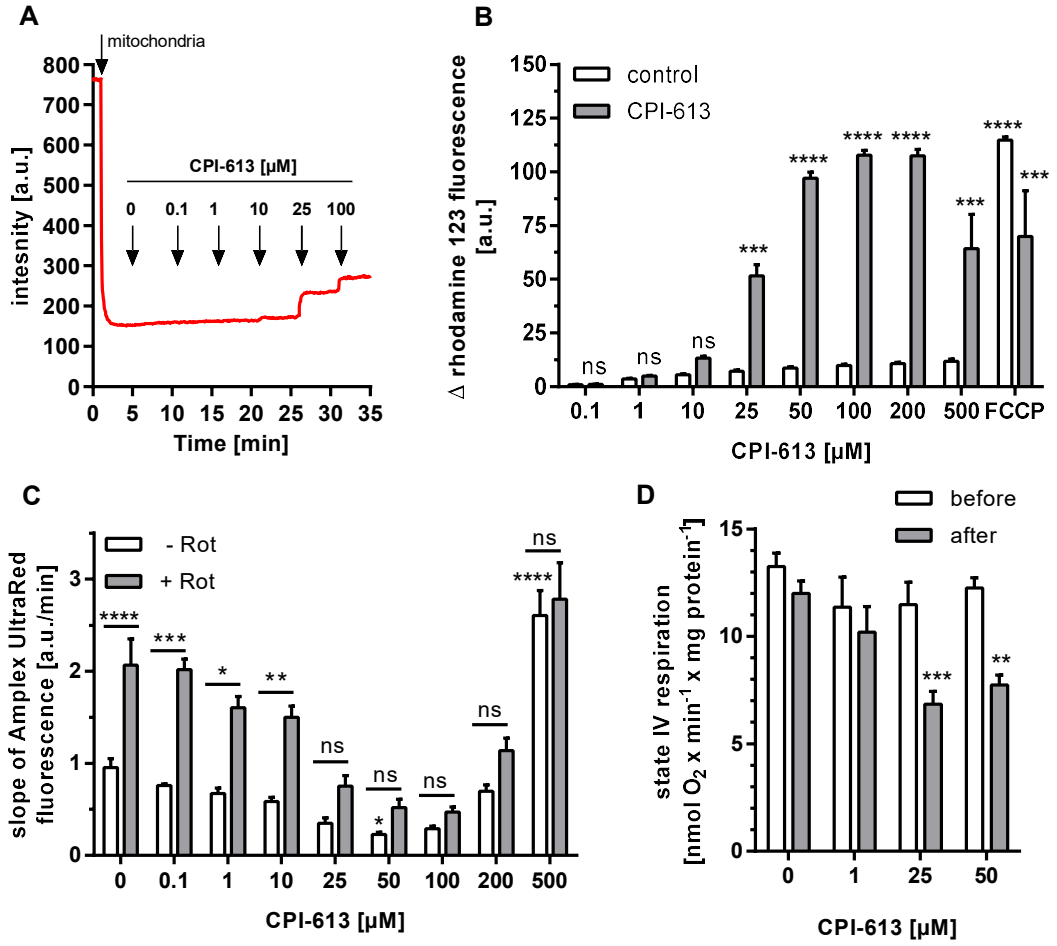

Figure 18: CPI-613 disrupts mitochondria and their function.
(A) Assessment of CPI-613-triggered loss of membrane potential in isolated mitochondria via rhodamine 123 fluorescence. (B) Graphical evaluation of A. (C) Measurement of membrane potential using Amplex UltraRed fluorescence assay in isolated mitochondria upon 0-500 µM CPI-613. FCCP was used as positive control. (D) Assessment of state IV respiration in CPI-613-treated mitochondria. Data is presented as mean + SEM (n≥6). ns: p>0.05; *p<0.05; **p<0.01; ***p<0.001; ****p<0.0001 vs. control or sample without Rotenone, respectively; 2-way ANOVA.

Summing up, CPI-613 effectively disrupted isolated mitochondria in low double-digit µM concentrations, which was reflected by the loss of membrane potential and state IV respiration. Surprisingly, the mitochondrial loss of functionality was accompanied by ROS reduction.

4.1.2. Mitochondria in CRC cells lose function upon CPI-613

While it has been demonstrated in 4.1.1 that CPI-613 disrupts mitochondrial function in a cell free assay at concentrations below 25 µM, the effects of CPI-613 on CRC cells and their mitochondria was to be evaluated in a next step. Therefore, ROS levels, mitochondrial membrane potential and mitochondrial number along with flux of oxidative phosphorylation (OXPHOS) were analysed in CRC cells.

ROS levels were quantified by flow cytometry using CM-H_2DCFDA as described in 3.2.5.4. HCT116 cells were treated with CPI-613 for 2 h (Figure 19A+C). Additionally, tBOOH served as positive control. A significant rise in ROS levels to 1.5-fold of the control was measured using 150 µM CPI-613. In cells treated with 300 µM CPI-613, ROS levels reached 2.5-fold of the control, ranging the levels of the positive control. In a next step, membrane potential of mitochondria in CRC cells was analysed using JC-1 staining (Figure 19B+D). Red-fluorescent JC-1 aggregates are formed in vital mitochondria with intact membrane potential, while green-fluorescent JC-1 monomers indicate depolarised mitochondria. Rotenone (1 µM, 24 h) and Valinomycin were applied as positive controls showing significant levels of damaged mitochondria. With respect to CPI-613, the highest dose (300 µM) only was able to alter mitochondrial membrane potential in HCT116 upon 1 h of incubation, leading to a loss of mitochondrial membrane potential in approx. 15% of treated HCT116 cells as compared to the positive control Rotenone.

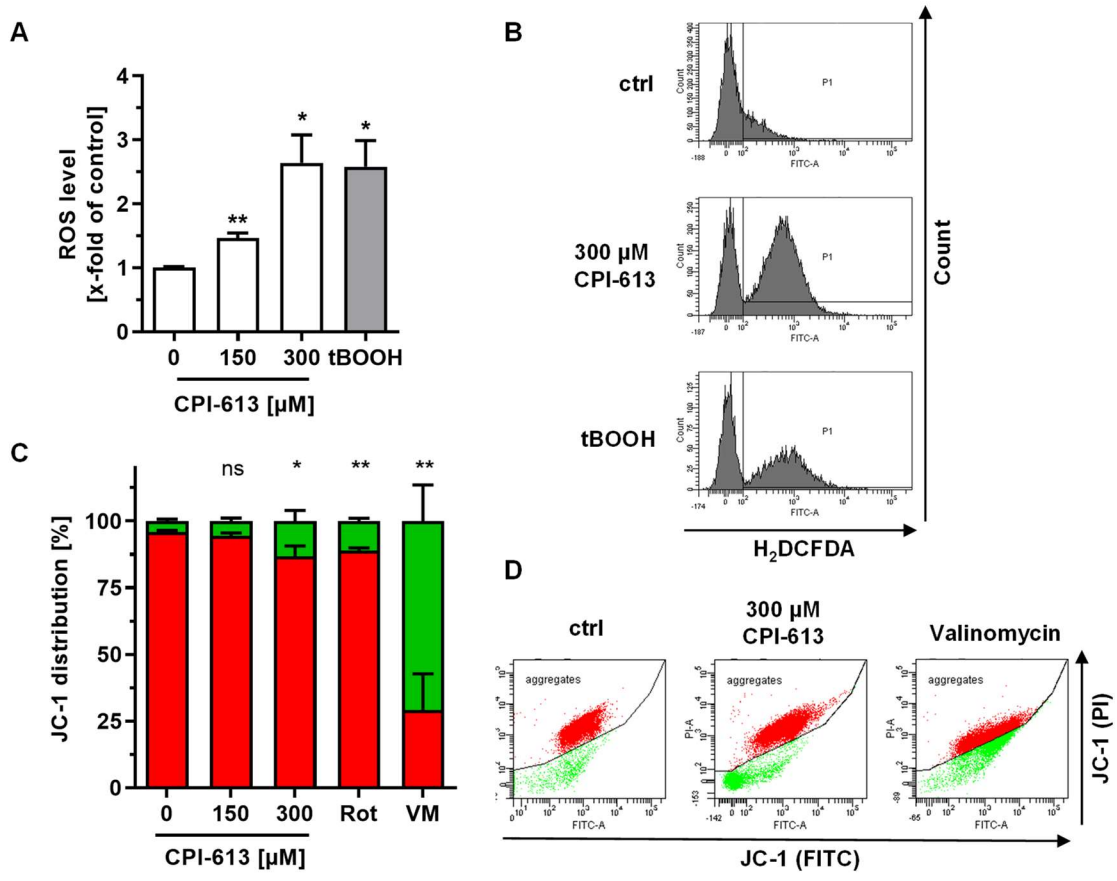

Figure 19: CPI-613 causes ROS formation and loss of membrane potential in CRC cells.
(A) ROS level in HCT116 upon CPI-613 incubation. Cells were treated for 2 h and measured by flow cytometry upon staining with H_2DCFDA. tBOOH (200 µM; 20 min) was included as positive control. Results displayed are mean + SEM (n=3). *p<0.05; **p<0.01; t-test. (B) Representative histograms of A. (C) Loss of mitochondrial membrane potential in CRC cells (HCT116) after 1 h of CPI-613 treatment. The respiratory complex I-inhibitor Rotenone (Rot; 1 µM; 24 h) and Valinomycin (VM) served as positive controls. Formation of JC-1 aggregates (red) versus monomers (green) was quantified by flow cytometry. Distribution is shown in relation to solvent control (0 µM). Data is presented as mean + SEM (n≥3). ns: p>0.05; *p<0.05; **p<0.01 vs. control; *t*-test. (D) Representative dot plots of C.

To assess the number of viable mitochondria in a semi-quantitative manner, CPI-613 (200 µM) was added for 24 h to HCT116 cells and cells underwent immunofluorescence staining with MitoTracker™ Orange and were subjected to confocal microscopy (Figure 20B). MitoTracker™ Orange fluorodye passively diffuses into cells and accumulates in active mitochondria having an intact mitochondrial membrane potential. The accumulation as aggregates occurs upon oxidation and by reaction with thiol-groups with its chloromethyl moiety to form aldehyde-fixable conjugates (Chazotte, 2011). The amount of MitoTracker™ intensity is therefore directly proportional to the number of intact mitochondria. Counterstaining of cell nuclei was performed using TO-PRO3. The quantification of the MitoTracker™ intensity per cell was reduced in those cells treated with CPI-613 as compared to DMSO-treated control cells by approx. 30% (Figure 20A). This effect, however, was not statistically significant. The positive control Rotenone in a concentration of 5 µM clearly abolished MitoTracker™ accumulation in HCT116 cells.

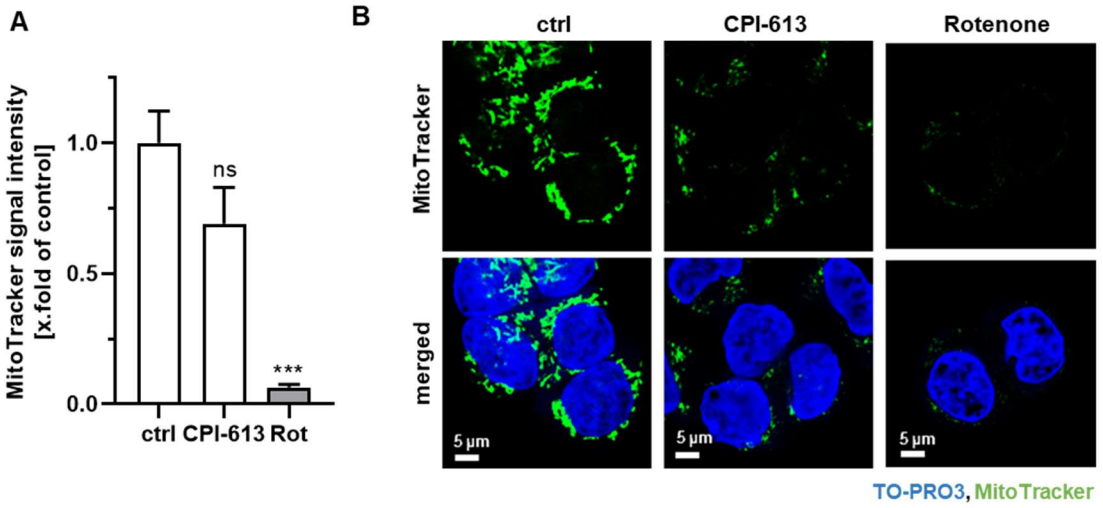

Figure 20: Mitochondrial number decreases upon CPI-613.
(A) HCT116 cells were incubated with either 200 µM CPI-613, solvent control or Rotenone (5 µM) for 24 h, stained for mitochondria using MitoTracker™, fixed and analysed using confocal microscopy. MitoTracker™ signals were quantified and related to control cells. Results are shown as mean + SEM (n=3, 5 sections each). ns: $p>0.05$; ***$p<0.001$ vs. control; *t*-test. (B) Representative pictures of A. Cell nuclei were stained using TO-PRO3 (blue) and mitochondria were visualised using MitoTracker™ (green).

The Seahorse Cell Mito Stress Test kit allows for assessment of mitochondrial function and causal differentiation of mitochondrial dysfunction. The following set of experiment was kindly performed by [redacted], and raw data was provided for further analysis. With the help of sequential injection of mitochondria-targeted compounds, different mitochondrial parameters can be measured within the Seahorse Cell Mito Stress Test Kit. During this process, oxygen consumption is directly quantified in HCT116 and HT29 cells treated with CPI-613 in comparison to untreated cells (Figure 21). Basal respiration is defined as the oxygen consumption rate at the start of the measurement

until the addition of Oligomycin, inhibiting ATP synthase and preventing stage III respiration and OXPHOS. The difference between basal respiration and the drop in oxygen consumption is referred to as ATP production-coupled respiration, while the remaining oxygen consumption is termed protein leak. Upon the supplementation with CCCP, the uncoupling of ATP synthesis and the chemiosmotic gradient, maximal respiration can be determined. The net amount between maximal and basal respiration is described as spare capacity. In a final step, the combination of Rotenone and Antimycin A lead to a complete interference with the electron transport chain due to inhibition of complex I and III, respectively, and oxygen consumption will drop to non-mitochondrial level.

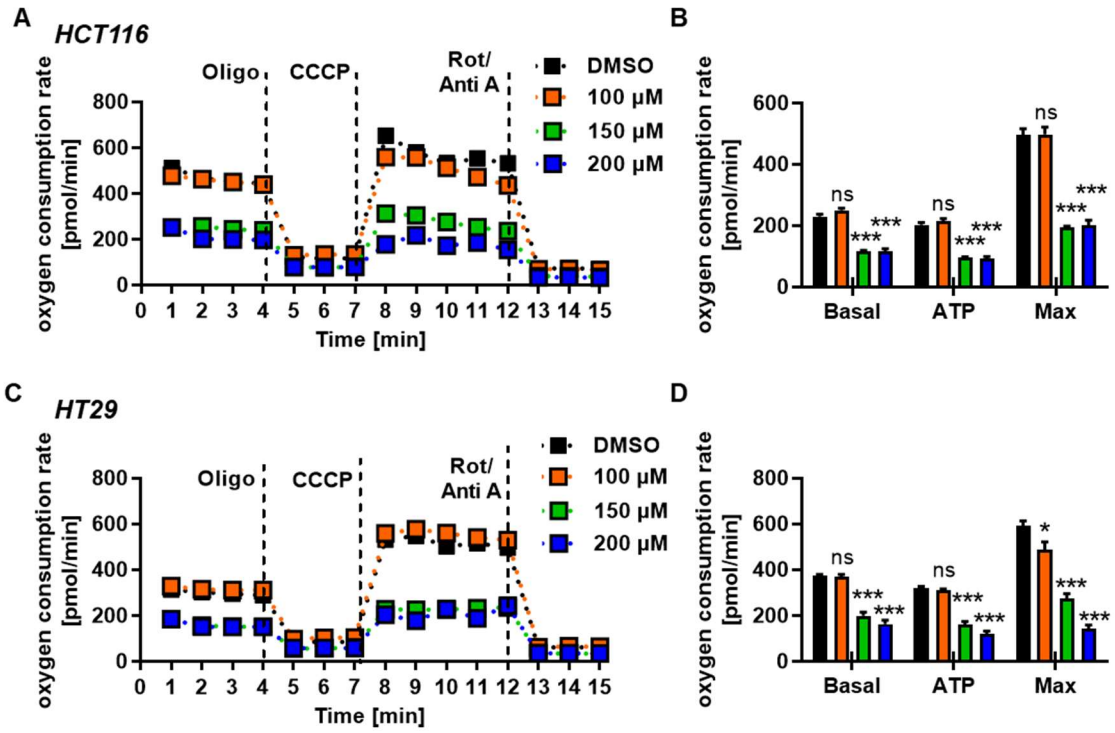

Figure 21: CPI-613 impairs oxygen consumption rate (OCR) of CRC cells.
HCT116 (A, B) or HT29 (C, D) cells were cultured and treated with indicated doses of CPI-613 for 24 h. Prior to analysis, cells were washed and kept in Seahorse assay media, containing L-glutamine, pyruvate and glucose. OCR was measured basally and after the addition of mitochondrial inhibitors Oligomycin (Oligo), CCCP and Rotenone/Antimycin A (Rot/Anti A). (A, C) Time courses indicate the impairment of basal respiration, mitochondrial ATP production and maximal respiration. (B, D) Quantification of basal respiration, mitochondrial ATP production and maximal respiration. Data are the mean + SEM (n=3-12 replicates from 3 biologically independent experiments). ns: $p>0.05$, *$p<0.05$, ***$p<0.001$ vs. control; 1-way-ANOVA.

HCT116 (Figure 21A+B) and HT29 (Figure 21C+D) cells were analysed using the Seahorse Cell Mito Stress Test Kit after incubation with increasing doses of CPI-613 for 24 h. While HCT116 cells treated with 100 µM CPI-613 only showed minimal reduction in maximal respiration, 150 and 200 µM CPI-613 lead to a dose-dependent reduction in basal, maximal as well as ATP-coupled respiration. Basal level as well as ATP-related energy production were halved, but maximal respiration and thus also spare capacity

were reduced to 25% of starting values. Generally, HT29 cells exhibited a lower basal oxygen consumption rate as compared to HCT116 cells. In HT29 cells, 100 µM CPI-613, surprisingly, lead to a slight increase in any type of mitochondrial respiration, however not statistically relevant. Both 150 and 200 µM CPI-613, in contrast, uncoupled mitochondrial basal, ATP-linked and maximal respiration and reduced mitochondrial function to 50%.

Concluding, incubation of CRC cells with CPI-613 lead to perpetuation of mitochondrial membrane potential integrity, timely followed by the formation of ROS and an overall reduction of intact mitochondria. At the same time, CPI-613 inhibited OXPHOS in HCT116 and HT29 in a dose-dependent manner. These insults might be crucially effecting cellular functionality and resulting in cytotoxicity.

4.2. CPI-613 as a Promising Building Block in the Treatment of CRC

As earlier demonstrated in this study, CPI-613 targets altered energy metabolism in colorectal cancer cells. This supports data described in other cell types in the literature. Based on this unique mode of action and being the first in this class of agents, its applicability in the treatment of CRC and the benefits derived from its inclusion shall be analysed *in vitro*.

4.2.1. Cytotoxicity of CPI-613 displays uniform, dose- and time-dependent and tumour-selective character

The dramatic attack of CPI-613 on mitochondria leads to the assumption that cytotoxicity might occur. While cytotoxicity of CPI-613 has been described for solid breast, kidney, lung and prostate cancer by Zachar et al. (2011), a detailed evaluation of its ability to reduce cell viability in a variety of CRC cells is lacking. The mother compound LA has been shown to be cytotoxic in some CRC cells with varying efficacy (Dörsam et al., 2015; Dörsam and Fahrer, 2016). To address this question, a panel of CRC cell lines with different genotypic statuses with respect to microsatellite stability, p53, KRAS and BRAF in addition to patient-derived cells was challenged with the lipoates CPI-613 and LA as well as the standard chemotherapeutic reference substances 5-Fluorouracil (5-FU) and Irinotecan (IT) (see Table 14). In order to assess the effect on healthy colonocytes adjacent to cancerous cells, non-transformed human colonic epithelial cells (HCEC) were carried along (Roig et al., 2010).

With respect to LA, IC_{50} values ranged between 266 and 1815 µM, this represents a 7-fold magnitude spread. For a clearer discrimination, cells were categorised as either resistant, depicted in red, or sensitive, depicted in green. While DLD-1 was the least sensitive cell line followed by HCT116, in particular MSS/p53-mt cell lines happened to be more vulnerable, led by HT29. Patient-derived HROC cells displayed a comparatively high IC_{50} value, which was also found in non-transformed HCEC cells.

In contrast, CPI-613 exhibited uniform cytotoxicity against all tested established cell lines with IC_{50} values between 155 to 187 µM - irrespective of the genotypic features. Both HCT116, as a representative of MSI/p53-wildtype cells, and HT29, as a representative of MSS/p53-mt cell, with IC_{50} values of 167 and 164 µM respectively are mid-table. The IC_{50} values increased gradually from patient-derived HROC cells to HCEC, which were the most resistant cells with an IC_{50} of 286 µM.

Looking at the cytostatics 5-FU and IT, for both anticancer drugs a wide range could be noted, which was more pronounced for 5-FU. For both 5-FU as well as IT, it becomes apparent that p53-wildtype cells are more vulnerable for these cytostatics indicated by lower IC_{50} values. For example, IC_{50} values for HCT116 were calculated to be 4 and 6 µM for 5-FU and IT, however for HT29 20 and 23 µM were determined. Whereas HROC cells happened to be dramatically more resistant to 5-FU than IT, HCEC cells were susceptible to both cytostatics.

As assessed in a series of ATP assays, uniform cytotoxicity was demonstrated for CPI-613 while its mother compound LA exhibited unpredictable responses. Furthermore, IC_{50} values indicated a superiority of CPI-613 with respect to tumour selectivity. Visualised in (Figure 22A), two representative CRC cell lines harbouring different genotypic equipment, namely HCT116 and HT29, were compared to non-transformed colonic epithelial cells HCEC in their response rate to either 500 µM LA or 200 µM CPI-613. Regarding LA, it is apparent that cell viability was only decreased to approx. 80% in both HCT116, as a resistant cell line, as well as HCEC but for HT29, cell viability dropped to approx. 20%. For CPI-613, however, 200 µM reduced cell viability below 20% in both CRC cell lines, while HCEC cells showed significantly less decrease in cell viability.

Table 18: Cytotoxicity screening in a panel of colon (cancer) cell lines based on IC_{50} values.
The panel comprised microsatellite-stable (MSS) / p53-wildtype in comparison to microsatellite-instable (MSI) / p53-mt CRC cells as well as patient-derived cells and non-transformed colonic epithelial cells (HCEC). Indicated cell lines were incubated with increasing doses of the lipoates CPI-613 and LA or cytostatics 5-FU and IT for 72 h followed by measurement of the cell viability using the ATP assay (n=3). Cell viability was normalised to solvent controls. Drug concentrations were transformed into log-scale and plotted against the cell viability. The curve was fitted by non-linear regression with variable slope, providing the indicated IC_{50} values.

cell line	*LA*	*CPI-613*	*5-FU*	*IT*
		MSI / p53-wildtype		
HCT116	1504	167	4	6
LS174T	1214	184	4	2
RKO	472	164	32	11
SW48	300	175	64	56
DLD-1	1815	155	4	52
		MSS / p53-mutant		
CacO-2	517	183	186	67
HT29	266	163	20	23
SW480	804	187	63	91
		patient-derived		
HROC278	1122	190	172	17
HROC60	754	211	1190	53
		non-transformed		
HCEC	1439	286	31	6

For common anticancer drugs used in first line therapy, the cytotoxicity is recorded to be dependent on p53, which is reflected in a resistance of p53-mt cell lines (Dörsam et al., 2015). Therefore, isogenic HCT116 cells bearing wildtype ($p53^{+/+}$) or p53 null ($p53^{-/-}$) status were used in order to assess the role of p53 in the cytotoxicity of CPI-613. As demonstrated in an ATP assay, no difference in cell viability reduction between HCT116-$p53^{+/+}$ and HCT116-$p53^{-/-}$ could be found. At any dose of CPI-613, cytotoxicity was not significantly different (Figure 22B). Another condition crucial for anticancer drug efficacy of first line therapy drugs is the necessity of cell proliferation. To address this question, proliferating HCT116 cells were arrested using chronic treatments of 5-FU or IT as described in 3.2.3.1. Cell cycle distribution analysis confirmed that chronically treated HCT116 cells with cytostatics to be halted in G2/M-phase (80% of cells treated with IT and 55% of cells treated with 5-FU) with a concomitant decrease of cells in S-phase, which lasted throughout the incubation period (Figure 22D+E). In Figure 22C, proliferating cells are compared to arrested cells using treatments with CPI-613, 5-FU or IT. Strikingly, neither arrested cell population responded to 10 µM 5-FU or IT anymore represented by no reduction in cell viability, whereas proliferating cells are reduced in their viability by about 75% each. Regarding CPI-613, a dose-dependent reduction of cell viability was found in all three populations. Response rate in arrested

cells was slightly less as compared to proliferating HCT116 cells, although at 200 µM CPI-613 the difference of IT-arrested cells was not different to proliferating HCT116 cells.

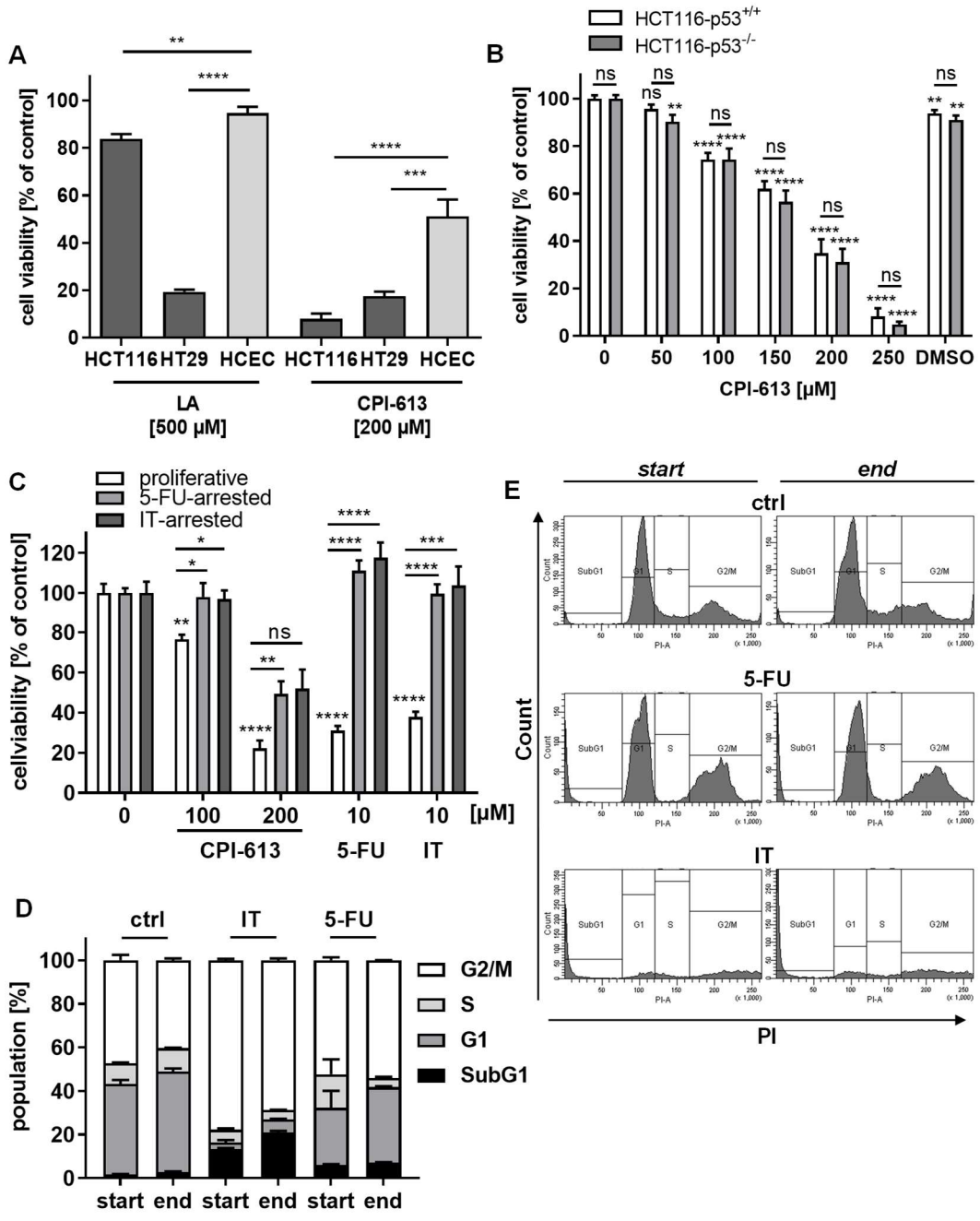

Figure 22: p53- and proliferation-independent as well as tumour-selective cytotoxicity of CPI-613. (A) Representative CRC cell lines (HCT116 and HT29; depicted in dark grey) next to non-transformed colonic epithelial cells (HCEC; depicted in light grey) were either exposed to 500 µM LA or 200 µM CPI-613 for 72 h and cell viability was determined based on ATP content. (n≥3) **p<0.01, ****p<0.0001 vs. other cell line as indicated; *t*-test. (B) Isogenic HCT116 cells proficient for wildtype p53 (depicted in white) or deficient for p53 (depicted in grey) underwent 72 h of CPI-613 treatment and cell viability was assessed using ATP assays. (n=5) ns: p>0.05, **p<0.01, *****p<0.0001 vs. control or between isogenic cell lines as indicated; *t*-test. (C) Proliferating (depicted in white) in comparison to arrested (depicted in grey/dark-grey) HCT116 cells were exposed to CPI-613 and measured as described in A. (n=3) ns: p>0.05, *p<0.05, **p<0.01, ***p<0.001, ****p<0.0001 vs. control or proliferating cells as indicated; *t*-test. (D) Proliferating and chronically treated HCT116 cells seeded for ATP assays in C underwent cell cycle distribution analysis at the beginning (start) and at the end (end) of the ATP assay to quantify the amount of arrested cells. A scheme of the experimental set up is depicted in Figure 14. (n=3) (E) Representative histograms of D.

Overall, CPI-613 displayed uniform cytotoxicity against a panel of CRC with a selectivity towards cells of cancerous origin, other than LA and standard chemotherapeutics. The mode of action, herein, was independent of p53 and cell proliferation was non-essential. The process of cytotoxicity and the associated induction of cell death, however, needs to be detailed further.

4.2.2. CPI-613 induces cell death, which is not mediated by caspases

Thus far, the reduction in cell viability upon CPI-613 was shown using ATP assays. To deepen the understanding of cell death induction upon CPI-613 treatment, further analysis was performed. The effect on the cell cycle distribution and particularly on the SubG1 fraction representing dead cells was assessed. Furthermore, apoptotic and necrotic cell death and the involvement of caspases were tested.

First, HCT116 cells were treated with increasing doses of CPI-613 (0, 150 and 200 µM) for different time points (24, 48 and 72 h) and measured by flow cytometry as depicted in Figure 23A and the representative histograms in Figure 23B. A dose- as well as time-dependent induction of SubG1 fraction could be observed. Effects of 150 µM CPI-613 were enhancing from insignificant increase (4%) to slight significant increase (8%) up to more than 42% cell death over the course of time. In HCT116 cells treated with 250 µM CPI-613 for 48h, more than 65% dead cells were measured. At the same time, a cell cycle arrest was not detectable at any condition.

The same set of experiments was performed in HT29 cells (Figure 23C+D). Similar effects were presented as in HCT116 cells, although, less pronounced. Cell death represented by the SubG1 fraction after 24 h of 250 µM CPI-613, for example, only accounted to approx. 15% but was found to be significant.

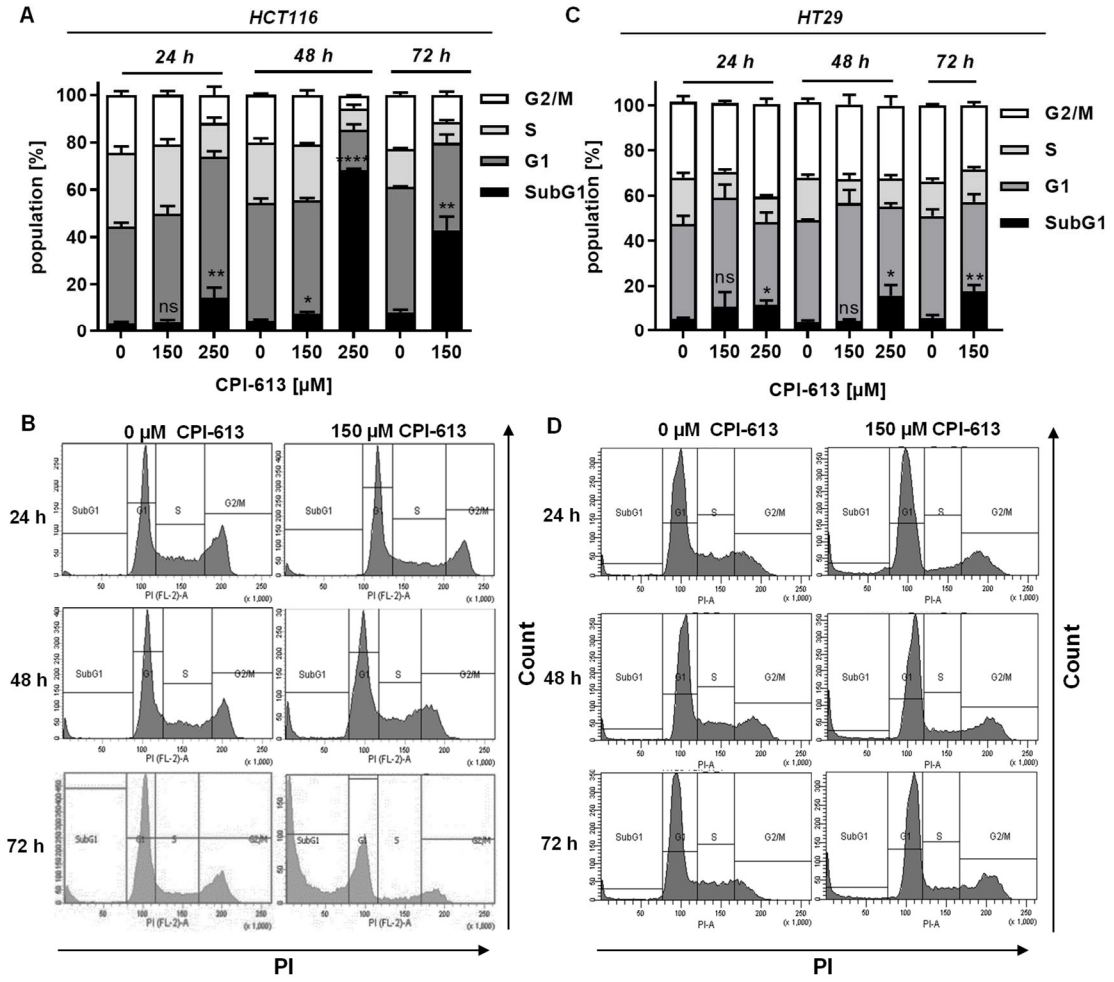

Figure 23: Induction of cell death and influence of CPI-613 on cell cycle distribution.
In a time- and dose-course over 24 to 72 h at 0 to 200 µM CPI-613, HCT116 (A and histograms in B) and HT29 (C and histograms in D) cells were treated and at indicated parameters analysed by flow cytometry with respect to cell cycle distribution and cell death induction represented by the SubG1 fraction. Results displayed are mean + SEM (n≥3). ns: p>0.05, *p<0.05, **p<0.01, ****p<0.0001 vs. control of the same time point; *t*-test.

Morphological changes in HCT116 (top panel) and HT29 (bottom panel) mainly manifested in rounding of the cells and detachment from the cell culture plate (Figure 24A).

Annexin V/PI staining of both cell lines confirmed the results of the cell cycle distribution analysis (Figure 24B+C). In here, 150 µM CPI-613 for 48 h did not significantly increase apoptotic or necrotic cells, but 250 µM CPI-613 lead to significant levels of cell death, which was more pronounced in HCT116 cells (30%) than in HT29 cells (18%). In both cell lines tested, late apoptosis or necrosis seemed to be the prevailing cell death pathway.

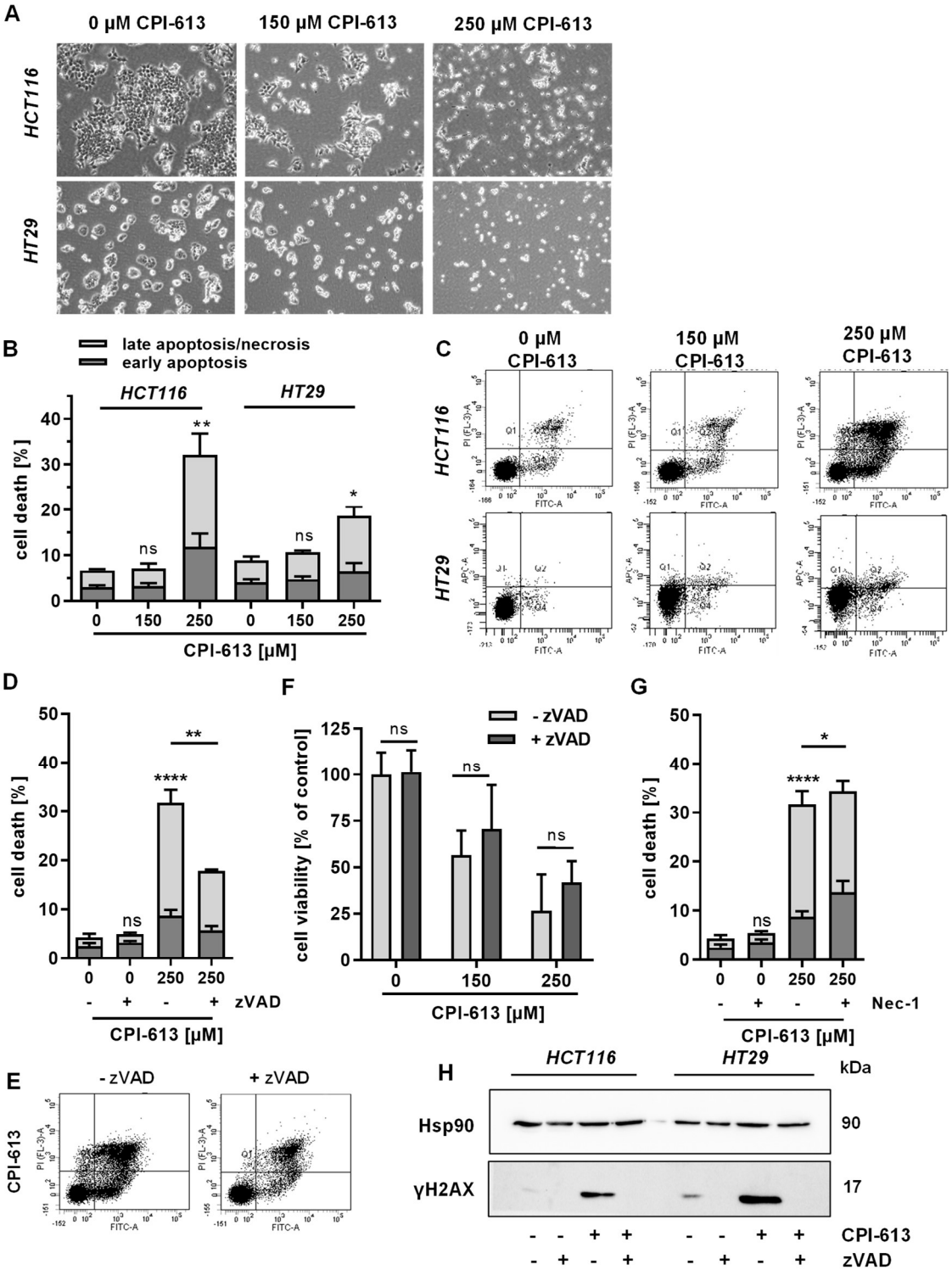

Figure 24: CPI-613 induces various types of cell death.
(A) Dose-dependent morphological changes in HCT116 (upper panel) and HT29 (lower panel) upon CPI-613 after 48 h. (B) Cell death measurement using AnnexinV/PI staining in HCT116 and HT29 cells. Cells were incubated with increasing CPI-613 doses for 48 h. (C) Representative dot plots for B are summarised. (D) Using the pan-caspase inhibitor zVAD, induced cell death attributable to apoptosis was evaluated in HCT116 after 48 h. Treatment was performed as in B. (E) Representative dot plots for D are shown. (F) Cell viability assay using ATP measurement was assessed after 72 h of incubation with CPI-613 with or without zVAD. (G) Using the necroptosis inhibitor Necrostatin-1 (Nec-1), induced cell death attributable to necroptosis was evaluated in HCT116 after 48 h. Treatment was performed as in B. (H) Western Blot analysis following whole cell lysis and SDS-PAGE of cell death-associated γH2AX formation in HCT116 and HT29 cells after 48 h of incubation with CPI-613 with/without zVAD. Hsp90 was used as loading control. Data is presented as mean

+ SEM (n≥3). ns: p>0.05, *p<0.05, **p<0.01, ****p<0.0001 vs. control of the same time point or sample without inhibitor, respectively; *t*-test.

Derived from AnnexinV/PI measurements, primarily necrotic cell death is elicited upon CPI-613 treatment. Under necroptosis-inhibited condition with the application of Necrostatin-1 in further AnnexinV/PI measurements, cell death induction was not diminished (Figure 24G). Since caspases initiate, mediate and govern apoptosis (Shalini et al., 2015; Julien and Wells, 2017), their involvement in the cell death elicited by CPI-613 was analysed. To check the role of caspases, HCT116 cells were co-treated with the pan-caspase inhibitor zVAD as described in 3.2.1.3. The total amount of cell death measurable was reduced upon the addition of zVAD, indicating a rescue from cell death (Figure 24D+E). This observation was corroborated in an ATP assay using the same conditions and revealing the same trend, which unfortunately was not statistically significant (Figure 24F).

Cell death- or apoptosis-accompanied, DNA strand breaks in the context of DNA fragmentation can be formed and labelled with γH2AX (Rogakou et al., 2000). The formation of γH2AX was shown to be essential for DNA fragmentation in apoptosis but not in the activation of Caspase-3 (Lu et al., 2006). Assessed in a Western Blot analysis of the DNA strand break marker γH2AX (Kinner et al., 2008; Zhao et al., 2019), the phosphorylation of Histone 2AX is dramatically increased in both HCT116 and HT29 cells treated with 200 µM CPI-613, which is abolished once caspases are inhibited using zVAD (Figure 24H).

Since cell death analysis indicated an involvement of caspases in the type of cell death triggered by CPI-613, Caspase-3 cleavage and PARP-1 cleavage were assessed using Western Blot analysis. Herein, the cleavage of Caspase-3, an executing caspase, results from the activation of the initiator Caspase-9 in the intrinsic apoptotic pathway or Caspase-8 in the extrinsic apoptotic pathway (Julien and Wells, 2017). The proenzyme of Caspase-3 (37 kDa in size) undergoes proteolytic processing at aspartic residues and forms two subunits, of which one is 17 kDa and one is 12 kDa big. As a downstream event, full length PARP-1 (116 kDa) is cleaved in apoptosis, resulting in the formation of a fragment with 85 kDa. The described cleavage leads to inactivation of PARP-1.

Using 150 and 200 µM CPI-613, HCT116 and HT29 cells were treated for either 24 or 48 h and Caspase-3 and PARP-1 cleavage were monitored using Western Blot analysis (Figure 25). As a positive control and as apoptosis inducer, HCT116 cells were treated with 1 µM of the protein kinase inhibitor Staurosporine for 16 h and HT29 cells were incubated with 500 µM LA for 72 h (Dörsam et al., 2015). Both treatments give rise to

cleaved Caspase-3 alongside cleaved PARP-1. For none of the cell lines or incubation conditions with CPI-613, neither Caspase-3 nor PARP-1 cleavage could be detected.

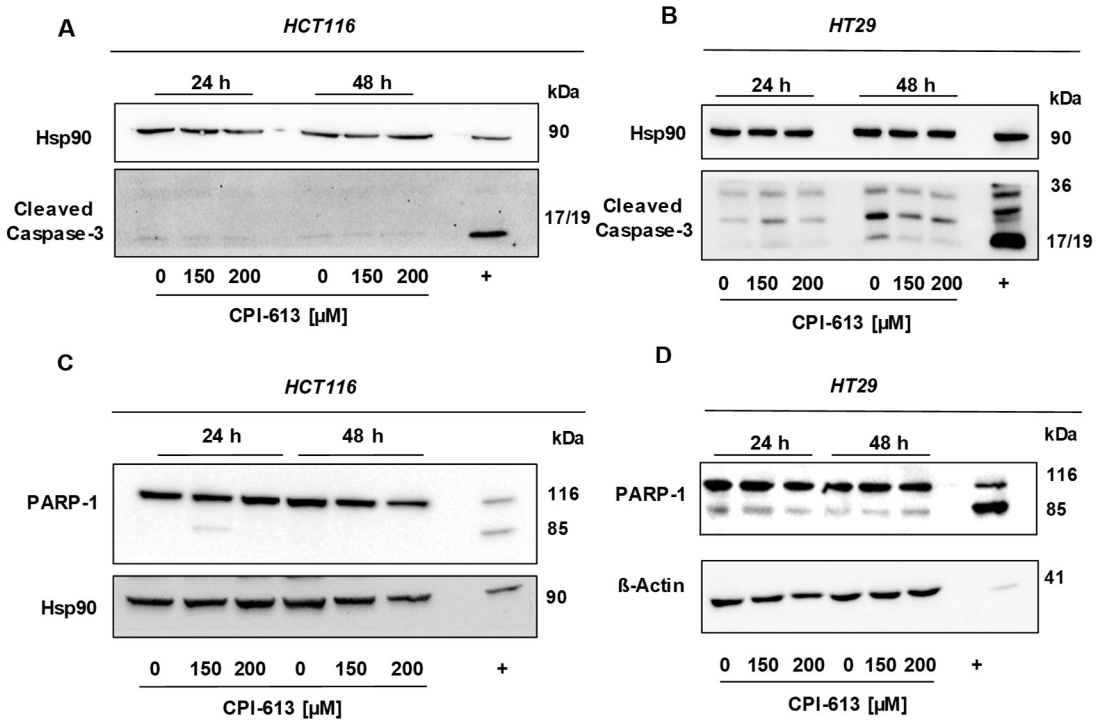

Figure 25: CPI-613-triggered cell death is independent of caspase activity.
Caspase-3 (A, B) as well as PARP-1 cleavage (C, D) were detected using Western Blot analysis following whole cell lysis of HCT116 (A, C) and HT29 (B, D) cells upon indicated time points and CPI-613 concentrations. Positive controls included 1 µM Staurosporine for 16 h in HCT116 (A, C) and 500 µM LA for 72 h in HT29 (B, D). Positive controls had to be chosen cell line-specifically. Either Hsp90 or β-Actin served as loading control.

To sum up, the cell death elicited upon CPI-613 was cell line-independent and increased over time and dose and was not preceded by a cell cycle arrest. Both apoptosis and necrosis contributed to the cell death induced, showing redundancy. Apoptosis induction was not primarily dependent on Caspase-3 activity, but other caspases (e.g. Caspase-2) might be involved since the pan-caspase inhibitor zVAD showed a rescuing effect.

4.2.3. Autophagy is increased upon CPI-613

The molecular recycling process of excessive or dysfunctional macromolecules and organelles, called autophagy, is widely regarded as a means of survival in cancer cells, which is in particular activated upon nutrient starvation, hypoxia (White, 2015) or drug treatment and was also shown to be activated upon LA treatment (Göder et al., 2015). Thus, the impact of CPI-613 on autophagy levels in cancerous cells merits elucidation.

To address this question, two different cell lines were treated with increasing doses of CPI-613 for 48 h and autophagy levels were quantified by flow cytometry using CytoID®

Green dye (Figure 26). Representative histograms are shown in Figure 26B. The bacterial genotoxin *cytolethal distending toxin* (CDT) served as positive control, which was reported previously to induce autophagy in HCT116 cells (Seiwert et al., 2017). In HCT116, autophagy levels were slightly elevated with increasing doses of CPI-613 to approximately 1.75-times of the control upon 200 µM CPI-613 (Figure 26A, left panel). In HT29, the rise in autophagy was more pronounced, reflected in a 2.8-fold increase upon 200 µM CPI-613 (Figure 26B, right panel).

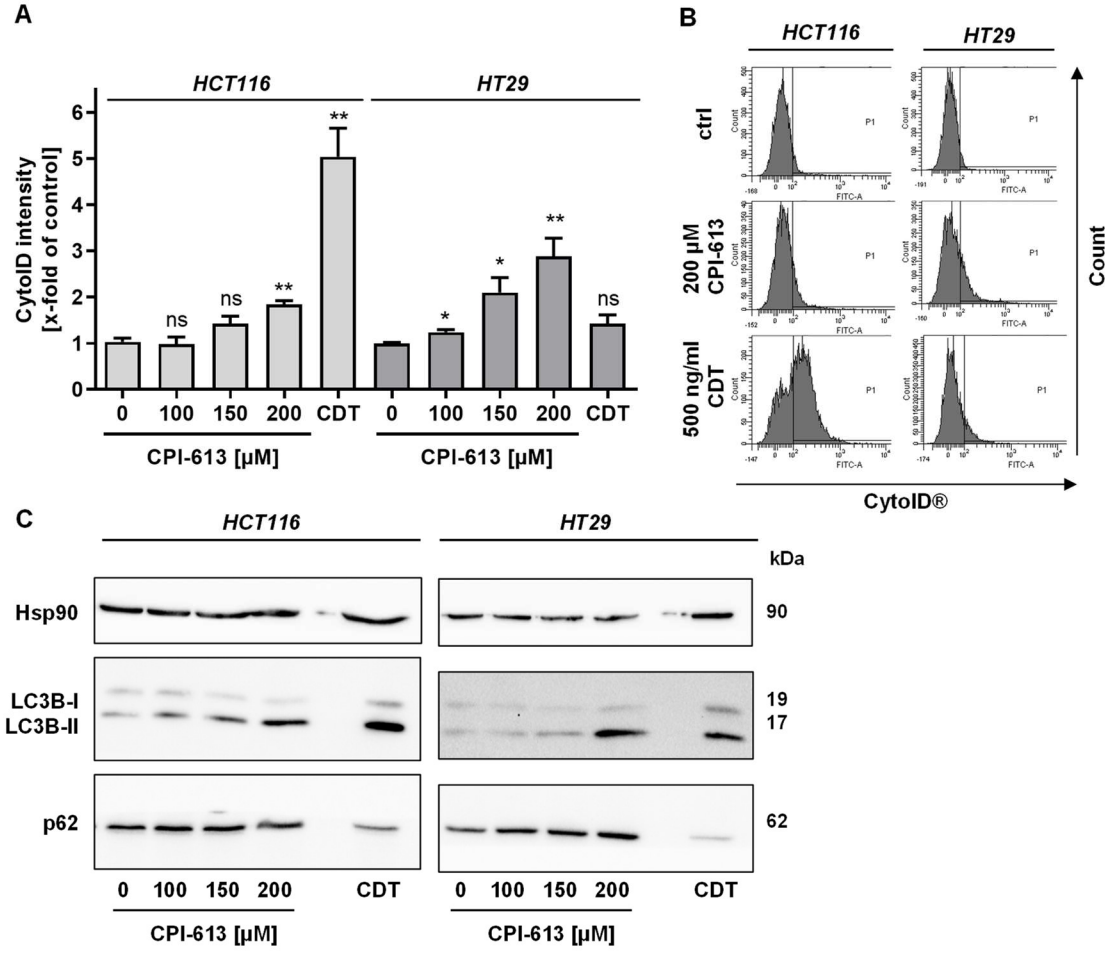

Figure 26: CPI-613 induces autophagy in CRC cells.
(A) Autophagy levels were determined using the CytoID® Green Autophagy Detection Kit after 48 h of incubation with increasing doses of CPI-613 in HCT116 (left panel) and HT29 (right panel). The bacterial toxin CDT (500 ng/ml) was used as positive control. Data is plotted as mean + SEM (n=3). ns: $p>0.05$, *$p<0.05$, **$p<0.01$ vs. control; *t*-test. (B) Western Blot analysis of the autophagy marker LC3B and the autophagy receptor p62. Cells were incubated for 48 h, harvested, lysed and subjected to SDS-PAGE and Western Blot analysis. Hsp90 served as loading control.

For the verification of autophagy induction, Western Blot analysis of the autophagy marker LC3B and the autophagy receptor and substrate p62 was conducted. LC3B-I was consistently converted to LC3B-II with increasing dose, while p62 increased, which is true for both HCT116 (Figure 26C, left panel) and HT29 (Figure 26C, right panel). In CDT-treated cells, LC3B-II increased strongly with concomitant reduction in p62 in both

cell lines. However, the CytoID® measurement showed an increase of autophagy levels by a factor of 5 in HCT116 but no significant increase in HT29 cells.

Taken together, the increase in CytoID® intensity and the autophagy marker LC3B-II indicated an increased formation of autophagosomes upon CPI-613, which was comparable to the cellular response in CRC cells upon incubation with the lipoate LA in the literature (Göder et al., 2015).

4.2.4. Genotoxicity testing of CPI-613

The principle of 5-FU, IT and oxaliplatin as cytostatics used in first line therapy of CRC is their DNA damaging mode of action (see 1.1.2.2). Although CPI-613 is designed to exclusively target mitochondrial energy metabolism, its application as drug besides the treatment of tumours requires a genotoxicity assessment. In this context, an InCellWestern (Figure 27A+B) plus a Western Blot analysis (Figure 27C) of the DNA damage marker γH2AX were performed as indicator tests in a first approach. Additionally, an alkaline Comet Assay to detect DNA double and single strand breaks and alkali labile sites (Figure 27A+B) were performed in a next step. All assays were conducted in a p53-wildtype cell line, HCT116, and a p53-mt cell line, HT29.

Either HCT116 or HT29 cells were incubated with increasing doses of CPI-613 (0-250 µM) for 24 h (Figure 27A+B). As positive control, 5-FU (10 µM) or Etoposide (5 µM) were used, which induced a 2.5-fold increase of γH2AX signal in both cell lines. In none of the treatments, any significant increase in γH2AX using the InCellWestern technique could be detected. When analysing γH2AX levels using Western Blot detection (Figure 27C), up to 150 µM CPI-613 did not increase γH2AX signalling in both cell lines. For HCT116, however, the highest dose (250 µM) slightly increased γH2AX, which is in accordance with DNA damage response signalling in cells undergoing cell death as seen in Figure 24A and H.

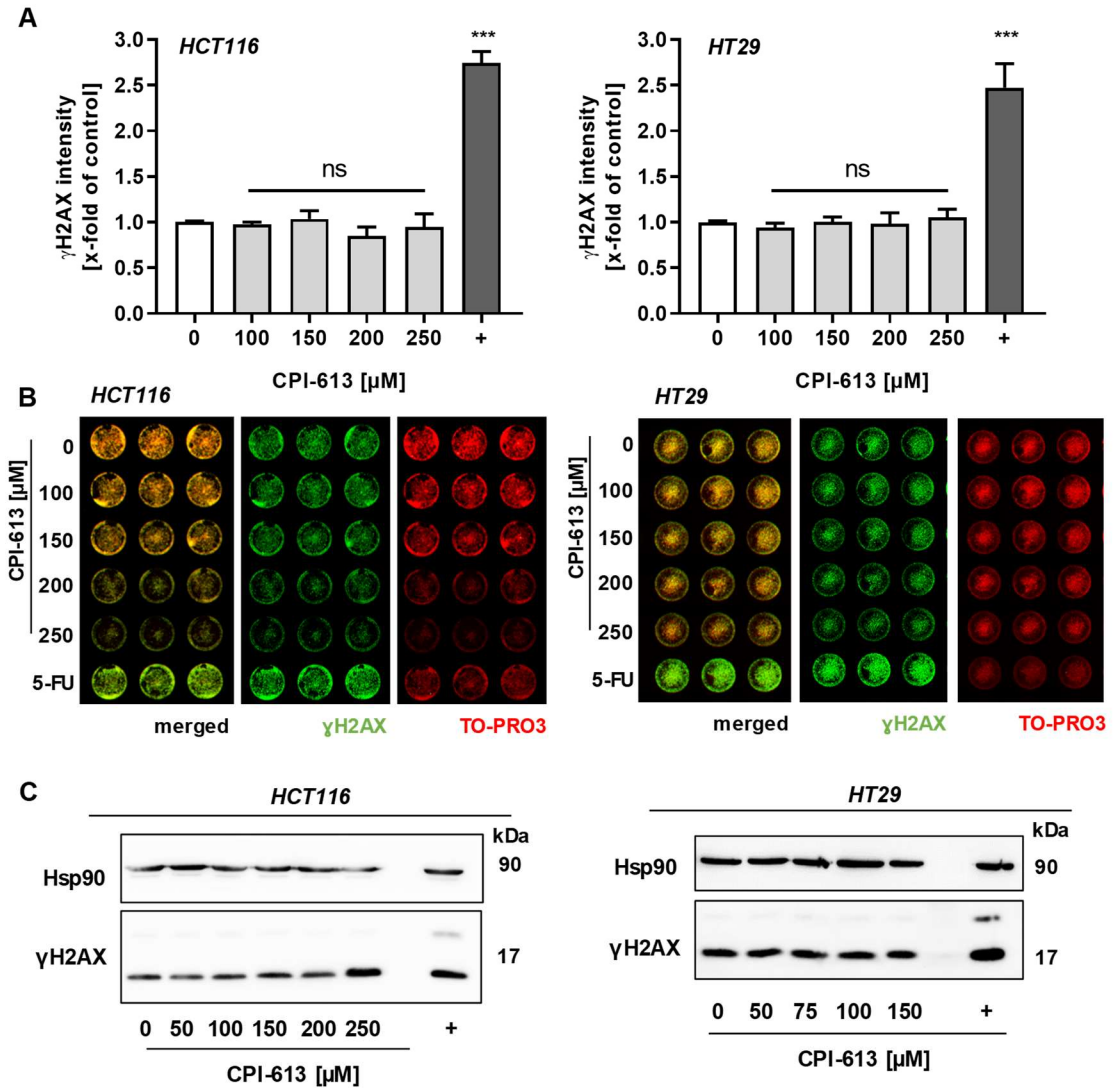

Figure 27: CPI-613 lacks genotoxicity.
(A) InCellWestern analysis of γH2AX in HCT116 (left panel) and HT29 (right panel) cells after 24 h at indicated doses. 5-FU (10 µM) was used as positive control. Data presented depicts mean + SEM (n=3). ns: $p>0.05$, ***$p<0.001$ vs. control; *t*-test. (B) Representative InCellWestern acquisitions of A. (C) HCT116 (left panel) and HT29 cells (right panel) were incubated with increasing doses of CPI-613 next to a positive control (5 µM Etoposide) and underwent Western Blot analysis for γH2AX. Hsp90 was visualised as loading control.

When cells were subjected to the alkaline Comet Assay, none of the doses tested (50-200 µM) elevated the tail moment as depicted in Figure 28A with representative comet photographs in Figure 28B in HCT116. In HT29 cells, a slight increase in γH2AX signal could be detected, which was not of statistical significance. As positive control, cells were treated with 200 µM tBOOH for 30 min.

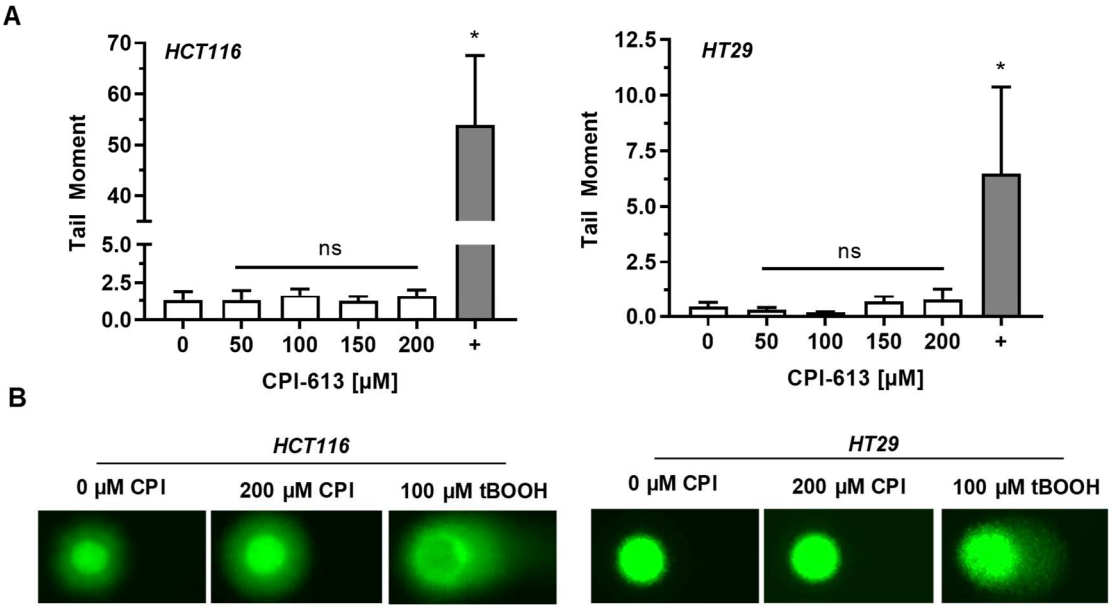

Figure 28: CPI-613 does not induce DNA strand breaks.
(A) Evaluation of alkaline Comet Assays in HCT116 (left panel) and HT29 (right panel) cells after 24 h of incubation with indicated doses. As positive control, cells were treated for 30 min with 200 µM tBOOH. Data presented depicts mean + SEM (n=3). ns: $p>0.05$, *$p<0.05$ vs. control; *t*-test. (B) Representative images of A.

Since CPI-613 was shown to elevate intracellular ROS levels (see Figure 19) and increased ROS levels are linked to increased oxidative nuclear DNA damage (Barzilai and Yamamoto, 2004), the potential of CPI-613 to cause oxidative DNA damage was investigated. Hence, a sensitive second approach to detect oxidative DNA damage, the FPG-modified alkaline Comet Assay as described in 3.2.6.2.1 was exploited.

As shown in Figure 29A, HCT116 cells were treated with either 100 or 200 µM CPI-613 and subjected to FPG incubation and the alkaline Comet Assay. During the FPG incubation, the bacterial enzyme FPG recognises oxidised purines (particularly 8-hydroxy-guanine) and hydrolytically cleaves the N-glycosidic bond, which gives rise to an apurinic site (Serre et al., 2002). Additionally, FPG cleaves the C3 phosphate bond at the 3' end of the apurinic site, which leads to a single strand break that can be detected in the alkaline Comet Assay. Incubation with 50 µM tBOOH for 20 min served as positive control. Once again, DNA damage in terms of tail moment was not significantly increased upon CPI-613 treatment. When including the aforementioned FPG incubation, the basal tail moment in the control rises. This rise could also be seen in CPI-613- or tBOOH-treated cells. However, the increase in tail moment as compared to the corresponding control was not significant for CPI-613. Representative photographs of the Comet IV software are shown in Figure 29B.

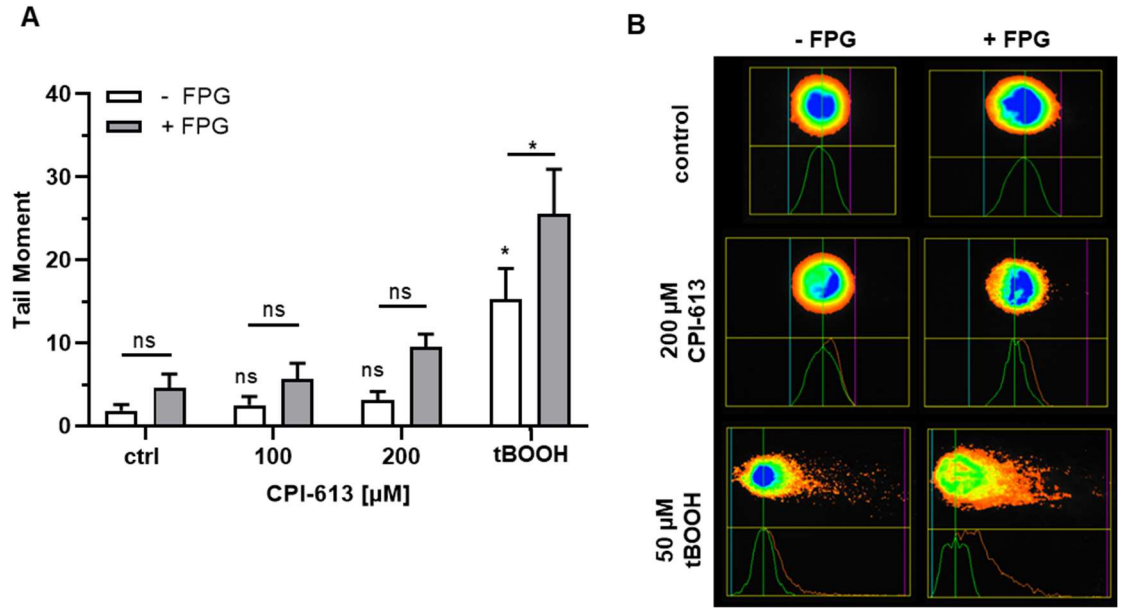

Figure 29: CPI-613 induces insignificant ROS-damage.
(A) HCT116 cells have been treated for 24 h with noted doses of CPI-613. While 50 µM tBOOH for 20 min served as positive control, cells underwent alkaline Comet Assay with supplementation with/without FPG (1 mg/ml). Data presented equals mean + SEM (n=4). ns: $p>0.05$, *$p<0.05$ vs. control or sample without FPG, respectively; 2-way-ANOVA. (B) Representative photographs of comet records of A.

In a nutshell, CPI-613 did not directly induce DNA damage in the form of persistent DNA single or double strand breaks. The formation of γH2AX was associated solely with cell death. As a secondary effect, however, ROS generated upon CPI-613 exposure might lead to oxidative DNA damage culminating in incessant mutations, which, however, was not proven in the studies outlined above.

4.3. Synergism of Lipoates and Standard Chemotherapeutic Agents in the Treatment of CRC

Nowadays, adjuvant chemotherapeutic regimen in all fields of oncology rely on the approach to combine several anticancer drugs with partially redundant or subsidiary modes of action. The rationale for combining such drugs is to a) prevent evolution of resistance, b) minimise side effects or toxicities and c) to increase efficacy (Bayat Mokhtari et al., 2017). While the previous experiments (sections 4.2) revealed CPI-613 as a promising agent in the treatment of CRC on a monotherapy-basis, its combination effect with standard chemotherapeutics is yet to be assessed. For the mother substance LA, a synergism with the anti-metabolite 5-FU has been demonstrated elsewhere (Dörsam et al., 2015; Neitzel et al., 2019). The following studies were conducted in order to assess beneficial combination effects.

4.3.1. Synergism modelling indicates beneficial combination effect

The golden standard for the evaluation of combination effects in pharmacology is the Chou Talalay method as detailed in Chou (2006), Chou (2010) and section 3.2.4. Summarizing the obtained CI values based on performed ATP assays, Figure 30A gives an overview of the combination of the lipoates CPI-613 and LA with the cytostatics 5-FU and IT. In HCT116 cells, the combination of CPI-613 and IT acted with the most distinctive synergism with a CI value as low as 0.39. Moreover, the combination of CPI-613 and 5-FU alongside LA and 5-FU or IT showed slight synergism in HCT116 with CI values of 0.87 and 0.89 or 0.82, respectively. In contrast, the combination of IT with either CPI-613 or LA in HT29 cells yielded a CI value greater than 1, 1.31 and 1.83, respectively, indicating an antagonistic combination effect. The combined application of any lipoate with 5-FU, however, resulted in CI values of 0.65 and 0.72, which represents significant synergism. Regarding the patient-derived cell line HROC278, no distinctive pattern manifested. While the combination of IT and LA as well 5-FU and CPI-613 was simply additive, 5-FU and LA had a positive combination effect, but IT and CPI-613 acted antagonistically.

In order to determine the concentration of any substance, which would result in the most promising response in combination regimen for future experiments, cell viability assays with a wide range of drug concentrations and their combinations were performed and Combenefit analysis were run as described in 3.2.4. Results were plotted as 3D model using the Highest Single Agent (HSA) model, in which those concentration points with best synergistic outcomes are coloured in blue and those concentration points with worst synergistic outcomes are coloured in red. Obtained from Figure 30B, for any substance, the upper concentration range was determined to be the most suitable. For CPI-613, a dose of 150 µM was found to fit best, which is also in accordance with its uniform IC_{50} across the CRC panel tested (see 4.2.1). To embrace the fact that HCT116 are more vulnerable to 5-FU and IT than HT29, moderate concentrations of 10 µM 5-FU and 20 µM IT were chosen to meet a compromise (see 4.2.1). Combenefit analysis were not performed for LA, however, 500 µM was chosen for further experiments as to reflect a concentration with moderate toxicity for both cell lines (see 4.2.1).

A

CI	CPI-613	LA
HCT116		
IT	0.39 (+++)	0.82 (++)
5-FU	0.87 (+)	0.89 (+)
HT29		
IT	1.31 (--)	1.83 (---)
5-FU	0.65 (+++)	0.72 (++)
HROC278		
IT	1.38 (--)	0.92 (±)
5-FU	1.10 (±)	0.79 (++)

B

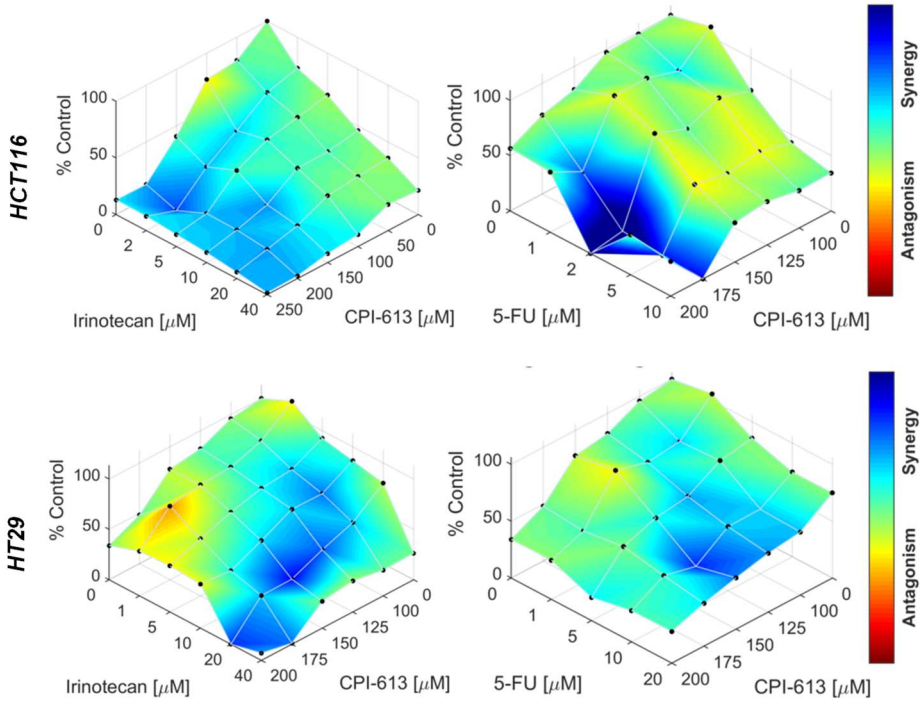

Figure 30: CPI-613 synergises with standard chemotherapeutics.
(A) The table summarises calculations of combination indices (CI) using the Chou Talalay method of lipoates (CPI-613, LA) together with standard chemotherapeutics (IT, 5-FU) in a variety of CRC cells. Modelling is based on cell viability data compiled using ATP assays after 72 h of incubation using the constant ratio approach. (B) 3D models generated by Combenefit software visualise the combination treatments allowing optimal dose choice for further experiments. Underlying data are gathered using ATP assays with a 6x6 matrix with an incubation time of 72 h. For both methodologies arithmetically averaged data of three independent experiments were used for analysis.

Having identified the optimal dose combinations and the most promising combinations of anticancer agents, detailed assessment using a variety of endpoints was conducted.

4.3.2. Cell death potentiates upon combination treatment

Addressing the endpoint of cell death in more detail, cell death measurements by flow cytometry in the form of AnnexinV/PI staining as depicted in 3.2.5.2 were performed with an incubation time of 48 h in HCT116 and HT29 cells.

Looking at HCT116, CPI-613 and LA only slightly induced cell death, but 5-FU and IT alone raised cell death rates significantly to approximately 25% each (Figure 31A). In particular, the combination of any cytostatic with CPI-613 potentiated cell death induction, which was less obvious when using LA as combinatory substance. The most promising combination derived from this assay was CPI-613 plus IT.

As expectable from IC_{50} values (see 4.2.1), HT29 cells reacted with increased cell death rates upon incubation with LA but decreased cell death induction upon IT and 5-FU as compared to HCT116 (Figure 31B). Again, both LA and CPI-613 potentiated cell death rates in combination with any anticancer drug used with the most beneficial outcome in cells treated with a regimen of IT and CPI-613.

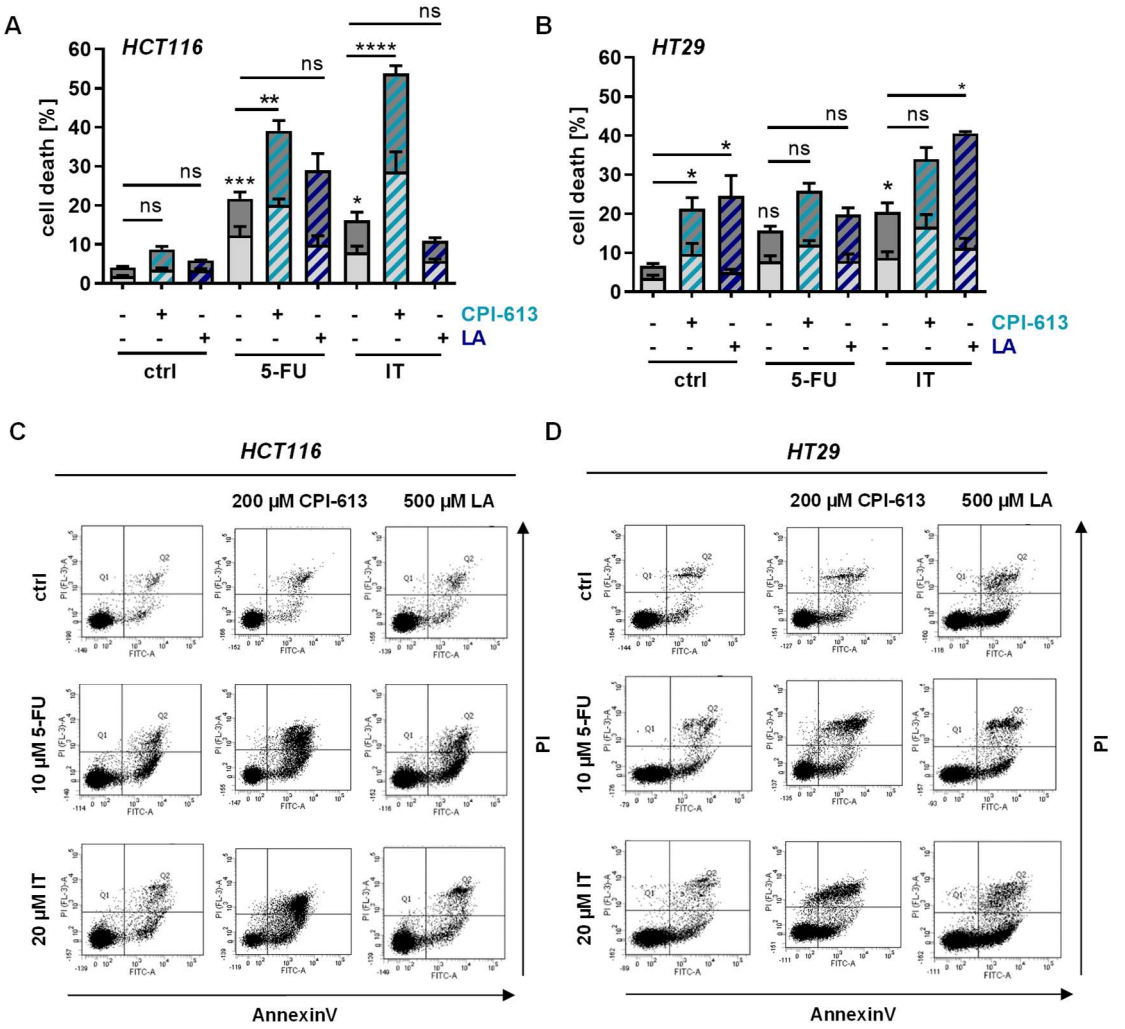

Figure 31: Cell death is potentiated upon combination of lipoates and chemotherapeutics.
Cell death was measured by flow cytometry using AnnexinV/PI staining after 48 h of incubation. Early apoptotic fraction is visualised in light grey, while late apoptosis/necrosis is coloured in dark grey. 200 µM CPI-613 or 500 µM LA were combined with 10 µM 5-FU or 20 µM IT, respectively, in HCT116 (A) and HT29 (B) cells. Data depicted represents mean + SEM (n=4). ns: p>0.05, *p>0.05, ** p>0.01, *** p<0.001, **** p<0.0001 vs. control or sample without additional lipoate treatment as indicated; 2-way-ANOVA. (C, D) Panel of representative dot plots of A and B, respectively.

In conclusion, especially CPI-613, other than LA, was able to potentiate cell death induction in any combination with standard chemotherapeutics.

4.3.3. Beneficial combination effect is not related to DNA damage levels

5-FU and IT represent genotoxic agents, which induce DNA damage in form of DNA strand breaks, which leads to the stabilisation of p53 (Lakin and Jackson, 1999; Pluquet and Hainaut, 2001; Williams and Schumacher, 2016). On the other hand, CPI-613, similar to LA, was shown to lack individual genotoxicity. The increase in cell death induction, however, might depend on altered DNA damage levels.

The tumour suppressor protein p53 is the most important regulator of cell cycle progression, apoptotic cell death and DNA damage response (Brady and Attardi, 2010; Williams and Schumacher, 2016). Upon stress or drug treatment, p53 is stabilised and activates a plethora of downstream target genes, including p21 as intervention in the cell cycle or BAX, PUMA and NOXA as pro-apoptotic genes necessary in the progression of programmed cell death (Chen, 2016; Williams and Schumacher, 2016).

To assess DNA damage levels and p53 stabilisation, Western Blot analysis of p53 and γH2AX in HCT116 (Figure 32A, left panel) and HT29 (Figure 32B, right panel) were performed. For HCT116 cells (Figure 32A, left panel), both standard chemotherapeutics 5-FU and IT induced γH2AX and stabilisation of p53. The stabilisation of p53 was more pronounced upon 5-FU, whereas a stronger induction of γH2AX and ubiquitinated species of γH2AX was notable upon IT. No increased levels of γH2AX were found upon CPI-613 treatment, but LA slightly induced γH2AX. In combination treatments, γH2AX induction triggered by 5-FU or IT was not altered upon addition of either LA or CPI-613. Both LA and CPI-613 alone depleted p53 protein. This depletion was also observed in cells treated with a combination of any cytostatic with any lipoate, although most pronounced in the combination of IT and LA. Of note, experiments in HCT116 and HT29 cells, which were incubated with either 150 or 200 µM CPI 613 for 24 or 48 h, and Western Blot analysis of p53 showed similar results (data not shown). Total p53 protein was depleted in HCT116 cells already after 24 h using 150 µM. This effect augmented with increasing dose and incubation time. However, in HT29 cells, bearing p53 with a gain of function mutation (R273H) (Rodrigues et al., 1990), p53 protein amounts was only depleted upon 200 µM CPI-613 for 48 h. Recently, the parental compound LA was shown to deplete p53 protein in CRC cells regardless of its mutation status (Neitzel et al., 2019). CPI-613, much like LA, treatment lead to a depletion of p53. In contrast,

treatment with standard chemotherapeutics, such as 5-FU or IT, trigger a stabilisation of p53.

With respect to HT29 cells (Figure 32A, right panel), both 5-FU and IT lead to an increase of γH2AX, which was, however, stronger upon 5-FU. Conversely, general stabilisation of p53 upon both anticancer drugs was notable, but with a greater emphasis upon IT. Induction of γH2AX and p53 protein were unaffected upon CPI-613 but increased upon LA monotreatment. For combination treatments, γH2AX levels were unaffected with regard to 5-FU plus any lipoate, but any combination with IT lead to a strong increase in γH2AX, whereas a p53 depletion in all cases of cytostatic plus lipoate was visible.

In order to quantify changes in γH2AX levels more sensitively, InCellWestern measurements were conducted (Figure 32B). Cells were herein treated as in Figure 32A. Looking at HCT116 cells (Figure 32B, left panel), no significant changes upon LA or CPI-613 alone were detected, although LA lead to a slight increase. As expected, both 5-FU and IT increased γH2AX levels strongly to more than 3- respectively 2.5-fold of the control. Using the combination of 5-FU and CPI-613, γH2AX levels dropped dramatically, while the combination of IT and CPI-613 slightly increased γH2AX levels, although not significantly. With respect to 5-FU and LA in a combination regimen, γH2AX amounts decreased moderately, while γH2AX levels upon the combination regimen of IT and LA were statistically unchanged. Considering HT29 cells (Figure 32B, right panel), neither LA nor CPI-613 induced γH2AX signalling. Comparable to HCT116 cells, 5-FU and IT promoted γH2AX, even if to a minor extent (2.5- and 2-fold). All trends observed in HCT116 for combination treatments held true for HT29, as well.

A master regulator of cell cycle progression is the p53-downstream target p21, also known as CDK inhibitor I. It links DNA damage to cell cycle arrest since p21 is activated upon p53 stabilisation (Abbas and Dutta, 2009; Karimian et al., 2016). Cell cycle arrest upon IT and 5-FU were demonstrated in Figure 22. An induction of p21 upon IT treatment was verified in both HCT116 as well as HT29 cells (Figure 32D), but only in HCT116 treatment with 5-FU lead to an increased expression of p21. These levels were slightly decreased in HCT116 cells upon the addition of CPI-613 or LA, which on their own did not induce p21. Interestingly, p21 could be detected in CPI-613-treated HT29 cells, with a band appearing at a higher molecular weight. LA, either alone or in combination with any cytostatic, did not result in an induction of p21, which, however, is reported in the literature as a p53-independent cellular response (Dörsam et al., 2015).

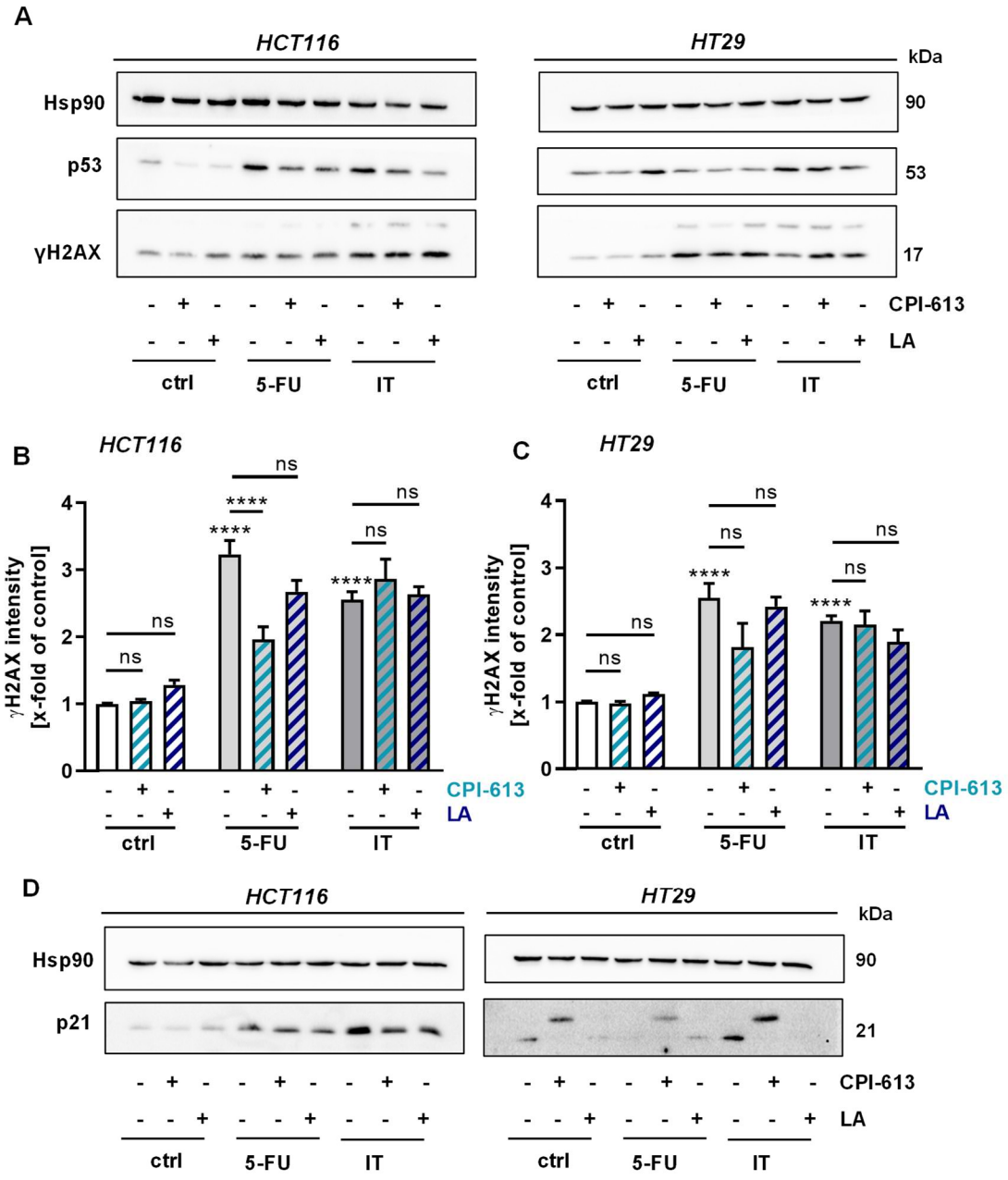

Figure 32: Influence of lipoates on genotoxicity of standard chemotherapeutics.
(A) Western Blot analysis of p53 and γH2AX in HCT116 (left panel) and HT29 (right panel) after 200 µM CPI-613 or 500 µM LA in combination with 10 µM 5-FU or 20 µM IT respectively for 24 h. InCellWestern analysis of γH2AX normalised to nuclear stain using TO-PRO3 after 24 h of CPI-613 or LA and chemotherapeutics in HCT116 (B) and HT29 (C). Data depicted represents mean + SEM (n=4). ns: p>0.05, **** p<0.0001 vs. control or sample without additional lipoate treatment as indicated; 2-way-ANOVA. (D) Western Blot analysis of cell cycle regulator p21 in HCT116 (left panel) and HT29 (right panel) treated as described in A.

Summing up, the combination of any lipoate with any anticancer drug used in the treatment of CRC did not alter DNA damage levels.

4.3.4. Influence of autophagy levels on combination effect

A number of agents used in the treatment of CRC are proven to induce autophagy as a means of cellular survival mechanism and a reaction to genotoxic insults or stress (Qiang et al., 2013; Zhang et al., 2015). Additionally, autophagy is described as process upregulated in cancer cells to overcome nutrient starvation (Folkerts et al., 2019). Göder et al. (2015) found LA to induce autophagy in CRC, for which indications upon CPI-613 exposure was reported earlier in this work (see 4.2.3). Whether the combination of lipoates and genotoxins results in changed autophagy levels, however, has not been addressed this far.

Utilizing the CytoID® Green Autophagy Detection kit, relative autophagy levels in HCT116 and HT29 cells were assessed upon combination regimen similar to those in Figure 31. A single treatment of CPI-613 and LA did not significantly induce autophagy levels in HCT116 although levels unambiguously increased (Figure 33A+C), whereas 5-FU and IT increased autophagy levels by a factor of 2 and 6, respectively. Surprisingly, a combination of both 5-FU or IT with CPI-613 dramatically abolished autophagy and autophagy levels dropped to basal levels in these cells. Contrary, the combination of LA with any cytostatic did not affect autophagy levels. Examining HT29 cells (Figure 33B+D), again neither LA nor CPI-613 induced autophagy significantly, even though an inducing trend was notable. This is in line with observations by Göder et al. (2015). Cytostatic treatments induced autophagy just as in HCT116, even if less marked (2- and 4-fold). A combination with CPI-613, similarly, lead to a decline in autophagy rates. LA, on the other hand, was not able to affect autophagy levels in cells exposed to combination treatments.

In order to verify the observed effects of CPI-613 single treatment and combination treatments with 5-FU and IT, Western Blot analysis of the autophagy marker LC3B and autophagy receptor p62 were performed (Figure 33D). Using HCT116 cells (Figure 33D, left panel), LC3B-II was primarily formed in cells treated with either CPI-613, 5-FU or IT alone. The p62 protein was almost not abundant in cells treated with 5-FU or IT but became visible again in combination treatments. In cells subjected to combination treatments, LC3B-II was mostly unaffected. For HT29 cells (Figure 33D, right panel), the autophagy receptor p62 was depleted in cells treated with cytostatics alone, but increased robustly in any cell sample treated with CPI-613. In particular in cells treated with cytostatics, a robust induction of LC3B-II was observed, whereas the addition of CPI-613 considerably reduced the amount of LC3B-II.

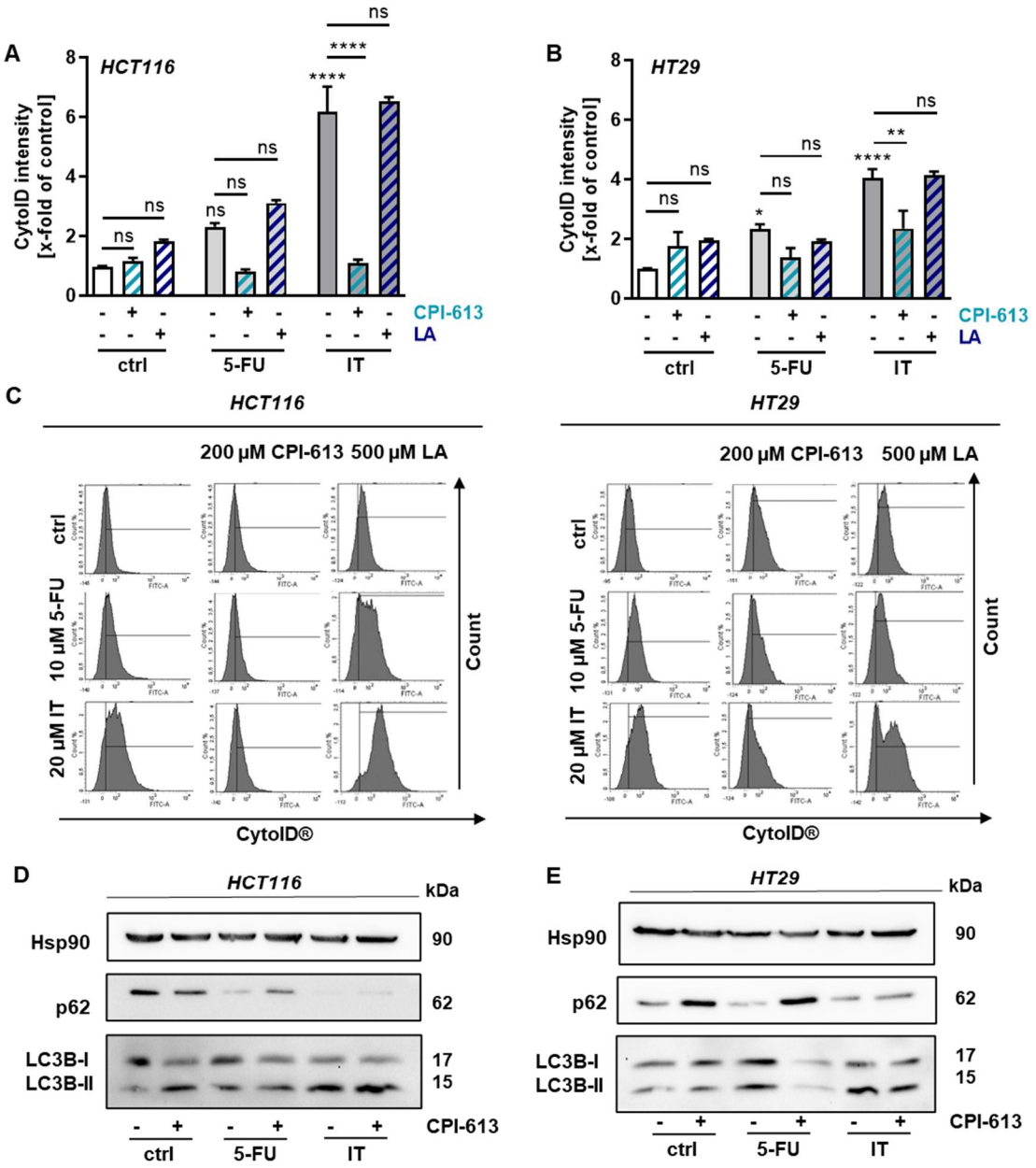

Figure 33: Effect on cytostatic-triggered autophagy in combination regimen.
(A, B) Autophagy levels were determined in cells which were treated for 48 h with 200 µM CPI-613 or 500 µM LA and 10 µM 5-FU or 20 µM IT, respectively. Upon harvesting and staining autophagosomes using CytoID®, autophagy levels were normalised to control cells. Results for HCT116 (A) and HT29 (B) cells are represented as mean + SEM (n≥3). ns: $p>0.05$, *$p<0.05$, ** $p<0.01$, **** $p<0.0001$ vs. control or sample without additional lipoate treatment as indicated; 2-way-ANOVA. (C) Overview of representative histograms of A and B. (D, E) Cells treated were subjected to whole cell lysis and Western Blot analysis of autophagy marker LC3B, autophagy receptor p62 and loading control Hsp90.

Concluding, the lipoate LA in combination regimen did not affect autophagy flux in anticancer drug-treated CRC cells. In contrast, the addition of CPI-613 to the anticancer drugs suppressed autophagy, which might play a role in the augmented cell death induction.

4.4. Proof of Therapeutic Efficacy of CPI-613 in Combination Treatments *in vivo*

In order to translate *in vitro* findings into the *in vivo* situation, two experimental approaches were used: a) a xenograft mouse model using the CRC cell lines HCT116 and HT29 and b) a model of chemically-induced CRC tumours based on the AOM/DSS model according to Dörsam et al. (2018) and Fahrer et al. (2015). The overall objective was to assess the therapeutic efficacy of CPI-613 as a monotherapy and to verify the synergism of CPI-613 in combination therapy together with IT.

Prior to pivotal xenograft mouse experiments, acute toxicity studies for CPI-613 have been conducted (data not shown). Herein, its tolerability represented by the lack of body weight loss and abnormal behaviour was demonstrated using a treatment scheme according to the following mouse experiments in dosages up to 50 mg/kg BW (3x/week).

4.4.1. Xenograft mouse studies confirm synergism of CPI-613 with IT

Xenograft experiments are commonly used throughout oncological research (Göder et al., 2015; Krumm et al., 2016). In the literature, CPI-613 has been tested in this type of experiment for lung and pancreatic cancer cell lines, but has never been applied in the context of CRC (see 1.3.2.5).

Xenograft studies were conducted in male BALB/c nu/nu mice of at least 7 weeks of age. Inoculation of CRC cells (HCT116 or HT29) was performed as described in 3.2.11.2.1. Upon initial growth of xenograft tumours for 7 days, a therapy of 4 consecutive weeks as depicted in Figure 34A and Figure 35A and described in 3.2.11.2.3 was carried out. Three times a week, body weight as well as tumour dimensions were recorded (see 3.2.11.2.2). Once termination criterion was met or at the end of the experiment, animals were sacrificed, tumours isolated and stored at -80°C after snap freezing in liquid nitrogen.

A first set of experiments was performed using HCT116 cells (Figure 34). The body weight gain diagram (Figure 34B) clearly shows that animals receiving CPI-613 (blue line) gradually gained body weight (+5% at the end of the experiment), comparable to control animals. Mice injected with IT (orange line) or the combination regimen (green line), however, slowly lost body weight up to 10%, with IT being the leading compound responsible for this toxicity. Remarkably, control animals did not survive the whole experimental time period and reached day 23 at a maximum due to fast tumour growth rates. Recorded tumour volumes are plotted in either absolute (Figure 34C) or relative (Figure 34D) numbers. Absolute tumour volumes of control animals steadily increased

over time with a steep tumour growth curve, which reached the maximum of 1500 mm³ after 23 days on average. The absolute tumour volumes were not significantly different to control animals when animals received IT alone, although the tumour growth had a delayed onset. Both CPI-613 and the combination regimen were able to inhibit tumour growth distinctly. Notably, the combination regimen showed the flattest tumour growth curve with a tumour volume of about 400 mm³ on average at the scheduled end of the experiment, which also underlines the superiority over single treatments.

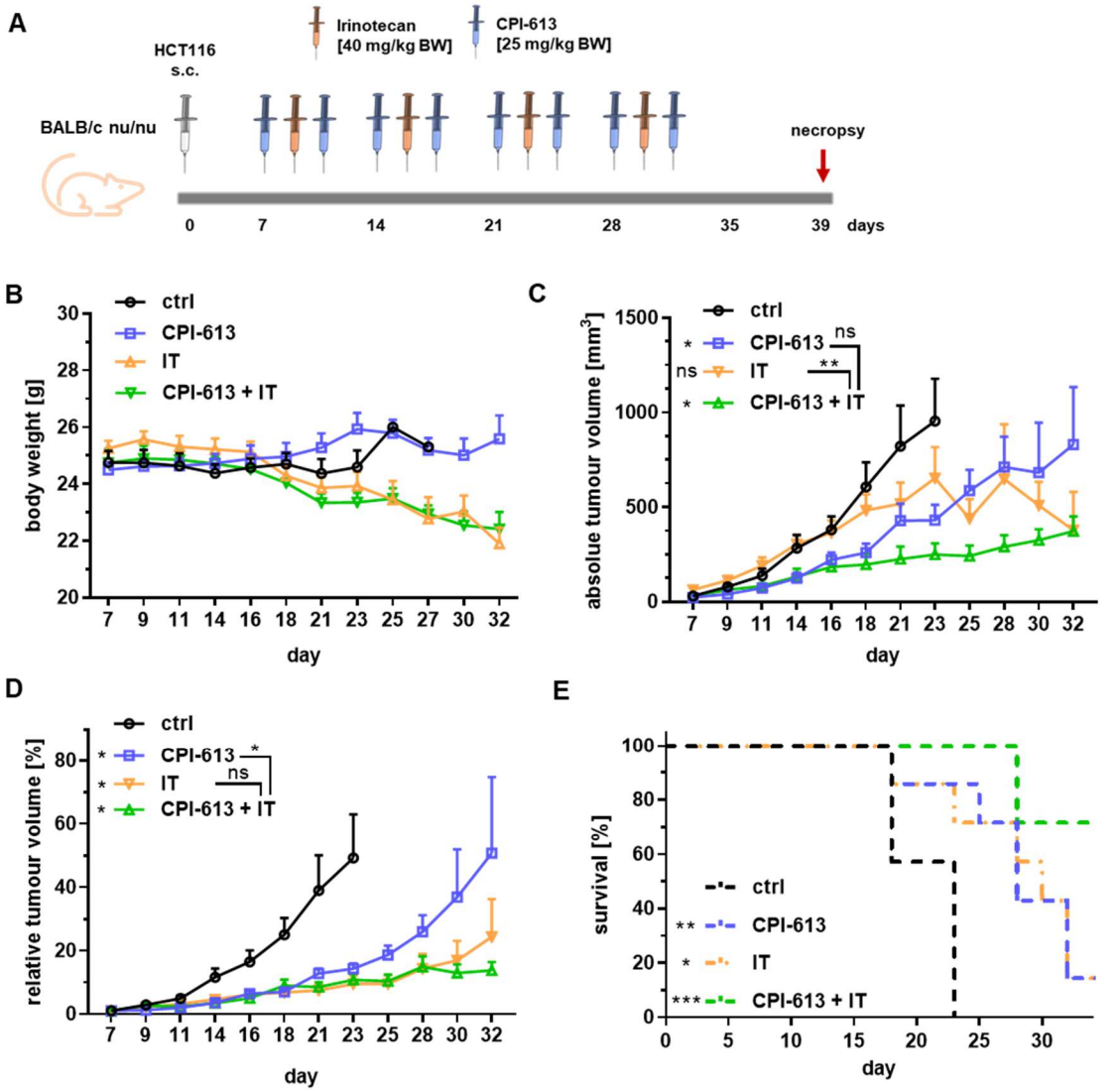

Figure 34: Antitumour activity of CPI-613 in comparison to IT in HCT116 xenograft model.
(A) Treatment scheme of male BALB/c mice. Inoculation of HCT116 cells was followed by 7 days of initial tumour growth. Tumours were treated for 4 consecutive weeks with alternating injections of CPI-613 and IT as indicated. Necropsy included isolation of the tumours. (B) Average body weight gain diagram of animals under treatment (n=7 animals/group). (C) Absolute and (D) relative tumour volume in mm³ or percent, respectively. (n=14 tumours/group). ns: p>0.05, *p<0.01, **p<0.01 vs. control animals or monotreatment as indicated; 2-way-ANOVA. (E) Survival analysis as Kaplan-Meier-curve and analysis using log-rank (Mantel Cox) test. (n=7 animals/group). *p<0.05, **p<0.01, ***p<0.001 vs. control animals; log-rank (Mantel Cox) test.

Considering relative tumour volumes, the ranking of the different therapy treatments becomes clearer when looking at the shape of the curves. While CPI-613 was not as effective as IT alone, the combination regimen was able to reduce tumour growth most potently. The strongly reduced tumour growth of animals receiving the combination regimen lead to an increased survival rate. Enhanced survival of animals receiving a combination of CPI-613 plus IT is easily notable in the corresponding Kaplan-Meier-curve and the significantly higher improved overall survival assessed by log-rank (Mantel Cox) test and a median survival of more than 40 days (Figure 34E). Animals receiving either CPI-613 or IT alone, nevertheless, showed improved survival outcome as compared to mock-treated animals with a median survival of 27 and 31 days, respectively, opposed to only 23 days in the control group.

Using the p53-mt HT29 cells, xenograft studies identical to HCT116 were conducted (Figure 35A). With respect to general toxicity/body weight gain, all treatment groups continuously increased in weight (Figure 35B). Notably, vehicle control animals lived no longer than 21 days and IT-treated animals had to be terminated at day 28 the latest. On average, animals of the CPI-613-group gained 13% body weight over the whole duration of the experiment. Rating absolute tumour volume progression over time (Figure 35C), control animals showed the fastest growing tumours with steep growth curves and an average of 1200 mm^3 tumour volume after 21 days. The curve of IT-treated tumours proceeds minimally above the tumour growth curve of CPI-613-treated animals. The strongest tumour inhibition was measurable in animals receiving a combination treatment of CPI-613 and IT, which was statistically more beneficial than monotherapies as well. Nonetheless, the average tumour size of this group was more than 900 mm^3 after 32 days. In the view of relative tumour volume values, CPI-613 and IT switch places in efficiency, while the combination regimen clearly showed best therapy outcome among all treatment groups (Figure 35D). Comparable to HCT116-xenografted mice, those animals in the combination regimen treatment group had best survival outcome, which was furthermore the only group having an advantage in comparison to control groups according to the log-rank (Mantel Cox) test on Kaplan-Meier-curves (Figure 35E). A median survival of 21 days in both control and CPI-613-treated animals was opposed to a median survival of 25 days in both IT- and combination treatment-receiving animals.

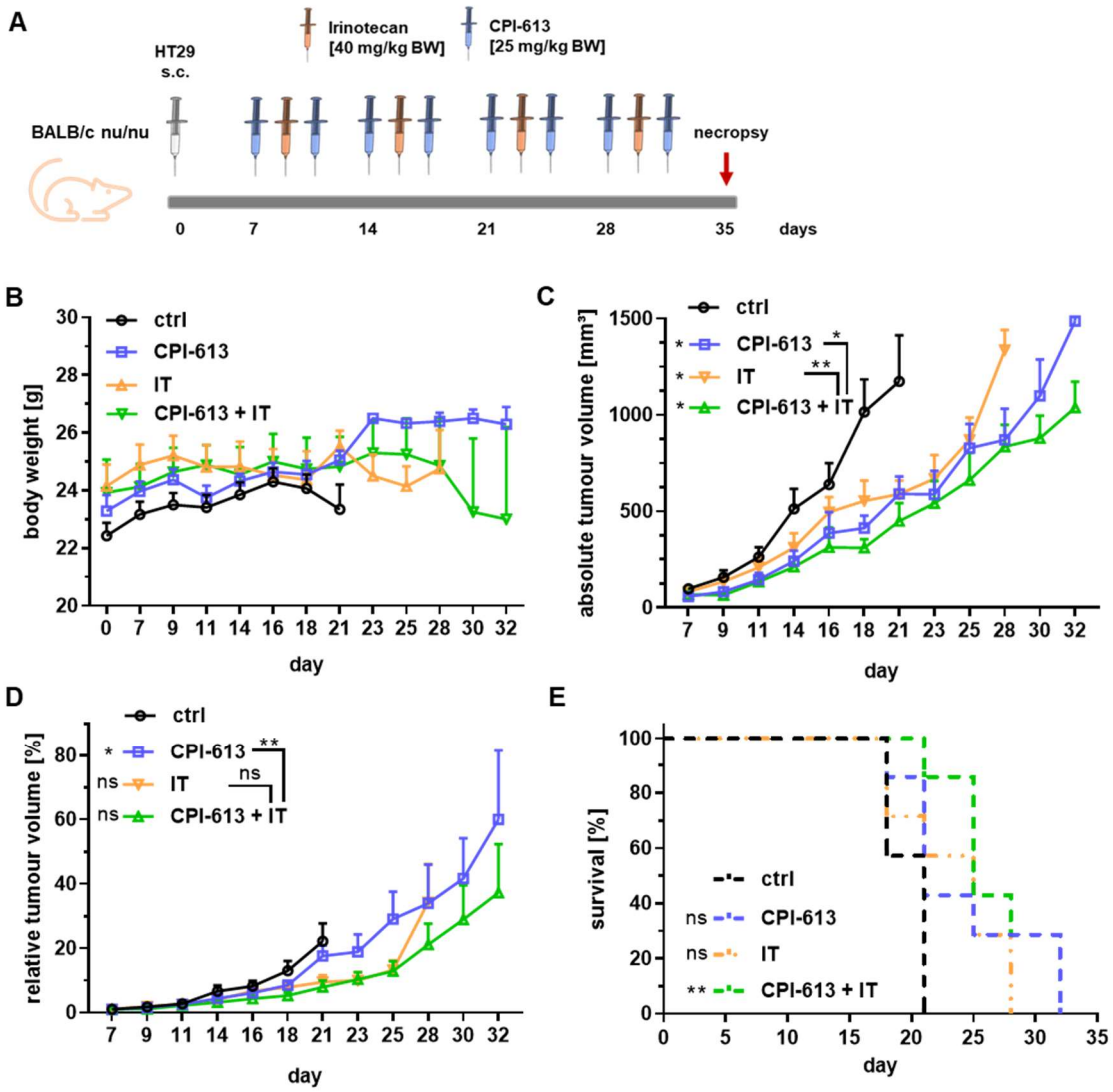

Figure 35: Antitumour activity of CPI-613 in comparison to IT in HT29 xenograft model.
(A) Treatment scheme of male BALB/c mice. Inoculation of HT29 cells was followed by 7 days of initial tumour growth. Tumours were treated for 4 consecutive weeks with alternating injections of CPI-613 and IT as indicated. Necropsy included isolation of the tumours. (B) Average body weight gain diagram of animals under treatment (n=7 animals/group). (C) Absolute and (D) relative tumour volume in mm³ or percent, respectively. (n=14 tumours/group). ns: $p>0.05$, *$p<0.01$, **$p<0.01$ vs. control animals or monotreatment as indicated; 2-way-ANOVA. (E) Survival analysis as Kaplan-Meier-Curve and analysis using log-rank (Mantel Cox) test. (n=7 animals/group). ns: $p>0.05$, **$p<0.01$ vs. control animals; log-rank (Mantel Cox) test.

Making use of histological HE overview staining of cryosections of the maximum diameter of isolated tumours, a comparison in terms of tumour size is possible (Figure 36; according to 3.2.11.2.5). Tumours of control animals showed the biggest tumour area, followed by CPI-613. Those tumours from animals having received a combination of CPI-613 and IT happen to be the smallest. In particular, HE stains of CPI-613- or combinatory treated-animals do not exclusively show hyperchromasia or bulky dark violet staining indicating condensed tumour areas, but in the centre of the sections light pink areas are notable, representing necrotic regions. Generally, the nucleus-plasma

relation within each of the tumours is shifted in favour of the nuclei, confirming the morphological transformation inherent of dysplasia, adenoma and carcinoma.

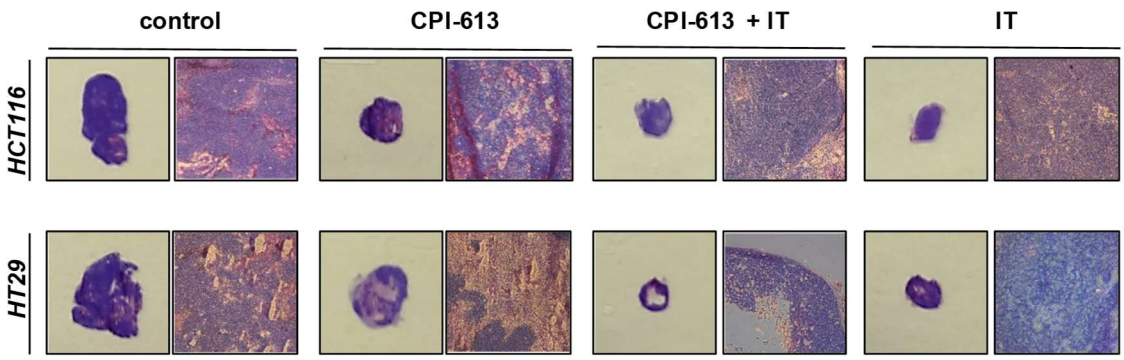

Figure 36: Histological overview staining of xenograft tumours.
HE staining of isolated tumours at maximum diameter of HCT116 (top panel) and HT29 (bottom panel) xenograft experiments. Cryosections of 10 µm were stained with haematoxylin and eosin and representative microscopic pictures at 20x magnification are summarised.

Xenograft tumours isolated at the end of each experiment were subjected to lysis, SDS-PAGE and Western Blot analysis of the DNA damage marker γH2AX, the levels of p53 protein and autophagy in terms of LC3B formation. Tumours isolated from mice inoculated with HCT116 cells were analysed and results are summarised in Figure 37A with the corresponding densitometric evaluation in Figure 37B. IT treatment lead to an induction of all three proteins analysed, namely p53, γH2AX and LC3B. A slight increase in p53 was also notable in CPI-613-treated mice. The level of γH2AX and LC3B in those animals receiving CPI-613 was unaffected. Interestingly, the combination of CPI-613 and IT resulted in suppressed induction of p53, γH2AX and LC3B as compared to CPI-613 alone. The same set of Western Blot analysis was performed on tumours isolated from mice inoculated with HT29 cells (Figure 37C+D). Generally, p53, γH2AX as well as LC3B did not show any difference between control and CPI-613-treated animals. Once more, IT strongly induced all three proteins of interest. Contrary to HCT116, combination treatments caused a result in-between of the single treatments.

In summary, the therapeutic efficacy and benefit of CPI-613 as a monotherapy or as part of a combination treatment together with IT could be shown in xenograft mouse experiments irrespective of the inoculated CRC cell line. Furthermore, the synergistic mode of action of CPI-613 and IT, which was described in 4.3, could be confirmed. The benefit included the slowing down of tumour growth, the prolonged survival comprising the increased median survival as compared to control animals and compared over treatment groups.

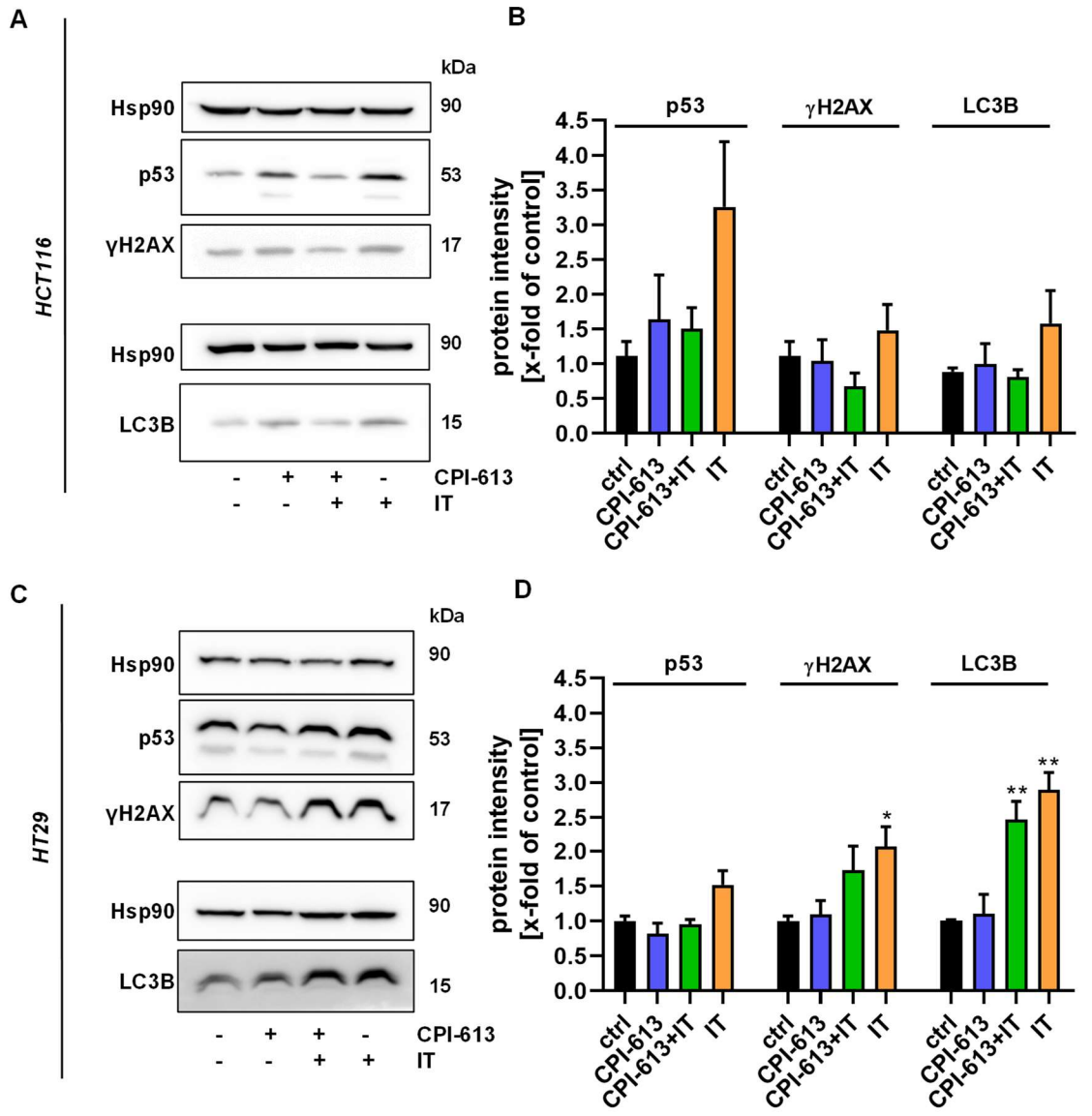

Figure 37: Effects on p53, γH2AX and LC3B protein levels in tumour tissue obtained from xenograft studies.
Snap frozen tumour segments were lysed, subjected to SDS-PAGE and Western Blot analysis. Shown are Western Blot analysis of p53, γH2AX and LC3B as well as the loading control Hsp90 in HCT116 (A) and HT29 (C) xenograft tumours as well as their densitometric evaluation (B, D) (n=4 for HCT116, n=3 for HT29). *p<0.01, **p<0.01 vs. control; *t*-test.

4.4.2. Chemically-induced CRC can be efficiently treated with CPI-613 plus IT in mice

Although xenograft experiments are an established tool to evaluate drug candidates, a more sophisticated approach is required to draw comprehensive conclusions. In order to meet this requirement, the murine AOM/DSS model for studying advanced colorectal carcinogenesis was applied in the following. Its robustness and applicability in studying therapeutics have been described and stated elsewhere (Robertis et al., 2011; Parang et al., 2016).

Colorectal tumours were induced in male C57BL/6 mice (7-9 weeks of age) using the AOM/DSS-model (see 3.2.11.3). Initial AOM injection using 10 mg/kg BW was followed by two cycles of 1% DSS in drinking water for 7 consecutive days followed by 14 days of rest in order to induce a significant amount of tumours (Figure 38A). Tumour burden and progression was monitored by mini-endoscopy throughout the tumour therapy at day 42, 56 (week 2) and 73 (week 4). Therapy lasted for 4 weeks as described in 3.2.11.3.4. Blood samples were collected alongside (see 3.2.11.3.6).

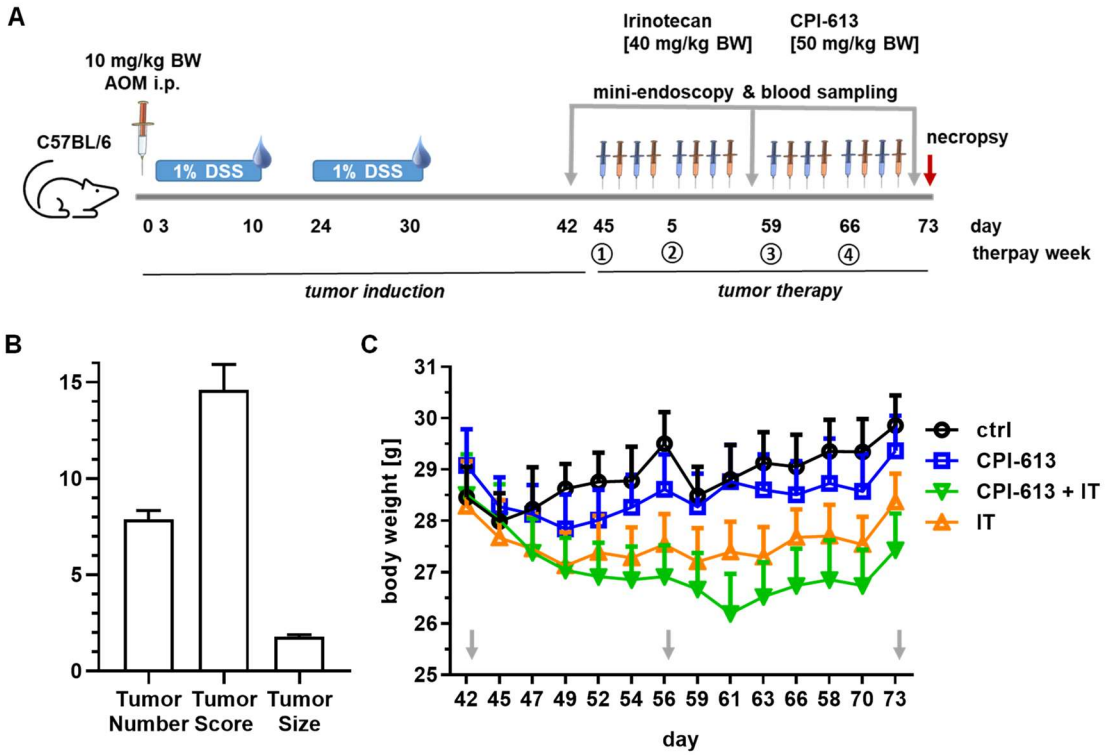

Figure 38: Chemically-induced CRC in mice.
(A) Scheme of tumour induction using 10 mg/kg BW AOM i.p. and two cycles of 1% DSS in drinking water for 7 days followed by tumour therapy of four consecutive weeks with alternating injections of CPI-613 and IT as depicted. Tumour number and size were monitored prior to the start of the therapy, in the middle (week 2) and at the end (week 4) using mini-endoscopy. Blood sampling at these time points was used for differential blood analysis. (B) Average tumour number, score and size at the start of the therapy (n=60). (C) Body weight curves of grouped animals. Gray arrows indicate time points of mini-endoscopic surveillance of tumour burden. Data are presented as mean + SEM.

Tumour prevalence was 100% in all animals undergoing mini-endoscopy at day 42. On average, animals had a tumour multiplicity of 7 to 8 with an average size of 1 to 2, resulting in an overall tumour score of approximately 14 to 15 prior to the start of the therapy at day 42 (Figure 38B). These numbers represent advanced or highly progressed CRC. Noteworthy, the tumour burden was inhomogeneous among all mice per experimental run (n=3), with the result that some animals bore either few little or many big tumours at the start of the therapy. Grouping was performed in order to compensate for these variances and to equal these parameters over the performance of

several set of experiments, i.e. mean tumour number and mean tumour score. While animals of the control group and animals receiving CPI-613 as monotherapy constantly gained body weight, animals treated with either IT as monotherapy or in combination with CPI-613 were subject to variation throughout therapy week 3 and 4 as depicted in Figure 38C. Body weights were slowly reducing in the first two weeks of therapy, but increased again in the last two weeks of therapy.

At day 56 (end of therapy week 2), a mini-endoscopy was performed in order to determine progression of number, tumour score and average tumour size of tumour-bearing mice. Results are summarised in Figure 39A-C with representative photographs in Figure 39D. Animals of the control group carried on average > 8 tumours per animal and although each of the therapy groups had slightly less tumours, these differences are not statistically significant (Figure 39A). With respect to tumour scores, the average overall score of animals receiving only vehicle control was about 20. CPI-613-treated animals followed with approx. 17, next to combinatory- and IT-treated animals with a mean score of 14 (Figure 39B). The average tumour size rose from 1-2 prior to the start of the therapy to 2-2.5 in control animals (Figure 39C). Animals under therapy with IT or the combination of CPI-613 and IT carried considerably smaller tumours with an average < 2. The differences between therapy groups, however, was not significantly different.

After completion of the therapy at day 73 (week 4), a terminal mini-endoscopy revealed therapy outcome in relation to average tumour number, score and size (Figure 39E-H). Tumour number among all groups ranged from 7-8 with no considerable change in multiplicity between groups or with respect to former mini-endoscopic evaluations (Figure 39E). Comparing the progress from therapy week 2 to therapy week 4, the tumour score in mock- and CPI-613-treated animals increased from 20 to 24 and 17 to 20 respectively, whereas animals injected with IT or the combination of IT and CPI-613 showed significantly reduced tumour scores from 18 and 17 to 15.5 and 15 (Figure 39F). The progression of average tumour size was comparable in all groups with a median increase of approximately 0.5 size points (Figure 39H). The most efficient compound in this experimental set-up was IT, since comparison of the remaining therapy groups uncovered no arithmetical variation. The monotherapy of CPI-613 showed no clear and measurable therapeutic benefit. The combination of CPI-613 and IT, unfortunately, did not dramatically increase therapeutic efficacy as compared to monotherapy with either CPI-613 or IT.

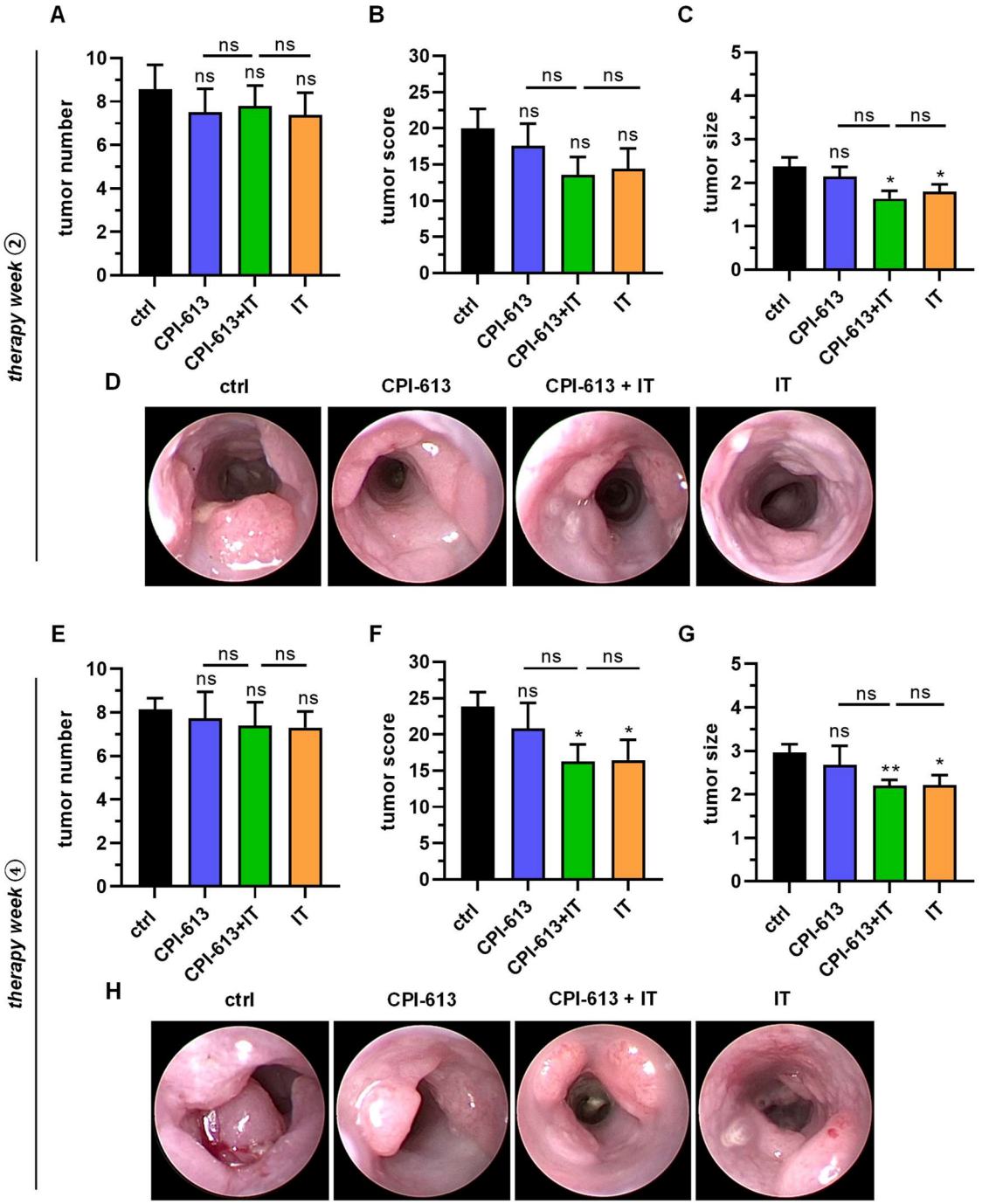

Figure 39: Therapeutic efficacy of CPI-613, IT and their combination in AOM/DSS-induced colorectal tumours.
After two weeks of therapy, average tumour number (A), average tumour score (B) and average tumour size (C) per group were monitored using mini-endoscopy. Overview of representative pictures taken during endoscopy is compiled in D. Upon completion of the therapy at week 4, average tumour number (E), average tumour score (F) and average tumour size (G) per group was evaluated using mini-endoscopy. Representative pictures taken during endoscopy are summarised in G. (n≥11 animals/group). ns: $p<0.05$, *$p<0.05$, **$p<0.01$ vs. control animals or monotreatment as indicated; 2-way-ANOVA.

Differential blood analysis was performed at day 56 and 73 to supplement toxicity data and to assess haematological effects of IT and CPI-613 as an indicator for bone marrow toxicity.

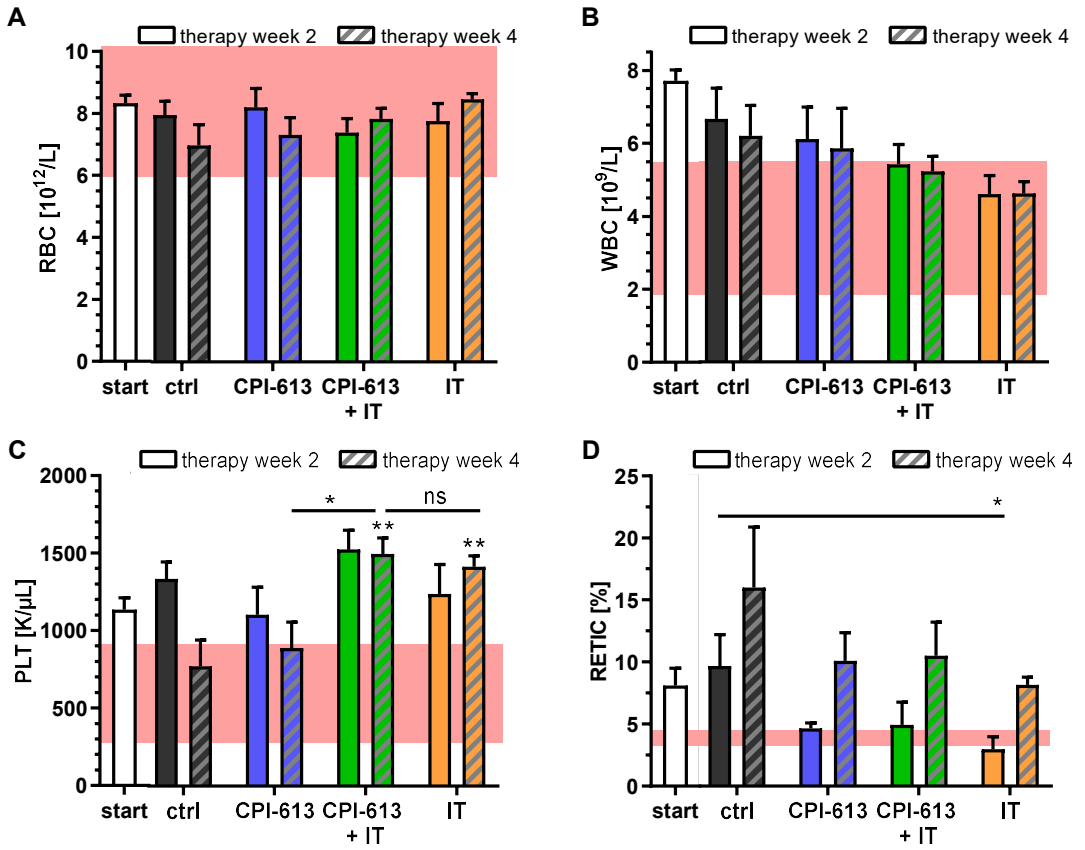

Figure 40: Differential blood analysis of animals undergoing AOM/DSS model coupled with therapy. Haematological surveillance of animals under treatment of red blood count (A), white blood count (B), platelet count (C) and reticulocyte abundance (D) determined at the same time as tumour burden. Red area represents physiological reference range. Column "start" describes the time point prior to the start of the therapy, day 42. (n≥6 animals/group/time point). ns: $p<0.05$, *$p<0.05$, **$p<0.01$ vs. sample of different time point or sample of the same time point of a different treatment group as indicated; *t*-test.

Red blood cell (RBC) count of control animals as well as CPI-613-treated animals dropped from 8 to 6.5 x 10^{12} erythrocytes per litre (Figure 40A). With respect to IT or the combination of IT and CPI-613, RBC rose from 7 to 8 x 10^{12} erythrocytes per litre. All of these values, nonetheless, are not statistically significant and lie within the historical reference range, as depicted using the light red area, speaking for an absence of anaemia. White blood cell (WBC) count dropped in every single group by 0.25-1 x 10^{9} leukocytes per litre during therapy (Figure 40B). Control animals along with animals of the CPI-613-group showed elevated WBC overall, indicating leucocytosis as a result from e.g. stress, inflammation or tumours. Moreover, IT is generally known to induce myelosuppression. The abnormally high platelet number (PLT) in all treatment groups > 900.000/µl decreased to normal range in control as well as CPI-613-treated animals (Figure 40C). Any animal injected with IT, either as single or combination treatment, showed elevated PLT/thrombocytosis compared to PLT counts prior to the start of the therapy, which did not normalise during therapeutic duration. Next, the percentual abundance of reticulocytes (RETIC) was determined as a marker for increased haematopoiesis, e.g. triggered by anaemia or increased blood loss. RETIC fraction

increased in every group over time (Figure 40D). Particularly, animals in the vehicle control group in week 2 and every other animal in week 4 showed highly enhanced abundance of RETIC with 8-16%, with the highest percentages in control animals.

Concluding, chemically-induced CRC tumours representing advanced CRC were successfully treated applying a combination regimen of CPI-613 plus IT, which was superior over monotherapies. The therapeutic benefit was primarily reflected in overall tumour score and average size, although not in tumour number or multiplicity. Herein, CPI-613 as a building block in the treatment scheme lacked additional haematological toxicity linked to the absence of bone marrow toxicity as compared to the control group.

5. DISCUSSION

Among cancer entities, CRC is the third most commonly diagnosed type of cancer (see 1.1). As specified in 1.1.2, standard chemotherapy for CRC patients is available, including the use of genotoxic agents in combination with biologicals. The prognosis of patients with advanced or metastasised CRC, however, is devastating. In the need for novel approaches, the lipoate CPI-613 and its derivates form a new class of agents, which attacks altered energy metabolism that is explained in detail in section 1.2. The aim of this study was to assess the applicability and efficacy of CPI-613 in comparison to its mother compound LA alone and in combination with standard chemotherapeutics in the treatment of CRC in cell culture and mouse models.

5.1. The Mode of Action of CPI-613: Targeting Mitochondria and Disrupting Their Function in Energy Metabolism in CRC

From its structural analogy to LA but its redox inertness, the mode of action of CPI-613 is to disrupt mitochondrial function and mitochondrial integrity (see section 1.3.2.2).

As visualised in Figure 18, isolated murine heart mitochondria showed mitochondrial membrane dissemination upon 25 µM CPI-613. Concomitantly, state IV respiration was impaired upon 25 µM CPI-613. At the same time, ROS generation and release from isolated murine heart mitochondria upon CPI-613 was dose-dependent (U-shaped). Low doses of CPI-613 (< 50 µM) reduced ROS formation, while high doses (> 100 µM) triggered increased ROS formation. For the first time, experiments were performed in isolated mitochondria to assess the result of exposure to CPI-613. O'Brien et al. (2017), Slade et al. (2017), Young et al. (2020) and Dogar et al. (2020) used 150 to 250 µM CPI-613 in isolated mitochondria to inhibit KGDH and PDH without addressing effects to mitochondrial integrity or function. The concentrations used in cell culture experiments are therefore not directly transferable to concentrations used in experiments using isolated mitochondria and vice versa. The used concentrations could, thus, represent concentrations that need to be reached intracellularly to disrupt mitochondrial integrity. A measurement of intracellular concentrations of CPI-613 in cell culture experiment is described nowhere. In CRC cell lines (Figure 19-Figure 21), CPI-613 increased ROS species at high doses (< 150 µM) and only moderately perpetuated mitochondrial membrane potential upon short incubation times (1-3 h). However, mitochondrial number was reduced, albeit not statistically significant (24 h, 200 µM CPI-613). Simultaneously, CPI-613 incubation reduced dose-dependently basal, maximal as well as ATP-coupled and spare capacity respiration in CRC cell lines (24 h, ≥ 150 µM).

Numerous studies assessed the effect of CPI-613 on mitochondrial ROS release, mitochondrial integrity, and mitochondrial function in mechanistic studies. In line with the observed effects in isolated mitochondria in this work, CPI-613 was applied as a ROS minimizing agent and pan-inhibitor for the production of $O2^{\cdot-}$ and H_2O_2 species in isolated murine liver mitochondria (5-150 µM) by Dogar et al. (2020), Slade et al. (2017) and O'Brien et al. (2017). In contrast but not necessarily contradicting, Stuart et al. (2014) found CPI-613 to elicit a ROS burst from the E3 subunit of KGDH in H460 lung cancer cells (16 h, > 60 µM). A similar ROS burst could be observed in CRC cells. Additionally, Zachar et al. (2011) illustrated irreversible mitochondrial membrane disruption in H460 lung cancer cells (> 1 h, 240 µM). A dissemination of mitochondrial membrane potential could also be measured in CRC cells, however, without addressing its reversibility. In line, increased ROS levels (12 h, 200 µM), which were reversible using NAC (5 µM) as antioxidant were reported by Zachar et al. (2011), and mitochondrial membrane potential dissipation (48 h, 200 µM) in pancreatic cancer cells was observed by Gao et al. (2020). Examining the disruption of mitochondrial structure, Gao et al. (2020) described an alteration in mitochondrial morphology in the form of reduced mitochondrial cristae junctions next to overall change of mitochondrial morphology in pancreatic cancer cell lines using transmission electron microscopy (45 min, 200 µM). Accordingly, Mordhorst et al. (2019) reported the mitochondrial number to be unchanged upon chronic treatment although mitochondrial membrane potential was decreased in porcine foetal fibroblasts (7 days, 100 µM). In this work, however, mitochondrial membrane potential was disrupted with concomitant reduction in mitochondrial number upon short-term exposure to CPI-613 in CRC cells as shown using MitoTracker™ staining. With respect to energy metabolism, TCA cycle flux in terms of maximal respiration capacity indicated by oxygen consumption rates was impaired in leukaemia cells (2 h, 5-50 µM) as demonstrated by Pardee et al. (2018). On the other hand, similar concentrations did not affect glioblastoma cells as determined by Oppermann et al. (2016). As a consequence of the TCA cycle inhibition, metabolomics data showed a reduction in metabolites down-stream of KGDH, such as succinate, fumarate and malate by Stuart et al. (2014). Additionally, the effect of CPI-613 is mainly mediated by the availability of different energy source (Zachar et al., 2011; Stuart et al., 2014). Interestingly, treatment with CPI-613 was able to induce a “reverse Warburg effect” in cancer-associated cells of the tumour microenvironment, as postulated by Bellio et al. (2019) and Mordhorst et al. (2019). As demonstrated in this work, CPI-613 dose-dependently impaired mitochondria respiration as shown using the Mito Cell Stress Test Kit. The impairment of mitochondrial respiration was measurable in basal, ATP-related and maximal respiration capacity. The effect of CPI-613 on mitochondrial respiration using the Mito Cell Stress Test Kit has, thus far,

not been described in the literature. The measurement of the extracellular acidification rate indicating glycolytic lactate production could supplement this set of experiment in the future.

5.2. CPI-613 Shows Benefits as a Potential Building Block in the Treatment of CRC

CPI-613 is the first representative of a new class of agents: mitochondrial disruptors targeting altered energy metabolism. In this work, the potential of CPI-613 as building block in the treatment of CRC was assessed using a variety of endpoints, such as cell death, using CRC cell lines. The cellular responses and benefits of CPI-613 as a chemotherapeutic agent in comparison to standard chemotherapeutic agents were exploited and characterised, as outlined in the following.

5.2.1. Cell death induction by CPI-613 in CRC cells

Established as well as patient-derived CRC cell lines were treated with increasing doses of CPI-613, LA as well as 5-FU and IT next to non-transformed colonic epithelial cells, which are representative for healthy colonic tissue. As described in section 1.2.2.1, numerous oncogenes and tumour suppressors alter energy metabolism in cancer cells and this could potentially lead to different susceptibility of CRC cell lines to vulnerability to CPI-613. Detailed in Table 18, a panel of CRC cell lines were tested with respect to sensitivity towards CPI-613. These CRC cell lines differed in their MSI-, p53-, BRAF- and KRAS-status and, therefore, rely to different proportions on aerobic glycolysis, OXPHOS and/or glutaminolysis.

Depicted in Figure 22, the cytotoxic profile of CPI-613 and its mother compound LA differ. Regarding LA, cell lines were grouped in sensitive and resistant cell lines. Dörsam et al. (2015) and Dörsam and Fahrer (2016) already described a wide range of IC_{50} values for LA in CRC cells. The vulnerability of some cell lines might result from varying expression levels of (drug) transporters, reliance on OXPHOS and concomitantly expression of PDH and KGDH and on mitochondrial spare capacity. However, the invariable IC_{50} values of CPI-613 point to the fact that, irrespective of the oncogenic or tumour suppressor configuration of CRC cells and the accompanied change in energy metabolism, CPI-613 has a broad spectrum of applicability. Surprisingly, the reliance on different energy metabolism pathways did not affect the vulnerability of the different cell lines to CPI-613. Zachar et al. (2011) screened a variety of cancer entities including bone marrow, breast, colorectal, kidney, lung, muscle, ovarian, pancreatic, prostate, and uterine cancer cells

and found an overall IC_{50} value range from 100 to 280 µM CPI-613. Gao et al. (2020) reported the median IC_{50} in pancreatic cancer cells to be 200 µM CPI-613. The average IC_{50} in CRC cell lines of 175 µM fits with this observation.

Furthermore, CPI-613 elicited uniform cytotoxicity in isogenic HCT116-$p53^{+/+}$ and HCT116-$p53^{-/-}$ cells and was applicable in arrested cells (Figure 22). As confirmed by cell cycle distribution analyses, arrested cells were obtained using a chronic treatment scheme of genotoxic agents, which was described in the literature to elicit senescence (Tato-Costa et al., 2016). For both IT and 5-FU, senescence induction with concomitant drug resistance is reported in CRC (Haug et al., 2008; Rudolf et al., 2012; Focaccetti et al., 2015; Altieri et al., 2017; Was et al., 2018). Therapy-induced senescent cells display a unique metabolism, which is characterised by a high glycolytic rate and elevated OXPHOS activity with increased reliance on the TCA cycle due to PDH upregulation (Sabbatinelli et al., 2019). This fact is likely to render these cells particularly vulnerable to treatment with CPI-613, which, on the other hand, could not be seen in this work.

Thus, CPI-613 acts as a p53- and proliferation-independent antineoplastic agent and is applicable also in formerly treated and drug-resistant CRC cells. In the literature, CPI-613 was described to be active independent of the cell cycle phase and of prevailing signal transduction pathways, tumour suppressor or oncogene mutations, i.e. p53-deficiency in AML or *KRAS* mutations in lung carcinoma cells (Zachar et al., 2011; Pardee et al., 2018), and was furthermore equally effective in cytostatic-resistant cell lines, i.e. Doxorubicin-resistant ovarian cancer cells and their non-resistant counterparts (Lee et al., 2014). Although chronic treatment of lung cancer cells (H460) with CPI-613 showed that subpopulations expressed stem cell-like properties and an EMT phenotype, Perera et al. (2015) described the ability of CPI-613 to eliminate both parent and resistant cells almost equally effective with increasing duration of treatment. Generally, it would be of interest to check for senescence induction by chronic CPI-613 treatment due to metabolic stress via senescence-associated β-Galactosidase staining and assessment of mediating proteins such as p16, p21 and E2F1 (Noren Hooten and Evans, 2017). In particular for aging but also in cancer, metabolic stress-, ROS- and mitochondrial dysfunction-associated senescence has been described, which, however, could occur in cancer cells due to treatment with CPI-613 (Nogueira et al., 2008; Ewald et al., 2010; Dörr et al., 2013; Pérez-Mancera et al., 2014; Wiley et al., 2016).

Already hypothesised by Zachar et al. (2011), CPI-613 also showed a tumour-selectivity in the context of CRC as it was already shown for lung and pancreatic cancer, which cannot be reported for LA (Figure 22). LA is described to have a broad range of IC_{50}

values in CRC cells, while its effect on non-transformed colonic epithelial cells, normal fibroblasts and peripheral blood lymphocytes is moderate (Dörsam and Fahrer, 2016). Generally, p53-wildtype cells are more susceptible to DNA damaging agents (Dörsam et al., 2015), which is also reflected in the IC_{50} calculations of 5-FU and IT. In principle, patient-derived HROC cell lines showed higher IC_{50} values for all compounds tested, which might be resulting from their lowered doubling time.

CPI-613 elicited time- and dose-dependent cell death without a preceding cell cycle arrest in p53-wt and p53-mt CRC cell lines (Figure 23). Lee et al. (2014) and Perera et al. (2012), on the other hand, found CPI-613 treatment to have impact on multiple cyclins (downregulation of *cyclin D3*, *E1*, *E2*, *F*, *A2*, *B1*) next to downregulation of p27, p19 and CDK2 *in vitro* in pancreatic, lung and gliosarcoma cell lines, which could indicate an effect on cell cycle progression – e.g. by inducing a cell cycle arrest. Generally, mitochondrial dysfunction and mitochondrial or metabolic stress can lead to cell cycle arrests upon checkpoint activation – also termed mitochondrial metabolic check points, which would fit the observations of the aforementioned studies (Mason and Rathmell, 2011; Mohrin and Chen, 2016; Ni and Qu, 2016). Standard chemotherapeutics in the treatment of CRC, such as 5-FU and IT, were repeatedly reported to induce DNA damage upon which DNA damage repair and a cell cycle arrest are induced. 5-FU induced an early G2/M phase arrest at low and a late G1 phase arrest at higher concentrations followed by apoptosis and/or mitotic catastrophe in HCT116 cells (Yoshikawa et al., 2001). Others reported the induction of an S phase arrest in HCT116 cells which is in line with its mode of action as described in 1.1.2.2.2 (Angelis et al., 2006). IT induced an S and a G2/M phase arrest in CaCo-2 cells in experiments performed by Kaku et al. (2015), similar to the observed effects in HCT116 cells in Figure 22. Upon IT treatment, HCT116 cells proficient of p53 underwent cell cycle arrest and sensitisation towards DNA damage, while HCT116 deficient in p53 underwent apoptosis directly (Blagosklonny and El-Deiry, 1998; Magrini et al., 2002; Gibson et al., 2011). The induction of e.g. a G2/M phase arrest by both 5-FU and IT in HCT116 cells, as seen in Figure 22, is most likely mediated by and dependent on p53 (Abal et al., 2004; Angelis et al., 2006; Adamsen et al., 2011). Furthermore, IT was shown to induce a p21-mediated S phase arrest in p53-transfected HT29 cells and a CDK1/cyclin B complex-mediated S phase arrest in p53-mt HT29 cells. Activated p53 increased the apoptotic rate and sensitivity to IT (Abal et al., 2004).

A set of flow cytometric AnnexinV/PI stainings to elaborate on cell death induction by CPI-613 confirmed the results from cell cycle distribution and Sub G1 fraction analysis (Figure 23). CPI-613 was shown to induce cell death in a dose- and time-dependent

manner in HCT116 and HT29 cells. In particular, AnnexinV- and PI-positive cells, representing late apoptotic/necrotic cell death, were detected. AnnexinV-positive but PI-negative cells, indicating cells undergoing (early) apoptosis, were detected as well, but to a lesser extent. Moreover, with the application of zVAD as pan-caspase-inhibitor and Nec-1 as a RIPK- and necroptosis-inhibitor it could be shown that not a single distinct type of cell death was elicited. This was already postulated by Zachar et al. (2011) with less sophisticated experiments in H460 lung cancer cells (2 h of treatment with 240 µM CPI-613), that were not clearly distinguishing the type of cell death elicited.

Treatment with cytotoxic doses of CPI-613 induced advanced cell death, which was accompanied by induction of γH2AX in HCT116 and HT29 cells. This type of γH2AX induction can be observed in DNA fragmentation in the context of apoptosis and nuclear degradation (Lu et al., 2006) and can also be observed as a so-called apoptotic ring in immunofluorescent staining in late apoptosis upon genotoxic insults and activated DNA damage response (Solier and Pommier, 2009, 2014). Since CPI-613 lacks genotoxicity as detailed later on, the observed γH2AX formation is likely attributable to cell death induction.

To further elucidate the type of cell death induced by CPI-613, Western Blot analysis (Figure 25) in HCT116 and HT29 cells were performed. Surprisingly, neither the effector Caspase-3 nor PARP-1 cleavage could be observed which are both late events in caspase-dependent apoptosis. Critical in this context is the observation of cell death as a time- and concentration-dependent cellular response. In the literature, shorter incubation times but higher concentrations of CPI-613 were used to study PARP-1 and caspase cleavage. Both PARP-1 as well as Caspase-3 cleavage were measured with concomitant apoptosis-associated morphological changes by Zachar et al. (2011) (24 h, 160 µM, H460 cells). In LNCaP prostate adenocarcinoma cells, apoptosis-related upregulation of NOXA was recorded by Arai et al. (2020) (5 h, 200 µM). Gao et al. (2020) reported apoptosis induction in pancreatic PANC1 and AsPC-1 cancer cells with increased levels of cleaved PARP, cleaved Caspase-3 and Bax and decreased levels of Bcl-2, which was ROS-dependent and related to mitochondrial insult, but autophagy and the activation of the AMPK-ACC-axis were dispensable. But Egawa et al. (2018) failed to find an upregulation of apoptosis in fibroblasts although they were able to detect necrosis in a combination treatment with chloroquine. Since the mitochondria and their metabolism are the sole target of CPI-613, it could be hypothesised that CPI-613 elicits the intrinsic mitochondria-mediated pathway of apoptosis. To check this, anti-apoptotic Bcl-2/Bcl-X_L and pro-apoptotic Bax/Bid levels as well as an analysis of cytochrome c release and cleavage of initiator caspases Caspase-9 and -7 could be performed.

Noteworthy, an interplay of different cell death types could be reason for observing increased cell death rates upon CPI-613. Therefore, detailed insight could be gained by combining cell death inhibitors and by addressing other forms of programmed cell deaths, e.g. necrosis, caspase-independent cell death, autophagic cell death parthanatos, anoikis, ferroptosis, oxeiptosis, alkaliptosis or autolysis (Waterhouse, 2003; Duprez et al., 2009; Ouyang et al., 2012; Galluzzi et al., 2018; Tang et al., 2019).

Given several observations described above including the central role of perpetuation of the mitochondria and the energetic homeostasis and focussing on the most probable cell death types, the following ideas and suggestions for experiments are presented:

- As the most probable type of cell death, caspase-independent cell death is observed in response to intrinsic apoptotic signals (Bröker et al., 2005; Kroemer and Martin, 2005; Tait and Green, 2008). Characteristics of caspase-independent cell death related to mitochondria are swollen cristae, mitochondrial outer membrane permeabilization and gradual loss of membrane potential, of which all of these features were observed in this work or in the literate in the context of CPI-613. Regarding the nucleus, DNA laddering and fragmentation do not necessarily occur in caspase-independent cell death, which was additionally found absent in the literature. In caspase-independent cell death, cells are generally AnnexinV negative and show abundant autophagosomes in the cytoplasm and lose their ability for proliferation but keep adhesion to the matrix. Most of these features were observed as well. Mitochondria play a central role in caspase-independent cell death since upon mitochondrial outer membrane permeabilization, intermembrane space proteins such as cytochrome c and the apoptosis-inducing factor AIF are released and activate cell death. Therefore, a translocation of the caspase-independent cell death mediator AIF to the nucleus would be an interesting endpoint for elucidation of cell death mechanisms upon CPI-613 (Cregan et al., 2004).
- In the context of CRC, cell death induction upon LA was linked to Caspase-2 (Dörsam et al., 2015). Caspase-2 is regarded as an orphan caspase due to its divergent role as initiator and executor caspase function in the process of cell death, which is commonly overlooked (Vakifahmetoglu-Norberg and Zhivotovsky, 2010). Inducing the intrinsic apoptosis pathway, Caspase-2 is activated upon endoplasmatic reticulum stress, mitotic catastrophe or imbalance of metabolism (Fava et al., 2012).
- Ferroptosis is another caspase-independent form of cell death, which is tightly linked to lipid peroxidation and glutathione-dependant elevated levels of ROS

(Stockwell et al., 2017; Galluzzi et al., 2018; Li et al., 2020). Dependent on iron availability, ferroptosis is associated with a perturbation of the intracellular microenvironment with ROS generation. It is result of oxidative insults and characterised by the involvement of the mitochondria (smaller mitochondria, reduced cristae, ruptured membranes) and associated with glutaminolysis. Crucial key regulators of ferroptosis include the p62-Keap1-Nrf2 pathway and p53/SLC7A11 interplay. With respect to observations using CPI-613, ferroptosis might potentially be elicited and could be further investigated.

- Oxeiptosis is a ROS-dependent, caspase-independent and KEAP-1 regulated type of cell death (Holze et al., 2018). NAC is the most important inhibitor of this pathway, which was shown in some studies in the literature to reverse effects presented after CPI-613 treatment.
- The rapid loss of adhesion to the matrix, however, would speak for anoikis, which is characterised by the loss of integrin-dependent anchorage (Paoli et al., 2013). Therefore, a screening for changes in integrin levels upon CPI-613 would be helpful.

It is of note that cell death pathways elicited upon CPI-613 might be specific for different types of cancer, especially in the light of solid tumours. A summary of the findings with respect to cell death can be found in Table 19.

Table 19: Summary of findings with respect to cell death induction upon CPI-613 in CRC cells.

Endpoint	*HCT116*	*HT29*
Cell morphology	cells were rounded and detached after 24 h of incubation	cells were rounded and detached after 24 h of incubation
Cell viability assay (ATP assays)	IC_{50} = 167 µM (similar IC_{50} in HCT116p53$^{-/-}$)	IC_{50} = 163 µM
Cell cycle distribution	at any time point (24, 48, 72 h), no cell cycle arrest could be measured	at any time point (24, 48, 72 h), no cell cycle arrest could be measured
Induction of cell death (SubG1 population)	cell death (expressed as SubG1 fraction) was induced in a dose- and time-dependent manner	cell death (expressed as SubG1 fraction) was induced in a dose- and time-dependent manner
Induction of apoptotic/ necrotic cell death (AnnexinV/PI staining)	apoptotic and necrotic cell death were induced after 48 h of incubation, necrosis was induced at a higher rate than apoptosis, cell death was induced at a higher rate than in HT29 cells	apoptotic and necrotic cell death were induced after 48 h of incubation, necrosis was induced at a higher rate than apoptosis, cell death was induced at a lower rate than in HCT116 cells
Formation of γH2AX	using cytotoxic doses of CPI-613, cell death induction was accompanied by γH2AX formation	using cytotoxic doses of CPI-613, cell death induction was accompanied by γH2AX formation
Effect of zVAD as pan-caspase-inhibitor	pan-caspase inhibition partially rescued cells from undergoing cell death, γH2AX formation was reversible	no assessment on the effect of zVAD on cell death induction was performed in this cell line, γH2AX formation was reversible
Effect of Nec-1 as necroptosis-inhibitor	inhibition of necroptosis did not change the level of cell death induction	no assessment on the effect of Nec-1 was performed in this cell line
Effect on p53	p53 protein was not stabilised, but depleted	p53 protein was not stabilised, but depleted
Cleavage of Caspase-3 and PARP-1 (Western Blot detection)	neither Caspase-3 nor PARP-1-cleavage could be detected	neither Caspase-3 nor PARP-1-cleavage could be detected

5.2.2. DNA damage is not induced upon CPI-613

While for standard chemotherapeutic agents, e.g. 5-FU and IT, it is their inherent cytotoxic characteristic to act genotoxic, the mode of action of CPI-613 does not allow a direct conclusion for its genotoxic potential. In the application as orphan drug and as anticancer agent, the standard battery of genotoxicity testing was not necessary according the ICH guidelines S9 (Non-clinical evaluation for anticancer pharmaceuticals) and S2 R1 (Genotoxicity testing and data interpretation for pharmaceuticals intended for human use). However, it is of interest to know the genotoxic potential of CPI-613 to evaluate the possibility of formation of secondary tumours upon treatment.

Instead of the standard genotoxic assay battery, the detection of γH2AX and the Comet Assay as indicator tests were performed in HCT116 and HT29 cells (Figure 27, Figure 28). Using both the alkaline as well as the FPG-modified Comet Assay, DNA single and double strand breaks and alkali labile sites as well as oxidative DNA damage (i.e. 8-Oxo-Guanine) should be detected, respectively (Albertini et al., 2000; Tice et al., 2000). The quantification of γH2AX in an InCellWestern and a Western Blot analysis was exploited as surrogate marker for DNA damage. Since none of these tests revealed an elevation in levels of aforementioned types of DNA damage upon CPI-613 treatment, DNA damage in terms of primary lesions and subsequent genotoxic activity of CPI-613 can be excluded. These results could be further corroborated by detection of e.g. 8-Oxo-Guanine in Slot Blot analysis, immunofluorescence imaging or HPLC quantification.

In comparison, the mother compound LA underwent the following analysis by Dörsam et al. (2015): Alkaline Comet Assay, formation of γH2AX and the involvement of p53. Dörsam et al. (2015) found LA in HCT116 and CaCo-2 cells to neither induce DNA damage as assessed in the alkaline Comet Assay nor to lead to the formation of γH2AX as shown in immunofluorescence staining. Furthermore, LA was evaluated with respect to its genotoxicity in a bacterial reverse mutation assay and an *in vivo* micronucleus test (Cremer et al., 2006). In the Ames test with and without metabolic activation using S9 mix, no mutagenicity was observed for LA using the standard set of *Salmonella Typhimurium* strains for both plate incorporation and pre-incubation assays. Using the TA97 strain which shows particular sensitivity to endogenous sulphhydryl compounds, a weak insignificant mutagenic response was recorded in the highest concentration (5000 mg/plate). Yet, this response was lower than effects of endogenously occurring L-cysteine. Additionally, a single oral administration of LA (825 mg/kg BW) did not significantly increase micronucleate polychromatic erythrocytes in male and female rats. Therefore, aneugenicity and clastogenicity for LA were excluded. Thus, LA is considered non-mutagenic and to have no genotoxic action potential. Underlining these findings, a

2 year-carcinogenicity study on LA in rats showed no evidence of carcinogenicity either (Cremer et al., 2006). As a hypothesis, LA could act as a secondary carcinogen by enhancing or setting the stage for alkylating agents, such as temozolomide, due to its ability to deplete MGMT. Depletion of MGMT leads to a reduced repair activity of O^6-methylguanine, the major DNA lesion introduced by temozolomide (Göder et al., 2015). With respect to mitochondrial DNA damage, LA has thus far been described to protect from mitochondrial DNA damage due to its anti-oxidative properties under physiological or supplementation conditions rather than inducing mitochondrial DNA damages itself (Savitha and Panneerselvam, 2007; Melli et al., 2008; Fogarty et al., 2013).

Much in contrast to standard chemotherapeutic agents that are used in the treatment of CRC, CPI-613 has a unique mode of action. By targeting the mitochondria and altered energy metabolism, this drug candidate greatly differs to 5-FU and IT. A crucial difference is the absence of a genotoxic mode of action by CPI-613. This feature has, so far, not been assessed or described in the literature.

5.2.3. CPI-613 treatment modulates autophagy

The catabolic process of autophagy describes the highly controlled process of lysosomal degradation of cytoplasmic components, either proteins or whole organelles. Targeting distinct substrates or organelles is termed selective autophagy, such as nucleophagy or mitophagy. While under physiological conditions, autophagy is described as an antitumourigenic process, autophagy in cancer cells promotes tumour progression (Kimmelman, 2011; Folkerts et al., 2019).

Standard chemotherapeutic agents induce autophagy at high rates. It is assumed that autophagy rates are increased to fuel the energy-demanding DNA damage response and to recycle enzymes involved in this process (Rodriguez-Rocha et al., 2011). In this work, both HCT116 and HT29 cells were found to respond to the chemotherapeutics 5-FU and IT with a great induction of autophagy as seen in CytoID® staining and Western Blot analysis (Figure 33). This finding is in line with some literature data and supports the data described therein. For example, 5-FU induced autophagy in HCT116 and HT29 cells and its inhibition was crucial to a potentiated anticancer effect by apoptosis (Li et al., 2009; Li et al., 2010a; Sasaki et al., 2010; Choi et al., 2012; Sasaki et al., 2012; Tang et al., 2016; Yang et al., 2018). Furthermore, autophagy mediates chemoresistance to 5-FU, which is a challenging clinical issue (Tang et al., 2016). Resistance to 5-FU lead to a reduced basal autophagy level in CRC cell lines but could also be overcome and re-

sensitised by autophagy inhibition (Sasaki et al., 2012; Schonewolf et al., 2014; Sui et al., 2014; Yao et al., 2017). 5-FU-induced autophagy was mediated by Bcl-2 and Bcl-X_L (Li et al., 2010a; Sui et al., 2014). Likewise, IT induced autophagy in HCT116 cells, inhibition sensitised CRC cells to drug therapy and resistance to IT was linked to increased autophagy in CRC cell lines, such as LoVo (Paillas et al., 2012; Stanislav et al., 2013; Chen et al., 2014). Furthermore, autophagic cell death was elicited upon 5-FU or IT treatment in apoptosis-deficient CRC cells and can, thus, display an alternative way of an anticancerogenic effect (Xiong et al., 2010).

Thus far, only a small number of publications assessed the relationship between CPI-613 and autophagy *in vitro*. Egawa et al. (2018) analysed the effect of CPI-613 in clear cell sarcoma cell lines and found CPI-613 to induce autophagosome formation, which was however not convincing due to one-sided designed experiments using the DALGreen agent. Abrogation of autophagic flux via chloroquine increased necrosis rates, which was a clear evidence for Egawa et al. (2018) that insufficient removal of CPI-613-triggered autophagy cargo culminates in cell death. Mordhorst et al. (2019) described an increase in autolysosomes via increased LysoTracker™ staining in porcine foetal fibroblasts upon CPI-613 and PS48-cotreatment, which followed decreased mitochondrial membrane potential upon CPI-613 alone, while mitochondrial number and size were unaffected. An effect with CPI-613 alone was not reported. They postulated changes in autophagy rates to mitigate mitochondrial damage. Most persuasively, Gao et al. (2020) recorded an increase of double-membraned vacuoles and an increase in LC3B-II with a concomitant decrease in p62 in pancreatic cancer cell lines. The induction of autophagy was found to be mediated via the AMPK-ULK1 pathway without contribution of or a change in mTOR protein levels. The changes in autophagy levels were found to be unconnected to the induction of cell death. Similarly, Boyle et al. (2018) described the induction of AMPK/TORC1-mediated mitophagy upon mitochondria-targeting drugs (3-carboxy proxyl nitroxide, Mito-Metformin) in wildtype and *KRAS*-mt CRC cells (HCT116, HT29) with concomitant abrogation of cancer cell proliferation.

In the presented data in Figure 26, sub-cytotoxic as well as cytotoxic concentrations of CPI-613 triggered a moderate increase in autophagy in CRC cells, independent of their p53-status. This was shown based on an increase in CytoID® staining and LC3B-II formation, but with concomitant increase in the autophagy substrate p62. In particular, the autophagosome formation was enhanced. Due to an increase of p62 instead of a reduction, it is not entirely clear whether the whole autophagic flux is triggered or whether CPI-613 disturbs the fusion of autophagosomes and autolysosomes. To address this question, further experiments using the autophagy inhibitor chloroquine and

Bafilomycin-A or a co-staining of autophagosomes and autolysosomes are needed (Seiwert et al., 2017). All these phenomena were also reported for its mother compound LA in CRC cells (Göder et al., 2015).

In here, macroautophagy was the major endpoint analysed with the CytoID® staining and LC3B-I/II ratio next to p62 levels as markers. However, since CPI-613 targets the mitochondria and leads to their disruption and collapse as detailed in section 5.1, mitophagy - selective autophagy - might be the key type of autophagy triggered. The term mitophagy describes the autophagic clearance of damaged or aged mitochondria. Dysfunctional mitochondria accumulate ROS due to a malfunctioning of OXPHOS and dissipation of their transmembrane potential, culminating in cell death. Therefore, mitophagy is a crucial mechanism of maintaining cellular homeostasis and a central part in mitochondrial quality control mechanism (Pickles et al., 2018; Yoo and Jung, 2018; Macleod, 2020). In here, sequestered mitochondria are hydrolytically degraded via lysosomes. Overall, three canonical pathways are identified in regulating mitophagy (Vara-Perez et al., 2019). First, the PINK1/Parkin pathway involves the accumulation of PINK1 on the outer mitochondrial membrane and recruitment of the E3 ubiquitin ligase Parkin. Upon ubiquitinylation on K48 and K63, mitochondrial proteins and whole mitochondria are targeted for the cargo receptor p62 and its LIR (LC3-interacting region) domain for LC3B, thereby bridging mitochondria to the autophagic machinery. Next, mitophagy can be performed by the hypoxia-induced FUNDC1 pathway, which involves its phosphorylation by the autophagy kinase ULK1. Another hypoxia-induced and HIF-1α-mediated pathway includes BNIP3/NIX, which are members of the Bcl-2 family and, thus, tightly linked to intrinsic apoptosis regulation. Both pathways involve direct binding of LC3B via LIR sequences without ubiquitin to the FUNDC1/BNIP3 receptors on the mitochondrial outer membrane, which direct mitochondria to the process of autophagy.

5.3. Synergism of CPI-613 With Standard Chemotherapeutics in the Treatment of CRC

Combination chemotherapy in any type of cancer is regarded as the key to enhance efficacy and in tandem to reduce toxic doses causing severe side effects, to tackle heterogenous tumours and to overcome resistance development and metastasis formation. In CRC therapy, the cornerstone of successful therapy is the combination of genotoxic compounds and antiangiogenic agents or inhibitors of the epidermal growth factor receptor as outlined in section 1.1.2.2 in detail. Notwithstanding, new elements or

building blocks in the treatment of advanced and disseminated CRC are urgently needed as stressed in chapter 1.1.1.

5.3.1. Efficacy of standard chemotherapeutics is improved in combination with CPI-613 in cell culture models

In this regard, the assessment of combinations of the lipoates LA and CPI-613 with the standard chemotherapeutic agents 5-FU and IT *in vitro* in HCT116 and HT29 CRC cells revealed a pool of beneficial combination effects. The enhanced cell death upon combination treatment might be due to the fact that two distinct subcellular targets are attacked. While lipoates, in particular CPI-613, lead to an imbalance in energy supply, the highly energy consuming pathways of autophagy and DNA damage response elicited upon treatment with chemotherapeutics, such as 5-FU and IT, cannot be fuelled. As a consequence, cells undergo cell death.

Using two synergism models, namely the Chou Talalay method and the Highest Single Agent (HSA) model, the most promising combination of CPI-613 and IT could be determined in HCT116 with respect to cell viability reduction. Looking at other endpoints, subsequent experiments addressing cell death rates, autophagy and DNA damage levels supported this observation not only for HCT116 cells but also for HT29 cells with a p53-independent mode of action.

The potentiation of cell death rates induced by a combination of 5-FU/IT and LA but in particular with CPI-613 (Figure 31) was primarily based on an abrogation of pro-survival autophagy induction (Figure 33) and accompanied by unaffected DNA damage levels (Figure 32). To underline these findings, the models of Chou Talalay would need to be applied in high-throughput set-ups of endpoints regarding cell death rates, autophagy and DNA damage levels in the future. These observations, however, allow for an application of lower amounts of genotoxic drugs (5-FU/IT) with a concomitant reduction on side effect occurrence in the clinic.

Thus far, a positive combination effect of LA with standard chemotherapeutic drugs in the treatment of CRC has been described for a variety of agents. Studies by Dörsam et al. (2015) and Neitzel et al. (2019) extensively described the synergism of 5-FU and LA in CRC cell lines, which are likely to be based on p53 depletion. The same holds true for the combination of LA and doxorubicin (Neitzel et al., 2019). Furthermore, Göder et al. (2015) reported LA and temozolomide to act potentiating in xenograft mouse experiments, which is mechanistically linked to the MGMT depleting activity of LA. Others

provided evidence for beneficial combination effects of LA and etoposide, ionizing radiation or cis-platin in CRC and lung cancer, respectively (Yoo et al., 2013; Puchsaka et al., 2016).

Coming back to the role of p53, CPI-613 treatment in sub-cytotoxic concentrations resulted in a depletion of p53. This effect was found in a p53-wt (HCT116) as well as p53-mt (HT29) CRC cell line in mono- and combination treatment (Figure 31). It can be speculated that the depletion of mutant p53 might attenuate metastatic and tumourigenic activity. As described earlier (see 5.1), CPI-613 can elicit a disbalance of the redox state of the cell. Generally, p53 was shown to be target of redox modulation (Bykov et al., 2009) and this could be the link to CPI-613-mediated depletion of p53. For LA, Neitzel et al (2019) described a depletion of p53 in a variety of CRC cell lines in a dose- and time-dependent manner in detail. Mechanistically, p53 protein degradation was attributable to proteasomal degradation upon ready ubiquitinylation. The transcription factor Nrf2 is induced upon oxidative stress and several studies demonstrated its activation upon LA (Tebay et al., 2015). However, neither autophagy nor Nrf2 induction were found to be obligatory for the depletion of p53, but it was postulated that the reactive disulphide bond of LA is needed to interact with p53. Commonly, treatment with genotoxic standard chemotherapeutics cause stabilization and accumulation of p53 followed by the activation of down-stream targets (Ju et al., 2007; Neitzel et al., 2019). For instance, 5-FU leads to an accumulation of p53 in HCT116 cells. In the scope of p53 activation, DNA damage response, cell cycle arrest and apoptotic cell death are regulated (Brady and Attardi, 2010). Post-translation modification via ubiquitylation and phosphorylation and cellular redox state largely control p53 on protein level (Dai and Gu, 2010; Kim et al., 2011). The synergism of CPI-613 in combination with 5-FU and IT might, therefore, also rely on the depletion of p53.

With little supporting data and experiments, CPI-613 was described to have a positive combination effect *in vitro* with doxorubicin, topotecan, paclitaxel/carboplatin, cytarabine, nilotinib, sorafenib and chloroquine in the context of AML, lung cancer or pancreatic cancer without addressing the underlying mechanism in detail (Lycan et al., 2016; Egawa et al., 2018; Pardee et al., 2018; Pardee et al., 2019). In clinical trials, CPI-613 is rarely used as single agent but is instead included in standard regimen (compare Pardee et al. (2014) and Table 7).

With a similar molecular target, dichloroacetate (DCA) can be compared to CPI-613 (see 1.2). In terms of combination treatment of DCA and standard anticancer drugs in CRC, some beneficial effects were reported in the literature. In four CRC cell lines (LS174T,

LoVo, SW620 and HT29), a combination of DCA (0-90 mM) and 5-FU (5-200 µM) showed synergistic action for the endpoints cell viability and cell death based on the median effect principle proposed by Chou and Talalay with CI values ranging from 0.42 to 0.75 (Tong et al., 2011a). On top, Liang et al. (2020) presented restoration of chemosensitivity in CRC to 5-FU through DCA *in vivo* and in a small retrospective cohort of patients. Additionally, antiangiogenic bevacizumab treatment lead to hypoxic adaption, which was reversed by DCA (50 mg/kg BW) and lead to synergistic therapeutic success in mouse xenografts in combination regimen (Kumar et al., 2013). Comparing to CPI-613, similar benefits were described. However, DCA did not find implementation into the treatment of CRC due to its failure in clinical trials (see 1.2.2).

5.3.2. Inhibition of tumour progression in murine xenograft and carcinogenesis models of CRC is pronounced in combination treatment of CPI-613 and IT

Inferring, CPI-613 has not been assessed in the context of CRC *in vivo* in xenograft or orthotopic tumour settings yet. To address this question, heterotrophic xenograft experiments were performed using HCT116 and HT29 cells with animals receiving either CPI-613 alone, IT alone or a combination of both, in which one IT administration was flanked by CPI-613 administrations per week. The rationale for this set up was to initiate energy starvation by application of CPI-613, which is exploited once energy-demanding DNA damage response is activated upon administration of IT. Another administration of CPI-613 afterwards shall drive tumour cells into undergoing cell death, either programmed or unprogrammed. To decide on the IT dose to be administered, a literature search was performed to decide on a concentration which reduces tumour growth moderately (Harris et al., 2005; McEwan et al., 2009; Pohl et al., 2009; Na et al., 2010; Na et al., 2011; Mudd et al., 2012; Yang et al., 2012; Shelton et al., 2013). The decision on the dose of CPI-613 was primarily based on publications by Zachar et al. (2011) and Lee et al. (2014).

As shown in chapter 4.4.1, 25 mg/kg BW CPI-613 alone twice per week was able to inhibit tumour growth and to prolong survival in HCT116 and HT29 xenografts. Comparing both xenograft settings, CPI-613 was equally potent to inhibit tumour growth represented by shifted growth curves. As expected from *in vitro* data, HCT116 xenografts were more sensitive to IT treatment (40 mg/kg BW once per week) as compared to HT29 xenografts, but a combination of IT and CPI-613 potentiated the anti-tumour effect and survival benefit. This synergistic action, nonetheless, was more pronounced in HCT116

xenografts. Again, these data underline the universal effect of CPI-613 irrespective of the p53-status. In combination regimen, Western Blot analysis of the xenograft tumours (Figure 37) revealed differential cellular response with respect to the markers p53 (cell death), γH2AX (DNA damage) and LC3B (autophagy) when comparing HCT116 and HT26 xenografts, but reactions to monotreatment of CPI-613 and IT were similar. *In vivo*, CPI-613 monotreatment did not significantly change levels of p53, γH2AX and LC3B, which is only partly in line with *in vitro* data. But IT treatment augmented levels of all three markers, which reflects *in vitro* findings strongly. To underline these results, future experiments like Western Blot analysis or immunofluorescence staining should focus on further markers with respect to proliferation such as PCNA and Ki67 or TUNEL staining to allow detection of cell death rates next to p62 as an autophagy substrate to complement analysis of autophagy.

A handful of studies assessed the ability of CPI-613 to inhibit tumour growth in murine xenograft experiments. Earliest, Zachar et al. (2011) demonstrated 10 mg/kg BW CPI-613 once weekly and Lee et al. (2014) reported 25 mg/kg BW CPI-613 once weekly to significantly reduce tumour cell growth in H460 lung and BxPC3 pancreatic cancer cell line xenografts, respectively. The tumour growth curve flattened almost completely and tumours did not grow anymore. An increased injection frequency was shown to add no further benefit, but administration of CPI-613 prolonged animal survival (Zachar et al., 2011). Li et al. (2019) used an orthotopic pancreatic cancer model to prove delivery of CPI-613 and its tumour growth inhibition activity. On the other hand, Egawa et al. (2018) failed to prove tumour growth inhibition using 25 mg/kg BW CPI-613 twice weekly in clear cell sarcoma HS-MM cell xenografts. Bellio et al. (2019) showed 12.5 mg/kg BW CPI-613 once weekly to decrease tumour growth in ovarian cancer xenografts using OVCAR3 cells, while 25 mg/kg BW CPI-613 once weekly completely abolished tumour growth. In this work, CPI-613 was injected at a concentration of 25 mg/kg BW and twice per week. The antitumour effect observed in CRC xenografts was not as distinctive as in the aforementioned studies, but a reduction in tumour growth was nonetheless proven. A remarkable effect in prolonging survival was shown for CRC xenografts, although experiments did not last as long as those described in Zachar et al. (2011). Concluding, CPI-613 needed to be injected at higher rate or concentration to achieve the same effects. Using BxPC3 xenografts, CPI-613 was shown to inhibit tumour progression more potently than the standard chemotherapeutic gemcitabine and, in general, the delivery of CPI-613 was verified using FDG-PET (Lee et al., 2014; Sai et al., 2017). The ability to inhibit tumour growth of CRC xenografts of CPI-613 was compared to IT in this work. As discussed earlier, CPI-613 performed superior to IT in both HCT116 and HT29 xenograft

tumours. Most interestingly, CPI-613 reduced cancer stem cell frequency as described by Bellio et al. (2019) and in section 1.3.2.5. Moreover, combination with carboplatin/paclitaxel, which are standard chemotherapeutic drugs in the treatment of ovarian cancer, and olaparib were performed but did not enhance the antitumour effect. Furthermore, CPI-613 pre-treatment of OVCAR3 cells diminished their tumourigenicity in a xenograft setting. In this work, CPI-613 was combined with IT. While the effect on cancer stem cell frequency was not an endpoint in this set of experiment, a detailed insight on the potentiating effect on the combination of these two anticancer drugs could be demonstrated. Thus far, CPI-613 has not been combined with IT or any other topo I inhibitor *in vivo* before although a positive combination effect with doxorubicin (topo II inhibitor) and topotecan (topo I inhibitor) was reported in Pardee et al. (2012) and Lycan et al. (2016), respectively.

For the first time ever, the efficacy of CPI-613 was tested in a carcinogen-induced model of (colorectal) cancer. In this approach, the AOM/DSS model was chosen, which is extensively used to study colon carcinogenesis and allows for therapy studies via drug intervention (Robertis et al., 2011; Parang et al., 2016).

Therapeutic intervention in AOM-DSS-induced CRC tumours was performed in mice bearing 7-8 tumours with an average size of 1-2 and an overall tumour score of 14-15, which reflects an advanced stage of CRC. The therapeutic scheme of 4 weeks was extrapolated from the previously applied regimen in the xenograft mouse studies and literature-based doses for IT to induce minimal effects for monotreatment with the standard chemotherapeutic agent (Kondo et al., 2018; Zhu et al., 2019).

Overall, treatment with CPI-613 alone did reduce tumour number, score or size as determined using mini-endoscopic surveillance after 2 and 4 weeks of therapy in comparison to control animals, although not statistically significant. On the other hand, administration of IT alone as standard chemotherapeutic agent lead to a significant decrease of tumour sizes and hence also tumour score, but not tumour number, after 2 and 4 weeks of therapy. Although not recordable in tumour number, tumour size and score were most profoundly decreased in combination regimen of CPI-613 and IT after 2 and 4 weeks of therapy, thus stressing the amelioration of CPI-613 as combination agent for IT.

The antitumour effect of IT on advanced chemically-induced CRC in this work was weak as compared to literature data (Kondo et al., 2018; Zhu et al., 2019). For example, Kondo et al. (2018) used the AOM/DSS model to induce tumours representing very early CRC formation prior to the start of the chemotherapeutic intervention. Exact numbers on

tumour burden was not given in their publication. Chemotherapy was designed to include four cycles. One cycle composed of IT in a dose of 60 mg/kg BW with a frequency of once times per week for 3 consecutive weeks followed by two weeks of rest. Using a different mouse strain (HR-1), IT was shown to reduce tumour number from 28 tumours per mouse in the control to less than 3 tumours per mouse. Daily oral administration of vitamin C was found to enhance the antitumour effect of IT significantly by reducing the tumour number to approximately one tumour per mouse.

Other drugs targeting altered energy metabolism are discussed in section 1.2.2. Another drug targeting mitochondrial metabolism is the antidiabetic drug Metformin, which acts in pleiotropic ways. Among many effects, it is shown to inhibit mitochondrial respiration via complex I and is associated with bioenergetic reprogramming, also in CRC (Sośnicki et al., 2016; Kamarudin et al., 2019). The antitumour role of Metformin is discussed controversially. In this light, Wang et al. (2019) tested the effect of oral Metformin alone and in combination with 5-FU in the AOM/DSS model of advanced colitis-associated CRC in C57BL/6 mice. Upon CRC induction using 10% AOM and 2% DSS, Metformin was administered orally at a dose of 1% in drinking water on a daily basis and 5-FU was given as i.p. injection at 15 mg/kg BW every 3 days for 12 weeks. Metformin alone and in combination with 5-FU prevented loss in body weight gain and shortening of the colorectal length. Moreover, Metformin alone and in combination with 5-FU was able to reduce tumour incidence to approximately 50% and reduced the enlargement of tumours in score. In combination with 5-FU, Metformin ameliorated gastrointestinal side effects. A synergism or potentiation of effects, however, could not be shown in combination regimen. In this study, Metformin was mechanically found to protect mitochondrial structure of colorectal epithelial cells through the activation of the AMPK pathway. As discussed in section 1.2.2.1, HIF represents a key regulator in alteration of energy metabolism in cancer. In this context, Wei et al. (2020) assessed the therapeutic efficacy of oxaliplatin in combination with targeting HIF-1α in CRC using the AOM/DSS model and hoped to overcome chemoresistance. The compound Zebularine was found to lead to a degradation of HIF-1α and was combined with oxaliplatin in AOM/DSS-induced CRC in mice. Upon tumour induction in C57BL/6 mice using 12.5% AOM and 3.5% DSS, therapy was performed using oral administration of Zebularine (100 mg/kg BW) for 5 days per week for two weeks in total. While Zebularine was as potent as oxaliplatin (5 mg/kg BW) in reducing the number of tumours per mouse and the sum of the tumour diameter, a combination of the two drugs enhanced this effect to a great extent and acted synergistically. The studies of Wang et al. (2019) and Wei et al. (2020) show and underline the rationale and benefit of combining standard chemotherapeutics with drugs

targeting altered energy metabolism in CRC. Similar to the AOM/DSS model with subsequent therapy as performed in this work, synergism could be identified, which was pronounced to varying degrees.

As described in section 1.2.2.1, tumours arising from the AOM-DSS-sequence show reprogrammed metabolism similar to metabolic rewiring in human CRC (Cruz et al., 2017). It is, thus, surprising that CPI-613 as monotherapy did not show a significant effect, which, however, might be more pronounced once administering adapted doses of CPI-613. Bellio et al. (2019) postulated therapy using CPI-613 to abolish and overcome chemotherapeutic-mediated cancer stem cell formation and that the sequential application of CPI-613 was of utmost importance. With respect to IT, enhanced cancer stem cell formation and subsequent therapy resistance was described in CRC (Dylla et al., 2008; Angelis et al., 2016; Yang et al., 2017). Therefore, an assessment of cancer stem cell frequency in the described experimental set-up could be of great value.

Although the AOM/DSS model inherits many advantages, such as representation of heterogenous natural carcinogenesis and reproducibility, its limitations lay within its genetic characteristics and metastatic potential. Mutation of *KRAS* and β-catenin are frequent, but *APC* and *p53* are rarely affected and only some show microsatellite instability/defects of mismatch repair (Robertis et al., 2011). Moreover, the metastasis tendency in liver and lung is rare or even absent (Kobaek-Larsen et al., 2000; Derry et al., 2014).

While the investigated setting describes advanced CRC, the efficacy and combination effect of CPI-613 should be addressed in future experiments with settings reflecting early stages of CRC. This can be achieved by reducing the dose of initial AOM injection (e.g. to 7.5 mg/kg BW) and/or simultaneous reduction of the DSS dose (e.g. to 0.75%). Another approach could be to exclude those animals from therapy, which exceed pre-defined conditions in terms of tumour number, size and score as done by Schulz-Heddergott et al. (2018).

The differential blood analysis of C57BL/6J mice showed no indication of haematological or bone marrow toxicity of CPI-613, only with a small increase in reticulocyte abundance as compared to reference values (Mazzaccara et al., 2008). This observation is partly in accordance with data generated in minipigs and rats by Zachar et al. (2011) and Maturo (2010), respectively. Sternal bone marrow hyperplasia and an elevation in reticulocytes were recorded at toxic doses of CPI-613 (~ 60x the therapeutic dose), which was hypothesised to be secondary to inflammation. In humans, common recorded side effects include dysgeusia, hyponatremia, hypocalcaemia, nausea, vomiting and acute

kidney injury but also lymphopenia for CPI-613 single agent administration (Pardee et al., 2014; Lycan et al., 2016; Anderson et al., 2018a). Lymphopenia was, however, not detected in this work in the context of the AOM/DSS model. For IT-treated animals, thrombocytosis could be derived from measured platelet counts next to neutropenia. Along with diarrhoea, the most common side effects of IT treatment in humans include neutropenia, which is reflected in the drop of WBC in IT-treated C57BL/6J mice. Noteworthy, CPI-613 did not aggravate the haematological alterations in IT-treated animals in the combination regimen. Understandable, differential blood analysis was not conducted in nude mice because these mice strains do not possess physiological haematopoiesis and haematopoietic adaption due to their athymia (Bamberger et al., 1977; Aggio and Lozzio, 1979).

Future studies of AOM/DSS-induced CRC tumours and chemotherapeutic intervention with CPI-613 and/or IT should be in accordance with Western Blot analysis and suggestions presented for xenograft mouse studies. Overview analysis using H&E staining and immunohistochemistry evaluation should be performed on Swiss roles of the distal and proximal colon separately, and also freshly isolated tumour biopsies during mini-endoscopy could be analysed in a more sophisticated approach.

6. CONCLUSION AND PERSPECTIVES

6.1. Conclusion

The four-step-approach as described in Chapter 2 was applied in order to determine the potential synergism. Overall, the underlying experiments of this work demonstrated a sound basis for the conclusion on the synergism of lipoates and standard chemotherapeutics in the treatment of CRC in cell culture and mouse models. Preceding, mechanistic studies were performed to characterise the features and consequences of treatment with lipoate CPI-613 in CRC cell lines. The findings and proposed molecular mechanism of action is outlined in Figure 41.

First, it was shown mechanistically that the mitochondrial disrupting mode of action of CPI-613 could be confirmed in the context of CRC. The mode of action was expressed as disturbance of mitochondrial integrity and function as well as energy metabolism in isolated mitochondria and CRC cell lines, which was shown in measurements of mitochondrial membrane potential and oxygen consumption rates. The enhanced release of ROS was shown to be highly dose-dependent but inconclusive, while the reduction of mitochondrial number was statistically not significant. Most of these results are in accordance with observations described in the literature, which, however, did not link all these effects in their totality and did not address CRC as cancer entity.

Second, CPI-613 was found to inherit no genotoxic trait but to induce robustly and reliably cytotoxicity and cell death of various types in CRC cells (e.g. apoptosis and necrosis). Thus and novel, the mode of action was shown to be exclusively targeting the mitochondria and not the nucleus. For the first time ever, the genotoxic potential of CPI-613 was evaluated in this work. Furthermore, sophisticated approaches were applied to elucidate on the cell death induction upon CPI-613 shedding light on the particular pathways involved. Complementary, a line of evidences described the induction of autophagy as a cellular response to CPI-613 in more detail. The majority of these observations were in line with findings generated with the mother compound LA available in the literature.

Third, both lipoates (LA and CPI-613) were tested in a series of cytotoxicity assays in combination with standard chemotherapeutics (5-FU, IT) in CRC cell lines. While combination regimen of CPI-613 and standard chemotherapeutics are described in the literature, an assessment of CPI-613 in combination with 5-FU and IT in the context of CRC was completely unexplored thus far. A mechanistic link between the disturbance of the energy metabolism and the subsequent synergism with genotoxic agents could be

provided herein. In general, lipoates displayed synergism once combined with 5-FU or IT. The combination of CPI-613 and IT was determined to be the most promising combination *in vitro* in terms of potentiated cell death induction, DNA damage levels and autophagy. These findings were, then, transferred into *in vivo* models of CRC.

Fourth, CPI-613 was proven to be therapeutically efficient in xenograft mouse studies as single agent and partly superior to monotherapy with IT as standard therapeutic agent. This was reflected in enhanced animal survival and tumour growth inhibition. Furthermore, the combination of CPI-613 with IT was shown to act synergistically to these endpoints in xenograft studies originating from two genetically different CRC cell lines. Moreover, CPI-613 was applied for the first time in a model of chemically-induced tumours and evaluated as a therapeutic building block in this setting. In chemically-induced CRC in mice, CPI-613 as a single agent was not able to impact tumour progression but, at least, did not show additional toxic side effects (e.g. haematoxicity). Nevertheless, the inclusion of CPI-613 to a therapy regimen of IT lead to a significant reducing effect on tumour score in animals bearing advanced tumour stages, which underlines the findings of the *in vitro* studies with respect to synergism.

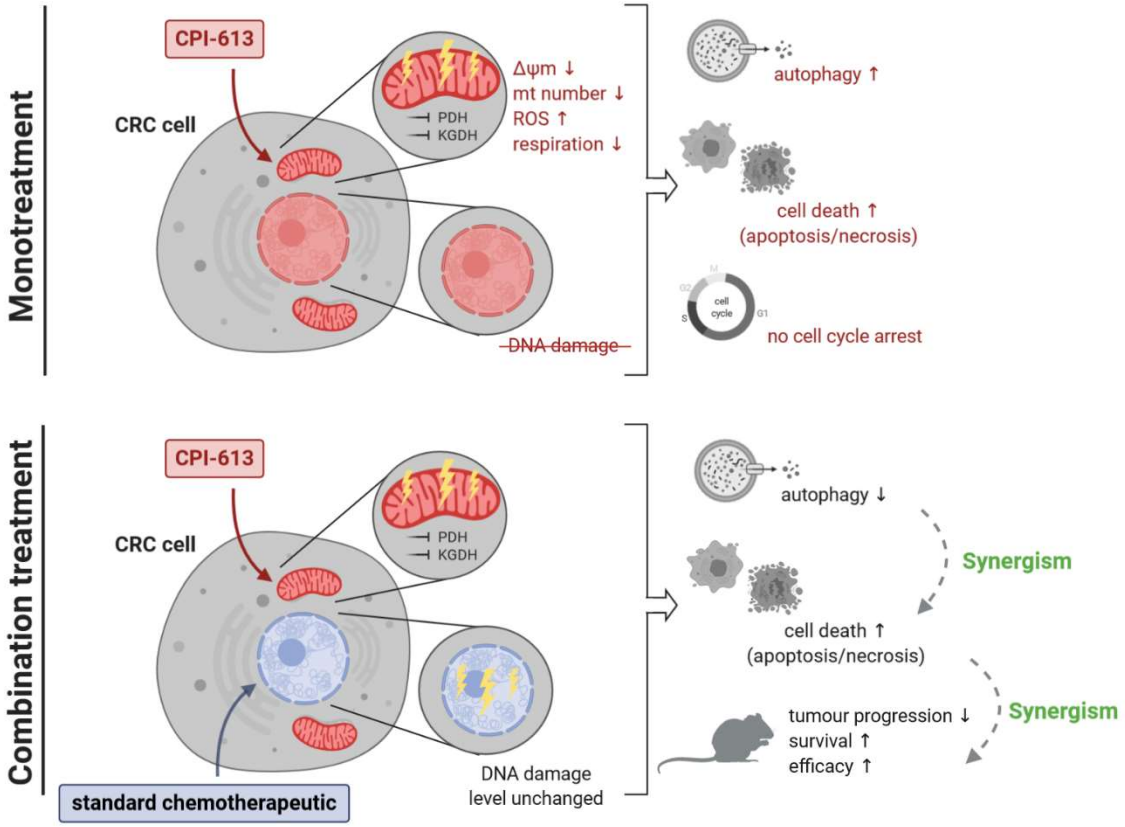

Figure 41: Synergism model of CPI-613 in combination with standard chemotherapeutics in the treatment of CRC.
(created using BioRender)

Concluding, the hypothesised synergism could be verified in this work, which provides the necessary data to suggest the inclusion of CPI-613 as a building block in the treatment of early as well as advanced or metastatic CRC. These findings are novel and have implications for the choice of new drug targets and in tailoring CRC therapy, in particular for patients with advanced or disseminated CRC. Furthermore, an insight on the underlying molecular mechanism for a synergistic combination effect is presented.

6.2. Perspective

While the data presented in this work demonstrate a sophisticated set of novel insights into the mechanism, benefits and applicability of CPI-613 in combination with standard chemotherapeutics in the context of CRC, suggestions for further studies are given and described below with a focus on molecular triggers and links. Moreover, some preliminary results are presented with respect to the ability of CPI-613 to affect metastasis formation and epithelial-to-mesenchymal transition (EMT).

6.2.1. Suggestion for future experiments

To elucidate further on the tumour-selectivity of CPI-613, cell death measurements in organoids as a technique of 3D cell culture could be performed. Ripani et al. (2020) used murine intestinal organoids and colonic tumouroids from AOM/DSS-treated mice and compared the effects of thiazolides, which target the mitochondrial respiration chain. This technique could be used for assessing CPI-613 as well.

Taking up the experiments performed to characterise the cell death induction upon CPI-613, additional studies on the molecular mechanism driving this cellular response would be desirable. In a first step, qPCR analysis of cell death-related target genes could be performed, including genes like *Fas-R*, *Fas-L*, *Noxa*, *Puma*, *Survivin*, *Bcl-2*, *Bcl-X_L*, *Bid*, *Bax*, *p21*, *p16*, in cells treated with CPI-613 alone and in combination with IT or 5-FU. As described in section 5.2.1, the translocalisation of AIF and the involvement of Caspase-2 could add insight into the cell death mechanism elicited upon CPI-613 and combination regimen (Dörsam et al., 2015). Furthermore, the regulators AMPK and c-MYC should be addressed as a molecular link between mitochondrial stress and cell death induction in CRC cells (Sertel et al., 2010; Gao et al., 2020; Ripani et al., 2020).

With reference to the Comet Assays performed with CPI-613, this set of experiments demonstrated the lack of genotoxicity to nuclear DNA in the form of DNA strand breaks or oxidative DNA damage upon ROS formation. Given the proximity, ROS-induced DNA damage is a common feature in mitochondria and found to be more extensive than

nuclear DNA damage (Yakes and van Houten, 1997). Although efficient base excision repair is abundant in mitochondria, ROS-related mitochondrial DNA damage persists for an extended amount of time (Croteau and Bohr, 1997; Bohr, 2002). Mitochondrial DNA damage precedes loss of mitochondrial function, energy depletion and cell death (van Houten et al., 2016). Therefore, in a next step, the mutagenic potential of CPI-613 on mitochondrial DNA could be assessed, e.g. by using next-generation-sequencing (NGS).

Although conclusive data is presented describing the autophagy-inducing effect of CPI-613, the question whether CPI-613 as a mitochondria-directed drug might be eliciting selective autophagy to the mitochondria, termed mitophagy, remains to be answered. Experimental verification of general induction of mitophagy as a part of cellular response to CPI-613 could include the colocalization of LC3B and mitochondria, visualised using MitoTracker™, in immunofluorescence imaging (Ding and Yin, 2012). As described earlier, CPI-613 treatment resulted in a reduction of total mitochondrial number, which would indicate a higher rate of mitochondrial reduction than autophagy rate or new mitochondrial biogenesis. However, the increase in LC3B was accompanied by a reduction in the mitochondrial membrane protein TOM20 (data not shown), which would point to an induction of selective mitophagy. To further address the exact elicited pathway, Western Blot analysis of PINK1/Parkin, FUNDC1 and BNIP3 are conceivable. These analyses should go hand in hand with measurement of the mitochondrial membrane potential. CCCP, for example, could serve as positive control in HCT116 cells in this type of experiment (Dolman et al., 2013; Abdrakhmanov et al., 2019). Addressing mitophagy and its relation to CPI-613 would be interesting since mitophagy is a mechanism to cope with metabolic stress, was shown to be implicated in carcinogensis and plays an important role in metabolic rewiring, the induction of cell death and chemotherapeutic resistance (White, 2007; Altman and Rathmell, 2012; Chang et al., 2017; Gross and Graef, 2020).

The chemical induction of CRC via the AOM/DSS model was chosen in this work to examine the potential of CPI-613 alone and in combination with standard chemotherapeutic agents. Further preclinical animal models of CRC are available to elucidate the therapeutic efficacy of CPI-613 or the combination of CPI-613 with standard chemotherapeutics or biologicals in more detail (Robertis et al., 2011; Johnson and Fleet, 2013b; McIntyre et al., 2015; Bürtin et al., 2020). To fully address the influence of oncogenic mutations and the consequent metabolic rewiring, xenografts of isogenic cell lines (HCT116-*KRAS* or HCT116-*BRAF*) could be tested. Xenograft studies are valuable for initial testing but limited in their representativeness in terms of metastasis formation and microenvironmental factors. At first, patient organoids could be cultured and used

for testing on CPI-613. This would initially represent the heterogenicity of CRC tumours. To overcome limitations of cell cultures, patient-derived xenografts (PDXs) could be used to represent clinical and molecular heterogenicity of tumours next to examining metastasis and to represent a more natural microenvironment, although the human stromal cells will soon be replaced by host stromal cells. Orthotopic xenografts can help to include a more natural microenvironment and to assess metastasis formations, however, surgical implantation is needed for this approach. Next to the AOM/DSS model, another sophisticated approach could be genetically-modified mice strains, such as $APC^{min/+}$ mice. The role of APC has been described in section 1.1. The $APC^{min/+}$ strain represents sporadic CRC but fails to show extensive metastasis formation since they represent early stages of carcinogenesis. Furthermore, APC mutant mice possess predominantly tumours in the small intestine. Therefore, strains with restricting tumours to the colon would need to be selected (e.g. $APC^{580S/580S}$).

6.2.2. Preliminary Data: Effect of CPI-613 on Epithelial-To-Mesenchymal Transition

At the time of diagnosis, more than 25% of CRC patients suffer from metastasis, in most cases located in liver or lung, and 18% of patients with curative resection show progress with early recurrence, both indicators for poor prognosis (Sadahiro et al., 2003; Scheer and Auer, 2009; Riihimäki et al., 2016; Lin et al., 2018). Standard chemotherapeutic agents do not bear the potential to inhibit metastasis formation, of which crucial events are the gain of migration and invasion properties as well the epithelial-to-mesenchymal transition (EMT) (Brabletz et al., 2005).

EMT describes a transient and reversible process in which epithelial cells gain a mesenchymal phenotype via a complex interplay of intra- and extra-cellular remodelling based on signalling pathways, transcription factors, cell surface and extracellular matrix proteins (Kalluri and Weinberg, 2009; Roche, 2018). Within this process, numerous profound morphological and phenotypic changes occur. Epithelial cells lose their characteristics of apico-basolateral cell polarity, adhesion and strong cell-cell contact and undergo reorganisation of cytoskeletal architecture in order to gain migratory and invasive properties, which are characterised by a spindle-like shape, anterior-posterior polarisation and little focal cell-cell contact (Voulgari and Pintzas, 2009; Nieto, 2011; Lamouille et al., 2014; Tania et al., 2014; Cao et al., 2015). Mesenchymal cells are of pluripotent stemness-like character and, thus, EMT is regarded as a mechanism for giving rise to cancer stem cells (CSCs) (Singh and Settleman, 2010; Dave et al., 2012).

In general, EMT is physiological in embryogenesis (e.g. in gastrulation and neural tube formation) and in wound healing, but pathological in organ fibrosis and cancer progression and metastasis. In order to distinguish, EMT can be subdivided into three types, of which Type 3 describes part of the metastatic process of cancer cells (Zeisberg and Neilson, 2009). In Type 3 metastasis-linked EMT and the metastasis cascade, primary epithelial tumour cells of solid tumours leave a primary tumour, migrate to new tissue and reform a secondary tumour (Aceto et al., 2015; Mittal, 2018). Upon repression of E-Cadherin, epithelial tumour cells gain migratory features and lose cell-cell adhesion. Gaining invasiveness, these cells locally invade the basal lamina and intravasate into the blood vessel entering the systemic blood stream becoming circulating tumour cells (CTCs). Once reaching the metastasis site, CTCs extravasate from the blood stream into the tissue and undergo the reverse process called mesenchymal-to-epithelial transition (MET) in order to settle as micro-metastasis and upon clonal expansion form a distant marco-metastasis. Furthermore, EMT can drive epithelial cells into fibroblasts which shape part of the tumour microenvironment (Talbot et al., 2012). As an additional disadvantage to promoting metastasis formation, EMT was shown to confer senescence and to promote evasion from immune surveillance (Terry et al., 2017). For the induction of EMT, a variety of extracellular stimuli from the tumour microenvironment were identified such as inflammatory cytokines, growth factors and stress such as hypoxia (Roche, 2018). Among triggers, Wnt/β-catenin and TGF-β/SMAD were discovered in CRC (Vincan and Barker, 2008; Tang et al., 2013). But EMT is also induced by chronic treatment with genotoxic agents such as oxaliplatin or 5-FU and eventually coupled with prior induction of senescence (Yang et al., 2006; Tato-Costa et al., 2016). Core EMT regulators are transcription factors such as SNAIL/SLUG, ZEB1/2 and TWIST1/2 (Voulgari and Pintzas, 2009; Lamouille et al., 2014). The effector proteins are represented by a loss in epithelial markers E-Cadherin, claudins and occludins with concomitant increase in mesenchymal markers N-Cadherin, Vimentin and Fibronectin with an induction in associated metastasis formation and poor prognosis in CRC (Cao et al., 2015). As a detrimental consequence, upregulation of EMT is tightly linked to the formation of metastasis, leading to poor prognosis and represents a challenge in cancer therapy due to the formation of EMT-mediated drug-resistances (Du and Shim, 2016). Clinical research recently focussed on targeting EMT (Marcucci et al., 2016). In the context of CRC, drugs under investigation in clinical trials include LY2109761, Sorafenib/Regorafenib and Emodin (Zhang et al., 2009; Li et al., 2010b; Zou et al., 2011; Voon et al., 2017).

Some basic experiments were performed in order to evaluate the potential of CPI-613 to diminish or to suppress these features and are presented in the following as preliminary data.

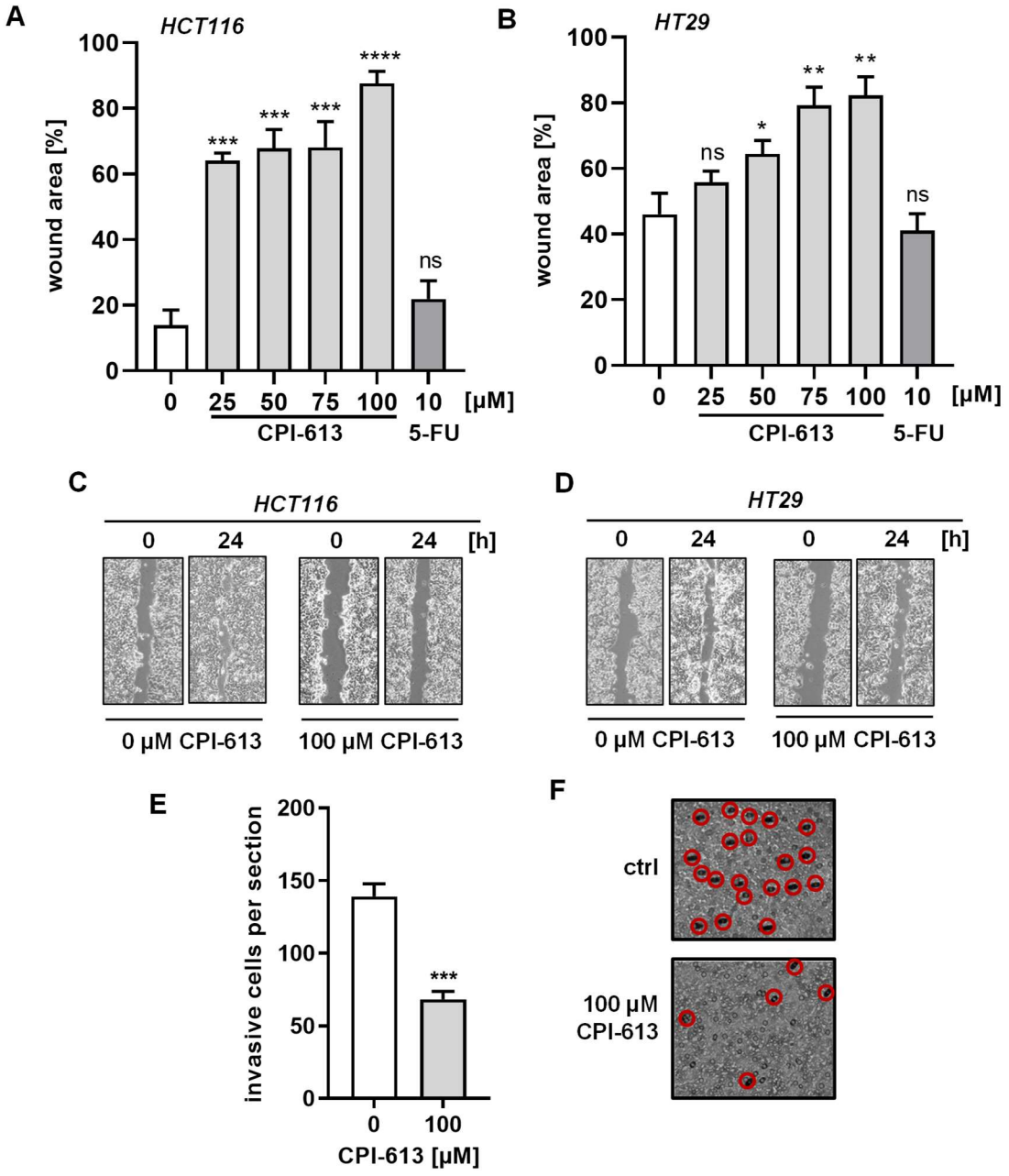

Figure 42: CPI-613 impairs migration and invasion of CRC cells.
(A, B) Wound healing assays were performed using HCT116 (A) and HT29 (B) cells over a period of 24 h in serum-diminished medium and with increasing doses of CPI-613. 5 µM 5-FU served as representative for standard chemotherapeutics. Data presented are mean + SEM (n≥3). ns: p>0.05, *p<0.05, **p<0.01, ****p<0.001, ****p<0.0001; *t*-test. (C, D) Representative microscopic photographs of 0 and 100 µM CPI-613 at t = 0 h and t = 24 h of A and B. (E) Quantification of a Boyden-chamber-based invasion assay using extracellular matrix. HCT116 cells were treated with 100 µM CPI-613 and invasive cells were stained and counted per section of view. Results are plotted as mean + SEM (n=3). ***p<0.001 vs. control; *t*-test. (F) Representative photographs of E. Encircled in red are stained invasive cells.

Making use of the wound healing assay, migratory behaviour of HCT116 (Figure 42A+C) and HT29 (Figure 42B+D) cells was assessed. Experiments were performed under

serum-starving conditions (1% FCS) to eliminate proliferation effects. Gap closure based on migration was monitored at different time points of which results of 24 h are depicted in Figure 42A+B. Regarding HCT116, control cells were able to migrate fast and close the wound with a residual wound area of less than 15% after 24 h.

Doses as low as 25 µM CPI-613 inhibited the migratory ability of these cells, represented by a residual wound area of more than 60%. This effect was dose-dependent and a dose of 100 µM CPI-613 resulted in a gap closure of less than 10% with a residual wound area of more than 90%. The standard chemotherapeutic 5-FU was not able to alter migration in HCT116 cells at all. While HT29 cells generally exhibit lower basal levels of migration, visible in the residual wound area of control cells (0 µM) of more than 40%, CPI-613 was also dose-dependently abolishing migration in this cell line with e.g. a residual wound area of more than 80% upon the incubation with 100 µM CPI-613 (Figure 42B). Again, 5-FU did not influence migration as compared to control cells. In order to analyse invasiveness of HCT116 cells, a Boyden Chamber-based invasion assays with extracellular matrix (ECM)-coated inserts was conducted (Figure 42E+F). Clearly visible in Figure 42E and F, cells treated with 100 µM CPI-613 were reduced in their invasion ability by approx. two thirds.

Since N-Cadherin is a mediator of invasion and migration (Derycke and Bracke, 2004; Hazan et al., 2004; Shih and Yamada, 2012), a Western Blot analysis of N-Cadherin protein levels was executed in HCT116 (Figure 43A+C left panel) and HT29 (Figure 43B+C right panel) cells. While E-Cadherin protein levels were unchanged in both cell lines upon incubation with CPI-613, N-Cadherin was depleted with increasing doses after 24 h. In HCT116 cells, N-Cadherin levels were depleted gradually over dose and reached less than one fourth at the highest dose. In HT29 cells, N-Cadherin levels were only moderately depleted with a remaining N-Cadherin level of 50% at the highest dose used.

Concluding, CPI-613 lead to a remarkable reduction of migratory as well as invasive properties of CRC cells, which is likely mediated by N-Cadherin depletion and seems to be independent of the p53 status. This might have a beneficial effect on reduction of metastasis formation.

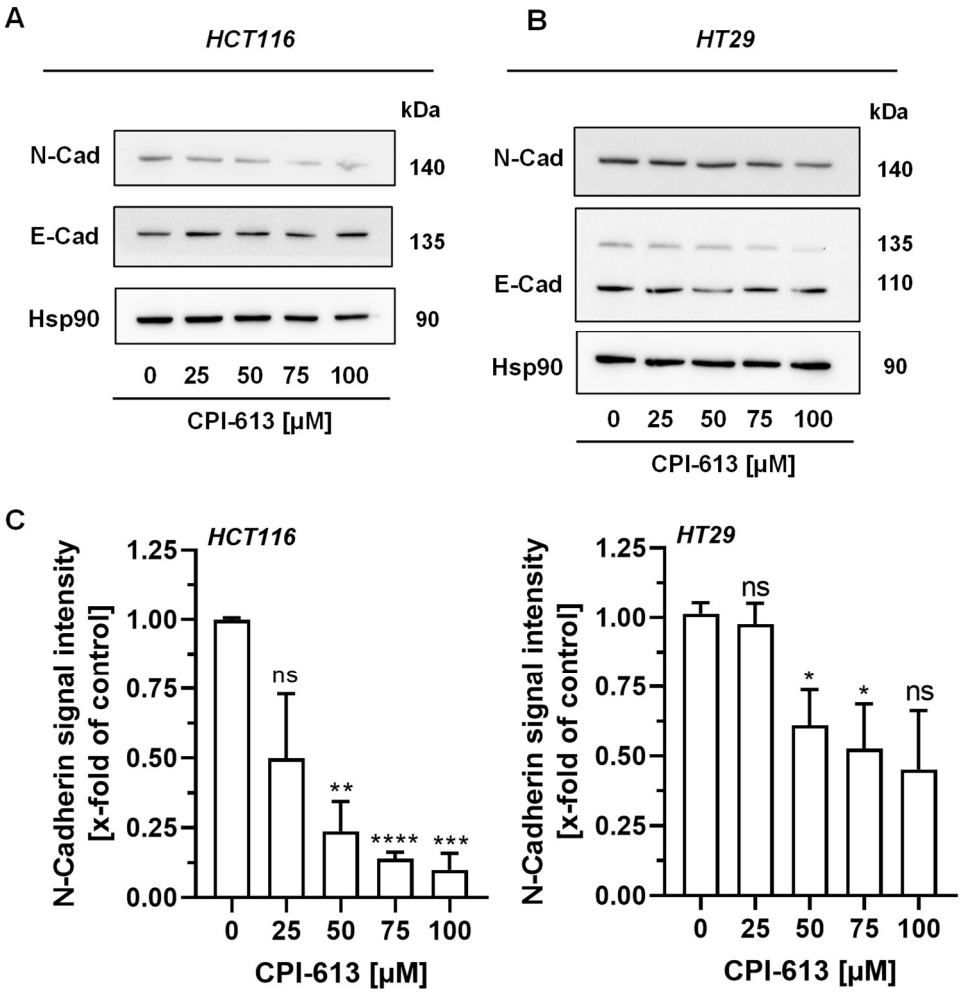

Figure 43: CPI-613 leads to depletion of migration-regulating N-Cadherin.
(A, B) Cells were treated with indicated doses of CPI-613 for 24 h and subjected to Western Blot analysis after lysis in 1x Lämmli-buffer. N-Cadherin (N-Cad) and E-Cadherin (E-Cad) were visualised along with the loading control Hsp90. (C) Quantification of N-Cadherin protein levels in HCT116 (left panel) and HT29 (right panel) cells upon CPI-613 incubation for 24 h as performed in A and B. Results are plotted as mean + SEM (n=3). ns: $p>0.05$, *$p<0.05$ **$p<0.01$, ***$p<0.001$, ****$p<0.0001$ vs. control; *t*-test.

Thus far, such effects have not been extensively described for CPI-613 in the literature. Perera et al. (2015) detected an upregulation of EMT markers (i.e. SLUG), mesenchymal markers and morphological changes upon chronic treatment of H460 lung cancer cells with CPI-613. These stem cell-like induced cells were less sensitive to CPI-613 as compared to parent cells by a factor of <2. Little convincing, Egawa et al. (2018) described CPI-613 to minimise mesenteric metastasis formation *in vivo* in SCID mice in the context of clear cell sarcoma, but this effect could only be found in combination with the autophagy-inhibitor chloroquine.

Although the preliminary results point to a contribution of CPI-613 to abrogate metastasis formation by the inhibition of EMT, further experiments are necessary to verify this effect. In experimental studies, not a single assay can cover the entire complex process of EMT, but an integrated testing strategy is needed (Yang et al., 2020). Moreover, it needs to be

taken into account that EMT is a transitional process with many intermediate or hybrid forms, which, however, are still regarded as able to metastasise. Using cell culture experiments, future studies could include a qPCR screening of the mRNA levels of EMT-markers as detailed above in CRC cell lines upon acute and/or chronic treatment with CPI-613 using suitable positive controls, such as TGF-β or chronic 5-FU treatment, in a first approach. In a next step, the potentially EMT-minimising or -reversing effect of CPI-613 on 5-FU-indued EMT in a sequential co-treatment could be assessed. Using immunofluorescence imaging or Western Blot analysis, the expression of EMT-markers on protein levels could be verified. Furthermore, immunofluorescence staining of Actin stress fibres could reveal the contribution of CPI-613 on the process of EMT or its abrogation (Shankar and Nabi, 2015). A flow-cytometric analysis of integrin levels and matrix metalloproteases could further deepen the picture of the effects of CPI-613 on EMT and metastasis abrogation (Radisky and Radisky, 2010). *In vivo*, a patient derived xenograft (PDX) model of cells or tissue originating from metastatic tumours or tumours from the metastatic site could be one useful approach. In here, HROC cells could be utilised. Generally, mouse models of CRC, which are either genetically-engineered or carcinogen-induced, rarely develop metastasis (Tong et al., 2011b; Johnson and Fleet, 2013a). Alternatively, orthotopic implantation of human CRC cells (e.g. HCT116, HT29 or CaCo-2) into cecum or rectum of immunodeficient mice leads to high rates of metastasis in lymph nodes, lung, liver and peritoneum. While this setting mimics vascular spread to distant sites, intrasplenic, intrahepatic or intraportal injection yields primarily but reproducibly hepatic metastasis. In here and allowing live imaging of metastatic burden, mice are injected with Luciferase-transfected HCT116 either into the tail vain to yield lung metastasis or into the spleen to yield liver metastasis with preceding system transportation (Khanna and Hunter, 2005). On this basis, experiments using a model of metastasis in immunosuppressive mice could shed light on the applicability of CPI-613 to target Type 3 EMT in cancer settings.

ACKNOWLEDGEMENTS

[redacted]

[redacted]

CURRICULUM VITAE

::: PERSONAL DETAILS

Name **Carina Neitzel**

[redacted]

::: ACADEMIC EDUCATION

since 09/2016 **Doctoral thesis**

09/2016 - 12/2017	Institute of Toxicology, University Medical Centre in Mainz, Germany
01/2018 - 12/2018	Rudolf-Buchheim-Institute of Pharmacology of the Justus-Liebig-University in Gießen, Germany
01/2018 - 09/2019	Department of Food Chemistry and Toxicology, Technical University Kaiserslautern in Kaiserslautern, Germany
Supervision	Prof Dr Jörg Fahrer
Funding	Wilhelm Sander Stiftung

since 01/2017 **Training for Expert Toxicologists** (DGPT)

10/2013 - 02/2016 **Master of Science Toxicology** (1.5)
Heinrich-Heine-University Düsseldorf, Germany

09/2010 - 09/2013 **Bachelor of Science Forensic Science** (1.3)
Hochschule Bonn-Rhein-Sieg in Rheinbach, Germany

09/2012 - 09/2013 **Bachelor of Science Forensic and Analytical Sciences** (First Class)
Robert Gordon University Aberdeen, Aberdeen, United Kingdom

06/2010 **Allgemeine Hochschulreife** (1.6)
Albert Einstein Schule in Schwalbach am Taunus, Germany

[redacted]

PUBLICATIONS

Neitzel, C.; Fahrer, J. (2020): CPI-613 targets mitochondria and synergizes with genotoxic anticancer drugs in colorectal cancer therapy. *In preparation*.

Neitzel, C.; Demuth, P.; Wittmann, S.; Fahrer, J. (2020): Targeting Altered Energy Metabolism in Colorectal Cancer: Oncogenic Reprogramming, the Central Role of the TCA Cycle and Therapeutic Opportunities. Cancers 12 (7), 1731.

Neitzel, C., Seiwert, N., Göder, A., Diehl, E., Weber, C., Nagel, G., Stroh, S., Rasenberger, B., Christmann, M., and Fahrer, J. (2019). Lipoic Acid Synergizes with Antineoplastic Drugs in Colorectal Cancer by Targeting p53 for Proteasomal Degradation. Cells *8*.

Neitzel, C., Seiwert, N., Stroh, S., Frisan, T., Audebert, M., Toulany, M., Kaina, B., and Fahrer, J. (2017). AKT2 Suppresses Pro-Survival Autophagy Triggered by DNA Double-Strand Breaks in Colorectal Cancer Cells. Cell Death & Disease *8*, e3019.

Mimmler, M.; Peter, S.; Kraus, A.; Stroh, S.; Nikolova, T.; Seiwert, N.; Hasselwander, S.; **Neitzel, C.**; Haub, J.; and Monien, B.H.; et al. (2016). DNA Damage Response Curtails Detrimental Replication Stress and Chromosomal Instability Induced by the Dietary Carcinogen PhIP. Nucleic Acids Research *44*.

CONFERENCE ATTENDANCES

05/2019	8th Mildred Scheel Cancer Conference Bonn Poster presentation
04/2019	Nachwuchswissenschaftler Meeting Günzburg Oral presentation
02/2019	4th German Pharm-Tox Summit (DGPT) Stuttgart Oral presentation
09/2018	1st University Cancer Centre Mainz Science Day Mainz Poster presentation (honoured with poster prize)
09/2018	Frankfurt Cancer Conference Frankfurt Poster presentation
03/2018	3rd German Pharm-Tox Summit (DGPT) Göttingen Poster presentation
10/2017	Gesellschaft für Umwelt- und Mutationsforschung Nachwuchsförderung Würzburg Oral presentation
11/2016	Symposium “DNA damage response, genetic instability and cancer” Mainz Oral presentation

REFERENCES

Abal, M., Bras-Goncalves, R., Judde, J.-G., Fsihi, H., Cremoux, P. de, Louvard, D., Magdelenat, H., Robine, S., and Poupon, M.-F. (2004). Enhanced sensitivity to irinotecan by Cdk1 inhibition in the p53-deficient HT29 human colon cancer cell line. Oncogene *23*, 1737-1744. https://doi.org/10.1038/sj.onc.1207299.

Abbas, T., and Dutta, A. (2009). p21 in cancer: intricate networks and multiple activities. Nature reviews. Cancer *9*, 400-414. https://doi.org/10.1038/nrc2657.

Abdrakhmanov, A., Kulikov, A.V., Luchkina, E.A., Zhivotovsky, B., and Gogvadze, V. (2019). Involvement of mitophagy in cisplatin-induced cell death regulation. Biological chemistry *400*, 161-170. https://doi.org/10.1515/hsz-2018-0210.

Abolhassani, M., Guais, A., Sanders, E., Campion, F., Fichtner, I., Bonte, J., Baronzio, G., Fiorentini, G., Israël, M., and Schwartz, L. (2012). Screening of well-established drugs targeting cancer metabolism: reproducibility of the efficacy of a highly effective drug combination in mice. Investigational new drugs *30*, 1331-1342. https://doi.org/10.1007/s10637-011-9692-7.

Aceto, N., Toner, M., Maheswaran, S., and Haber, D.A. (2015). En Route to Metastasis: Circulating Tumor Cell Clusters and Epithelial-to-Mesenchymal Transition. Trends in cancer *1*, 44-52. https://doi.org/10.1016/j.trecan.2015.07.006.

Adamsen, B.L., Kravik, K.L., and Angelis, P.M. de (2011). DNA damage signaling in response to 5-fluorouracil in three colorectal cancer cell lines with different mismatch repair and TP53 status. International journal of oncology *39*, 673-682. https://doi.org/10.3892/ijo.2011.1080.

Aggio, M.C., and Lozzio, B.B. (1979). Hematopoiesis of hereditarily asplenic-athymic (lasat) mice. Experimental hematology *7*, 197-205.

Ahmed, D., Eide, P.W., Eilertsen, I.A., Danielsen, S.A., Eknæs, M., Hektoen, M., Lind, G.E., and Lothe, R.A. (2013). Epigenetic and genetic features of 24 colon cancer cell lines. Oncogenesis *2*, e71. https://doi.org/10.1038/oncsis.2013.35.

Albertini, R.J., Anderson, D., Douglas, G.R., Hagmar, L., Hemminki, K., Merlo, F., Natarajan, A.T., Norppa, H., Shuker, D.E.G., and Tice, R., et al. (2000). IPCS guidelines for the monitoring of genotoxic effects of carcinogens in humans. Mutation Research/Reviews in Mutation Research *463*, 111-172. https://doi.org/10.1016/S1383-5742(00)00049-1.

Alistar, A., Morris, B.B., Desnoyer, R., Klepin, H.D., Hosseinzadeh, K., Clark, C., Cameron, A., Leyendecker, J., D'Agostino, R., and Topaloglu, U., et al. (2017). Safety and tolerability of the first-in-class agent CPI-613 in combination with modified FOLFIRINOX in patients with metastatic pancreatic cancer: a single-centre, open-label, dose-escalation, phase 1 trial. The Lancet. Oncology *18*, 770-778. https://doi.org/10.1016/S1470-2045(17)30314-5.

Alistar, A.T., Desnoyers, R., D'Agostino, R.J., and Pasche, B. (2016). CPI-613 enhances FOLFIRINOX response rate in stage IV pancreatic cancer. Annals of Oncology *27*, vi228. https://doi.org/10.1093/annonc/mdw371.67.

Alistar, A.T., Morris, B., Harrison, L., Bickenbach, K., Ginder, N., Proulx, J., McIlwain, L., and Luther, S. (2019). GA CPI 613: A single arm, open-label phase I study of CPI-613 in combination with gemcitabine and nab-paclitaxel for patients with locally advanced or metastatic pancreatic cancer. JCO *37*, TPS459-TPS459. https://doi.org/10.1200/JCO.2019.37.4_suppl.TPS459.

Almquist, D.R., Ahn, D.H., and Bekaii-Saab, T.S. (2020). The Role of Immune Checkpoint Inhibitors in Colorectal Adenocarcinoma. BioDrugs : clinical immunotherapeutics, biopharmaceuticals and gene therapy *34*, 349-362. https://doi.org/10.1007/s40259-020-00420-3.

Altieri, P., Murialdo, R., Barisione, C., Lazzarini, E., Garibaldi, S., Fabbi, P., Ruggeri, C., Borile, S., Carbone, F., and Armirotti, A., et al. (2017). 5-fluorouracil causes endothelial cell senescence: potential protective role of glucagon-like peptide 1. British journal of pharmacology *174*, 3713-3726. https://doi.org/10.1111/bph.13725.

Altman, B.J., and Rathmell, J.C. (2012). Metabolic stress in autophagy and cell death pathways. Cold Spring Harbor perspectives in biology *4*, a008763. https://doi.org/10.1101/cshperspect.a008763.

Anderson, E.M., Zhang, J., Russell, G., Bowline, I.G., Thyagarajan, B., Li, D., Ma, L., Anderson, E.R., and Murea, M. (2018a). A Single-Center Retrospective Study of Acute Kidney Injury Incidence in Patients With Advanced Malignancies Treated With Antimitochondrial Targeted Drug. Kidney International Reports *4*, 310-320. https://doi.org/10.1016/j.ekir.2018.10.021.

Anderson, N.M., Mucka, P., Kern, J.G., and Feng, H. (2018b). The emerging role and targetability of the TCA cycle in cancer metabolism. Protein & cell *9*, 216-237. https://doi.org/10.1007/s13238-017-0451-1.

Anderson, R.G., Ghiraldeli, L.P., and Pardee, T.S. (2018c). Mitochondria in cancer metabolism, an organelle whose time has come? Biochimica et biophysica acta. Reviews on cancer *1870*, 96-102. https://doi.org/10.1016/j.bbcan.2018.05.005.

Angelis, M.L. de, Zeuner, A., Policicchio, E., Russo, G., Bruselles, A., Signore, M., Vitale, S., Luca, G. de, Pilozzi, E., and Boe, A., et al. (2016). Cancer Stem Cell-Based Models of Colorectal Cancer Reveal Molecular Determinants of Therapy Resistance. Stem cells translational medicine *5*, 511-523. https://doi.org/10.5966/sctm.2015-0214.

Angelis, P.M. de, Svendsrud, D.H., Kravik, K.L., and Stokke, T. (2006). Cellular response to 5-fluorouracil (5-FU) in 5-FU-resistant colon cancer cell lines during treatment and recovery. Molecular cancer *5*, 20. https://doi.org/10.1186/1476-4598-5-20.

Applegate, M.A.B., Humphries, K.M., and Szweda, L.I. (2008). Reversible inhibition of alpha-ketoglutarate dehydrogenase by hydrogen peroxide: glutathionylation and protection of lipoic acid. Biochemistry *47*, 473-478. https://doi.org/10.1021/bi7017464.

Arai, S., Chen, S., Xie, L., and Balk, S.P. (2020). Ubiquitin Ligase MARCH5 Regulates Apoptosis through Mediation of Stress-Induced and NOXA-Dependent MCL1 Degradation.

Armaghany, T., Wilson, J.D., Chu, Q., and Mills, G. (2012). Genetic Alterations in Colorectal Cancer. Gastrointestinal Cancer Research : GCR *5*, 19-27.

Atlante, S., Visintin, A., Marini, E., Savoia, M., Dianzani, C., Giorgis, M., Sürün, D., Maione, F., Schnütgen, F., and Farsetti, A., et al. (2018). α-ketoglutarate dehydrogenase inhibition counteracts breast cancer-associated lung metastasis. Cell death & disease *9*, 756. https://doi.org/10.1038/s41419-018-0802-8.

Avagliano, A., Granato, G., Ruocco, M.R., Romano, V., Belviso, I., Carfora, A., Montagnani, S., and Arcucci, A. (2018). Metabolic Reprogramming of Cancer Associated Fibroblasts: The Slavery of Stromal Fibroblasts. BioMed research international *2018*, 6075403. https://doi.org/10.1155/2018/6075403.

Bamberger, E.G., Machado, E.A., and Lozzio, B.B. (1977). Hematopoiesis in hereditarily athymic mice. Laboratory animal science *27*, 43-49.

Barzilai, A., and Yamamoto, K.-I. (2004). DNA damage responses to oxidative stress. DNA repair *3*, 1109-1115. https://doi.org/10.1016/j.dnarep.2004.03.002.

Bayat Mokhtari, R., Homayouni, T.S., Baluch, N., Morgatskaya, E., Kumar, S., Das, B., and Yeger, H. (2017). Combination therapy in combating cancer. Oncotarget *8*, 38022-38043. https://doi.org/10.18632/oncotarget.16723.

Becker, C., Fantini, M.C., and Neurath, M.F. (2006). High resolution colonoscopy in live mice. Nature protocols *1*, 2900-2904. https://doi.org/10.1038/nprot.2006.446.

Bellio, C., DiGloria, C., Spriggs, D.R., Foster, R., Growdon, W.B., and Rueda, B.R. (2019). The Metabolic Inhibitor CPI-613 Negates Treatment Enrichment of Ovarian Cancer Stem Cells. Cancers *11*. https://doi.org/10.3390/cancers11111678.

Bendixen, C., Thomsen, B., Alsner, J., and Westergaard, O. (1990). Camptothecin-stabilized topoisomerase I-DNA adducts cause premature termination of transcription. Biochemistry *29*, 5613-5619. https://doi.org/10.1021/bi00475a028.

Beutler, E., Gelbart, T., and Demina, A. (1998). Racial variability in the UDP-glucuronosyltransferase 1 (UGT1A1) promoter: a balanced polymorphism for regulation of bilirubin metabolism? Proceedings of the National Academy of Sciences of the United States of America *95*, 8170-8174. https://doi.org/10.1073/pnas.95.14.8170.

Bi, X., Lin, Q., Foo, T.W., Joshi, S., You, T., Shen, H.-M., Ong, C.N., Cheah, P.Y., Eu, K.W., and Hew, C.-L. (2006). Proteomic analysis of colorectal cancer reveals alterations in metabolic pathways: mechanism of tumorigenesis. Molecular & cellular proteomics : MCP *5*, 1119-1130. https://doi.org/10.1074/mcp.M500432-MCP200.

Bigagli, E., Filippo, C. de, Castagnini, C., Toti, S., Acquadro, F., Giudici, F., Fazi, M., Dolara, P., Messerini, L., and Tonelli, F., et al. (2016). DNA copy number alterations, gene expression changes and disease-free survival in patients with colorectal cancer: a 10 year follow-up. Cellular oncology (Dordrecht) *39*, 545-558. https://doi.org/10.1007/s13402-016-0299-z.

Blagosklonny, M.V., and El-Deiry, W.S. (1998). Acute overexpression of wt p53 facilitates anticancer drug-induced death of cancer and normal cells. Int. J. Cancer *75*, 933-940. https://doi.org/10.1002/(SICI)1097-0215(19980316)75:6<933::AID-IJC17>3.0.CO;2-3.

Blouin, J.-M., Penot, G., Collinet, M., Nacfer, M., Forest, C., Laurent-Puig, P., Coumoul, X., Barouki, R., Benelli, C., and Bortoli, S. (2011). Butyrate elicits a metabolic switch in human colon cancer cells by targeting the pyruvate dehydrogenase complex. International journal of cancer *128*, 2591-2601. https://doi.org/10.1002/ijc.25599.

Boengler, K., Bulic, M., Schreckenberg, R., Schlüter, K.-D., and Schulz, R. (2017). The gap junction modifier ZP1609 decreases cardiomyocyte hypercontracture following ischaemia/reperfusion independent from mitochondrial connexin 43. British journal of pharmacology *174*, 2060-2073. https://doi.org/10.1111/bph.13804.

Bogaert, J., and Prenen, H. (2014). Molecular genetics of colorectal cancer. Annals of Gastroenterology *27*, 9-14.

Bohr, V.A. (2002). Repair of oxidative DNA damage in nuclear and mitochondrial DNA, and some changes with aging in mammalian cells1,2 1Guest Editor: Miral Dizdaroglu 2This article is part of a series of reviews on “Oxidative DNA Damage and Repair.” The full list of papers may be found on the homepage of the journal. Free Radical Biology and Medicine *32*, 804-812. https://doi.org/10.1016/S0891-5849(02)00787-6.

Bokemeyer, C., Köhne, C.-H., Ciardiello, F., Lenz, H.-J., Heinemann, V., Klinkhardt, U., Beier, F., Duecker, K., van Krieken, J.H., and Tejpar, S. (2015). FOLFOX4 plus cetuximab treatment and RAS mutations in colorectal cancer. European journal of cancer (Oxford, England : 1990) *51*, 1243-1252. https://doi.org/10.1016/j.ejca.2015.04.007.

Bonomi, F., and Pagani, S. (1986). Removal of ferritin-bound iron by DL-dihydrolipoate and DL-dihydrolipoamide. European journal of biochemistry *155*, 295-300. https://doi.org/10.1111/j.1432-1033.1986.tb09489.x.

Boyle, K.A., van Wickle, J., Hill, R.B., Marchese, A., Kalyanaraman, B., and Dwinell, M.B. (2018). Mitochondria-targeted drugs stimulate mitophagy and abrogate colon cancer cell proliferation. The Journal of biological chemistry *293*, 14891-14904. https://doi.org/10.1074/jbc.RA117.001469.

Brabletz, T., Hlubek, F., Spaderna, S., Schmalhofer, O., Hiendlmeyer, E., Jung, A., and Kirchner, T. (2005). Invasion and metastasis in colorectal cancer: epithelial-mesenchymal transition, mesenchymal-epithelial transition, stem cells and beta-catenin. Cells, tissues, organs *179*, 56-65. https://doi.org/10.1159/000084509.

Brady, C.A., and Attardi, L.D. (2010). p53 at a glance. Journal of cell science *123*, 2527-2532. https://doi.org/10.1242/jcs.064501.

Bray, F., Ferlay, J., Soerjomataram, I., Siegel, R.L., Torre, L.A., and Jemal, A. (2018). Global cancer statistics 2018: GLOBOCAN estimates of incidence and mortality worldwide for 36 cancers in 185 countries. CA: a cancer journal for clinicians *68*, 394-424. https://doi.org/10.3322/caac.21492.

Bröker, L.E., Kruyt, F.A.E., and Giaccone, G. (2005). Cell death independent of caspases: a review. Clinical cancer research : an official journal of the American Association for Cancer Research *11*, 3155-3162. https://doi.org/10.1158/1078-0432.CCR-04-2223.

Brosnan, J.T. (2003). Interorgan amino acid transport and its regulation. The Journal of nutrition *133*, 2068S-2072S. https://doi.org/10.1093/jn/133.6.2068S.

Brown, R.E., Short, S.P., and Williams, C.S. (2018). Colorectal Cancer and Metabolism. Current colorectal cancer reports *14*, 226-241. https://doi.org/10.1007/s11888-018-0420-y.

Bunik, V.I. (2003). 2-Oxo acid dehydrogenase complexes in redox regulation. European journal of biochemistry *270*, 1036-1042. https://doi.org/10.1046/j.1432-1033.2003.03470.x.

Bunik, V.I., Mkrtchyan, G., Grabarska, A., Oppermann, H., Daloso, D., Araujo, W.L., Juszczak, M., Rzeski, W., Bettendorff, L., and Fernie, A.R., et al. (2016). Inhibition of mitochondrial 2-oxoglutarate dehydrogenase impairs viability of cancer cells in a cell-specific metabolism-dependent manner. Oncotarget *7*, 26400-26421. https://doi.org/10.18632/oncotarget.8387.

Bürtin, F., Mullins, C.S., and Linnebacher, M. (2020). Mouse models of colorectal cancer: Past, present and future perspectives. World journal of gastroenterology *26*, 1394-1426. https://doi.org/10.3748/wjg.v26.i13.1394.

Bykov, V.J.N., Lambert, J.M.R., Hainaut, P., and Wiman, K.G. (2009). Mutant p53 rescue and modulation of p53 redox state. Cell cycle (Georgetown, Tex.) *8*, 2509-2517. https://doi.org/10.4161/cc.8.16.9382.

Cairns, R.A., Harris, I.S., and Mak, T.W. (2011). Regulation of cancer cell metabolism. Nature reviews. Cancer *11*, 85-95. https://doi.org/10.1038/nrc2981.

Cantor, J.R., and Sabatini, D.M. (2012). Cancer cell metabolism: one hallmark, many faces. Cancer discovery *2*, 881-898. https://doi.org/10.1158/2159-8290.CD-12-0345.

Cao, H., Xu, E., Liu, H., Wan, L., and Lai, M. (2015). Epithelial-mesenchymal transition in colorectal cancer metastasis: A system review. Pathology, research and practice *211*, 557-569. https://doi.org/10.1016/j.prp.2015.05.010.

Cardaci, S., Desideri, E., and Ciriolo, M.R. (2012). Targeting aerobic glycolysis: 3-bromopyruvate as a promising anticancer drug. Journal of bioenergetics and biomembranes *44*, 17-29. https://doi.org/10.1007/s10863-012-9422-7.

Chabot, G.G. (1997). Clinical pharmacokinetics of irinotecan. Clinical pharmacokinetics *33*, 245-259. https://doi.org/10.2165/00003088-199733040-00001.

Chang, J.Y., Yi, H.-S., Kim, H.-W., and Shong, M. (2017). Dysregulation of mitophagy in carcinogenesis and tumor progression. Biochimica et biophysica acta. Bioenergetics *1858*, 633-640. https://doi.org/10.1016/j.bbabio.2016.12.008.

Chazotte, B. (2011). Labeling mitochondria with MitoTracker dyes. Cold Spring Harbor protocols *2011*, 990-992. https://doi.org/10.1101/pdb.prot5648.

Chen, J. (2016). The Cell-Cycle Arrest and Apoptotic Functions of p53 in Tumor Initiation and Progression. Cold Spring Harbor perspectives in medicine *6*, a026104. https://doi.org/10.1101/cshperspect.a026104.

Chen, J.-Q., and Russo, J. (2012). Dysregulation of glucose transport, glycolysis, TCA cycle and glutaminolysis by oncogenes and tumor suppressors in cancer cells. Biochimica et biophysica acta *1826*, 370-384. https://doi.org/10.1016/j.bbcan.2012.06.004.

Chen, M.-C., Lee, N.-H., Ho, T.-J., Hsu, H.-H., Kuo, C.-H., Kuo, W.-W., Lin, Y.-M., Tsai, F.-J., Tsai, C.-H., and Huang, C.-Y. (2014). Resistance to irinotecan (CPT-11) activates epidermal growth factor receptor/nuclear factor kappa B and increases cellular metastasis and autophagy in LoVo colon cancer cells. Cancer Letters *349*, 51-60. https://doi.org/10.1016/j.canlet.2014.03.023.

Choi, J.-H., Yoon, J.S., Won, Y.-W., Park, B.-B., and Lee, Y.Y. (2012). Chloroquine enhances the chemotherapeutic activity of 5-fluorouracil in a colon cancer cell line via cell cycle alteration.

APMIS : acta pathologica, microbiologica, et immunologica Scandinavica *120*, 597-604. https://doi.org/10.1111/j.1600-0463.2012.02876.x.

Choi, S.Y., Yu, J.H., and Kim, H. (2009). Mechanism of alpha-lipoic acid-induced apoptosis of lung cancer cells. Annals of the New York Academy of Sciences *1171*, 149-155. https://doi.org/10.1111/j.1749-6632.2009.04708.x.

Chong, D., Ma, L., Liu, F., Zhang, Z., Zhao, S., Huo, Q., Zhang, P., Zheng, H., and Liu, H. (2017). Synergistic antitumor effect of 3-bromopyruvate and 5-fluorouracil against human colorectal cancer through cell cycle arrest and induction of apoptosis. Anti-cancer drugs *28*, 831-840. https://doi.org/10.1097/CAD.0000000000000517.

Chou, T.-C. (2006). Theoretical basis, experimental design, and computerized simulation of synergism and antagonism in drug combination studies. Pharmacological reviews *58*, 621-681. https://doi.org/10.1124/pr.58.3.10.

Chou, T.-C. (2010). Drug combination studies and their synergy quantification using the Chou-Talalay method. Cancer research *70*, 440-446. https://doi.org/10.1158/0008-5472.CAN-09-1947.

Collins, S.L., and Patterson, A.D. (2020). The gut microbiome: an orchestrator of xenobiotic metabolism. Acta pharmaceutica Sinica. B *10*, 19-32. https://doi.org/10.1016/j.apsb.2019.12.001.

Compton, C.C., and Greene, F.L. (2004). The staging of colorectal cancer: 2004 and beyond. CA: a cancer journal for clinicians *54*, 295-308. https://doi.org/10.3322/canjclin.54.6.295.

Contractor, T., and Harris, C.R. (2012). p53 negatively regulates transcription of the pyruvate dehydrogenase kinase Pdk2. Cancer research *72*, 560-567. https://doi.org/10.1158/0008-5472.CAN-11-1215.

Cregan, S.P., Dawson, V.L., and Slack, R.S. (2004). Role of AIF in caspase-dependent and caspase-independent cell death. Oncogene *23*, 2785-2796. https://doi.org/10.1038/sj.onc.1207517.

Cremer, D.R., Rabeler, R., Roberts, A., and Lynch, B. (2006). Safety evaluation of alpha-lipoic acid (ALA). Regulatory toxicology and pharmacology : RTP *46*, 29-41. https://doi.org/10.1016/j.yrtph.2006.06.004.

Cremolini, C., Di Bartolomeo, M., Amatu, A., Antoniotti, C., Moretto, R., Berenato, R., Perrone, F., Tamborini, E., Aprile, G., and Lonardi, S., et al. (2015a). BRAF codons 594 and 596 mutations identify a new molecular subtype of metastatic colorectal cancer at favorable prognosis. Annals of oncology : official journal of the European Society for Medical Oncology *26*, 2092-2097. https://doi.org/10.1093/annonc/mdv290.

Cremolini, C., Loupakis, F., Antoniotti, C., Lupi, C., Sensi, E., Lonardi, S., Mezi, S., Tomasello, G., Ronzoni, M., and Zaniboni, A., et al. (2015b). FOLFOXIRI plus bevacizumab versus FOLFIRI plus bevacizumab as first-line treatment of patients with metastatic colorectal cancer: updated overall survival and molecular subgroup analyses of the open-label, phase 3 TRIBE study. The Lancet. Oncology *16*, 1306-1315. https://doi.org/10.1016/S1470-2045(15)00122-9.

Cronan, J.E., Zhao, X., and Jiang, Y. (2005). Function, Attachment and Synthesis of Lipoic Acid in Escherichia coli. In Advances in microbial physiology, R.K. Poole, ed. (Amsterdam: Elsevier Academic), pp. 103–146.

Croteau, D.L., and Bohr, V.A. (1997). Repair of oxidative damage to nuclear and mitochondrial DNA in mammalian cells. The Journal of biological chemistry *272*, 25409-25412. https://doi.org/10.1074/jbc.272.41.25409.

Cruz, M.D., Ledbetter, S., Chowdhury, S., Tiwari, A.K., Momi, N., Wali, R.K., Bliss, C., Huang, C., Lichtenstein, D., and Bhattacharya, S., et al. (2017). Metabolic reprogramming of the premalignant colonic mucosa is an early event in carcinogenesis. Oncotarget *8*, 20543-20557. https://doi.org/10.18632/oncotarget.16129.

Cunningham, D., Atkin, W., Lenz, H.-J., Lynch, H.T., Minsky, B., Nordlinger, B., and Starling, N. (2010). Colorectal cancer. The Lancet *375*, 1030-1047. https://doi.org/10.1016/S0140-6736(10)60353-4.

Cunningham, D., Pyrhönen, S., James, R.D., Punt, C.J., Hickish, T.F., Heikkila, R., Johannesen, T.B., Starkhammar, H., Topham, C.A., and Awad, L., et al. (1998). Randomised trial of irinotecan plus supportive care versus supportive care alone after fluorouracil failure for patients with metastatic colorectal cancer. Lancet (London, England) *352*, 1413-1418. https://doi.org/10.1016/S0140-6736(98)02309-5.

Dahan, M. (2014). CPI-613, a non-redox active lipoic acid analog, causes hyper-phosphorylation of BCKDC E1α in H460 lung cancer cells in vitro. Thesis at Stony Brook Universtiy, New York, USA.

Dai, C., and Gu, W. (2010). p53 post-translational modification: deregulated in tumorigenesis. Trends in molecular medicine *16*, 528-536. https://doi.org/10.1016/j.molmed.2010.09.002.

Danenberg, P.V., Gustavsson, B., Johnston, P., Lindberg, P., Moser, R., Odin, E., Peters, G.J., and Petrelli, N. (2016). Folates as adjuvants to anticancer agents: Chemical rationale and mechanism of action. Critical reviews in oncology/hematology *106*, 118-131. https://doi.org/10.1016/j.critrevonc.2016.08.001.

Dang, L., Yen, K., and Attar, E.C. (2016). IDH mutations in cancer and progress toward development of targeted therapeutics. Annals of oncology : official journal of the European Society for Medical Oncology *27*, 599-608. https://doi.org/10.1093/annonc/mdw013.

Datta, S., Chowdhury, S., and Roy, H.K. (2017). Metabolism, microbiome and colorectal cancer. Aging *9*, 1086-1087. https://doi.org/10.18632/aging.101234.

Dave, B., Mittal, V., Tan, N.M., and Chang, J.C. (2012). Epithelial-mesenchymal transition, cancer stem cells and treatment resistance. Breast cancer research : BCR *14*, 202. https://doi.org/10.1186/bcr2938.

Daye, D., and Wellen, K.E. (2012). Metabolic reprogramming in cancer: unraveling the role of glutamine in tumorigenesis. Seminars in cell & developmental biology *23*, 362-369. https://doi.org/10.1016/j.semcdb.2012.02.002.

DeBerardinis, R.J., and Chandel, N.S. (2016). Fundamentals of cancer metabolism. Science advances *2*, e1600200. https://doi.org/10.1126/sciadv.1600200.

DeBerardinis, R.J., Lum, J.J., Hatzivassiliou, G., and Thompson, C.B. (2008). The biology of cancer: metabolic reprogramming fuels cell growth and proliferation. Cell metabolism *7*, 11-20. https://doi.org/10.1016/j.cmet.2007.10.002.

Deenen, M.J., Meulendijks, D., Cats, A., Sechterberger, M.K., Severens, J.L., Boot, H., Smits, P.H., Rosing, H., Mandigers, C.M.P.W., and Soesan, M., et al. (2016). Upfront Genotyping of DPYD*2A to Individualize Fluoropyrimidine Therapy: A Safety and Cost Analysis. Journal of clinical oncology : official journal of the American Society of Clinical Oncology *34*, 227-234. https://doi.org/10.1200/JCO.2015.63.1325.

Derangère, V., Fumet, J.D., Boidot, R., Bengrine, L., Limagne, E., Chevriaux, A., Vincent, J., Ladoire, S., Apetoh, L., and Rébé, C., et al. (2016). Does bevacizumab impact anti-EGFR therapy efficacy in metastatic colorectal cancer? Oncotarget *7*, 9309-9321. https://doi.org/10.18632/oncotarget.7008.

Derry, M.M., Raina, K., Agarwal, R., and Agarwal, C. (2014). Characterization of azoxymethane-induced colon tumor metastasis to lung in a mouse model relevant to human sporadic colorectal cancer and evaluation of grape seed extract efficacy. Experimental and toxicologic pathology : official journal of the Gesellschaft fur Toxikologische Pathologie *66*, 235-242. https://doi.org/10.1016/j.etp.2014.02.003.

Derycke, L.D.M., and Bracke, M.E. (2004). N-cadherin in the spotlight of cell-cell adhesion, differentiation, embryogenesis, invasion and signalling. The International journal of developmental biology *48*, 463-476. https://doi.org/10.1387/ijdb.041793ld.

Di Veroli, G.Y., Fornari, C., Wang, D., Mollard, S., Bramhall, J.L., Richards, F.M., and Jodrell, D.I. (2016). Combenefit: an interactive platform for the analysis and visualization of drug combinations. Bioinformatics (Oxford, England) *32*, 2866-2868. https://doi.org/10.1093/bioinformatics/btw230.

Diasio, R.B., and Harris, B.E. (1989). Clinical pharmacology of 5-fluorouracil. Clinical pharmacokinetics *16*, 215-237. https://doi.org/10.2165/00003088-198916040-00002.

Ding, W.-X., and Yin, X.-M. (2012). Mitophagy: mechanisms, pathophysiological roles, and analysis. Biological chemistry *393*, 547-564. https://doi.org/10.1515/hsz-2012-0119.

Dogar, I., Dixon, S., Gill, R., Young, A., Mallay, S., Oldford, C., and Mailloux, R.J. (2020). C57BL/6J mice upregulate catalase to maintain the hydrogen peroxide buffering capacity of liver mitochondria. Free radical biology & medicine *146*, 59-69. https://doi.org/10.1016/j.freeradbiomed.2019.10.409.

Dolman, N.J., Chambers, K.M., Mandavilli, B., Batchelor, R.H., and Janes, M.S. (2013). Tools and techniques to measure mitophagy using fluorescence microscopy. Autophagy *9*, 1653-1662. https://doi.org/10.4161/auto.24001.

Dong, L., and Neuzil, J. (2019). Targeting mitochondria as an anticancer strategy. Cancer communications (London, England) *39*, 63. https://doi.org/10.1186/s40880-019-0412-6.

Doong, S.L., and Dolnick, B.J. (1988). 5-Fluorouracil substitution alters pre-mRNA splicing in vitro. The Journal of biological chemistry *263*, 4467-4473.

Dörr, J.R., Yu, Y., Milanovic, M., Beuster, G., Zasada, C., Däbritz, J.H.M., Lisec, J., Lenze, D., Gerhardt, A., and Schleicher, K., et al. (2013). Synthetic lethal metabolic targeting of cellular senescence in cancer therapy. Nature *501*, 421-425. https://doi.org/10.1038/nature12437.

Dörsam, B., and Fahrer, J. (2016). The disulfide compound α-lipoic acid and its derivatives: A novel class of anticancer agents targeting mitochondria. Cancer Letters *371*, 12-19. https://doi.org/10.1016/j.canlet.2015.11.019.

Dörsam, B., Göder, A., Seiwert, N., Kaina, B., and Fahrer, J. (2015). Lipoic acid induces p53-independent cell death in colorectal cancer cells and potentiates the cytotoxicity of 5-fluorouracil. Archives of toxicology *89*, 1829-1846. https://doi.org/10.1007/s00204-014-1434-0.

Dörsam, B., Seiwert, N., Foersch, S., Stroh, S., Nagel, G., Begaliew, D., Diehl, E., Kraus, A., McKeague, M., and Minneker, V., et al. (2018). PARP-1 protects against colorectal tumor induction, but promotes inflammation-driven colorectal tumor progression. Proceedings of the National Academy of Sciences of the United States of America *115*, E4061-E4070. https://doi.org/10.1073/pnas.1712345115.

Du, B., and Shim, J.S. (2016). Targeting Epithelial-Mesenchymal Transition (EMT) to Overcome Drug Resistance in Cancer. Molecules (Basel, Switzerland) *21*. https://doi.org/10.3390/molecules21070965.

Duprez, L., Wirawan, E., Vanden Berghe, T., and Vandenabeele, P. (2009). Major cell death pathways at a glance. Microbes and infection *11*, 1050-1062. https://doi.org/10.1016/j.micinf.2009.08.013.

Dylla, S.J., Beviglia, L., Park, I.-K., Chartier, C., Raval, J., Ngan, L., Pickell, K., Aguilar, J., Lazetic, S., and Smith-Berdan, S., et al. (2008). Colorectal cancer stem cells are enriched in xenogeneic tumors following chemotherapy. PLoS ONE *3*, e2428. https://doi.org/10.1371/journal.pone.0002428.

Egawa, Y., Saigo, C., Kito, Y., Moriki, T., and Takeuchi, T. (2018). Therapeutic potential of CPI-613 for targeting tumorous mitochondrial energy metabolism and inhibiting autophagy in clear cell sarcoma. PLoS ONE *13*. https://doi.org/10.1371/journal.pone.0198940.

Eng, C., Kiuru, M., Fernandez, M.J., and Aaltonen, L.A. (2003). A role for mitochondrial enzymes in inherited neoplasia and beyond. Nature reviews. Cancer *3*, 193-202. https://doi.org/10.1038/nrc1013.

Engstrand, J., Nilsson, H., Strömberg, C., Jonas, E., and Freedman, J. (2018). Colorectal cancer liver metastases - a population-based study on incidence, management and survival. BMC cancer *18*, 78. https://doi.org/10.1186/s12885-017-3925-x.

Ewald, J.A., Desotelle, J.A., Wilding, G., and Jarrard, D.F. (2010). Therapy-induced senescence in cancer. Journal of the National Cancer Institute *102*, 1536-1546. https://doi.org/10.1093/jnci/djq364.

Fahrer, J., Frisch, J., Nagel, G., Kraus, A., Dörsam, B., Thomas, A.D., Reißig, S., Waisman, A., and Kaina, B. (2015). DNA repair by MGMT, but not AAG, causes a threshold in alkylation-induced colorectal carcinogenesis. Carcinogenesis *36*, 1235-1244. https://doi.org/10.1093/carcin/bgv114.

Falcone, A., Ricci, S., Brunetti, I., Pfanner, E., Allegrini, G., Barbara, C., Crinò, L., Benedetti, G., Evangelista, W., and Fanchini, L., et al. (2007). Phase III trial of infusional fluorouracil, leucovorin, oxaliplatin, and irinotecan (FOLFOXIRI) compared with infusional fluorouracil, leucovorin, and irinotecan (FOLFIRI) as first-line treatment for metastatic colorectal cancer: the Gruppo Oncologico Nord Ovest. Journal of clinical oncology : official journal of the American Society of Clinical Oncology *25*, 1670-1676. https://doi.org/10.1200/JCO.2006.09.0928.

Favoriti, P., Carbone, G., Greco, M., Pirozzi, F., Pirozzi, R.E.M., and Corcione, F. (2016). Worldwide burden of colorectal cancer: a review. Updates in surgery *68*, 7-11. https://doi.org/10.1007/s13304-016-0359-y.

Fedorova, M.S., Kudryavtseva, A.V., Lakunina, V.A., Snezhkina, A.V., Volchenko, N.N., Slavnova, E.N., Danilova, T.V., Sadritdinova, A.F., Melnikova, N.V., and Belova, A.A., et al.

(2015). Downregulation of OGDHL expression is associated with promoter hypermethylation in colorectal cancer. Mol Biol *49*, 608-617. https://doi.org/10.1134/S0026893315040044.

Feron, O. (2009). Pyruvate into lactate and back: from the Warburg effect to symbiotic energy fuel exchange in cancer cells. Radiotherapy and oncology : journal of the European Society for Therapeutic Radiology and Oncology *92*, 329-333. https://doi.org/10.1016/j.radonc.2009.06.025.

Feuerecker, B., Pirsig, S., Seidl, C., Aichler, M., Feuchtinger, A., Bruchelt, G., and Senekowitsch-Schmidtke, R. (2012). Lipoic acid inhibits cell proliferation of tumor cells in vitro and in vivo. Cancer biology & therapy *13*, 1425-1435. https://doi.org/10.4161/cbt.22003.

Fischer, F., Baerenfaller, K., and Jiricny, J. (2007). 5-Fluorouracil is efficiently removed from DNA by the base excision and mismatch repair systems. Gastroenterology *133*, 1858-1868. https://doi.org/10.1053/j.gastro.2007.09.003.

Focaccetti, C., Bruno, A., Magnani, E., Bartolini, D., Principi, E., Dallaglio, K., Bucci, E.O., Finzi, G., Sessa, F., and Noonan, D.M., et al. (2015). Effects of 5-Fluorouracil on Morphology, Cell Cycle, Proliferation, Apoptosis, Autophagy and ROS Production in Endothelial Cells and Cardiomyocytes. PLoS ONE *10*. https://doi.org/10.1371/journal.pone.0115686.

Fogarty, M.C., Devito, G., Hughes, C.M., Burke, G., Brown, J.C., McEneny, J., Brown, D., McClean, C., and Davison, G.W. (2013). Effects of α-lipoic acid on mtDNA damage after isolated muscle contractions. Medicine and science in sports and exercise *45*, 1469-1477. https://doi.org/10.1249/MSS.0b013e31828bf31e.

Folkerts, H., Hilgendorf, S., Vellenga, E., Bremer, E., and Wiersma, V.R. (2019). The multifaceted role of autophagy in cancer and the microenvironment. Medicinal research reviews *39*, 517-560. https://doi.org/10.1002/med.21531.

Fujita, K.-i., Kubota, Y., Ishida, H., and Sasaki, Y. (2015). Irinotecan, a key chemotherapeutic drug for metastatic colorectal cancer. World journal of gastroenterology *21*, 12234-12248. https://doi.org/10.3748/wjg.v21.i43.12234.

Galluzzi, L., Vitale, I., Aaronson, S.A., Abrams, J.M., Adam, D., Agostinis, P., Alnemri, E.S., Altucci, L., Amelio, I., and Andrews, D.W., et al. (2018). Molecular mechanisms of cell death: recommendations of the Nomenclature Committee on Cell Death 2018. Cell death and differentiation *25*, 486-541. https://doi.org/10.1038/s41418-017-0012-4.

Ganapathy-Kanniappan, S., Vali, M., Kunjithapatham, R., Buijs, M., Syed, L.H., Rao, P.P., Ota, S., Kwak, B.K., Loffroy, R., and Geschwind, J.F. (2010). 3-bromopyruvate: a new targeted antiglycolytic agent and a promise for cancer therapy. Current pharmaceutical biotechnology *11*, 510-517. https://doi.org/10.2174/138920110791591427.

Gao, L., Xu, Z., Huang, Z., Tang, Y., Yang, D., Huang, J., He, L., Liu, M., Chen, Z., and Teng, Y. (2020). CPI-613 rewires lipid metabolism to enhance pancreatic cancer apoptosis via the AMPK-ACC signaling. Journal of experimental & clinical cancer research : CR *39*, 73. https://doi.org/10.1186/s13046-020-01579-x.

Ghoshal, K., and Jacob, S.T. (1994). Specific inhibition of pre-ribosomal RNA processing in extracts from the lymphosarcoma cells treated with 5-fluorouracil. Cancer research *54*, 632-636.

Gibson, F.S., Gupta, D., Shorr, R., and Rodriguez, R. (2011). An Efficient, Economical Synthesis of the Novel Anti-tumor Agent CPI-613. Org. Process Res. Dev. *15*, 855-857. https://doi.org/10.1021/op200091t.

Gibson, G.E., Blass, J.P., Beal, M.F., and Bunik, V. (2005). The α-Ketoglutarate–Dehydrogenase Complex: A Mediator Between Mitochondria and Oxidative Stress in Neurodegeneration. MN *31*, 43-64. https://doi.org/10.1385/MN:31:1-3:043.

Göder, A., Nagel, G., Kraus, A., Dörsam, B., Seiwert, N., Kaina, B., and Fahrer, J. (2015). Lipoic acid inhibits the DNA repair protein O 6-methylguanine-DNA methyltransferase (MGMT) and triggers its depletion in colorectal cancer cells with concomitant autophagy induction. Carcinogenesis *36*, 817-831. https://doi.org/10.1093/carcin/bgv070.

Golshani, G., and Zhang, Y. (2020). Advances in immunotherapy for colorectal cancer: a review. Therapeutic advances in gastroenterology *13*, 1756284820917527. https://doi.org/10.1177/1756284820917527.

Golub, D., Iyengar, N., Dogra, S., Wong, T., Bready, D., Tang, K., Modrek, A.S., and Placantonakis, D.G. (2019). Mutant Isocitrate Dehydrogenase Inhibitors as Targeted Cancer Therapeutics. Frontiers in oncology *9*, 417. https://doi.org/10.3389/fonc.2019.00417.

Gori, S., Inno, A., Belluomini, L., Bocus, P., Bisoffi, Z., Russo, A., and Arcaro, G. (2019). Gut microbiota and cancer: How gut microbiota modulates activity, efficacy and toxicity of antitumoral therapy. Critical reviews in oncology/hematology *143*, 139-147. https://doi.org/10.1016/j.critrevonc.2019.09.003.

Gross, A.S., and Graef, M. (2020). Mechanisms of Autophagy in Metabolic Stress Response. Journal of molecular biology *432*, 28-52. https://doi.org/10.1016/j.jmb.2019.09.005.

Grothey, A., van Cutsem, E., Sobrero, A., Siena, S., Falcone, A., Ychou, M., Humblet, Y., Bouché, O., Mineur, L., and Barone, C., et al. (2013). Regorafenib monotherapy for previously treated metastatic colorectal cancer (CORRECT): an international, multicentre, randomised, placebo-controlled, phase 3 trial. The Lancet *381*, 303-312. https://doi.org/10.1016/S0140-6736(12)61900-X.

Gruenberger, T., Bridgewater, J., Chau, I., García Alfonso, P., Rivoire, M., Mudan, S., Lasserre, S., Hermann, F., Waterkamp, D., and Adam, R. (2015). Bevacizumab plus mFOLFOX-6 or

FOLFOXIRI in patients with initially unresectable liver metastases from colorectal cancer: the OLIVIA multinational randomised phase II trial. Annals of oncology : official journal of the European Society for Medical Oncology *26*, 702-708. https://doi.org/10.1093/annonc/mdu580.

Gupta, R., Sinha, S., and Paul, R.N. (2018). The impact of microsatellite stability status in colorectal cancer. Current problems in cancer *42*, 548-559. https://doi.org/10.1016/j.currproblcancer.2018.06.010.

Haenen, G.R.M.M., and Bast, A. (1991). Scavenging of hypochlorous acid by lipoic acid. Biochemical Pharmacology *42*, 2244-2246. https://doi.org/10.1016/0006-2952(91)90363-A.

Hagland, H.R., Berg, M., Jolma, I.W., Carlsen, A., and Søreide, K. (2013). Molecular pathways and cellular metabolism in colorectal cancer. Digestive surgery *30*, 12-25. https://doi.org/10.1159/000347166.

Hall, D., Ybazeta, G., Destro-Bisol, G., Petzl-Erler, M.L., and Di Rienzo, A. (1999). Variability at the uridine diphosphate glucuronosyltransferase 1A1 promoter in human populations and primates. Pharmacogenetics *9*, 591-599.

Hamabe, A., Yamamoto, H., Konno, M., Uemura, M., Nishimura, J., Hata, T., Takemasa, I., Mizushima, T., Nishida, N., and Kawamoto, K., et al. (2014). Combined evaluation of hexokinase 2 and phosphorylated pyruvate dehydrogenase-E1α in invasive front lesions of colorectal tumors predicts cancer metabolism and patient prognosis. Cancer science *105*, 1100-1108. https://doi.org/10.1111/cas.12487.

Hammoud, M.A., McCutcheon, I.E., Elsouki, R., Schoppa, D., and Patt, Y.Z. (1996). Colorectal carcinoma and brain metastasis: distribution, treatment, and survival. Annals of surgical oncology *3*, 453-463. https://doi.org/10.1007/BF02305763.

Hamouda, N., Sano, T., Oikawa, Y., Ozaki, T., Shimakawa, M., Matsumoto, K., Amagase, K., Higuchi, K., and Kato, S. (2017). Apoptosis, Dysbiosis and Expression of Inflammatory Cytokines are Sequential Events in the Development of 5-Fluorouracil-Induced Intestinal Mucositis in Mice. Basic & clinical pharmacology & toxicology *121*, 159-168. https://doi.org/10.1111/bcpt.12793.

Han, D., Handelman, G., Marcocci, L., Sen, C.K., Roy, S., Kobuchi, H., Tritschler, H.J., Flohé, L., and Packer, L. (1997). Lipoic acid increases de novo synthesis of cellular glutathione by improving cystine utilization. BioFactors (Oxford, England) *6*, 321-338. https://doi.org/10.1002/biof.5520060303.

Hanahan, D., and Weinberg, R.A. (2000). The Hallmarks of Cancer. Cell *100*, 57-70. https://doi.org/10.1016/S0092-8674(00)81683-9.

Hanahan, D., and Weinberg, R.A. (2011). Hallmarks of cancer: the next generation. Cell *144*, 646-674. https://doi.org/10.1016/j.cell.2011.02.013.

Handelman, G.J., Han, D., Tritschler, H., and Packer, L. (1994). α-Lipoic acid reduction by mammalian cells to the dithiol form, and release into the culture medium. Biochemical Pharmacology *47*, 1725-1730. https://doi.org/10.1016/0006-2952(94)90298-4.

Hao, Y., Samuels, Y., Li, Q., Krokowski, D., Guan, B.-J., Wang, C., Jin, Z., Dong, B., Cao, B., and Feng, X., et al. (2016). Oncogenic PIK3CA mutations reprogram glutamine metabolism in colorectal cancer. Nature communications *7*, 11971. https://doi.org/10.1038/ncomms11971.

Harris, S.M., Mistry, P., Freathy, C., Brown, J.L., and Charlton, P.A. (2005). Antitumour activity of XR5944 in vitro and in vivo in combination with 5-fluorouracil and irinotecan in colon cancer cell lines. British journal of cancer *92*, 722-728. https://doi.org/10.1038/sj.bjc.6602403.

Haug, K., Kravik, K.L., and Angelis, P.M. de (2008). Cellular response to irinotecan in colon cancer cell lines showing differential response to 5-fluorouracil. Anticancer research *28*, 583-592.

Hazan, R.B., Qiao, R., Keren, R., Badano, I., and Suyama, K. (2004). Cadherin switch in tumor progression. Annals of the New York Academy of Sciences *1014*, 155-163. https://doi.org/10.1196/annals.1294.016.

Hecht, J.R., Mitchell, E., Chidiac, T., Scroggin, C., Hagenstad, C., Spigel, D., Marshall, J., Cohn, A., McCollum, D., and Stella, P., et al. (2009). A randomized phase IIIB trial of chemotherapy, bevacizumab, and panitumumab compared with chemotherapy and bevacizumab alone for metastatic colorectal cancer. Journal of clinical oncology : official journal of the American Society of Clinical Oncology *27*, 672-680. https://doi.org/10.1200/JCO.2008.19.8135.

Heinemann, V., Weikersthal, L.F. von, Decker, T., Kiani, A., Vehling-Kaiser, U., Al-Batran, S.-E., Heintges, T., Lerchenmüller, C., Kahl, C., and Seipelt, G., et al. (2014). FOLFIRI plus cetuximab versus FOLFIRI plus bevacizumab as first-line treatment for patients with metastatic colorectal cancer (FIRE-3): a randomised, open-label, phase 3 trial. The Lancet. Oncology *15*, 1065-1075. https://doi.org/10.1016/S1470-2045(14)70330-4.

Hiratsuka, T., Inomata, M., Kono, Y., Yokoyama, S., Shiraishi, N., and Kitano, S. (2013). DHL-TauZnNa, a newly synthesized α-lipoic acid derivative, induces autophagy in human colorectal cancer cells. Oncology reports *29*, 2140-2146. https://doi.org/10.3892/or.2013.2394.

Ho, N., and Coomber, B.L. (2015). Pyruvate dehydrogenase kinase expression and metabolic changes following dichloroacetate exposure in anoxic human colorectal cancer cells. Experimental cell research *331*, 73-81. https://doi.org/10.1016/j.yexcr.2014.12.006.

Holze, C., Michaudel, C., Mackowiak, C., Haas, D.A., Benda, C., Hubel, P., Pennemann, F.L., Schnepf, D., Wettmarshausen, J., and Braun, M., et al. (2018). Oxeiptosis, a ROS-induced

caspase-independent apoptosis-like cell-death pathway. Nature immunology *19*, 130-140. https://doi.org/10.1038/s41590-017-0013-y.

Hoque, M.O., Kim, M.S., Ostrow, K.L., Liu, J., Wisman, G.B.A., Park, H.L., Poeta, M.L., Jeronimo, C., Henrique, R., and Lendvai, A., et al. (2008). Genome-wide promoter analysis uncovers portions of the cancer methylome. Cancer research *68*, 2661-2670. https://doi.org/10.1158/0008-5472.CAN-07-5913.

Hoskins, J.M., Goldberg, R.M., Qu, P., Ibrahim, J.G., and McLeod, H.L. (2007). UGT1A1*28 genotype and irinotecan-induced neutropenia: dose matters. Journal of the National Cancer Institute *99*, 1290-1295. https://doi.org/10.1093/jnci/djm115.

Hsu, P.P., and Sabatini, D.M. (2008). Cancer cell metabolism: Warburg and beyond. Cell *134*, 703-707. https://doi.org/10.1016/j.cell.2008.08.021.

Hutton, J.E., Wang, X., Zimmerman, L.J., Slebos, R.J.C., Trenary, I.A., Young, J.D., Li, M., and Liebler, D.C. (2016). Oncogenic KRAS and BRAF Drive Metabolic Reprogramming in Colorectal Cancer. Molecular & cellular proteomics : MCP *15*, 2924-2938. https://doi.org/10.1074/mcp.M116.058925.

Iyer, L., King, C.D., Whitington, P.F., Green, M.D., Roy, S.K., Tephly, T.R., Coffman, B.L., and Ratain, M.J. (1998). Genetic predisposition to the metabolism of irinotecan (CPT-11). Role of uridine diphosphate glucuronosyltransferase isoform 1A1 in the glucuronidation of its active metabolite (SN-38) in human liver microsomes. The Journal of clinical investigation *101*, 847-854. https://doi.org/10.1172/JCI915.

Iyer, L., and Ratain, M.J. (1998). Clinical pharmacology of camptothecins. Cancer chemotherapy and pharmacology *42 Suppl*, S31-43. https://doi.org/10.1007/s002800051077.

Jasperson, K.W., Tuohy, T.M., Neklason, D.W., and Burt, R.W. (2010). Hereditary and familial colon cancer. Gastroenterology *138*, 2044-2058. https://doi.org/10.1053/j.gastro.2010.01.054.

Jass, J.R. (2007). Classification of colorectal cancer based on correlation of clinical, morphological and molecular features. Histopathology *50*, 113-130. https://doi.org/10.1111/j.1365-2559.2006.02549.x.

Jeon, M.J., Kim, W.G., Lim, S., Choi, H.-J., Sim, S., Kim, T.Y., Shong, Y.K., and Kim, W.B. (2016). Alpha lipoic acid inhibits proliferation and epithelial mesenchymal transition of thyroid cancer cells. Molecular and cellular endocrinology *419*, 113-123. https://doi.org/10.1016/j.mce.2015.10.005.

Jo, Y.S., Oh, H.R., Kim, M.S., Yoo, N.J., and Lee, S.H. (2016). Frameshift mutations of OGDH, PPAT and PCCA genes in gastric and colorectal cancers. Neoplasma *63*, 681-686. https://doi.org/10.4149/neo_2016_504.

Joachim, C., Macni, J., Drame, M., Pomier, A., Escarmant, P., Veronique-Baudin, J., and Vinh-Hung, V. (2019). Overall survival of colorectal cancer by stage at diagnosis: Data from the Martinique Cancer Registry. Medicine *98*, e16941. https://doi.org/10.1097/MD.0000000000016941.

Johnson, C.M., Wei, C., Ensor, J.E., Smolenski, D.J., Amos, C.I., Levin, B., and Berry, D.A. (2013). Meta-analyses of colorectal cancer risk factors. Cancer causes & control : CCC *24*, 1207-1222. https://doi.org/10.1007/s10552-013-0201-5.

Johnson, R.L., and Fleet, J.C. (2013a). Animal models of colorectal cancer. Cancer metastasis reviews *32*, 39-61. https://doi.org/10.1007/s10555-012-9404-6.

Johnson, R.L., and Fleet, J.C. (2013b). Animal models of colorectal cancer. Cancer metastasis reviews *32*, 39-61. https://doi.org/10.1007/s10555-012-9404-6.

Jones, R.G., and Thompson, C.B. (2009). Tumor suppressors and cell metabolism: a recipe for cancer growth. Genes & development *23*, 537-548. https://doi.org/10.1101/gad.1756509.

Jones, W., Li, X., Qu, Z.-c., Perriott, L., Whitesell, R.R., and May, J.M. (2002). Uptake, recycling, and antioxidant actions of α-lipoic acid in endothelial cells. Free Radical Biology and Medicine *33*, 83-93. https://doi.org/10.1016/S0891-5849(02)00862-6.

Jordan, S.W., and Cronan, J.E. ((1997)). [19] Biosynthesis of lipoic acid and posttranslational modification with lipoic acid in Escherichia coli. In Vitamins and coenzymes (New York: Acad. Press), pp. 176–183.

Ju, J., Schmitz, J.C., Song, B., Kudo, K., and Chu, E. (2007). Regulation of p53 expression in response to 5-fluorouracil in human cancer RKO cells. Clinical cancer research : an official journal of the American Association for Cancer Research *13*, 4245-4251. https://doi.org/10.1158/1078-0432.CCR-06-2890.

Juang, H.-H. (2004). Modulation of mitochondrial aconitase on the bioenergy of human prostate carcinoma cells. Molecular genetics and metabolism *81*, 244-252. https://doi.org/10.1016/j.ymgme.2003.12.009.

Julien, O., and Wells, J.A. (2017). Caspases and their substrates. Cell death and differentiation *24*, 1380-1389. https://doi.org/10.1038/cdd.2017.44.

Kafara, P., Icard, P., Guillamin, M., Schwartz, L., and Lincet, H. (2015). Lipoic acid decreases Mcl-1, Bcl-xL and up regulates Bim on ovarian carcinoma cells leading to cell death. Journal of ovarian research *8*, 36. https://doi.org/10.1186/s13048-015-0165-z.

Kagan, V.E., Shvedova, A., Serbinova, E., Khan, S., Swanson, C., Powell, R., and Packer, L. (1992). Dihydrolipoic acid—a universal antioxidant both in the membrane and in the aqueous

phase. Biochemical Pharmacology *44*, 1637-1649. https://doi.org/10.1016/0006-2952(92)90482-X.

Kaku, Y., Tsuchiya, A., Kanno, T., and Nishizaki, T. (2015). Irinotecan induces cell cycle arrest, but not apoptosis or necrosis, in Caco-2 and CW2 colorectal cancer cell lines. Pharmacology *95*, 154-159. https://doi.org/10.1159/000381029.

Kalluri, R., and Weinberg, R.A. (2009). The basics of epithelial-mesenchymal transition. The Journal of clinical investigation *119*, 1420-1428. https://doi.org/10.1172/JCI39104.

Kamarudin, M.N.A., Sarker, M.M.R., Zhou, J.-R., and Parhar, I. (2019). Metformin in colorectal cancer: molecular mechanism, preclinical and clinical aspects. Journal of experimental & clinical cancer research : CR *38*, 491. https://doi.org/10.1186/s13046-019-1495-2.

Kanamaru, R., Kakuta, H., Sato, T., Ishioka, C., and Wakui, A. (1986). The inhibitory effects of 5-fluorouracil on the metabolism of preribosomal and ribosomal RNA in L-1210 cells in vitro. Cancer chemotherapy and pharmacology *17*, 43-46. https://doi.org/10.1007/BF00299864.

Kankotia, S., and Stacpoole, P.W. (2014). Dichloroacetate and cancer: new home for an orphan drug? Biochimica et biophysica acta *1846*, 617-629. https://doi.org/10.1016/j.bbcan.2014.08.005.

Karimian, A., Ahmadi, Y., and Yousefi, B. (2016). Multiple functions of p21 in cell cycle, apoptosis and transcriptional regulation after DNA damage. DNA repair *42*, 63-71. https://doi.org/10.1016/j.dnarep.2016.04.008.

Kawada, K., Toda, K., and Sakai, Y. (2017). Targeting metabolic reprogramming in KRAS-driven cancers. International journal of clinical oncology *22*, 651-659. https://doi.org/10.1007/s10147-017-1156-4.

Kennedy, K.M., and Dewhirst, M.W. (2010). Tumor metabolism of lactate: the influence and therapeutic potential for MCT and CD147 regulation. Future oncology (London, England) *6*, 127-148. https://doi.org/10.2217/fon.09.145.

Keum, N., and Giovannucci, E. (2019). Global burden of colorectal cancer: emerging trends, risk factors and prevention strategies. Nature reviews. Gastroenterology & hepatology *16*, 713-732. https://doi.org/10.1038/s41575-019-0189-8.

Khalaj-Kondori, M., Hosseinnejad, M., Hosseinzadeh, A., Behroz Sharif, S., and Hashemzadeh, S. (2020). Aberrant hypermethylation of OGDHL gene promoter in sporadic colorectal cancer. Current problems in cancer *44*, 100471. https://doi.org/10.1016/j.currproblcancer.2019.03.001.

Khan, A., Andrews, D., and Blackburn, A.C. (2016). Long-term stabilization of stage 4 colon cancer using sodium dichloroacetate therapy. World journal of clinical cases *4*, 336-343. https://doi.org/10.12998/wjcc.v4.i10.336.

Khanna, C., and Hunter, K. (2005). Modeling metastasis in vivo. Carcinogenesis *26*, 513-523. https://doi.org/10.1093/carcin/bgh261.

Kim, D.-H., Kundu, J.K., and Surh, Y.-J. (2011). Redox modulation of p53: mechanisms and functional significance. Molecular carcinogenesis *50*, 222-234. https://doi.org/10.1002/mc.20709.

Kimmelman, A.C. (2011). The dynamic nature of autophagy in cancer. Genes & development *25*, 1999-2010. https://doi.org/10.1101/gad.17558811.

Kinner, A., Wu, W., Staudt, C., and Iliakis, G. (2008). Gamma-H2AX in recognition and signaling of DNA double-strand breaks in the context of chromatin. Nucleic acids research *36*, 5678-5694. https://doi.org/10.1093/nar/gkn550.

Ko, F.C., Liu, J.M., Chen, W.S., Chiang, J.K., Lin, T.C., and Lin, J.K. (1999). Risk and patterns of brain metastases in colorectal cancer: 27-year experience. Diseases of the colon and rectum *42*, 1467-1471. https://doi.org/10.1007/BF02235049.

Kobaek-Larsen, M., Thorup, I., Diederichsen, A., Fenger, C., and Hoitinga, M.R. (2000). Review of colorectal cancer and its metastases in rodent models: comparative aspects with those in humans. Comparative medicine *50*, 16-26.

Koike, M., and Koike, K. (1976). Structure, assembly and function of mammalian alpha-keto acid dehydrogenase complexes. Advances in biophysics, 187-227.

Kondo, K., Sano, R., Goto, K., Hiramoto, K., and Ooi, K. (2018). Administration of High-Dose Vitamin C and Irinotecan Ameliorates Colorectal Cancer Induced by Azoxymethane and Dextran Sodium Sulfate in Mice. Biological & pharmaceutical bulletin *41*, 1797-1803. https://doi.org/10.1248/bpb.b18-00453.

Kopetz, S., Desai, J., Chan, E., Hecht, J.R., O'Dwyer, P.J., Maru, D., van Morris, Janku, F., Dasari, A., and Chung, W., et al. (2015). Phase II Pilot Study of Vemurafenib in Patients With Metastatic BRAF-Mutated Colorectal Cancer. Journal of clinical oncology : official journal of the American Society of Clinical Oncology *33*, 4032-4038. https://doi.org/10.1200/JCO.2015.63.2497.

Korotchkina, L.G., and Patel, M.S. (2001). Site specificity of four pyruvate dehydrogenase kinase isoenzymes toward the three phosphorylation sites of human pyruvate dehydrogenase. The Journal of biological chemistry *276*, 37223-37229. https://doi.org/10.1074/jbc.M103069200.

Koukourakis, M.I., Giatromanolaki, A., Harris, A.L., and Sivridis, E. (2006). Comparison of metabolic pathways between cancer cells and stromal cells in colorectal carcinomas: a metabolic survival role for tumor-associated stroma. Cancer research *66*, 632-637. https://doi.org/10.1158/0008-5472.CAN-05-3260.

Kroemer, G., and Martin, S.J. (2005). Caspase-independent cell death. Nature medicine *11*, 725-730. https://doi.org/10.1038/nm1263.

Kroemer, G., and Pouyssegur, J. (2008). Tumor cell metabolism: cancer's Achilles' heel. Cancer cell *13*, 472-482. https://doi.org/10.1016/j.ccr.2008.05.005.

Krumm, A., Barckhausen, C., Kücük, P., Tomaszowski, K.-H., Loquai, C., Fahrer, J., Krämer, O.H., Kaina, B., and Roos, W.P. (2016). Enhanced Histone Deacetylase Activity in Malignant Melanoma Provokes RAD51 and FANCD2-Triggered Drug Resistance. Cancer research *76*, 3067-3077. https://doi.org/10.1158/0008-5472.CAN-15-2680.

Kubicka, S., Greil, R., André, T., Bennouna, J., Sastre, J., van Cutsem, E., Moos, R. von, Osterlund, P., Reyes-Rivera, I., and Müller, T., et al. (2013). Bevacizumab plus chemotherapy continued beyond first progression in patients with metastatic colorectal cancer previously treated with bevacizumab plus chemotherapy: ML18147 study KRAS subgroup findings. Annals of oncology : official journal of the European Society for Medical Oncology *24*, 2342-2349. https://doi.org/10.1093/annonc/mdt231.

Kumar, K., Wigfield, S., Gee, H.E., Devlin, C.M., Singleton, D., Li, J.-L., Buffa, F., Huffman, M., Sinn, A.L., and Silver, J., et al. (2013). Dichloroacetate reverses the hypoxic adaptation to bevacizumab and enhances its antitumor effects in mouse xenografts. Journal of molecular medicine (Berlin, Germany) *91*, 749-758. https://doi.org/10.1007/s00109-013-0996-2.

Kunz, C., Focke, F., Saito, Y., Schuermann, D., Lettieri, T., Selfridge, J., and Schär, P. (2009). Base excision by thymine DNA glycosylase mediates DNA-directed cytotoxicity of 5-fluorouracil. PLoS biology *7*, e91. https://doi.org/10.1371/journal.pbio.1000091.

Lakin, N.D., and Jackson, S.P. (1999). Regulation of p53 in response to DNA damage. Oncogene *18*, 7644-7655. https://doi.org/10.1038/sj.onc.1203015.

Lamar, Z.S., Isom, S., Vaidya, R., Beaven, A.W., and McIver, Z.A. (2016). Phase I Dose-Escalation Study of Cpi-613, in Combination with Bendamustine, in Relapsed or Refractory T-Cell Non-Hodgkin Lymphoma. Blood *128*, 4163. https://doi.org/10.1182/blood.V128.22.4163.4163.

Lamouille, S., Xu, J., and Derynck, R. (2014). Molecular mechanisms of epithelial-mesenchymal transition. Nature reviews. Molecular cell biology *15*, 178-196. https://doi.org/10.1038/nrm3758.

Leclerc, D., Pham, D.N.T., Lévesque, N., Truongcao, M., Foulkes, W.D., Sapienza, C., and Rozen, R. (2017). Oncogenic role of PDK4 in human colon cancer cells. British journal of cancer *116*, 930-936. https://doi.org/10.1038/bjc.2017.38.

Lee, H.S., Na, M.H., and Kim, W.K. (2010). alpha-Lipoic acid reduces matrix metalloproteinase activity in MDA-MB-231 human breast cancer cells. Nutrition research (New York, N.Y.) *30*, 403-409. https://doi.org/10.1016/j.nutres.2010.06.009.

Lee, K.C., Maturo, C., Perera, C.N., Luddy, J., Rodriguez, R., and Shorr, R. (2014). Translational assessment of mitochondrial dysfunction of pancreatic cancer from in vitro gene microarray and animal efficacy studies, to early clinical studies, via the novel tumor-specific anti-mitochondrial agent, CPI-613. Annals of Translational Medicine *2*. https://doi.org/10.3978/j.issn.2305-5839.2014.05.08.

Lee, K.C., Shorr, R., Rodriguez, R., Maturo, C., Boteju, L.W., and Sheldon, A. (2011). Formation and anti-tumor activity of uncommon in vitro and in vivo metabolites of CPI-613, a novel anti-tumor compound that selectively alters tumor energy metabolism. Drug metabolism letters *5*, 163-182. https://doi.org/10.2174/187231211796904991.

Leitlinienprogramm Onkologie (2019). S3-Leitlinie Kolorektales Karzinom.

Li, J., Cao, F., Yin, H.-L., Huang, Z.-J., Lin, Z.-T., Mao, N., Sun, B., and Wang, G. (2020). Ferroptosis: past, present and future. Cell death & disease *11*, 88. https://doi.org/10.1038/s41419-020-2298-2.

Li, J., Hou, N., Faried, A., Tsutsumi, S., and Kuwano, H. (2010a). Inhibition of autophagy augments 5-fluorouracil chemotherapy in human colon cancer in vitro and in vivo model. European journal of cancer (Oxford, England : 1990) *46*, 1900-1909. https://doi.org/10.1016/j.ejca.2010.02.021.

Li, J., Hou, N., Faried, A., Tsutsumi, S., Takeuchi, T., and Kuwano, H. (2009). Inhibition of autophagy by 3-MA enhances the effect of 5-FU-induced apoptosis in colon cancer cells. Annals of surgical oncology *16*, 761-771. https://doi.org/10.1245/s10434-008-0260-0.

Li, J., Qin, S., Xu, R., Yau, T.C.C., Ma, B., Pan, H., Xu, J., Bai, Y., Chi, Y., and Wang, L., et al. (2015a). Regorafenib plus best supportive care versus placebo plus best supportive care in Asian patients with previously treated metastatic colorectal cancer (CONCUR): a randomised, double-blind, placebo-controlled, phase 3 trial. The Lancet Oncology *16*, 619-629. https://doi.org/10.1016/S1470-2045(15)70156-7.

Li, R., Liang, J., Ni, S., Zhou, T., Qing, X., Li, H., He, W., Chen, J., Li, F., and Zhuang, Q., et al. (2010b). A mesenchymal-to-epithelial transition initiates and is required for the nuclear reprogramming of mouse fibroblasts. Cell stem cell *7*, 51-63. https://doi.org/10.1016/j.stem.2010.04.014.

Li, W., Saud, S.M., Young, M.R., Chen, G., and Hua, B. (2015b). Targeting AMPK for cancer prevention and treatment. Oncotarget *6*, 7365-7378. https://doi.org/10.18632/oncotarget.3629.

Li, Y., Zhao, Z., Liu, H., Fetse, J.P., Jain, A., Lin, C.-Y., and Cheng, K. (2019). Development of a Tumor-Responsive Nanopolyplex Targeting Pancreatic Cancer Cells and Stroma. ACS applied materials & interfaces *11*, 45390-45403. https://doi.org/10.1021/acsami.9b15116.

Liang, Y., Hou, L., Li, L., Li, L., Zhu, L., Wang, Y., Huang, X., Hou, Y., Zhu, D., and Zou, H., et al. (2020). Dichloroacetate restores colorectal cancer chemosensitivity through the p53/miR-149-3p/PDK2-mediated glucose metabolic pathway. Oncogene *39*, 469-485. https://doi.org/10.1038/s41388-019-1035-8.

Lin, J., Peng, J., Zhao, Y., Luo, B., Zhao, Y., Deng, Y., Sui, Q., Gao, Y., Zeng, Z., and Lu, Z., et al. (2018). Early recurrence in patients undergoing curative resection of colorectal liver oligometastases: identification of its clinical characteristics, risk factors, and prognosis. Journal of cancer research and clinical oncology *144*, 359-369. https://doi.org/10.1007/s00432-017-2538-8.

Liu, H., Wang, J., He, T., Becker, S., Zhang, G., Li, D., and Ma, X. (2018). Butyrate: A Double-Edged Sword for Health? Advances in nutrition (Bethesda, Md.) *9*, 21-29. https://doi.org/10.1093/advances/nmx009.

Liu, L.F., Desai, S.D., Li, T.K., Mao, Y., Sun, M., and Sim, S.P. (2000). Mechanism of action of camptothecin. Annals of the New York Academy of Sciences *922*, 1-10. https://doi.org/10.1111/j.1749-6632.2000.tb07020.x.

Liu, X., Cheng, D., Kuang, Q., Liu, G., and Xu, W. (2014). Association of UGT1A1*28 polymorphisms with irinotecan-induced toxicities in colorectal cancer: a meta-analysis in Caucasians. The pharmacogenomics journal *14*, 120-129. https://doi.org/10.1038/tpj.2013.10.

Longley, D.B., Harkin, D.P., and Johnston, P.G. (2003). 5-fluorouracil: mechanisms of action and clinical strategies. Nature reviews. Cancer *3*, 330-338. https://doi.org/10.1038/nrc1074.

Loupakis, F., Cremolini, C., Masi, G., Lonardi, S., Zagonel, V., Salvatore, L., Cortesi, E., Tomasello, G., Ronzoni, M., and Spadi, R., et al. (2014a). Initial therapy with FOLFOXIRI and bevacizumab for metastatic colorectal cancer. The New England journal of medicine *371*, 1609-1618. https://doi.org/10.1056/NEJMoa1403108.

Loupakis, F., Cremolini, C., Salvatore, L., Masi, G., Sensi, E., Schirripa, M., Michelucci, A., Pfanner, E., Brunetti, I., and Lupi, C., et al. (2014b). FOLFOXIRI plus bevacizumab as first-line treatment in BRAF mutant metastatic colorectal cancer. European journal of cancer (Oxford, England : 1990) *50*, 57-63. https://doi.org/10.1016/j.ejca.2013.08.024.

Lozy, F., and Karantza, V. (2012). Autophagy and cancer cell metabolism. Seminars in cell & developmental biology *23*, 395-401. https://doi.org/10.1016/j.semcdb.2012.01.005.

Lu, C., Zhu, F., Cho, Y.-Y., Tang, F., Zykova, T., Ma, W.-y., Bode, A.M., and Dong, Z. (2006). Cell apoptosis: requirement of H2AX in DNA ladder formation, but not for the activation of caspase-3. Molecular cell *23*, 121-132. https://doi.org/10.1016/j.molcel.2006.05.023.

Lu, C.-W., Lin, S.-C., Chien, C.-W., Lin, S.-C., Lee, C.-T., Lin, B.-W., Lee, J.-C., and Tsai, S.-J. (2011). Overexpression of pyruvate dehydrogenase kinase 3 increases drug resistance and

early recurrence in colon cancer. The American journal of pathology *179*, 1405-1414. https://doi.org/10.1016/j.ajpath.2011.05.050.

Luengo, A., Gui, D.Y., and Vander Heiden, M.G. (2017). Targeting Metabolism for Cancer Therapy. Cell chemical biology *24*, 1161-1180. https://doi.org/10.1016/j.chembiol.2017.08.028.

Lycan, T.W., Pardee, T.S., Petty, W.J., Bonomi, M., Alistar, A., Lamar, Z.S., Isom, S., Chan, M.D., Miller, A.A., and Ruiz, J. (2016). A Phase II Clinical Trial of CPI-613 in Patients with Relapsed or Refractory Small Cell Lung Carcinoma. PLoS ONE *11*, e0164244. https://doi.org/10.1371/journal.pone.0164244.

Macleod, K.F. (2020). Mitophagy and Mitochondrial Dysfunction in Cancer. Annu. Rev. Cancer Biol. *4*, 41-60. https://doi.org/10.1146/annurev-cancerbio-030419-033405.

Magrini, R., Bhonde, M.R., Hanski, M.-L., Notter, M., Scherübl, H., Boland, C.R., Zeitz, M., and Hanski, C. (2002). Cellular effects of CPT-11 on colon carcinoma cells: dependence on p53 and hMLH1 status. International journal of cancer *101*, 23-31. https://doi.org/10.1002/ijc.10565.

Maletzki, C., Huehns, M., Knapp, P., Waukosin, N., Klar, E., Prall, F., and Linnebacher, M. (2015). Functional Characterization and Drug Response of Freshly Established Patient-Derived Tumor Models with CpG Island Methylator Phenotype. PLoS ONE *10*, e0143194. https://doi.org/10.1371/journal.pone.0143194.

Man, F.M. de, Goey, A.K.L., van Schaik, R.H.N., Mathijssen, R.H.J., and Bins, S. (2018). Individualization of Irinotecan Treatment: A Review of Pharmacokinetics, Pharmacodynamics, and Pharmacogenetics. Clinical pharmacokinetics *57*, 1229-1254. https://doi.org/10.1007/s40262-018-0644-7.

Manna, S.K., Tanaka, N., Krausz, K.W., Haznadar, M., Xue, X., Matsubara, T., Bowman, E.D., Fearon, E.R., Harris, C.C., and Shah, Y.M., et al. (2014). Biomarkers of coordinate metabolic reprogramming in colorectal tumors in mice and humans. Gastroenterology *146*, 1313-1324. https://doi.org/10.1053/j.gastro.2014.01.017.

Marcucci, F., Stassi, G., and Maria, R. de (2016). Epithelial-mesenchymal transition: a new target in anticancer drug discovery. Nature reviews. Drug discovery *15*, 311-325. https://doi.org/10.1038/nrd.2015.13.

Markowitz, S.D., and Bertagnolli, M.M. (2009). Molecular origins of cancer: Molecular basis of colorectal cancer. The New England journal of medicine *361*, 2449-2460. https://doi.org/10.1056/NEJMra0804588.

Marley, A.R., and Nan, H. (2016). Epidemiology of colorectal cancer. International Journal of Molecular Epidemiology and Genetics *7*, 105-114.

Martinez-Outschoorn, U.E., Lisanti, M.P., and Sotgia, F. (2014). Catabolic cancer-associated fibroblasts transfer energy and biomass to anabolic cancer cells, fueling tumor growth. Seminars in cancer biology *25*, 47-60. https://doi.org/10.1016/j.semcancer.2014.01.005.

Martínez-Reyes, I., and Chandel, N.S. (2020). Mitochondrial TCA cycle metabolites control physiology and disease. Nature communications *11*, 102. https://doi.org/10.1038/s41467-019-13668-3.

Mason, E.F., and Rathmell, J.C. (2011). Cell metabolism: an essential link between cell growth and apoptosis. Biochimica et biophysica acta *1813*, 645-654. https://doi.org/10.1016/j.bbamcr.2010.08.011.

Mathijssen, R.H., van Alphen, R.J., Verweij, J., Loos, W.J., Nooter, K., Stoter, G., and Sparreboom, A. (2001). Clinical pharmacokinetics and metabolism of irinotecan (CPT-11). Clinical cancer research : an official journal of the American Association for Cancer Research *7*, 2182-2194.

Maturo (2010). Uncommon Toxicologic Profile at Toxic Doses of CPI-613 (an Agent Selectively Alters Tumor Energy Metabolism) in Rats and Minipigs Reflects Novel Mechanism. American Journal of Pharmacology and Toxicology *5*, 183-208. https://doi.org/10.3844/ajptsp.2010.183.208.

Mayer, R.J., van Cutsem, E., Falcone, A., Yoshino, T., Garcia-Carbonero, R., Mizunuma, N., Yamazaki, K., Shimada, Y., Tabernero, J., and Komatsu, Y., et al. (2015). Randomized trial of TAS-102 for refractory metastatic colorectal cancer. The New England journal of medicine *372*, 1909-1919. https://doi.org/10.1056/NEJMoa1414325.

Mayers, R.M., Butlin, R.J., Kilgour, E., Leighton, B., Martin, D., Myatt, J., Orme, J.P., and Holloway, B.R. (2003). AZD7545, a novel inhibitor of pyruvate dehydrogenase kinase 2 (PDHK2), activates pyruvate dehydrogenase in vivo and improves blood glucose control in obese (fa/fa) Zucker rats. Biochemical Society transactions *31*, 1165-1167. https://doi.org/10.1042/bst0311165.

Mazzaccara, C., Labruna, G., Cito, G., Scarfò, M., Felice, M. de, Pastore, L., and Sacchetti, L. (2008). Age-Related Reference Intervals of the Main Biochemical and Hematological Parameters in C57BL/6J, 129SV/EV and C3H/HeJ Mouse Strains. PLoS ONE *3*. https://doi.org/10.1371/journal.pone.0003772.

McEwan, J.F., Windsor, M.L., and Cullis-Hill, S.D. (2009). Antibodies to prion protein inhibit human colon cancer cell growth. Tumour biology : the journal of the International Society for Oncodevelopmental Biology and Medicine *30*, 141-147. https://doi.org/10.1159/000225243.

McIntyre, R.E., Buczacki, S.J.A., Arends, M.J., and Adams, D.J. (2015). Mouse models of colorectal cancer as preclinical models. BioEssays : news and reviews in molecular, cellular and developmental biology *37*, 909-920. https://doi.org/10.1002/bies.201500032.

McLain, A.L., Szweda, P.A., and Szweda, L.I. (2011). α-Ketoglutarate dehydrogenase: a mitochondrial redox sensor. Free radical research *45*, 29-36. https://doi.org/10.3109/10715762.2010.534163.

Melli, G., Taiana, M., Camozzi, F., Triolo, D., Podini, P., Quattrini, A., Taroni, F., and Lauria, G. (2008). Alpha-lipoic acid prevents mitochondrial damage and neurotoxicity in experimental chemotherapy neuropathy. Experimental neurology *214*, 276-284. https://doi.org/10.1016/j.expneurol.2008.08.013.

Meulendijks, D., Henricks, L.M., Sonke, G.S., Deenen, M.J., Froehlich, T.K., Amstutz, U., Largiadèr, C.R., Jennings, B.A., Marinaki, A.M., and Sanderson, J.D., et al. (2015). Clinical relevance of DPYD variants c.1679TG, c.1236GA/HapB3, and c.1601GA as predictors of severe fluoropyrimidine-associated toxicity: a systematic review and meta-analysis of individual patient data. The Lancet. Oncology *16*, 1639-1650. https://doi.org/10.1016/S1470-2045(15)00286-7.

Michikoshi, H., Nakamura, T., Sakai, K., Suzuki, Y., Adachi, E., Matsugo, S., and Matsumoto, K. (2013). α-Lipoic acid-induced inhibition of proliferation and met phosphorylation in human non-small cell lung cancer cells. Cancer Letters *335*, 472-478. https://doi.org/10.1016/j.canlet.2013.03.008.

Mimmler, M., Peter, S., Kraus, A., Stroh, S., Nikolova, T., Seiwert, N., Hasselwander, S., Neitzel, C., Haub, J., and Monien, B.H., et al. (2016). DNA Damage Response Curtails Detrimental Replication Stress and Chromosomal Instability Induced by the Dietary Carcinogen PhIP. Nucleic acids research *44*. https://doi.org/10.1093/nar/gkw791.

Mittal, V. (2018). Epithelial Mesenchymal Transition in Tumor Metastasis. Annual review of pathology *13*, 395-412. https://doi.org/10.1146/annurev-pathol-020117-043854.

Mohrin, M., and Chen, D. (2016). The mitochondrial metabolic checkpoint and aging of hematopoietic stem cells. Current opinion in hematology *23*, 318-324. https://doi.org/10.1097/MOH.0000000000000244.

Montagnani, F., Chiriatti, A., Turrisi, G., Francini, G., and Fiorentini, G. (2011). A systematic review of FOLFOXIRI chemotherapy for the first-line treatment of metastatic colorectal cancer: improved efficacy at the cost of increased toxicity. Colorectal disease : the official journal of the Association of Coloproctology of Great Britain and Ireland *13*, 846-852. https://doi.org/10.1111/j.1463-1318.2010.02206.x.

Moolenbeek, C., and Ruitenberg, E.J. (1981). The "Swiss roll": a simple technique for histological studies of the rodent intestine. Laboratory animals *15*, 57-59. https://doi.org/10.1258/002367781780958577.

Moore, J.D., Staniszewska, A., Shaw, T., D'Alessandro, J., Davis, B., Surgenor, A., Baker, L., Matassova, N., Murray, J., and Macias, A., et al. (2014). VER-246608, a novel pan-isoform ATP competitive inhibitor of pyruvate dehydrogenase kinase, disrupts Warburg metabolism and induces context-dependent cytostasis in cancer cells. Oncotarget *5*, 12862-12876. https://doi.org/10.18632/oncotarget.2656.

Mordhorst, B.R., Kerns, K.C., Schauflinger, M., Zigo, M., Murphy, S.L., Ross, R.M., Wells, K.D., Green, J.A., Sutovsky, P., and Prather, R.S. (2019). Pharmacologic treatment with CPI-613 and PS48 decreases mitochondrial membrane potential and increases quantity of autolysosomes in porcine fibroblasts. Scientific reports *9*, 9417. https://doi.org/10.1038/s41598-019-45850-4.

Morrell, J.A., Orme, J., Butlin, R.J., Roche, T.E., Mayers, R.M., and Kilgour, E. (2003). AZD7545 is a selective inhibitor of pyruvate dehydrogenase kinase 2. Biochemical Society transactions *31*, 1168-1170. https://doi.org/10.1042/bst0311168.

Mudd, S.R., Holich, K.D., Voorbach, M.J., Cole, T.B., Reuter, D.R., Tapang, P., Bukofzer, G., Chakravartty, A., Donawho, C.K., and Palma, J.P., et al. (2012). Pharmacodynamic evaluation of irinotecan therapy by FDG and FLT PET/CT imaging in a colorectal cancer xenograft model. Molecular imaging and biology *14*, 617-624. https://doi.org/10.1007/s11307-011-0529-8.

Mullen, A.R., Hu, Z., Shi, X., Jiang, L., Boroughs, L.K., Kovacs, Z., Boriack, R., Rakheja, D., Sullivan, L.B., and Linehan, W.M., et al. (2014). Oxidation of alpha-ketoglutarate is required for reductive carboxylation in cancer cells with mitochondrial defects. Cell reports *7*, 1679-1690. https://doi.org/10.1016/j.celrep.2014.04.037.

Müller, M.F., Ibrahim, A.E.K., and Arends, M.J. (2016). Molecular pathological classification of colorectal cancer. Virchows Archiv : an international journal of pathology *469*, 125-134. https://doi.org/10.1007/s00428-016-1956-3.

Murphy, N., Moreno, V., Hughes, D.J., Vodicka, L., Vodicka, P., Aglago, E.K., Gunter, M.J., and Jenab, M. (2019). Lifestyle and dietary environmental factors in colorectal cancer susceptibility. Molecular aspects of medicine *69*, 2-9. https://doi.org/10.1016/j.mam.2019.06.005.

Na, Y.-S., Jung, K.-A., Kim, S.-M., Hong, Y.S., Ryu, M.-H., Jang, S.J., Moon, D.H., Cho, D.-H., Kim, J.C., and Lee, J.S., et al. (2011). The histone deacetylase inhibitor PXD101 increases the efficacy of irinotecan in in vitro and in vivo colon cancer models. Cancer chemotherapy and pharmacology *68*, 389-398. https://doi.org/10.1007/s00280-010-1495-6.

Na, Y.-S., Kim, S.-M., Jung, K.-A., Yang, S.-J., Hong, Y.S., Ryu, M.-H., Ro, S., Cho, D.-H., Kim, J.C., and Jin, D.-H., et al. (2010). Effects of the HDAC inhibitor CG2 in combination with

irinotecan, 5-fluorouracil, or oxaliplatin on HCT116 colon cancer cells and xenografts. Oncology reports *24*, 1509-1514. https://doi.org/10.3892/or_00001012.

Neitzel, C., Demuth, P., Wittmann, S., and Fahrer, J. (2020). Targeting Altered Energy Metabolism in Colorectal Cancer: Oncogenic Reprogramming, the Central Role of the TCA Cycle and Therapeutic Opportunities. Cancers *12*, 1731. https://doi.org/10.3390/cancers12071731.

Neitzel, C., Seiwert, N., Göder, A., Diehl, E., Weber, C., Nagel, G., Stroh, S., Rasenberger, B., Christmann, M., and Fahrer, J. (2019). Lipoic Acid Synergizes with Antineoplastic Drugs in Colorectal Cancer by Targeting p53 for Proteasomal Degradation. Cells *8*. https://doi.org/10.3390/cells8080794.

Nguyen, H.T., and Duong, H.-Q. (2018). The molecular characteristics of colorectal cancer: Implications for diagnosis and therapy. Oncology letters *16*, 9-18. https://doi.org/10.3892/ol.2018.8679.

Ni, F., and Qu, C.-K. (2016). A metabolic stress-induced cell cycle checkpoint in stem cells. Cell Cycle *15*, 2539-2540. https://doi.org/10.1080/15384101.2016.1204851.

Nieto, M.A. (2011). The ins and outs of the epithelial to mesenchymal transition in health and disease. Annual review of cell and developmental biology *27*, 347-376. https://doi.org/10.1146/annurev-cellbio-092910-154036.

Nogueira, V., Park, Y., Chen, C.-C., Xu, P.-Z., Chen, M.-L., Tonic, I., Unterman, T., and Hay, N. (2008). Akt determines replicative senescence and oxidative or oncogenic premature senescence and sensitizes cells to oxidative apoptosis. Cancer cell *14*, 458-470. https://doi.org/10.1016/j.ccr.2008.11.003.

Noren Hooten, N., and Evans, M.K. (2017). Techniques to Induce and Quantify Cellular Senescence. Journal of visualized experiments : JoVE. https://doi.org/10.3791/55533.

O'Brien, M., Chalker, J., Slade, L., Gardiner, D., and Mailloux, R.J. (2017). Protein S-glutathionylation alters superoxide/hydrogen peroxide emission from pyruvate dehydrogenase complex. Free radical biology & medicine *106*, 302-314. https://doi.org/10.1016/j.freeradbiomed.2017.02.046.

Ohdo, S., Makinosumi, T., Ishizaki, T., Yukawa, E., Higuchi, S., Nakano, S., and Ogawa, N. (1997). Cell cycle-dependent chronotoxicity of irinotecan hydrochloride in mice. The Journal of pharmacology and experimental therapeutics *283*, 1383-1388.

Oppermann, H., Schnabel, L., Meixensberger, J., and Gaunitz, F. (2016). Pyruvate attenuates the anti-neoplastic effect of carnosine independently from oxidative phosphorylation. Oncotarget *7*, 85848-85860. https://doi.org/10.18632/oncotarget.13039.

Ostrow, K.L., Park, H.L., Hoque, M.O., Kim, M.S., Liu, J., Argani, P., Westra, W., van Criekinge, W., and Sidransky, D. (2009). Pharmacologic unmasking of epigenetically silenced genes in breast cancer. Clinical cancer research : an official journal of the American Association for Cancer Research *15*, 1184-1191. https://doi.org/10.1158/1078-0432.CCR-08-1304.

Ou, P., Tritschler, H.J., and Wolff, S.P. (1995). Thioctic (lipoic) acid: a therapeutic metal-chelating antioxidant? Biochemical Pharmacology *50*, 123-126. https://doi.org/10.1016/0006-2952(95)00116-H.

Ouyang, L., Shi, Z., Zhao, S., Wang, F.-T., Zhou, T.-T., Liu, B., and Bao, J.-K. (2012). Programmed cell death pathways in cancer: a review of apoptosis, autophagy and programmed necrosis. Cell proliferation *45*, 487-498. https://doi.org/10.1111/j.1365-2184.2012.00845.x.

Packer, L., Kraemer, K., and Rimbach, G. (2001). Molecular aspects of lipoic acid in the prevention of diabetes complications. Nutrition *17*, 888-895. https://doi.org/10.1016/S0899-9007(01)00658-X.

Paillas, S., Causse, A., Marzi, L., Medina, P. de, Poirot, M., Denis, V., Vezzio-Vie, N., Espert, L., Arzouk, H., and Coquelle, A., et al. (2012). MAPK14/p38α confers irinotecan resistance to TP53-defective cells by inducing survival autophagy. Autophagy *8*, 1098-1112. https://doi.org/10.4161/auto.20268.

Paoli, P., Giannoni, E., and Chiarugi, P. (2013). Anoikis molecular pathways and its role in cancer progression. Biochimica et biophysica acta *1833*, 3481-3498. https://doi.org/10.1016/j.bbamcr.2013.06.026.

Parang, B., Barrett, C.W., and Williams, C.S. (2016). AOM/DSS Model of Colitis-Associated Cancer. Methods in molecular biology (Clifton, N.J.) *1422*, 297-307. https://doi.org/10.1007/978-1-4939-3603-8_26.

Pardee, T.S., Anderson, R.G., Pladna, K.M., Isom, S., Ghiraldeli, L.P., Miller, L.D., Chou, J.W., Jin, G., Zhang, W., and Ellis, L.R., et al. (2018). A Phase I Study of CPI-613 in Combination with High-Dose Cytarabine and Mitoxantrone for Relapsed or Refractory Acute Myeloid Leukemia. Clinical cancer research : an official journal of the American Association for Cancer Research *24*, 2060-2073. https://doi.org/10.1158/1078-0432.CCR-17-2282.

Pardee, T.S., DeFord-Watts, L.M., Peronto, E., Levitan, D.A., Hurd, D.D., Kridel, S., Harrelson, R., Manuel, M., Lyerly, S., and Powell, B.L. (2012). Evaluation of the first-in-class antimitochondrial metabolism agent CPI-613 in hematologic malignancies. JCO *30*, 6524. https://doi.org/10.1200/jco.2012.30.15_suppl.6524.

Pardee, T.S., Lee, K., Luddy, J., Maturo, C., Rodriguez, R., Isom, S., Miller, L.D., Stadelman, K.M., Levitan, D., and Hurd, D., et al. (2014). A phase I study of the first-in-class antimitochondrial metabolism agent, CPI-613, in patients with advanced hematologic

malignancies. Clinical cancer research : an official journal of the American Association for Cancer Research *20*, 5255-5264. https://doi.org/10.1158/1078-0432.CCR-14-1019.

Pardee, T.S., Luther, S., Buyse, M., Powell, B.L., and Cortes, J. (2019). Devimistat in combination with high dose cytarabine and mitoxantrone compared with high dose cytarabine and mitoxantrone in older patients with relapsed/refractory acute myeloid leukemia: ARMADA 2000 Phase III study. Future oncology (London, England) *15*, 3197-3208. https://doi.org/10.2217/fon-2019-0201.

Pardee, T.S., Stadelman, K., Isom, S., Ellis, L.R., Berenzon, D., Hurd, D.D., Howard, D.S., Harrelson, R., Manuel, M., and Dralle, S., et al. (2015). Activity of the mitochondrial metabolism inhibitor cpi-613 in combination with high dose Ara-C (HDAC) and mitoxantrone in high risk relapsed or refractory acute myeloid leukemia (AML). JCO *33*, 7015. https://doi.org/10.1200/jco.2015.33.15_suppl.7015.

Park, S., Jeon, J.H., Min, B.K., Ha, C.M., Thoudam, T., Park, B.Y., and Lee, I.K. (2018). Role of the Pyruvate Dehydrogenase Complex in Metabolic Remodeling: Differential Pyruvate Dehydrogenase Complex Functions in Metabolism. Diabetes & metabolism journal *42*, 270-281. https://doi.org/10.4093/dmj.2018.0101.

Patanaphan, V., and Salazar, O.M. (1993). Colorectal cancer: metastatic patterns and prognosis. Southern medical journal *86*, 38-41.

Patel, M.S., and Korotchkina, L.G. (2003). The biochemistry of the pyruvate dehydrogenase complex. Biochem. Mol. Biol. Educ. *31*, 5-15. https://doi.org/10.1002/bmb.2003.494031010156.

Patel, M.S., Nemeria, N.S., Furey, W., and Jordan, F. (2014). The pyruvate dehydrogenase complexes: structure-based function and regulation. The Journal of biological chemistry *289*, 16615-16623. https://doi.org/10.1074/jbc.R114.563148.

Patton, J.R. (1993). Ribonucleoprotein particle assembly and modification of U2 small nuclear RNA containing 5-fluorouridine. Biochemistry *32*, 8939-8944. https://doi.org/10.1021/bi00085a027.

Pavlova, N.N., and Thompson, C.B. (2016). The Emerging Hallmarks of Cancer Metabolism. Cell metabolism *23*, 27-47. https://doi.org/10.1016/j.cmet.2015.12.006.

Peeters, M., Price, T.J., Cervantes, A., Sobrero, A.F., Ducreux, M., Hotko, Y., André, T., Chan, E., Lordick, F., and Punt, C.J.A., et al. (2010). Randomized phase III study of panitumumab with fluorouracil, leucovorin, and irinotecan (FOLFIRI) compared with FOLFIRI alone as second-line treatment in patients with metastatic colorectal cancer. Journal of clinical oncology : official journal of the American Society of Clinical Oncology *28*, 4706-4713. https://doi.org/10.1200/JCO.2009.27.6055.

Perera, C.N., Rodriguez, R., and Shorr, R. (04152012). Abstract 3807: Regulation of pancreatic, gliosarcoma and non-small cell lung cancer via CPI-613, a novel anticancer therapeutic agent. In Experimental and Molecular Therapeutics (American Association for Cancer Research), p. 3807.

Perera, C.N., Rodriguez, R., and Shorr, R. Abstract A65: Heterogeneous response of H460 non-small lung carcinoma cells to CPI-613, a novel compound that selectively alters tumor energy metabolism. In Translational and Therapeutic Potential 2015, A65-A65.

Pérez-Mancera, P.A., Young, A.R.J., and Narita, M. (2014). Inside and out: the activities of senescence in cancer. Nature reviews. Cancer *14*, 547-558. https://doi.org/10.1038/nrc3773.

Pettersen, H.S., Visnes, T., Vågbø, C.B., Svaasand, E.K., Doseth, B., Slupphaug, G., Kavli, B., and Krokan, H.E. (2011). UNG-initiated base excision repair is the major repair route for 5-fluorouracil in DNA, but 5-fluorouracil cytotoxicity depends mainly on RNA incorporation. Nucleic acids research *39*, 8430-8444. https://doi.org/10.1093/nar/gkr563.

Philip, P.A., Buyse, M.E., Alistar, A.T., Rocha Lima, C.M., Luther, S., Pardee, T.S., and van Cutsem, E. (2019). A Phase III open-label trial to evaluate efficacy and safety of CPI-613 plus modified FOLFIRINOX (mFFX) versus FOLFIRINOX (FFX) in patients with metastatic adenocarcinoma of the pancreas. Future oncology (London, England) *15*, 3189-3196. https://doi.org/10.2217/fon-2019-0209.

Pickles, S., Vigié, P., and Youle, R.J. (2018). Mitophagy and Quality Control Mechanisms in Mitochondrial Maintenance. Current biology : CB *28*, R170-R185. https://doi.org/10.1016/j.cub.2018.01.004.

Pietrantonio, F., Petrelli, F., Coinu, A., Di Bartolomeo, M., Borgonovo, K., Maggi, C., Cabiddu, M., Iacovelli, R., Bossi, I., and Lonati, V., et al. (2015). Predictive role of BRAF mutations in patients with advanced colorectal cancer receiving cetuximab and panitumumab: a meta-analysis. European journal of cancer (Oxford, England : 1990) *51*, 587-594. https://doi.org/10.1016/j.ejca.2015.01.054.

Pluquet, O., and Hainaut, P. (2001). Genotoxic and non-genotoxic pathways of p53 induction. Cancer Letters *174*, 1-15. https://doi.org/10.1016/S0304-3835(01)00698-X.

Pohl, M., Stricker, I., Schoeneck, A., Schulmann, K., Klein-Scory, S., Schwarte-Waldhoff, I., Hasmann, M., Tannapfel, A., Schmiegel, W., and Reinacher-Schick, A. (2009). Antitumor activity of the HER2 dimerization inhibitor pertuzumab on human colon cancer cells in vitro and in vivo. Journal of cancer research and clinical oncology *135*, 1377-1386. https://doi.org/10.1007/s00432-009-0579-3.

Puchsaka, P., Chaotham, C., and Chanvorachote, P. (2016). α-Lipoic acid sensitizes lung cancer cells to chemotherapeutic agents and anoikis via integrin β1/β3 downregulation. International journal of oncology *49*, 1445-1456. https://doi.org/10.3892/ijo.2016.3624.

Qiang, L., Wu, C., Ming, M., Viollet, B., and He, Y.-Y. (2013). Autophagy controls p38 activation to promote cell survival under genotoxic stress. The Journal of biological chemistry *288*, 1603-1611. https://doi.org/10.1074/jbc.M112.415224.

Qiu, M., Hu, J., Yang, D., Cosgrove, D.P., and Xu, R. (2015). Pattern of distant metastases in colorectal cancer: a SEER based study. Oncotarget *6*, 38658-38666. https://doi.org/10.18632/oncotarget.6130.

Qiu, Y., Cai, G., Zhou, B., Li, D., Zhao, A., Xie, G., Li, H., Cai, S., Xie, D., and Huang, C., et al. (2014). A distinct metabolic signature of human colorectal cancer with prognostic potential. Clinical cancer research : an official journal of the American Association for Cancer Research *20*, 2136-2146. https://doi.org/10.1158/1078-0432.CCR-13-1939.

Qu, D., Shen, L., Liu, S., Li, H., Ma, Y., Zhang, R., Wu, K., Yao, L., Li, J., and Zhang, J. (2017). Chronic inflammation confers to the metabolic reprogramming associated with tumorigenesis of colorectal cancer. Cancer biology & therapy *18*, 237-244. https://doi.org/10.1080/15384047.2017.1294292.

Radisky, E.S., and Radisky, D.C. (2010). Matrix metalloproteinase-induced epithelial-mesenchymal transition in breast cancer. Journal of mammary gland biology and neoplasia *15*, 201-212. https://doi.org/10.1007/s10911-010-9177-x.

Randerath, K., Tseng, W.C., Harris, J.S., and Lu, L.J. (1983). Specific effects of 5-fluoropyrimidines and 5-azapyrimidines on modification of the 5 position of pyrimidines, in particular the synthesis of 5-methyluracil and 5-methylcytosine in nucleic acids. Recent results in cancer research. Fortschritte der Krebsforschung. Progres dans les recherches sur le cancer *84*, 283-297. https://doi.org/10.1007/978-3-642-81947-6_22.

Reckzeh, E.S., Karageorgis, G., Schwalfenberg, M., Ceballos, J., Nowacki, J., Stroet, M.C.M., Binici, A., Knauer, L., Brand, S., and Choidas, A., et al. (2019). Inhibition of Glucose Transporters and Glutaminase Synergistically Impairs Tumor Cell Growth. Cell chemical biology *26*, 1214-1228.e25. https://doi.org/10.1016/j.chembiol.2019.06.005.

Reid, M.A. (2020). 9 - Cancer Metabolism.

Reitzer, L.J., Wice, B.M., and Kennell, D. (1979). Evidence that glutamine, not sugar, is the major energy source for cultured HeLa cells. The Journal of biological chemistry *254*, 2669-2676.

Reljanovic, M., Reichel, G., Rett, K., Lobisch, M., Schuette, K., Möller, W., Tritschler, H.J., and Mehnert, H. (1999). Treatment of diabetic polyneuropathy with the antioxidant thioctic acid

(alpha-lipoic acid): a two year multicenter randomized double-blind placebo-controlled trial (ALADIN II). Alpha Lipoic Acid in Diabetic Neuropathy. Free radical research *31*, 171-179. https://doi.org/10.1080/10715769900300721.

Retter, A.S. (2012). Translational assessment of the efficacy of CPI-613 against pancreatic cancer in animal models versus patients with stage IV disease. JCO *30*, 3075. https://doi.org/10.1200/jco.2012.30.15_suppl.3075.

Retter, A.S., Shorr, R., Rodriguez, R., Hoffman, K., Volterra, F., Hoffman, A.D., Huppert, N., and Lee, K. (2010). Phase I trial of CPI-613, a lipoic acid analog, and gemcitabine in patients with advanced solid tumors. JCO *28*, e13136-e13136. https://doi.org/10.1200/jco.2010.28.15_suppl.e13136.

Riihimäki, M., Hemminki, A., Sundquist, J., and Hemminki, K. (2016). Patterns of metastasis in colon and rectal cancer. Scientific reports *6*, 29765. https://doi.org/10.1038/srep29765.

Ripani, P., Delp, J., Bode, K., Delgado, M.E., Dietrich, L., Betzler, V.M., Yan, N., Scheven, G. von, Mayer, T.U., and Leist, M., et al. (2020). Thiazolides promote G1 cell cycle arrest in colorectal cancer cells by targeting the mitochondrial respiratory chain. Oncogene *39*, 2345-2357. https://doi.org/10.1038/s41388-019-1142-6.

Robert Koch-Institut (2015). Krebs in Deutschland | 2015/2016 | Darm C8-C20.

Robertis, M. de, Massi, E., Poeta, M.L., Carotti, S., Morini, S., Cecchetelli, L., Signori, E., and Fazio, V.M. (2011). The AOM/DSS murine model for the study of colon carcinogenesis: From pathways to diagnosis and therapy studies. Journal of carcinogenesis *10*, 9. https://doi.org/10.4103/1477-3163.78279.

Rocha Lima, C.M.S.P., Alistar, A.T., Desnoyers, R.J., Sorscher, S., Yacoub, G.H., van Dressler, E.M., Pardee, T.S., Grant, S.C., Luther, S., and Butler, D., et al. (2019). A phase I clinical trial of fluorouracil (5-FU) + devimistat (CPI-613) combination in previously treated patients (pts) with metastatic colorectal cancer (MCR). JCO *37*, e15054-e15054. https://doi.org/10.1200/JCO.2019.37.15_suppl.e15054.

Roche, J. (2018). The Epithelial-to-Mesenchymal Transition in Cancer. Cancers *10*. https://doi.org/10.3390/cancers10020052.

Roche, T.E., Baker, J.C., Yan, X., Hiromasa, Y., Gong, X., Peng, T., Dong, J., Turkan, A., and Kasten, S.A. (2001). Distinct regulatory properties of pyruvate dehydrogenase kinase and phosphatase isoforms. In Progress in nucleic acid research and molecular biology, K. Moldave, ed. (San Diego, Calif.: Academic Press), pp. 33–75.

Roche, T.E., Hiromasa, Y., Turkan, A., Gong, X., Peng, T., Yan, X., Kasten, S.A., Bao, H., and Dong, J. (2003). Essential roles of lipoyl domains in the activated function and control of

pyruvate dehydrogenase kinases and phosphatase isoform 1. European journal of biochemistry *270*, 1050-1056. https://doi.org/10.1046/j.1432-1033.2003.03468.x.

Rochette, L., Ghibu, S., Richard, C., Zeller, M., Cottin, Y., and Vergely, C. (2013). Direct and indirect antioxidant properties of α-lipoic acid and therapeutic potential. Molecular nutrition & food research *57*, 114-125. https://doi.org/10.1002/mnfr.201200608.

Rodriguez-Rocha, H., Garcia-Garcia, A., Panayiotidis, M.I., and Franco, R. (2011). DNA damage and autophagy. Mutation research *711*, 158-166. https://doi.org/10.1016/j.mrfmmm.2011.03.007.

Rogakou, E.P., Nieves-Neira, W., Boon, C., Pommier, Y., and Bonner, W.M. (2000). Initiation of DNA fragmentation during apoptosis induces phosphorylation of H2AX histone at serine 139. The Journal of biological chemistry *275*, 9390-9395. https://doi.org/10.1074/jbc.275.13.9390.

Roig, A.I., Eskiocak, U., Hight, S.K., Kim, S.B., Delgado, O., Souza, R.F., Spechler, S.J., Wright, W.E., and Shay, J.W. (2010). Immortalized epithelial cells derived from human colon biopsies express stem cell markers and differentiate in vitro. Gastroenterology *138*, 1012-21.e1-5. https://doi.org/10.1053/j.gastro.2009.11.052.

Romero-Garcia, S., Lopez-Gonzalez, J.S., Báez-Viveros, J.L., Aguilar-Cazares, D., and Prado-Garcia, H. (2011). Tumor cell metabolism: an integral view. Cancer biology & therapy *12*, 939-948. https://doi.org/10.4161/cbt.12.11.18140.

Rothenberg, M.L., Oza, A.M., Bigelow, R.H., Berlin, J.D., Marshall, J.L., Ramanathan, R.K., Hart, L.L., Gupta, S., Garay, C.A., and Burger, B.G., et al. (2003). Superiority of oxaliplatin and fluorouracil-leucovorin compared with either therapy alone in patients with progressive colorectal cancer after irinotecan and fluorouracil-leucovorin: interim results of a phase III trial. JCO *21*, 2059-2069. https://doi.org/10.1200/JCO.2003.11.126.

Rougier, P., van Cutsem, E., Bajetta, E., Niederle, N., Possinger, K., Labianca, R., Navarro, M., Morant, R., Bleiberg, H., and Wils, J., et al. (1998). Randomised trial of irinotecan versus fluorouracil by continuous infusion after fluorouracil failure in patients with metastatic colorectal cancer. Lancet (London, England) *352*, 1407-1412. https://doi.org/10.1016/S0140-6736(98)03085-2.

Rowland, A., Dias, M.M., Wiese, M.D., Kichenadasse, G., McKinnon, R.A., Karapetis, C.S., and Sorich, M.J. (2015). Meta-analysis of BRAF mutation as a predictive biomarker of benefit from anti-EGFR monoclonal antibody therapy for RAS wild-type metastatic colorectal cancer. British journal of cancer *112*, 1888-1894. https://doi.org/10.1038/bjc.2015.173.

Rudolf, E., John, S., and Cervinka, M. (2012). Irinotecan induces senescence and apoptosis in colonic cells in vitro. Toxicology letters *214*, 1-8. https://doi.org/10.1016/j.toxlet.2012.08.004.

Sabbatinelli, J., Prattichizzo, F., Olivieri, F., Procopio, A.D., Rippo, M.R., and Giuliani, A. (2019). Where Metabolism Meets Senescence: Focus on Endothelial Cells. Frontiers in physiology *10*, 1523. https://doi.org/10.3389/fphys.2019.01523.

Sadahiro, S., Suzuki, T., Ishikawa, K., Nakamura, T., Tanaka, Y., Masuda, T., Mukoyama, S., Yasuda, S., Tajima, T., and Makuuchi, H., et al. (2003). Recurrence patterns after curative resection of colorectal cancer in patients followed for a minimum of ten years. Hepato-gastroenterology *50*, 1362-1366.

Sai, K.S., Zachar, Z., Almaguel, F., Stuart, S.D., Dahan, M.S., Guardado, M., Rideout, S., Wang, M., Sattiraju, A., and Bingham, P.M., et al. (2017). Abstract 2867: FDG-PET imaging as a potential biomarker of mitochondrial targeting by CPI-613, a novel inhibitor of mitochondrial metabolism, 2867. https://doi.org/10.1158/1538-7445.AM2017-2867.

Saltz, L., Badarinath, S., Dakhil, S., Bienvenu, B., Harker, W.G., Birchfield, G., Tokaz, L.K., Barrera, D., Conkling, P.R., and O'Rourke, M.A., et al. (2012). Phase III trial of cetuximab, bevacizumab, and 5-fluorouracil/leucovorin vs. FOLFOX-bevacizumab in colorectal cancer. Clinical colorectal cancer *11*, 101-111. https://doi.org/10.1016/j.clcc.2011.05.006.

Santi, D.V., McHenry, C.S., and Sommer, H. (1974). Mechanism of interaction of thymidylate synthetase with 5-fluorodeoxyuridylate. Biochemistry *13*, 471-481. https://doi.org/10.1021/bi00700a012.

Sartore-Bianchi, A., Trusolino, L., Martino, C., Bencardino, K., Lonardi, S., Bergamo, F., Zagonel, V., Leone, F., Depetris, I., and Martinelli, E., et al. (2016). Dual-targeted therapy with trastuzumab and lapatinib in treatment-refractory, KRAS codon 12/13 wild-type, HER2-positive metastatic colorectal cancer (HERACLES): a proof-of-concept, multicentre, open-label, phase 2 trial. The Lancet. Oncology *17*, 738-746. https://doi.org/10.1016/S1470-2045(16)00150-9.

Sasaki, K., Tsuno, N.H., Sunami, E., Kawai, K., Hongo, K., Hiyoshi, M., Kaneko, M., Murono, K., Tada, N., and Nirei, T., et al. (2012). Resistance of colon cancer to 5-fluorouracil may be overcome by combination with chloroquine, an in vivo study. Anti-cancer drugs *23*, 675-682. https://doi.org/10.1097/CAD.0b013e328353f8c7.

Sasaki, K., Tsuno, N.H., Sunami, E., Tsurita, G., Kawai, K., Okaji, Y., Nishikawa, T., Shuno, Y., Hongo, K., and Hiyoshi, M., et al. (2010). Chloroquine potentiates the anti-cancer effect of 5-fluorouracil on colon cancer cells. BMC cancer *10*, 370. https://doi.org/10.1186/1471-2407-10-370.

Satoh, K., Yachida, S., Sugimoto, M., Oshima, M., Nakagawa, T., Akamoto, S., Tabata, S., Saitoh, K., Kato, K., and Sato, S., et al. (2017). Global metabolic reprogramming of colorectal cancer occurs at adenoma stage and is induced by MYC. Proceedings of the National Academy of Sciences of the United States of America *114*, E7697-E7706. https://doi.org/10.1073/pnas.1710366114.

Satoh, S., Shindoh, M., Min, J.Z., Toyo'oka, T., Fukushima, T., and Inagaki, S. (2008). Selective and sensitive determination of lipoyllysine (protein-bound alpha-lipoic acid) in biological specimens by high-performance liquid chromatography with fluorescence detection. Analytica chimica acta *618*, 210-217. https://doi.org/10.1016/j.aca.2008.05.001.

Saunier, E., Antonio, S., Regazzetti, A., Auzeil, N., Laprévote, O., Shay, J.W., Coumoul, X., Barouki, R., Benelli, C., and Huc, L., et al. (2017). Resveratrol reverses the Warburg effect by targeting the pyruvate dehydrogenase complex in colon cancer cells. Scientific reports *7*, 6945. https://doi.org/10.1038/s41598-017-07006-0.

Savitha, S., and Panneerselvam, C. (2007). Mitigation of age-dependent oxidative damage to DNA in rat heart by carnitine and lipoic acid. Mechanisms of ageing and development *128*, 206-212. https://doi.org/10.1016/j.mad.2006.11.029.

Scheer, A., and Auer, R.A.C. (2009). Surveillance after curative resection of colorectal cancer. Clinics in colon and rectal surgery *22*, 242-250. https://doi.org/10.1055/s-0029-1242464.

Schmoll, H.-J., Haustermans, K., Price, T.J., Nordlinger, B., Hofheinz, R., Daisne, J.-F., Janssens, J., Brenner, B., Schmidt, P., and Reinel, H., et al. (2018). Preoperative chemoradiotherapy and postoperative chemotherapy with capecitabine +/- oxaliplatin in locally advanced rectal cancer: Final results of PETACC-6. JCO *36*, 3500. https://doi.org/10.1200/JCO.2018.36.15_suppl.3500.

Schonewolf, C.A., Mehta, M., Schiff, D., Wu, H., Haffty, B.G., Karantza, V., and Jabbour, S.K. (2014). Autophagy inhibition by chloroquine sensitizes HT-29 colorectal cancer cells to concurrent chemoradiation. World journal of gastrointestinal oncology *6*, 74-82. https://doi.org/10.4251/wjgo.v6.i3.74.

Schulz-Heddergott, R., Stark, N., Edmunds, S.J., Li, J., Conradi, L.-C., Bohnenberger, H., Ceteci, F., Greten, F.R., Dobbelstein, M., and Moll, U.M. (2018). Therapeutic Ablation of Gain-of-Function Mutant p53 in Colorectal Cancer Inhibits Stat3-Mediated Tumor Growth and Invasion. Cancer cell *34*, 298-314.e7. https://doi.org/10.1016/j.ccell.2018.07.004.

Schupke, H., Hempel, R., Peter, G., Hermann, R., Wessel, K., Engel, J., and Kronbach, T. (2001). New metabolic pathways of alpha-lipoic acid. Drug metabolism and disposition: the biological fate of chemicals *29*, 855-862.

Sciacovelli, M., and Frezza, C. (2016). Oncometabolites: Unconventional triggers of oncogenic signalling cascades. Free radical biology & medicine *100*, 175-181. https://doi.org/10.1016/j.freeradbiomed.2016.04.025.

Seiwert, N., Heylmann, D., Hasselwander, S., and Fahrer, J. (2020). Mechanism of colorectal carcinogenesis triggered by heme iron from red meat. Biochimica et biophysica acta. Reviews on cancer *1873*, 188334. https://doi.org/10.1016/j.bbcan.2019.188334.

Seiwert, N., Neitzel, C., Stroh, S., Frisan, T., Audebert, M., Toulany, M., Kaina, B., and Fahrer, J. (2017). AKT2 suppresses pro-survival autophagy triggered by DNA double-strand breaks in colorectal cancer cells. Cell death & disease *8*, e3019. https://doi.org/10.1038/cddis.2017.418.

Semenza, G.L. (2008). Tumor metabolism: cancer cells give and take lactate. The Journal of clinical investigation *118*, 3835-3837. https://doi.org/10.1172/JCI37373.

Semenza, G.L. (2010a). Defining the role of hypoxia-inducible factor 1 in cancer biology and therapeutics. Oncogene *29*, 625-634. https://doi.org/10.1038/onc.2009.441.

Semenza, G.L. (2010b). HIF-1: upstream and downstream of cancer metabolism. Current opinion in genetics & development *20*, 51-56. https://doi.org/10.1016/j.gde.2009.10.009.

Serre, L., Pereira de Jésus, K., Boiteux, S., Zelwer, C., and Castaing, B. (2002). Crystal structure of the Lactococcus lactis formamidopyrimidine-DNA glycosylase bound to an abasic site analogue-containing DNA. The EMBO journal *21*, 2854-2865. https://doi.org/10.1093/emboj/cdf304.

Sertel, S., Eichhorn, T., Simon, C.H., Plinkert, P.K., Johnson, S.W., and Efferth, T. (2010). Pharmacogenomic Identification of c-Myc/Max-Regulated Genes Associated with Cytotoxicity of Artesunate towards Human Colon, Ovarian and Lung Cancer Cell Lines. Molecules *15*, 2886-2910. https://doi.org/10.3390/molecules15042886.

Shahruzaman, S.H., Fakurazi, S., and Maniam, S. (2018). Targeting energy metabolism to eliminate cancer cells. Cancer management and research *10*, 2325-2335. https://doi.org/10.2147/CMAR.S167424.

Shalini, S., Dorstyn, L., Dawar, S., and Kumar, S. (2015). Old, new and emerging functions of caspases. Cell death and differentiation *22*, 526-539. https://doi.org/10.1038/cdd.2014.216.

Shankar, J., and Nabi, I.R. (2015). Actin cytoskeleton regulation of epithelial mesenchymal transition in metastatic cancer cells. PLoS ONE *10*, e0119954. https://doi.org/10.1371/journal.pone.0119954.

Shay, K.P., Michels, A.J., Li, W., Kong, A.-N.T., and Hagen, T.M. (2012). Cap-independent Nrf2 translation is part of a lipoic acid-stimulated detoxification stress response. Biochimica et biophysica acta *1823*, 1102-1109. https://doi.org/10.1016/j.bbamcr.2012.04.002.

Shay, K.P., Moreau, R.F., Smith, E.J., Smith, A.R., and Hagen, T.M. (2009). Alpha-lipoic acid as a dietary supplement: molecular mechanisms and therapeutic potential. Biochimica et biophysica acta *1790*, 1149-1160. https://doi.org/10.1016/j.bbagen.2009.07.026.

Shelton, J.W., Waxweiler, T.V., Landry, J., Gao, H., Xu, Y., Wang, L., El-Rayes, B., and Shu, H.-K.G. (2013). In vitro and in vivo enhancement of chemoradiation using the oral PARP

inhibitor ABT-888 in colorectal cancer cells. International journal of radiation oncology, biology, physics *86*, 469-476. https://doi.org/10.1016/j.ijrobp.2013.02.015.

Shi, D.-Y., Liu, H.-L., Stern, J.S., Yu, P.-Z., and Liu, S.-L. (2008). Alpha-lipoic acid induces apoptosis in hepatoma cells via the PTEN/Akt pathway. FEBS letters *582*, 1667-1671. https://doi.org/10.1016/j.febslet.2008.04.021.

Shih, W., and Yamada, S. (2012). N-cadherin as a key regulator of collective cell migration in a 3D environment. Cell adhesion & migration *6*, 513-517. https://doi.org/10.4161/cam.21766.

Sigel, H., Prijs, B., McCormick, D.B., and Shih, J.C.H. (1978). Stability and structure of binary and ternary complexes of α-lipoate and lipoate derivatives with Mn2+, Cu2+, and Zn2+ in solution. Archives of Biochemistry and Biophysics *187*, 208-214. https://doi.org/10.1016/0003-9861(78)90025-5.

Simbula, G., Columbano, A., Ledda-Columbano, G.M., Sanna, L., Deidda, M., Diana, A., and Pibiri, M. (2007). Increased ROS generation and p53 activation in alpha-lipoic acid-induced apoptosis of hepatoma cells. Apoptosis : an international journal on programmed cell death *12*, 113-123. https://doi.org/10.1007/s10495-006-0487-9.

Singh, A., and Settleman, J. (2010). EMT, cancer stem cells and drug resistance: an emerging axis of evil in the war on cancer. Oncogene *29*, 4741-4751. https://doi.org/10.1038/onc.2010.215.

Slade, L., Chalker, J., Kuksal, N., Young, A., Gardiner, D., and Mailloux, R.J. (2017). Examination of the superoxide/hydrogen peroxide forming and quenching potential of mouse liver mitochondria. Biochimica et biophysica acta. General subjects *1861*, 1960-1969. https://doi.org/10.1016/j.bbagen.2017.05.010.

Smith, A.R., Shenvi, S.V., Widlansky, M., Suh, J.H., and Hagen, T.M. (2004). Lipoic acid as a potential therapy for chronic diseases associated with oxidative stress. Current medicinal chemistry *11*, 1135-1146. https://doi.org/10.2174/0929867043365387.

Snezhkina, A.V., Krasnov, G.S., Zaretsky, A.R., Zhavoronkov, A., Nyushko, K.M., Moskalev, A.A., Karpova, I.Y., Afremova, A.I., Lipatova, A.V., and Kochetkov, D.V., et al. (2016). Differential expression of alternatively spliced transcripts related to energy metabolism in colorectal cancer. BMC genomics *17*, 1011. https://doi.org/10.1186/s12864-016-3351-5.

Sobin, L.H., and Fleming, I.D. (1997). TNM classification of malignant tumors, fifth edition (1997). Cancer *80*, 1803-1804. https://doi.org/10.1002/(SICI)1097-0142(19971101)80:9<1803::AID-CNCR16>3.0.CO;2-9.

Sobrero, A.F., Maurel, J., Fehrenbacher, L., Scheithauer, W., Abubakr, Y.A., Lutz, M.P., Vega-Villegas, M.E., Eng, C., Steinhauer, E.U., and Prausova, J., et al. (2008). EPIC: phase III trial of cetuximab plus irinotecan after fluoropyrimidine and oxaliplatin failure in patients with metastatic

colorectal cancer. Journal of clinical oncology : official journal of the American Society of Clinical Oncology *26*, 2311-2319. https://doi.org/10.1200/JCO.2007.13.1193.

Soga, T. (2013). Cancer metabolism: key players in metabolic reprogramming. Cancer science *104*, 275-281. https://doi.org/10.1111/cas.12085.

Solier, S., and Pommier, Y. (2009). The apoptotic ring: a novel entity with phosphorylated histones H2AX and H2B and activated DNA damage response kinases. Cell cycle (Georgetown, Tex.) *8*, 1853-1859. https://doi.org/10.4161/cc.8.12.8865.

Solier, S., and Pommier, Y. (2014). The nuclear γ-H2AX apoptotic ring: implications for cancers and autoimmune diseases. Cellular and molecular life sciences : CMLS *71*, 2289-2297. https://doi.org/10.1007/s00018-013-1555-2.

Song, M., Kim, S.-H., Im, C.Y., and Hwang, H.-J. (2018). Recent Development of Small Molecule Glutaminase Inhibitors. Current topics in medicinal chemistry *18*, 432-443. https://doi.org/10.2174/1568026618666180525100830.

Sośnicki, S., Kapral, M., and Węglarz, L. (2016). Molecular targets of metformin antitumor action. Pharmacological reports : PR *68*, 918-925. https://doi.org/10.1016/j.pharep.2016.04.021.

Souglakos, J., Androulakis, N., Syrigos, K., Polyzos, A., Ziras, N., Athanasiadis, A., Kakolyris, S., Tsousis, S., Kouroussis, C., and Vamvakas, L., et al. (2006). FOLFOXIRI (folinic acid, 5-fluorouracil, oxaliplatin and irinotecan) vs FOLFIRI (folinic acid, 5-fluorouracil and irinotecan) as first-line treatment in metastatic colorectal cancer (MCC): a multicentre randomised phase III trial from the Hellenic Oncology Research Group (HORG). British journal of cancer *94*, 798-805. https://doi.org/10.1038/sj.bjc.6603011.

Spallotta, F., Cencioni, C., Atlante, S., Garella, D., Cocco, M., Mori, M., Mastrocola, R., Kuenne, C., Guenther, S., and Nanni, S., et al. (2018). Stable Oxidative Cytosine Modifications Accumulate in Cardiac Mesenchymal Cells From Type2 Diabetes Patients: Rescue by α-Ketoglutarate and TET-TDG Functional Reactivation. Circulation research *122*, 31-46. https://doi.org/10.1161/CIRCRESAHA.117.311300.

Staker, B.L., Hjerrild, K., Feese, M.D., Behnke, C.A., Burgin, A.B., and Stewart, L. (2002). The mechanism of topoisomerase I poisoning by a camptothecin analog. Proceedings of the National Academy of Sciences of the United States of America *99*, 15387-15392. https://doi.org/10.1073/pnas.242259599.

Stanislav, J., Mls, J., Červinka, M., and Rudolf, E. (2013). The role of autophagic cell death and apoptosis in irinotecan-treated p53 null colon cancer cells. Anti-cancer agents in medicinal chemistry *13*, 811-820. https://doi.org/10.2174/18715206113130050015.

Starkov, A.A., Fiskum, G., Chinopoulos, C., Lorenzo, B.J., Browne, S.E., Patel, M.S., and Beal, M.F. (2004). Mitochondrial alpha-ketoglutarate dehydrogenase complex generates reactive

oxygen species. The Journal of neuroscience : the official journal of the Society for Neuroscience *24*, 7779-7788. https://doi.org/10.1523/JNEUROSCI.1899-04.2004.

Stockwell, B.R., Friedmann Angeli, J.P., Bayir, H., Bush, A.I., Conrad, M., Dixon, S.J., Fulda, S., Gascón, S., Hatzios, S.K., and Kagan, V.E., et al. (2017). Ferroptosis: A Regulated Cell Death Nexus Linking Metabolism, Redox Biology, and Disease. Cell *171*, 273-285. https://doi.org/10.1016/j.cell.2017.09.021.

Stuart, S.D., Guardado, M., Dahan, M., Bingham, P.M., and Zachar, Z. (012016). Abstract A61: Tumor metabolic remodeling can modulate anticancer drug response: CPI-613 attack on tumor cell mitochondrial metabolism is mediated by metabolite availability. In Therapeutic Targets From Cancer (American Association for Cancer Research), A61-A61.

Stuart, S.D., Schauble, A., Gupta, S., Kennedy, A.D., Keppler, B.R., Bingham, P.M., and Zachar, Z. (2014). A strategically designed small molecule attacks alpha-ketoglutarate dehydrogenase in tumor cells through a redox process. Cancer & metabolism *2*, 4. https://doi.org/10.1186/2049-3002-2-4.

Suh, J.H., Shenvi, S.V., Dixon, B.M., Liu, H., Jaiswal, A.K., Liu, R.-M., and Hagen, T.M. (2004). Decline in transcriptional activity of Nrf2 causes age-related loss of glutathione synthesis, which is reversible with lipoic acid. Proceedings of the National Academy of Sciences of the United States of America *101*, 3381-3386. https://doi.org/10.1073/pnas.0400282101.

Sui, X., Kong, N., Wang, X., Fang, Y., Hu, X., Xu, Y., Chen, W., Wang, K., Li, D., and Jin, W., et al. (2014). JNK confers 5-fluorouracil resistance in p53-deficient and mutant p53-expressing colon cancer cells by inducing survival autophagy. Scientific reports *4*, 4694. https://doi.org/10.1038/srep04694.

Sun, L., Suo, C., Li, S.-T., Zhang, H., and Gao, P. (2018). Metabolic reprogramming for cancer cells and their microenvironment: Beyond the Warburg Effect. Biochimica et biophysica acta. Reviews on cancer *1870*, 51-66. https://doi.org/10.1016/j.bbcan.2018.06.005.

Sun, Y., Liu, Z., Zou, X., Lan, Y., Sun, X., Wang, X., Zhao, S., Jiang, C., and Liu, H. (2015). Mechanisms underlying 3-bromopyruvate-induced cell death in colon cancer. Journal of bioenergetics and biomembranes *47*, 319-329. https://doi.org/10.1007/s10863-015-9612-1.

Suzuki, Y.J., Tsuchiya, M., and Packer, L. (1991). Thioctic acid and dihydrolipoic acid are novel antioxidants which interact with reactive oxygen species. Free radical research communications *15*, 255-263. https://doi.org/10.3109/10715769109105221.

Tabernero, J., Yoshino, T., Cohn, A.L., Obermannova, R., Bodoky, G., Garcia-Carbonero, R., Ciuleanu, T.-E., Portnoy, D.C., van Cutsem, E., and Grothey, A., et al. (2015). Ramucirumab versus placebo in combination with second-line FOLFIRI in patients with metastatic colorectal carcinoma that progressed during or after first-line therapy with bevacizumab, oxaliplatin, and a

fluoropyrimidine (RAISE): a randomised, double-blind, multicentre, phase 3 study. The Lancet. Oncology *16*, 499-508. https://doi.org/10.1016/S1470-2045(15)70127-0.

Tait, S.W.G., and Green, D.R. (2008). Caspase-independent cell death: leaving the set without the final cut. Oncogene *27*, 6452-6461. https://doi.org/10.1038/onc.2008.311.

Takaishi, N., Yoshida, K., Satsu, H., and Shimizu, M. (2007). Transepithelial transport of alpha-lipoic acid across human intestinal Caco-2 cell monolayers. Journal of agricultural and food chemistry *55*, 5253-5259. https://doi.org/10.1021/jf063624i.

Talbot, L.J., Bhattacharya, S.D., and Kuo, P.C. (2012). Epithelial-mesenchymal transition, the tumor microenvironment, and metastatic behavior of epithelial malignancies. International Journal of Biochemistry and Molecular Biology *3*, 117-136.

Tang, D., Kang, R., Berghe, T.V., Vandenabeele, P., and Kroemer, G. (2019). The molecular machinery of regulated cell death. Cell research *29*, 347-364. https://doi.org/10.1038/s41422-019-0164-5.

Tang, J.-C., Feng, Y.-L., Liang, X., and Cai, X.-J. (2016). Autophagy in 5-Fluorouracil Therapy in Gastrointestinal Cancer: Trends and Challenges. Chinese medical journal *129*, 456-463. https://doi.org/10.4103/0366-6999.176069.

Tang, Y., Herr, G., Johnson, W., Resnik, E., and Aho, J. (2013). Induction and analysis of epithelial to mesenchymal transition. Journal of visualized experiments : JoVE. https://doi.org/10.3791/50478.

Tania, M., Khan, M.A., and Fu, J. (2014). Epithelial to mesenchymal transition inducing transcription factors and metastatic cancer. Tumour biology : the journal of the International Society for Oncodevelopmental Biology and Medicine *35*, 7335-7342. https://doi.org/10.1007/s13277-014-2163-y.

Tarrado-Castellarnau, M., Atauri, P. de, and Cascante, M. (2016). Oncogenic regulation of tumor metabolic reprogramming. Oncotarget *7*, 62726-62753. https://doi.org/10.18632/oncotarget.10911.

Tataranni, T., and Piccoli, C. (2019). Dichloroacetate (DCA) and Cancer: An Overview towards Clinical Applications. Oxidative medicine and cellular longevity *2019*, 8201079. https://doi.org/10.1155/2019/8201079.

Tato-Costa, J., Casimiro, S., Pacheco, T., Pires, R., Fernandes, A., Alho, I., Pereira, P., Costa, P., Castelo, H.B., and Ferreira, J., et al. (2016). Therapy-Induced Cellular Senescence Induces Epithelial-to-Mesenchymal Transition and Increases Invasiveness in Rectal Cancer. Clinical colorectal cancer *15*, 170-178.e3. https://doi.org/10.1016/j.clcc.2015.09.003.

Tebay, L.E., Robertson, H., Durant, S.T., Vitale, S.R., Penning, T.M., Dinkova-Kostova, A.T., and Hayes, J.D. (2015). Mechanisms of activation of the transcription factor Nrf2 by redox stressors, nutrient cues, and energy status and the pathways through which it attenuates degenerative disease. Free radical biology & medicine *88*, 108-146. https://doi.org/10.1016/j.freeradbiomed.2015.06.021.

Teichert, J., Hermann, R., Ruus, P., and Preiss, R. (2003). Plasma kinetics, metabolism, and urinary excretion of alpha-lipoic acid following oral administration in healthy volunteers. Journal of clinical pharmacology *43*, 1257-1267. https://doi.org/10.1177/0091270003258654.

Teichert, J., Kern, J., Tritschler, H.J., Ulrich, H., and Preiss, R. (1998). Investigations on the pharmacokinetics of alpha-lipoic acid in healthy volunteers. International journal of clinical pharmacology and therapeutics *36*, 625-628.

Terry, S., Savagner, P., Ortiz-Cuaran, S., Mahjoubi, L., Saintigny, P., Thiery, J.-P., and Chouaib, S. (2017). New insights into the role of EMT in tumor immune escape. Molecular oncology *11*, 824-846. https://doi.org/10.1002/1878-0261.12093.

Tice, R.R., Agurell, E., Anderson, D., Burlinson, B., Hartmann, A., Kobayashi, H., Miyamae, Y., Rojas, E., Ryu, J.-C., and Sasaki, Y.F. (2000). Single cell gel/comet assay: Guidelines for in vitro and in vivo genetic toxicology testing. Environ. Mol. Mutagen. *35*, 206-221. https://doi.org/10.1002/(SICI)1098-2280(2000)35:3<206::AID-EM8>3.0.CO;2-J.

Tol, J., Koopman, M., Cats, A., Rodenburg, C.J., Creemers, G.J.M., Schrama, J.G., Erdkamp, F.L.G., Vos, A.H., van Groeningen, C.J., and Sinnige, H.A.M., et al. (2009). Chemotherapy, bevacizumab, and cetuximab in metastatic colorectal cancer. The New England journal of medicine *360*, 563-572. https://doi.org/10.1056/NEJMoa0808268.

Tong, J., Xie, G., He, J., Li, J., Pan, F., and Liang, H. (2011a). Synergistic Antitumor Effect of Dichloroacetate in Combination with 5-Fluorouracil in Colorectal Cancer. Journal of Biomedicine and Biotechnology *2011*. https://doi.org/10.1155/2011/740564.

Tong, Y., Yang, W., and Koeffler, H.P. (2011b). Mouse models of colorectal cancer. Chinese Journal of Cancer *30*, 450-462. https://doi.org/10.5732/cjc.011.10041.

Tran, B., Kopetz, S., Tie, J., Gibbs, P., Jiang, Z.-Q., Lieu, C.H., Agarwal, A., Maru, D.M., Sieber, O., and Desai, J. (2011). Impact of BRAF mutation and microsatellite instability on the pattern of metastatic spread and prognosis in metastatic colorectal cancer. Cancer *117*, 4623-4632. https://doi.org/10.1002/cncr.26086.

Tretter, L., and Adam-Vizi, V. (2005). Alpha-ketoglutarate dehydrogenase: a target and generator of oxidative stress. Philosophical transactions of the Royal Society of London. Series B, Biological sciences *360*, 2335-2345. https://doi.org/10.1098/rstb.2005.1764.

Trinidad, A.G., Whalley, N., Rowlinson, R., Delpuech, O., Dudley, P., Rooney, C., and Critchlow, S.E. (2017). Pyruvate dehydrogenase kinase 4 exhibits a novel role in the activation of mutant KRAS, regulating cell growth in lung and colorectal tumour cells. Oncogene *36*, 6164-6176. https://doi.org/10.1038/onc.2017.224.

Tveit, K.M., Guren, T., Glimelius, B., Pfeiffer, P., Sorbye, H., Pyrhonen, S., Sigurdsson, F., Kure, E., Ikdahl, T., and Skovlund, E., et al. (2012). Phase III trial of cetuximab with continuous or intermittent fluorouracil, leucovorin, and oxaliplatin (Nordic FLOX) versus FLOX alone in first-line treatment of metastatic colorectal cancer: the NORDIC-VII study. Journal of clinical oncology : official journal of the American Society of Clinical Oncology *30*, 1755-1762. https://doi.org/10.1200/JCO.2011.38.0915.

Valcarcel-Jimenez, L., Gaude, E., Torrano, V., Frezza, C., and Carracedo, A. (2017). Mitochondrial Metabolism: Yin and Yang for Tumor Progression. https://doi.org/10.17863/CAM.15824.

van Cutsem, E., Lenz, H.-J., Köhne, C.-H., Heinemann, V., Tejpar, S., Melezínek, I., Beier, F., Stroh, C., Rougier, P., and van Krieken, J.H., et al. (2015). Fluorouracil, leucovorin, and irinotecan plus cetuximab treatment and RAS mutations in colorectal cancer. Journal of clinical oncology : official journal of the American Society of Clinical Oncology *33*, 692-700. https://doi.org/10.1200/JCO.2014.59.4812.

van Cutsem, E., Tabernero, J., Lakomy, R., Prenen, H., Prausová, J., Macarulla, T., Ruff, P., van Hazel, G.A., Moiseyenko, V., and Ferry, D., et al. (2012). Addition of aflibercept to fluorouracil, leucovorin, and irinotecan improves survival in a phase III randomized trial in patients with metastatic colorectal cancer previously treated with an oxaliplatin-based regimen. Journal of clinical oncology : official journal of the American Society of Clinical Oncology *30*, 3499-3506. https://doi.org/10.1200/JCO.2012.42.8201.

van de Mark, K., Chen, J.S., Steliou, K., Perrine, S.P., and Faller, D.V. (2003). Alpha-lipoic acid induces p27Kip-dependent cell cycle arrest in non-transformed cell lines and apoptosis in tumor cell lines. Journal of cellular physiology *194*, 325-340. https://doi.org/10.1002/jcp.10205.

van der Geest, L.G.M., Lam-Boer, J.'t., Koopman, M., Verhoef, C., Elferink, M.A.G., and Wilt, J.H.W. de (2015). Nationwide trends in incidence, treatment and survival of colorectal cancer patients with synchronous metastases. Clinical & experimental metastasis *32*, 457-465. https://doi.org/10.1007/s10585-015-9719-0.

van Houten, B., Hunter, S.E., and Meyer, J.N. (2016). Mitochondrial DNA damage induced autophagy, cell death, and disease. Frontiers in bioscience (Landmark edition) *21*, 42-54.

Vara-Perez, M., Felipe-Abrio, B., and Agostinis, P. (2019). Mitophagy in Cancer: A Tale of Adaptation. Cells *8*. https://doi.org/10.3390/cells8050493.

Vazquez, A., Kamphorst, J.J., Markert, E.K., Schug, Z.T., Tardito, S., and Gottlieb, E. (2016). Cancer metabolism at a glance. Journal of cell science *129*, 3367-3373. https://doi.org/10.1242/jcs.181016.

Vincan, E., and Barker, N. (2008). The upstream components of the Wnt signalling pathway in the dynamic EMT and MET associated with colorectal cancer progression. Clinical & experimental metastasis *25*, 657-663. https://doi.org/10.1007/s10585-008-9156-4.

Vogelstein, B., Fearon, E.R., Hamilton, S.R., Kern, S.E., Preisinger, A.C., Leppert, M., Nakamura, Y., White, R., Smits, A.M., and Bos, J.L. (1988). Genetic alterations during colorectal-tumor development. The New England journal of medicine *319*, 525-532. https://doi.org/10.1056/NEJM198809013190901.

Voon, D.C., Huang, R.Y., Jackson, R.A., and Thiery, J.P. (2017). The EMT spectrum and therapeutic opportunities. Molecular oncology *11*, 878-891. https://doi.org/10.1002/1878-0261.12082.

Voulgari, A., and Pintzas, A. (2009). Epithelial-mesenchymal transition in cancer metastasis: mechanisms, markers and strategies to overcome drug resistance in the clinic. Biochimica et biophysica acta *1796*, 75-90. https://doi.org/10.1016/j.bbcan.2009.03.002.

Vuik, F.E., Nieuwenburg, S.A., Bardou, M., Lansdorp-Vogelaar, I., Dinis-Ribeiro, M., Bento, M.J., Zadnik, V., Pellisé, M., Esteban, L., and Kaminski, M.F., et al. (2019). Increasing incidence of colorectal cancer in young adults in Europe over the last 25 years. Gut *68*, 1820-1826. https://doi.org/10.1136/gutjnl-2018-317592.

Waitkus, M.S., Diplas, B.H., and Yan, H. (2018). Biological Role and Therapeutic Potential of IDH Mutations in Cancer. Cancer cell *34*, 186-195. https://doi.org/10.1016/j.ccell.2018.04.011.

Wallace, B.D., Wang, H., Lane, K.T., Scott, J.E., Orans, J., Koo, J.S., Venkatesh, M., Jobin, C., Yeh, L.-A., and Mani, S., et al. (2010). Alleviating cancer drug toxicity by inhibiting a bacterial enzyme. Science (New York, N.Y.) *330*, 831-835. https://doi.org/10.1126/science.1191175.

Wang, S.-Q., Cui, S.-X., and Qu, X.-J. (2019). Metformin inhibited colitis and colitis-associated cancer (CAC) through protecting mitochondrial structures of colorectal epithelial cells in mice. Cancer biology & therapy *20*, 338-348. https://doi.org/10.1080/15384047.2018.1529108.

Warburg, O., Wind, F., and Negelein, E. (1927). THE METABOLISM OF TUMORS IN THE BODY. The Journal of General Physiology *8*, 519-530.

Ward, P.S., and Thompson, C.B. (2012). Metabolic reprogramming: a cancer hallmark even warburg did not anticipate. Cancer cell *21*, 297-308. https://doi.org/10.1016/j.ccr.2012.02.014.

Was, H., Czarnecka, J., Kominek, A., Barszcz, K., Bernas, T., Piwocka, K., and Kaminska, B. (2018). Some chemotherapeutics-treated colon cancer cells display a specific phenotype being

a combination of stem-like and senescent cell features. Cancer biology & therapy *19*, 63-75. https://doi.org/10.1080/15384047.2017.1385675.

Waterhouse, N.J. (2003). The cellular energy crisis: mitochondria and cell death. Medicine and science in sports and exercise *35*, 105-110. https://doi.org/10.1097/00005768-200301000-00017.

Wei, T.-T., Lin, Y.-T., Tang, S.-P., Luo, C.-K., Tsai, C.-T., Shun, C.-T., and Chen, C.-C. (2020). Metabolic targeting of HIF-1α potentiates the therapeutic efficacy of oxaliplatin in colorectal cancer. Oncogene *39*, 414-427. https://doi.org/10.1038/s41388-019-0999-8.

Wenzel, U., Nickel, A., and Daniel, H. (2005). alpha-Lipoic acid induces apoptosis in human colon cancer cells by increasing mitochondrial respiration with a concomitant O2-*-generation. Apoptosis : an international journal on programmed cell death *10*, 359-368. https://doi.org/10.1007/s10495-005-0810-x.

White, E. (2007). Role of the metabolic stress responses of apoptosis and autophagy in tumor suppression. Ernst Schering Foundation symposium proceedings, 23-34. https://doi.org/10.1007/2789_2008_087.

White, E. (2015). The role for autophagy in cancer. The Journal of clinical investigation *125*, 42-46. https://doi.org/10.1172/JCI73941.

Wieland, O.H. (1983). The mammalian pyruvate dehydrogenase complex: structure and regulation. Reviews of physiology, biochemistry and pharmacology *96*, 123-170. https://doi.org/10.1007/BFb0031008.

Wiley, C.D., Velarde, M.C., Lecot, P., Liu, S., Sarnoski, E.A., Freund, A., Shirakawa, K., Lim, H.W., Davis, S.S., and Ramanathan, A., et al. (2016). Mitochondrial Dysfunction Induces Senescence with a Distinct Secretory Phenotype. Cell metabolism *23*, 303-314. https://doi.org/10.1016/j.cmet.2015.11.011.

Williams, A.B., and Schumacher, B. (2016). p53 in the DNA-Damage-Repair Process. Cold Spring Harbor perspectives in medicine *6*. https://doi.org/10.1101/cshperspect.a026070.

Wohlhueter, R.M., McIvor, R.S., and Plagemann, P.G. (1980). Facilitated transport of uracil and 5-fluorouracil, and permeation of orotic acid into cultured mammalian cells. Journal of cellular physiology *104*, 309-319. https://doi.org/10.1002/jcp.1041040305.

Wyatt, M.D., and Wilson, D.M. (2009). Participation of DNA repair in the response to 5-fluorouracil. Cellular and molecular life sciences : CMLS *66*, 788-799. https://doi.org/10.1007/s00018-008-8557-5.

Xiong, H.-y., Guo, X.-L., Bu, X.-x., Zhang, S.-S., Ma, N.-n., Song, J.-R., Hu, F., Tao, S.-f., Sun, K., and Li, R., et al. (2010). Autophagic cell death induced by 5-FU in Bax or PUMA deficient

human colon cancer cell. Cancer Letters *288*, 68-74. https://doi.org/10.1016/j.canlet.2009.06.039.

Yadav, V., Marracci, G., Lovera, J., Woodward, W., Bogardus, K., Marquardt, W., Shinto, L., Morris, C., and Bourdette, D. (2005). Lipoic acid in multiple sclerosis: a pilot study. Multiple sclerosis (Houndmills, Basingstoke, England) *11*, 159-165. https://doi.org/10.1191/1352458505ms1143oa.

Yakes, F.M., and van Houten, B. (1997). Mitochondrial DNA damage is more extensive and persists longer than nuclear DNA damage in human cells following oxidative stress. Proceedings of the National Academy of Sciences of the United States of America *94*, 514-519. https://doi.org/10.1073/pnas.94.2.514.

Yamasaki, M., Iwase, M., Kawano, K., Sakakibara, Y., Suiko, M., Ikeda, M., and Nishiyama, K. (2014). α-Lipoic acid suppresses migration and invasion via downregulation of cell surface β1-integrin expression in bladder cancer cells. Journal of clinical biochemistry and nutrition *54*, 18-25. https://doi.org/10.3164/jcbn.13-57.

Yan, H., Parsons, D.W., Jin, G., McLendon, R., Rasheed, B.A., Yuan, W., Kos, I., Batinic-Haberle, I., Jones, S., and Riggins, G.J., et al. (2009). IDH1 and IDH2 mutations in gliomas. The New England journal of medicine *360*, 765-773. https://doi.org/10.1056/NEJMoa0808710.

Yang, A.D., Fan, F., Camp, E.R., van Buren, G., Liu, W., Somcio, R., Gray, M.J., Cheng, H., Hoff, P.M., and Ellis, L.M. (2006). Chronic oxaliplatin resistance induces epithelial-to-mesenchymal transition in colorectal cancer cell lines. Clinical cancer research : an official journal of the American Association for Cancer Research *12*, 4147-4153. https://doi.org/10.1158/1078-0432.CCR-06-0038.

Yang, H., Higgins, B., Kolinsky, K., Packman, K., Bradley, W.D., Lee, R.J., Schostack, K., Simcox, M.E., Kopetz, S., and Heimbrook, D., et al. (2012). Antitumor activity of BRAF inhibitor vemurafenib in preclinical models of BRAF-mutant colorectal cancer. Cancer research *72*, 779-789. https://doi.org/10.1158/0008-5472.CAN-11-2941.

Yang, J., Antin, P., Berx, G., Blanpain, C., Brabletz, T., Bronner, M., Campbell, K., Cano, A., Casanova, J., and Christofori, G., et al. (2020). Guidelines and definitions for research on epithelial-mesenchymal transition. Nature reviews. Molecular cell biology *21*, 341-352. https://doi.org/10.1038/s41580-020-0237-9.

Yang, J.-W., Zhang, Q.-H., and Liu, T. (2018). Autophagy facilitates anticancer effect of 5-fluorouracil in HCT-116 cells. Journal of cancer research and therapeutics *14*, S1141-S1147. https://doi.org/10.4103/0973-1482.204898.

Yang, Y., Wang, G., Zhu, D., Huang, Y., Luo, Y., Su, P., Chen, X., and Wang, Q. (2017). Epithelial-mesenchymal transition and cancer stem cell-like phenotype induced by Twist1

contribute to acquired resistance to irinotecan in colon cancer. International journal of oncology *51*, 515-524. https://doi.org/10.3892/ijo.2017.4044.

Yao, C.W., Kang, K.A., Piao, M.J., Ryu, Y.S., Fernando, P.M.D.J., Oh, M.C., Park, J.E., Shilnikova, K., Na, S.-Y., and Jeong, S.U., et al. (2017). Reduced Autophagy in 5-Fluorouracil Resistant Colon Cancer Cells. Biomolecules & therapeutics *25*, 315-320. https://doi.org/10.4062/biomolther.2016.069.

Yoo, S.-M., and Jung, Y.-K. (2018). A Molecular Approach to Mitophagy and Mitochondrial Dynamics. Molecules and cells *41*, 18-26. https://doi.org/10.14348/molcells.2018.2277.

Yoo, T.-H., Lee, J.-H., Chun, H.-S., and Chi, S.-G. (2013). α-Lipoic acid prevents p53 degradation in colon cancer cells by blocking NF-κB induction of RPS6KA4. Anti-cancer drugs *24*, 555-565. https://doi.org/10.1097/CAD.0b013e32836181eb.

Yoshikawa, R., Kusunoki, M., Yanagi, H., Noda, M., Furuyama, J.I., Yamamura, T., and Hashimoto-Tamaoki, T. (2001). Dual antitumor effects of 5-fluorouracil on the cell cycle in colorectal carcinoma cells: a novel target mechanism concept for pharmacokinetic modulating chemotherapy. Cancer research *61*, 1029-1037.

Yoshino, T., Mizunuma, N., Yamazaki, K., Nishina, T., Komatsu, Y., Baba, H., Tsuji, A., Yamaguchi, K., Muro, K., and Sugimoto, N., et al. (2012). TAS-102 monotherapy for pretreated metastatic colorectal cancer: a double-blind, randomised, placebo-controlled phase 2 trial. The Lancet. Oncology *13*, 993-1001. https://doi.org/10.1016/S1470-2045(12)70345-5.

Young, A., Oldford, C., and Mailloux, R.J. (2020). Lactate dehydrogenase supports lactate oxidation in mitochondria isolated from different mouse tissues. Redox biology *28*, 101339. https://doi.org/10.1016/j.redox.2019.101339.

Yuan, L., Zhang, S., Li, H., Yang, F., Mushtaq, N., Ullah, S., Shi, Y., An, C., and Xu, J. (2018). The influence of gut microbiota dysbiosis to the efficacy of 5-Fluorouracil treatment on colorectal cancer. Biomedicine & pharmacotherapy = Biomedecine & pharmacotherapie *108*, 184-193. https://doi.org/10.1016/j.biopha.2018.08.165.

Zachar, Z., Marecek, J., Maturo, C., Gupta, S., Stuart, S.D., Howell, K., Schauble, A., Lem, J., Piramzadian, A., and Karnik, S., et al. (2011). Non-redox-active lipoate derivates disrupt cancer cell mitochondrial metabolism and are potent anticancer agents in vivo. Journal of molecular medicine (Berlin, Germany) *89*, 1137-1148. https://doi.org/10.1007/s00109-011-0785-8.

Zacharakis, M., Xynos, I.D., Lazaris, A., Smaro, T., Kosmas, C., Dokou, A., Felekouras, E., Antoniou, E., Polyzos, A., and Sarantonis, J., et al. (2010). Predictors of survival in stage IV metastatic colorectal cancer. Anticancer research *30*, 653-660.

Zehnpfennig, B., Wiriyasermkul, P., Carlson, D.A., and Quick, M. (2015). Interaction of α-Lipoic Acid with the Human Na+/Multivitamin Transporter (hSMVT). The Journal of biological chemistry *290*, 16372-16382. https://doi.org/10.1074/jbc.M114.622555.

Zeisberg, M., and Neilson, E.G. (2009). Biomarkers for epithelial-mesenchymal transitions. The Journal of clinical investigation *119*, 1429-1437. https://doi.org/10.1172/JCI36183.

Zhang, B., Halder, S.K., Zhang, S., and Datta, P.K. (2009). Targeting transforming growth factor-beta signaling in liver metastasis of colon cancer. Cancer Letters *277*, 114-120. https://doi.org/10.1016/j.canlet.2008.11.035.

Zhang, S.-J., Ge, Q.-F., Guo, D.-W., Hu, W.-X., and Liu, H.-Z. (2010). Synthesis and anticancer evaluation of alpha-lipoic acid derivatives. Bioorganic & medicinal chemistry letters *20*, 3078-3083. https://doi.org/10.1016/j.bmcl.2010.03.112.

Zhang, S.-M., Shang, Z.-F., and Zhou, P.-K. (2015). Autophagy as the effector and player in DNA damage response of cells to genotoxicants. Toxicol. Res. *4*, 613-622. https://doi.org/10.1039/C5TX00043B.

Zhang, Y., and Yang, J.-M. (2013). Altered energy metabolism in cancer: a unique opportunity for therapeutic intervention. Cancer biology & therapy *14*, 81-89. https://doi.org/10.4161/cbt.22958.

Zhao, H., Huang, X., Halicka, H.D., and Darzynkiewicz, Z. (2019). Detection of Histone H2AX Phosphorylation on Ser-139 as an Indicator of DNA Damage. Current protocols in cytometry *89*, e55. https://doi.org/10.1002/cpcy.55.

Zhu, X.-H., Lang, H.-D., Wang, X.-L., Hui, S.-C., Zhou, M., Kang, C., Yi, L., Mi, M.-T., and Zhang, Y. (2019). Synergy between dihydromyricetin intervention and irinotecan chemotherapy delays the progression of colon cancer in mouse models. Food & function *10*, 2040-2049. https://doi.org/10.1039/c8fo01756e.

Zou, J., Luo, H., Zeng, Q., Dong, Z., Wu, D., and Liu, L. (2011). Protein kinase CK2α is overexpressed in colorectal cancer and modulates cell proliferation and invasion via regulating EMT-related genes. Journal of translational medicine *9*, 97. https://doi.org/10.1186/1479-5876-9-97.

ANNEX

Assay (time points)		Culture Plate		Cell Line					
				HCT116			HT29		others (per well)
ATP assays using arrested cells	**(72 h)**	white 96-half-well-plate		$2.5x10^3$ / well			$3.75x10^3$ / well		**HCT116-p53-/-:** $3.25x10^3$ **LS-174T:** $2.5x10^3$ **RKO:** $2.5x10^{53}$ **SW48:** $3.25x10^3$ **DLD-1:** $2.5x10^3$ **CaCO-2:** $3.25x10^3$ **SW480:** $2.5x10^3$ **HROC60:** $5x10^3$ **HROC278:** $4x10^3$ **HCEC:** $0.5x10^3$
ATP assays using arrested cells	**(7 d, 72 h)**	10 cm dish for induction of arrest;	white 96-half-well-plate for ATP assay	10 cm dish: $5x10^5$	96-half-well-plates: $1x10^4$/well (HCT116-a)		-		-
Cell cycle distribution	**(24, 48, 72 h)**	6 cm dish		24 h: $5x10^5$	48 h: $2.5x10^5$	72 h: $1.25x10^5$	24 h: $5x10^5$	48 h: $2.5x10^5$ / 72 h: $1.25x10^5$	-
Measurement of AnnexinV/PI or CytoID®	**(48h)**	3.5 cm dish			$1x10^5$			$1x10^5$	-
Measurement of ROS or JC-1	**(1-2 h)**	3.5 cm dish			$4x10^5$			-	-
In Cell Western	**(24 h)**	black 96-well-plate with transparent bottom			$2x10^4$ / well			$2x10^4$ /well	-
Comet Assay	**(24 h)**	3.5 cm dish			$2x10^5$			$2x10^5$	-
Immuno-fluorescence staining MitoTracker™	**(24 h)**	3.5 cm dish with cover slips			$2x10^5$			-	-
Invasion CytoSelect™ Assay	**(48 h)**	insert			$5x10^5$/ml			-	-
MitoStress Test Kit Seahorse	**(24 h)**	96-well-plate of kit			$8x10^5$/well			$8x10^5$/well	-
Xenograft experiments in nude mice		per flank in 200 µl medium			$5x10^6$			$2x10^6$	-
Migration Wound Healing Assay	**(24 h)**	6-well-plate			$2x10^6$ /well			$2x10^6$ /well	-
Western Blot samples	**(24 / 48 h)**	3.5 cm dish		24 h: $2x10^5$	48 h: $1x10^5$	-	24 h: $2.5x10^5$	48 h: $1.25x10^5$	-

Table Annex- 1: Overview of seeded cell densities for the different cell culture experiments.

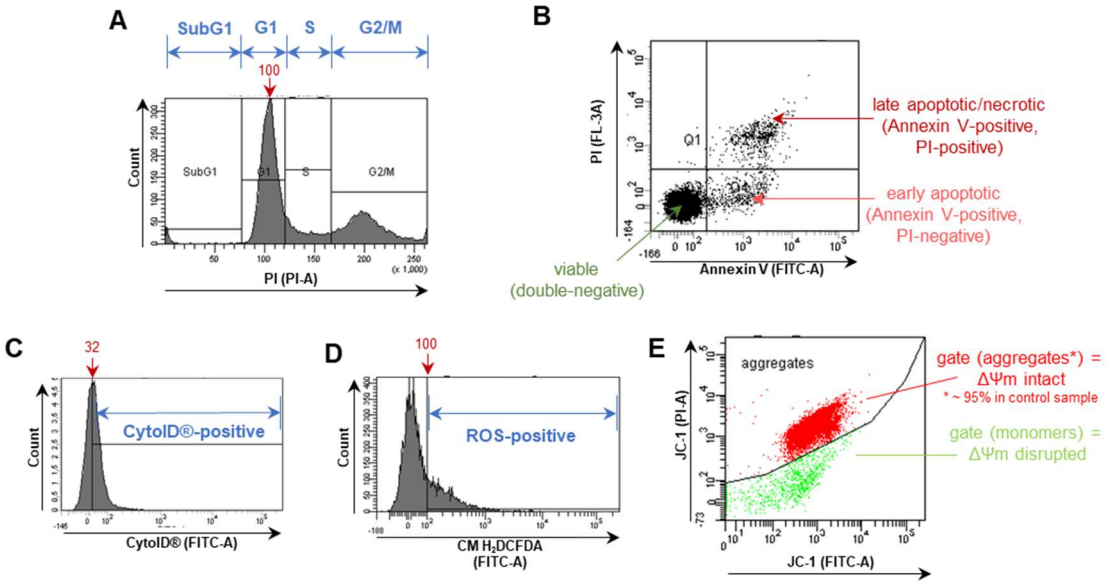

Figure Annex- 1: Gating strategy of flow cytometry methods.

Pictures show schematic gating strategies of flow cytometry methods. (A) For cell cycle distribution analysis, the PI signal was measured using PI-A. Histograms were used to visualise the cell cycle distribution. The peak belonging to the G1 phase was adjusted to 100 (x1,000) and gates for SubG1, G1, S and G2/M were fixed for the entire experimental runs. (B) In cell death measurements using Annexin V-FITC and PI, dot plots visualising Annexin V signal intensity measured with the FITC-A channel versus PI signal intensity measured with the FL-3A channel were used to assess the rates of apoptotic/necrotic cell death. Double-negative cells, depicted in green, represent viable cells. Annexin V-positive but PI-negative cells, shown in light red, stand for early apoptotic cells, while double-positive cells, illustrated in dark red, undergo late apoptotic/necrotic cell death. Gating using squares was fixed throughout all experimental runs. (C) To assess autophagy levels, CytoID® Green Dye was used and measured using the channel FITC-A. When plotting the histograms, the peak in the control sample was set to align with a mean signal intensity of 32. (D) When measuring relative ROS levels, the signal intensity of CM H_2DCFDA was measured using the FITC-A channel. The control sample was adjusted to show a mean signal intensity of 100. (E) Measuring the change in mitochondrial membrane potential (ΔΨm), JC-1 staining was used. Aggregates and monomers of the JC-1 dye were quantified by using dot plots of PI-A versus FITC-A. Gates were chosen to show approximately 95% of cells as aggregates in the untreated control sample and gating was fixed throughout all experimental runs.